Centralized Monitoring of 10kV Cable Based Radial Distribution Networks

Steen M. Munk

second edition
31st of August 1995

A thesis submitted for the degree of
Doctor of Philosophy

Industrial Research Education Programme EF467,
the Academy of Technical Sciences,
the Electronics Institute & the Power Engineering Department of the
Technical University of Denmark
and the Department of Research and Development of NESA A/S

Udgivet af/Published by:
- **Elektronisk Institut**
  bygning 349, Danmarks Tekniske Universitet
  DK–2800 Lyngby
  Danmark
  (+45) 4525 3885, fax: (+45) 4588 0117

i samarbejde med/in cooperation with:
- **NESA A/S**
  Udviklingsafdelingen
  Strandvejen 102
  DK–2900 Hellerup
  Danmark
  (+45) 3948 1010, fax: (+45) 3948 1011

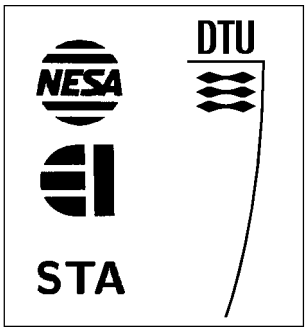

Denne afhandling er katalogiseret i NESA's Udviklingsafdelings nummersystem som rapport:
#UD 1995-051

Preface

This thesis was written as the final part of the Industrial Research Education Programme EF467, (Erhvervsforskerprojekt), that was in process from the 1st of December 1992 to the 31st of May 1995.

This project was concerned with an investigation on alternative methods for distribution network monitoring — so-called centralized monitoring.

The work was partly funded by the MINISTRY OF INDUSTRY and administered by a committee under the ACADEMY OF TECHNICAL SCIENCES, (ATV).

Industrial research education programmes are organized as a collaboration among the candidate, ATV, a university and a company.
The candidate is employed with the company and matriculated with the university. The requirements of this kind of Ph.D.–education programme are described in [ATV, 1994].

This project was set up as a collaboration between the TECHNICAL UNIVERSITY OF DENMARK, (DTU), represented by the ELECTRONICS INSTITUTE and the ELECTRICAL POWER ENGINEERING DEPARTMENT, and the electricity distribution utility NESA A/S, see also the syllabus of the project; [Nielsen *et al.*, 1993].

The project steering committee was: R&D Manager, B.Sc. Willy Bergstrøm-Poulsen,.....NESA A/S
Associate Professor, M.Sc., Arne Hejde Nielsen,.....DTU
Associate Prof., Ph.D., M.Sc. Knud Ole Helgesen Pedersen,. DTU
Manager, M.Sc. Torben Rahbek,.....NESA A/S
Associate Professor, Ph.D., M.Sc. John Aasted Sørensen,....DTU
Chief Engineer, Ph.D., M.Sc. Henrik Weldingh, ... DELRI/DEFU

As an offspring of this Ph.D.–programme, four students pursuing a Masters degree have worked on related topics and submitted theses, see [Høg, 1994], [Jespersen, 1994], [Lauritsen, 1995] and [Nielsen, 1995].

DK–2900 Hellerup, 31st of August, 1995 Steen M. Munk

Throughout this thesis European decimal notation has been applied where possible.

Contents

Sammenfatning på dansk

I denne ph.d.–afhandling beskrives begrebet *Centraliseret overvågning af el-distributionsnetværk.*
På grundlag af de primære måleværdier; tre fasestrømme og tre fase-jord spændinger, der kan måles ved udføringen af en distributionsradial, undersøges det om tilstrækkelig information kan uddrages, således at en 10kV distributionsradial vil kunne overvåges udfra disse målinger.

Afhandlingen beskriver arbejdet med at skabe indblik i 10kV radiale distributionsnetværks egenskaber som overføringsmedium af signaler, der er opstået i forbindelse med en tilstandsændring i netværket.
Tilstandsændring beskrives i afhandlingen ved begrebet *hændelse.* Efter at en hændelse er *detekteret*, skal den *identificeres.*
Arbejdet med disse emner har eftervist, at centraliseret overvågning er mulig.
Projektet er nået til begyndelsen af arbejdet med at udvikle metoder til automatiseret identifikation af hændelser.

Forsøg på en idriftværende distributionsradial har vist, at ganske mange detaljer fra en hændelse et sted i netværket når frem til hovedstationen, hvor *O*bservations *P*unktet for et centraliseret overvågningssystem vil være placeret.
I *OP*'et måles med højkvalitetsmåleudstyr, således at strømme og spændinger måles i en båndbredde på ca. 10kHz.
Analyse af målinger, foretaget i forbindelse med forsøg, antyder, at strømmålinger er mere krævende end spændingsmålinger.
Forsøgene og deres tilrettelæggelse er beskrevet i denne afhandling.

Den store båndbredde skal sikre at transienter, der opstår ved en tilstandsændring, vil blive opsamlet af registreringsudstyret.
Som noget nyt, i forhold til den gængse måde, at anskue højspændingssystemer på, er det i denne fremstilling en fundamental antagelse, at 50Hz-komponenten ikke er den eneste kilde til indsigt i aktiviteten i netværket.
P.g.a. 50Hz-komponentens kraftige amplitude, i forhold til alle andre komponenter i frekvensspektret, sker analysen af målingerne i to spor. Et *grundtonespor* og et *restsignalspor.* Disse to begreber er væsentlige i det samlede begrebsæt, der er udviklet i forbindelse med dette projekt.

Estimaterne af grundtonekomponenterne af strømmene bruges til detektion af hændelser. Den følgende identifikation skal baseres både på grundtonekomponenten og på restsignalet.

Udfra nogle af de målinger, der blev foretaget på en radial i drift, vises det at der, for lavspændingshændelser, hvor signalerne først har passeret en distributionstransformer, kan ses spor af frekvenskomponenter over ca. 2,5kHz.

Endvidere vises det, at det er muligt at opstille modeller for hændelser og, udfra målingerne, estimere parametrene.
Forsøg med to meget ens motorer, placeret det samme sted i netværket, har godtgjort, at det er muligt at kende forskel på start og stop af disse to maskiner.
Dette regnes for et af projektets meget vigtige resultater.

Begrebet *Ækvivalent Elektrisk Afstand* introduceres og det indledende arbejde med dets definition beskrives.

Abstract in English

This Ph.D.–thesis describes the concept of *Centralized Monitoring of Distribution Networks.*
On the basis of the primary measurements that may be measured where a feeder leaves the substation; three phase currents and three phase-ground voltages, it is investigated if sufficient information is available to monitor a distribution feeder.

The thesis describes the work on gaining insight into radial distribution feeders as the means for transferring signals that arise as the result of a change of state in the network. *Change of state* is in this thesis termed *event.* After the *detection* of an event, it must be *classified.*
Work on these topics has demonstrated that centralized monitoring is possible.
The project is now so far that work on the development of methods for automated identification of events may commence.

Experiments on a feeder in operation have shown that detailed information from an event somewhere in the network reaches the substation, where the *O*bservation *P*oint of a centralized monitoring system is located.
At the *OP* measurements are taken with high quality equipment. Currents and voltages are measured in a bandwidth of about 10kHz.
Analysis of measurements, taken during experiments, indicates that current measurements are more demanding than voltage measurements.
The experiments and their preparation are described in this thesis.

The large bandwidth is required to ensure that transients that arise due to a change of state, may be captured by the equipment.
As something new, compared to the traditional way of regarding high voltage systems, it is in this work a fundamental assumption that the 50Hz component is not the only source of information about the activity in the network.
Because the 50Hz component is so strong, compared to other components in the frequency spectrum, the analysis is performed in two tracks. The *fundamental component* track and the *residual signal component* track. These two terms are important in the set of concepts that has been defined during this project.

The estimates of the fundamental frequency components of the currents are used for the detection of events. The subsequent identification is to be based on both the fundamental frequency component and the residual signal component.

With some of the measurements that were taken on a feeder in operation, it is shown that events that take place in the low voltage network, give rise to frequency components over 2,5kHz. This is remarkable since the signals have passed through a distribution transformer.

Furthermore, it is shown that it is possible to create models of events and, from the measurements, estimate the parameters.
Experiments with two similar motors, placed at the same location in the network, has shown that it is possible to distinguish the starting and stopping of the two. This result is regarded as one of the very important of the project.

The concept *Equivalent Electrical Distance* is introduced and the initial steps on the work on its definition are described.

Chapter 1

Distribution Network Monitoring

Distribution of electrical energy is done through a two-level network. The first level is the *transmission level*. This level transports the energy from where it is produced to nodes in the network from where it is *distributed*.
The second level is the *distribution level*. At this level the energy is distributed to the customers.

Up to the present, detailed monitoring of the electrical network has mainly been performed at transmission level.

At distribution level no real monitoring has been made. At the substations has been measured the voltages at the busbar and the currents into the feeders.
Hereby it has been possible to open circuit breakers in the event of a fault somewhere on a feeder.
This would extinct the fault but also deprive of supply all customers connected to the feeder until the location of the fault has been determined, the faulty part of the feeder isolated, and supply reestablished from other feeders.
The process might last for hours!

NESA A/S and other utilities in Danmark therefore initiated collaboration on the definition of the distribution network of the future, the so-called DSO–project[1].
This project started in the summer of 1991 and was scheduled to terminate by the end of 1994.
The DSO–project dealt with the definition of structures for monitoring and control of whole networks, so that, among many perspectives, rapid fault clearing would be possible.
The establishment of measuring points at virtually all transformer stations was a fundamental assumption. With every measuring point there must be a communication channel to transmit to locations in the network where processing should take place the measurements, or a pre-processed version of these. The project therefore was also concerned with the definition of ways to communicate data depending on the level in the hierarchy of the system.

It was estimated that a full implementation of a DSO–system would require an investment of DKK200.000.000 (1992 prices) only in NESA's area of operation; 500.000 customers supplied from 60 substations and 6.000 transformer stations. Such an investment would seem hard to motivate.

However, utilities are becoming more and more interested in *power quality*. With an increasing number of non-linear loads, customers encounter more and more frequently problems with malfunction, due to high levels of harmonics and switching transients.

The experiences from the DSO–project lead to the idea that it would be relevant to investigate if "many" of the measuring points could be suppressed and some of the money saved instead used on the establishment of smart monitoring systems, where advanced signal processing methods are applied to the measurements to extract as much information as possible in order to compensate for the limited number of measuring points. The idea lies in line with *nonintrusive appliance load monitoring*, see [Hart, 1992].

On occasion of DELRI[2], that already was the coordinator of the DSO–project, contact was established between the Technical University of Denmark and NESA A/S in order to initiate research on the topic

[1] DSO, **D**istributionsnettets **S**tyring og **O**vervågning. *Control and Monitoring of the Distribution Network.*
[2] DELRI, the **D**anish **EL**ectrical **R**esearch **I**nstitute.

***C**entralized **M**onitoring of **D**istribution **N**etworks*, CMDN.
This contact lead to this project; the DISMO–project[3].
The project was originally intended to be tightly coordinated with the DSO–project, but has developed into an independent project, even though it has been much inspired by DSO.

Elements of the ideas behind this project may also be seen in the light of *state estimation*.
State estimation is well-known in the transmission network. But, as opposed to the distribution network, in NESA's area of distribution, these are being operated as meshed networks, i.e. the topology is fundamentally different.
Still, the same is desired; on the basis of measurements an estimate of the state of the distribution feeder is calculated.
A thorough description of state estimation techniques may be found in [Schweppe and Wildes, 1970] and [Olesen, 1975].

Today NESA's customers still experience comparatively few "inconveniences" in their supply. Investigations have shown that most customers will not pay more to be ensured higher security in the delivery of electrical energy.
The fundamental idea was that distribution network monitoring must be cheap, however much desired by the utilities. Therefore the code word was, 'how little is enough?'. Meaning 'how few measuring points are required', and 'what is achieved by installing auxiliary measuring points along a feeder'?

The assumption was that distribution networks of the future would be cable based and meshed, but operated as being radial. Though NESA still operates overhead distribution feeders, the tendency is that the distribution network will be buried. This is partly a reaction to environmental demands from the population, both regarding the aesthetics in not having to look at the lines and also regarding concerns about magnetic fields, and partly because of the cost of maintaining underground networks is lower than for overhead lines.
The DISMO–project has therefore only worked with 10kV cable based radial distribution networks.

Distribution between substations and transformer stations takes place at 10kV level on a three phase Petersen Coil grounded system. From the transformer stations the customers are supplied from 0,4kV three phase networks with an active zero.
Normal small consumptions are supplied between one phase and zero, hence at 0,23kV level. Larger consumptions are supplied using all three phases.

The utility imposes on its customers that larger consumptions must be balanced, i.e. connected to all three phases.

Many interesting topics need attention in the context of CMDN. Originally was expected that a "machine" that actually could carry out centralized monitoring would be the result of the DISMO–project, as indicated in the syllabus of the project, which is rendered in [Nielsen *et al.*, 1993].
Also important questions were expected to be clarified such as; 'what is the pay-off of auxiliary measuring points along the feeder', 'what is the impact of decentralized electricity production' and 'what will be the "quality" of the monitoring scheme as a function of the quality of the measuring equipment'.

Yet other fundamental questions had to be tried first. This thesis describes how the original hypothesis behind starting the project has been proven valid: It is possible to see a great deal of the activity on the feeder from measurements available from only the substation supplying it.
During the first stages of the project it became obvious that DISMO was the opening of a new area of research in methods for monitoring distribution networks. Therefore, not much help was available in the literature.
The concepts that centralized monitoring of distribution networks are to be based upon had to be defined, and an investigation of the distribution network as a means for other than delivery to customers of electrical energy had to be made.
Though many interesting references may be found concerning higher frequencies in electrical networks, both on load modelling, and on the propagation of "disturbances" from the source to other locations in the network, very little evidence was found about how the information contained in harmonics and transients can actually be exploited.
The following references represent the wide variety of topics that are covered in the literature: [Mak, 1993]

[3]DISMO, **DIS**tribution Network **MO**nitoring.

[Girgis and McManis, 1989], [Morched and Kundur, 1987], [Heydt, 1989a], [Hiyama *et al.*, 1989] and [Beides and Heydt, 1991]. See also the bibliography on pages 109–116.

Transient analysis of electrical networks is not a new subject, see e.g. [Rüdenberg, 1950] and [Clarke, 1943]. Very often power engineers discussing transients, consider only the transient behaviour of the fundamental frequency component. Transient analysis in the sense of dissecting the waveform into detailed information on what happened is an area that has been devoted far less interest, though some newer references that pursue this idea may be found. In particular should be mentioned [Lehtonen, 1992] who describes ideas much in line with the hypothesis behind this project.

The traditional approach, when dealing with higher frequencies in power delivery, is to investigate the contents of harmonics.
Harmonics are defined under the assumption of stationarity. Distribution networks do not exhibit stationarity, at the best they may be regarded as quasi stationary. Therefore, in distribution networks, harmonics only give a very incomplete image of the activity on the feeder.

The hypothesis behind the project was therefore that if transients could be acquired and analysed along with an analysis of the stationary behaviour of the network, information could be extracted that could make up for the lack of measuring points. An important question that had to be addressed was therefore the choice of measuring equipment, see Section 6.2.

Having acquired the measurements the next important question to address is 'what to do'.
During the project a simulator of a CMDN–system has been developed. The state of development of this simulator contains the answers to many of the fundamental questions concerning the analysis system, see Chapters 5 and 6.

NESA maintains a data base on its network. It is believed that this is also done by other distribution utilities.
The data base of NESA contains very detailed information on what kind of cable is used and where, and on where two stretches of cables are connected by a socket joint.
An inquiry at the company has revealed that the effort of maintaining this data base is justified, because exact knowledge about the locations of joints is essential to be able to locate faults quickly.
A fundamental assumption has therefore been that exact knowledge about the topology of the network is available at all times.

The process of locating a fault is normally slow. It would be very interesting to utilities if it were possible to analyse post-fault measurements to give an estimate of the location. So that the repair team can be dispatched to almost the correct location.
However, it is not expected that every kind of fault is detectable using centralized monitoring.
An example of a kind of fault that would be of the utmost interest to electricity utilities to be able to detect is intermittent faults. E.g. water that slowly penetrates the insulation of a cable will cause intermittent faults. The water will cause a short circuit. The current flowing in the short circuit will boil away the water, and the fault will disappear. This might go on until the insulation is so damaged that a real, lasting fault occurs.
If it would be possible to tell where this takes place before a lasting fault settles, much would be gained.
For lasting faults with connection to ground, go that the distribution network, operated by NESA, is Petersen Coil grounded, this does that the fault current will be low. This fact does that it might be difficult to detect a fault in its steady state. It is therefore expected that lasting faults, with connection to ground, must be detected as they start.
Before steady state is reached, where the Petersen coil compensates for the fault, the network passes through a transition period during which a transient will arise. Of course, monitoring the current in the coil might give an indication of a fault.
For short circuits between phases, with or without connection to ground, will go that the currents will attain such a level, that they should be easily distinguishable. Furthermore, already installed protection devices will most likely react soon after the occurrence of such a fault.
It is expected that it will be possible to pin-point where in the network such a fault has occurred.

Automated fault localization has been, and is still a topic of much interest, but mainly in the transmission network, see [GEC Measurements, 1987] and [Phadke and Thorp, 1988].
The conditions in the transmission network are not directly transferable to the distribution network.

Between the two types of network there is a fundamental difference. Much money "passes through" the transmission network, hence more money is available for protection and monitoring equipment. Therefore there is no real problem in establishing the number of measuring points one might require — the number of nodes is also significantly smaller.
Many of the methods for fault location that are reported in the literature will not work very well in a distribution network, see also Appendix B.

This thesis describes whole new methods of processing measurements from electrical power systems. The reader will learn that quite much may be said on the activity in a radial distribution network, on the basis of very few measurements.

The combination of advanced signal processing methods and thorough insight into the behaviour of electric networks gives the potential of moving the border for what may be attained in the optimization of power systems.
This thesis gives an indication of the possibilities but also opens for future delvelopments.

There are still many aspects to investigate!

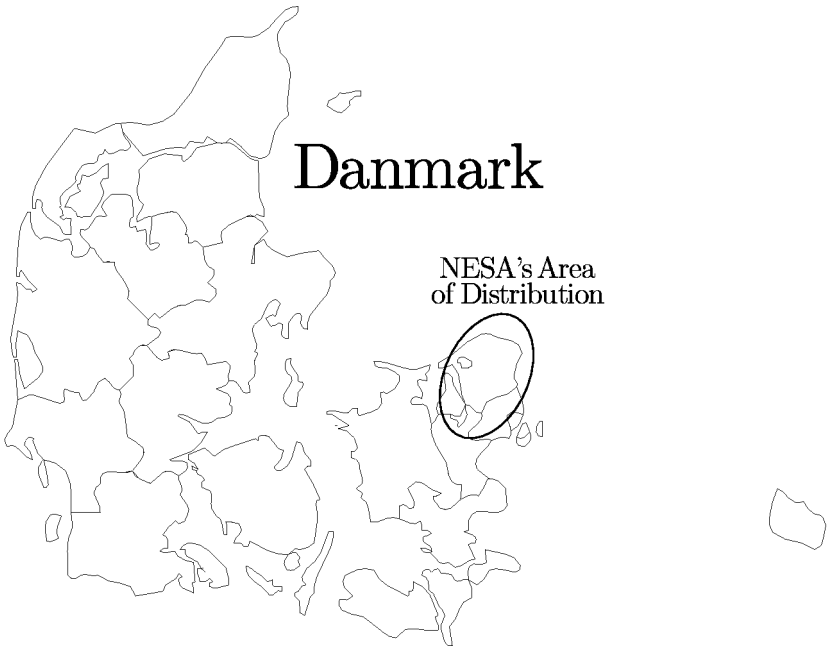

Figure 1.1: Danmark with Indication of NESA's Area of Distribution.

The main topics of the chapters are:

Chapter 2 defines fundamental concepts that are used throughout the thesis.

Chapter 3 describes the modelling that has been performed during the project.
An investigation on the signal transferring capabilities of cables is described.

Chapter 4 describes the preparation for the experiments and their execution.

Chapter 5 gives the outline of the DISMO–monitoring system.

Chapter 6 describes various signal processing methods that either have been incorporated in the DISMO–simulation system or have been used for investigations.
In Appendix A is rendered further material on the initial work on classification. Though the description has been put in the appendix, it is still important. It is placed there, because the investigations have not yet been concluded.

Chapter 7 shows the results of the analyses of the measurements based on the methods described in Chapter 6.

Chapter 2

Fundamental Concepts

Many concepts need definition in order to define a **C**entralized **M**onitoring of **D**istribution **N**etworks system and the environment in which it is to operate.

In Chapter 1 was specified that this project has only been concerned with radial cable based 10kV distribution feeders.
Actually, the voltage at the substations is maintained at 10,4kV, but colloquially this level is termed 'the 10kV level'. This term will also be used throughout this thesis.

In the future, distribution network monitoring will not only be the task of monitoring what takes place on one feeder alone. The entire network will have to be monitored as a whole, hence the activity on one feeder must be seen in the context of the state of the entire electrical network.
E.g. if the fundamental frequency is detected to pass its normal limits, it is most likely that the cause of this is not to be found on the feeder, but rather in the overlying network.

In this project, however, we only work with one feeder. This feeder was chosen on the basis of many parameters.
It should be conveniently located, so that access would be easy. There should be enough space at the substation so that measuring equipment could be installed at the busbar where the feeder is connected. These demands lead to the substation GLENTEGÅRD at Buddinge, a suburb North of København. Here the department of NESA that operates the network has offices. The 10kV system at this substation was the old open kind, thus there was plenty of space, see Figure 4.5 on page 32[1].

From the all in all 24 10kV feeders that are supplied from this substation, one that supplies both industrial and residential areas was chosen, henceforward denoted **A28**, see Figure 2.1.

NESA's customers are normally categorized into three groups:

1. Customers supplied directly from the 10kV level. By NESA termed "A–customers".
2. Customers supplied directly from the secondary side of a distribution transformer. By NESA termed "B–customers".
3. Customers supplied through the low-voltage network. By NESA termed "C–customers".

A few very large customers get supply directly from the transmission network, e.g. 132kV.
About 50% of the consumption is by C–customers.

The feeder **A28** supplies about 2200 customers from 16 transformers. The total yearly consumption is about 13GWh.
20 customers have a yearly consumption exceeding 50MWh and one has a yearly consumption exceeding 1GWh. This customer is the paint factory DYRUP A/S (B–customer) at Gladsaxe, about 4,8km from GLENTEGÅRD. From **A28** this customer is supplied from the transformer **5408**.

[1] After the experiments were performed, the 10kV substation at GLENTEGÅRD has been dismantled and replaced by a new compact station.

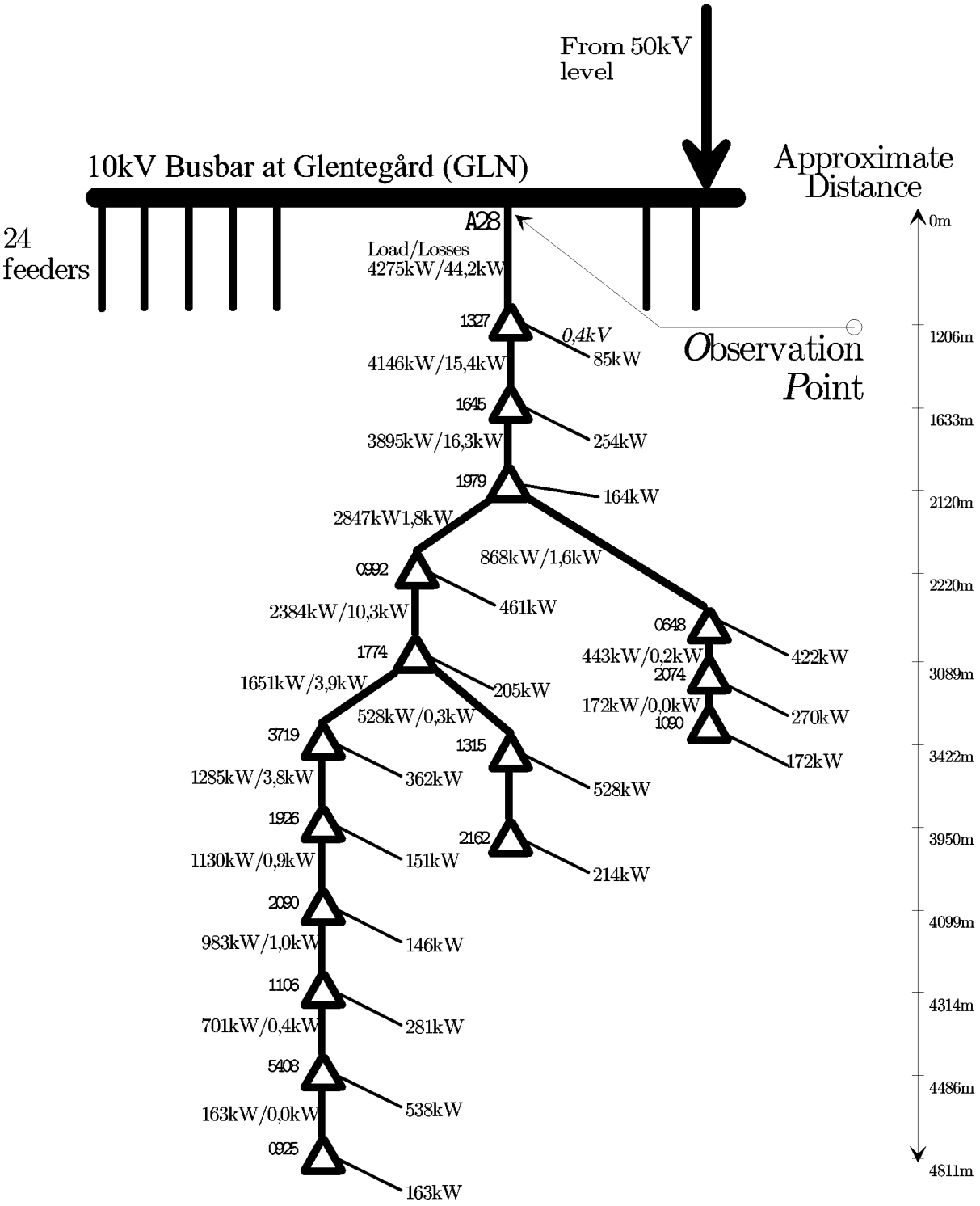

Figure 2.1: Schematic of the Feeder **A28**–SØBORGHAVE with Indication of Nominal Loads and Losses.

In power engineering it is a tradition to describe the network in its steady state condition. Therefore the above mentioned 10kV is a measure of the RMS–value of the fundamental component of the voltage between two phases. Such a measure is less suited for investigations in the context of centralized monitoring, because it levels out local deviations from stationarity. In other words; transients are not taken into account.
In this context transients are very important. Limiting the number of measuring points reduces the available amount of data. Therefore as much information as possible should be squeezed out of the actually available measurements.
Transients describe the "path" the network follows combining the steady states before and after an *event.*

Definition 1 Topology *describes the present network structure. The description is based on information on how the network is configured, i.e. the position of circuit dividers.*
Information on the electrical parameters is known from the network database, i.e. what kind of cable/overhead line is used and where, and where two stretches of cable/overhead line are connected by a joint.
The topology description is a function of time. When changes are made in the network this information must be included so as always to have an updated image of the network.

Definition 2 Event *covers a changing of the topology, but does not cover what caused the change. This means that "event" covers everything from switching on the light in the living room to faults directly on the 10kV cable.*

Definition 3 Detection *is the process of recognizing the occurence of an event.*

After having detected an event the next step will be to *classify* it.

Definition 4 Classification *means to determine the characteristics and the location of the event.*
In order to classify, detailed information is needed on the topology and about the wave forms of the three phase to ground voltages and the three currents.

In the following, unless otherwise stated, "voltage" means phase to ground voltage.
It is believed that suitable models for voltages and currents measured at the *O*bservation *P*oint are as indicated in Equations 2.1 and 2.2.

Definition 5 Observation Point *is the master measuring point of a feeder, as opposed to possible auxiliary measuring points that may be located along the feeder.*

Henceforward the *O*bservation *P*oint will be denoted the *OP*.

$$u_{OP}(t) = \sum_{m=0}^{\infty} \alpha_m(t)\,\cos(m\,\omega_0(t)\,t + \varphi_{voltage,\,m}(t)) + \nu_u(t) \tag{2.1}$$

$$i_{OP}(t) = \sum_{n=0}^{\infty} \beta_n(t)\,\cos(n\,\omega_0(t)\,t + \varphi_{current,\,n}(t)) + \nu_i(t) \tag{2.2}$$

Where $\nu_u(t)$ and $\nu_i(t)$ are band limited Gaussian white noise signals. $\omega_0 = 2\,\pi\,f_0$ denotes the fundamental frequency. $\alpha(t)$ and $\beta(t)$ are discussed in Section 6.1.
An investigation on the network frequency on Sjælland was carried out by NESA in 1978, see [NESA, 1978]. This was the best available material, but as it is believed that the conclusions are still valid today, it was decided to rely on that information.
This reference describes that the frequency normally does not deviate from 50Hz by more than ±0,1Hz. When the frequency exceeds this interval, it is regarded a disturbance.
In the following "measurements" means the vector $\boldsymbol{x}(t)$:

$$\boldsymbol{x}(t) = \begin{pmatrix} \boldsymbol{u}(t) \\ \boldsymbol{i}(t) \end{pmatrix} \tag{2.3}$$

Where the vectors $\boldsymbol{u}(t)$ and $\boldsymbol{i}(t)$ are defined as:

$$\boldsymbol{u}(t) = \begin{pmatrix} u_R(t) \\ u_S(t) \\ u_T(t) \end{pmatrix} \tag{2.4}$$

$$\boldsymbol{i}(t) = \begin{pmatrix} i_R(t) \\ i_S(t) \\ i_T(t) \end{pmatrix} \tag{2.5}$$

R, S and T is the description of the phase order used by NESA. This notation is applied throughout this thesis.
This notation corresponds to "a, b and c" or "1, 2 and 3" as used by other utilities.

It is assumed that the network may be regarded as being linear, thus when an event occurs in the network, the signals will propagate according to the following:

Let: $\boldsymbol{x}_{OP}$ denote the measurements taken at the *OP*.
$\boldsymbol{x}_q$ denote voltages and currents at a node somewhere on the feeder.
T denote the network topology function.
This is a function of time, describing the present topology of the network.
N_q denote the network transfer function from the node r to the *OP*.

Then:

$$\boldsymbol{x}_{OP} = \sum_{q=1}^{Q} N_q\,(T,\, \boldsymbol{x}_q) \tag{2.6}$$

Q denotes the number of nodes on the feeder.

As stated, the term *event* covers, in fact, that a transient has arisen. In order to detect an event, it must be required that the measuring system is capable of capturing transients.

In this context the transients occur somewhere in the network. Each node in the network is connected to the *OP* by a stretch of cable.
Cables behave much like lowpass filters, i.e. though high frequencies were injected at the location of the event, it must be expected that the bandwidth at the *OP* is limited.
To explain the signal transfer capabilities of cables a theoretical study was carried out, see Section 3.1.1. This investigation has substantiated an hypothesis behind the project, that measurements should be taken in at least 10kHz bandwidth.

In the following, unless otherwise specified, "measurements" means high quality measurements, i.e. large dynamic range and large bandwidth.

The electrical system is conceived to work at one frequency; the *fundamental frequency*. All other components are undesired.
Normally, the contents at the fundamental frequency, or the *fundamental component*, is much stronger than the other components. It therefore seems reasonable to consider the total contents in the frequency spectrum as the sum of two parts; the fundamental component and the *residual component*. This terminology will be used throughout this thesis, see also Section 6.4.

The measurements $\boldsymbol{x}(t)$ may thus be written as:

$$\boldsymbol{x}(t) = \boldsymbol{x}_0 + \boldsymbol{z}(t) \tag{2.7}$$

Where $\boldsymbol{z}(t)$ is the residual component.

To associate an event to possible locations in the network, it is possible to define two different distances based on geometrical and electrical concepts respectively:

Definition 6 Equivalent Geometric Distance *is an estimate of the position in the network of the event. The estimation is based on all available topology information and all available information contained in the measurements.*

In Appendix B is discussed a method that is used in a commercially available distance relay for transmission lines. The algorithm translates an *electrical distance* into an estimate of the *Equivalent Geometric Distance.*

Definition 7 Electrical Distance *is a measure in Ω's of the location in the network of an event. E.g. the electrical distance of a short circuit to ground, seen from the OP under the assumption of zero ground impedance, will be the impedance of the line to the fault.*

For a network that branches out or for events that do not have zero impedance, the link between the *electrical distance* and the *equivalent geometric distance* is not trivial, see Section 8.3 and Appendix A.4.

Chapter 3

Modelling

Complementary to full-scale experiments, as described in Chapter 4, is modelling. Neither topic can stand alone. A good model must be verified against the real world, but deeper insight into any system requires models, where different parameters may be changed and the result seen.
As is illustrated in Chapter 4, it may be very cumbersome to prepare for, and to perform experiments on real systems. If one therefore has the need of seeing the result of changing various parameters on a real system, it might become extremely expensive and a very slow process.
The right approach therefore is to find the right balance between experiments on a real world system and experiments on a model.

Because of the size of the electrical system, modelling is a well-known exercise to power engineers. Since the early days of digital computers, complex simulation tools have evolved.
Despite having a very little attractive user interface, the EMTP[1] is still a very strong contender for the title as **the** power engineering simulation tool.
The program was originally in the public domain. Therefore its development was the result of the efforts of people of many different organizations. This has also done that the documentation of the program has suffered much. Until recently one could have a hard time finding proper documentation on certain routines.
In the mid-eighties an attempt to commercialize the EMTP was made by EPRI[2]. This lead to two lines of the EMTP; the EPRI–supported version, still called EMTP, and a version that was still kept in the public domain; the so-called ATP[3].
The last version before this was called `M39`.

The moving spirit behind ATP has been Dr. W. Scott Meyer of the **B**onneville the **P**ower **A**dministration in Oregon, U.S.A.
On the basis of all the old, incomplete documentation on EMTP and the newer, more complete on the routines that have been added to ATP, BPA is slowly working towards a complete ATP/EMTP reference.

Because of the "defacto standard"-status of the EMTP and of the continuing maintenance of ATP and its availability, it was decided that this tool should be used as a corner stone in this project.
Unfortunately it has not been possible to benefit from the revised RULE BOOK. Instead was used the old references.
RULE BOOK, see [LEC, 1992], is EMTP-terminology for *users manual*. Behind the RULE BOOK lies another collection of text, the so-called THEORY BOOK, see [Dommel and others, 1986].
It is on the basis of these two references and the newer material on ATP–extensions that BPA is working.

Over the years other interesting simulation tools have emerged. Among these PSPICE$_{TM}$ is becoming more and more suited for power engineering applications. The software features a very friendly user interface. It lacks, however, some of the "raw"power of ATP. Which is, in fact, the case for most such software. Therefore it is expected that ATP/EMTP for many years still will be in widespread use.

[1] **Electro Magnetic Transients Program.**
[2] **Electrical Power Research Institute.**
[3] **Alternative Transients Program.**

Common to network simulation tools is that they solve partial differential equations as described in Section 3.1.

The growing demand for better interfaces is reflected in an increasing number of papers on the subject, e.g. [Nayak *et al.*, 1995].

Supplementary tools to network simulation tools are also becoming more and more acknowledged. Among the many offers, packages like MATHCAD$_{TM}$ have been able to win the attention of power engineers. This is somewhat understandable, because this software features an extremely friendly user interface.

Of other important tools to do mathematical calculations should be mentioned both MATLAB$_{TM}$ and MATHEMATICA$_{TM}$.

MATLAB was conceived as an efficient general means of matrix calculation. Later versions of the program have featured more and more friendly user interfaces.

MATHEMATICA has won market shares as an important tool to do symbolic calculations.

Throughout this project simulations have been performed using the ATP for PC (DOS), MATLAB and MATHEMATICA for PC (WINDOWS) and whenever the above mentioned tools were insufficient, the solution was arrived at by programming in the C-programming language, using BORLAND's compiler.

3.1 Homogeneous Transmission Lines

Though distribution feeders are not homogeneous, when seen as a whole, they may be divided into parts that are homogeneous cables/overhead lines. The theory of homogeneous transmission lines apply for these parts.

This section renders the theory and concludes by defining the equivalent Π–element. The investigation is restricted to one-phase models.

Let the specific constants of the line be denoted by the terms given in Figure 3.1. These quantities are

R	resistance
L	inductance
G	conductance
C	capacitance

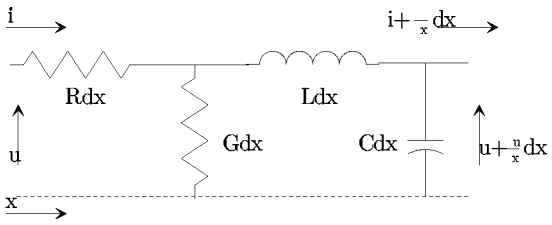

Figure 3.1: Infinitesimal Line.

all per length and per phase.

The corresponding differential equations are:

$$\frac{\partial u}{\partial x}\,dx = -\left(R\,dx\,i + L\,dx\frac{\partial i}{\partial t}\right) \Rightarrow \frac{\partial u}{\partial x} = -\left(R\,i + L\,\frac{\partial i}{\partial t}\right) \tag{3.1}$$

$$\frac{\partial i}{\partial x}\,dx = -\left(C\,dx\frac{\partial u}{\partial t} + G\,dx\,u\right) \Rightarrow \frac{\partial i}{\partial x} = -\left(C\,\frac{\partial u}{\partial t} + G\,u\right) \tag{3.2}$$

Equations 3.1 and 3.2 may be found in [Karlsson and Gjendal, 1986] and [Vørts, 1990]. Neither of the two deals with the solution in the general case, which involves Bessel functions. Instead the effort is restricted to the case, where the excitation is sinusoidal at a fixed frequency.

The general solution, however, might be of interest for deeper insight in the behaviour of transmission lines under transient conditions.

During the solution of the differential equations two quantities, γ; the *propagation coefficient* and Z_0; the *characteristic impedance*, are defined.

$$\gamma = \sqrt{(R + j\,\omega\,L)\,(G + j\,\omega\,C)} = \sqrt{z\,y}, \text{ for } \angle\gamma \in \left[0; \frac{\pi}{2}\right] \tag{3.3}$$

$$Z_0 = \sqrt{\frac{R + j\,\omega\,L}{G + j\,\omega\,C}} = \sqrt{\frac{z}{y}} = \frac{1}{Y_0}, \text{ for } \angle Z_0 \in \left[-\frac{\pi}{4}; \frac{\pi}{4}\right] \tag{3.4}$$

With Z_L denoting the load of the line, the *reflection coefficient* and the *transmission coefficient* may be defined.

$$\rho = \tau - 1 = \frac{Z_L - Z_0}{Z_L + Z_0} \tag{3.5}$$

$$\tau = 2\frac{Z_L}{Z_L + Z_0} \tag{3.6}$$

In the case where the excitation is sinusoidal, Equations 3.1 and 3.2 develop into:

$$\frac{du}{dx} = -(R + j\,\omega\,L)\,i \tag{3.7}$$

$$\frac{di}{dx} = -(G + j\,\omega\,C)\,u \tag{3.8}$$

Differentiation of Equations 3.7 and 3.8 with respect to x gives:

$$\frac{d^2u}{dx^2} = \gamma^2\,u \tag{3.9}$$

$$\frac{d^2i}{dx^2} = \gamma^2\,i \tag{3.10}$$

The solutions to these two differential equations are linear combinations of $e^{\gamma\,x}$ and $e^{-\gamma\,x}$. The solution to Equation 3.10 is: $i = I_1\,e^{\gamma\,x} + I_2\,e^{-\gamma\,x}$. To Equation 3.9 it is: $u = U_1\,e^{\gamma\,x} + U_2\,e^{-\gamma\,x}$.

The values of I_1, I_2, U_1 and U_2 depend on the conditions at the terminals of the line, i.e. the source and load impedances.

Considering the model shown in Figure 3.2 the expressions of Equations 3.11 and 3.12 may be given.

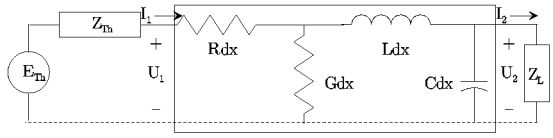

Figure 3.2: Transmission Line with Attached Load and Generator.

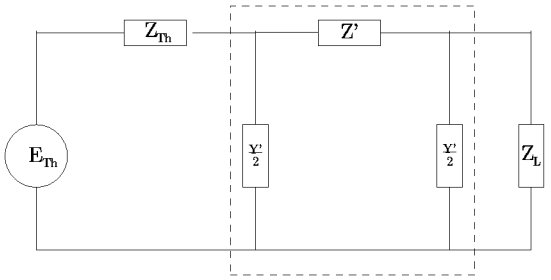

Figure 3.3: Equivalent Π-Element.

$$u(x) = u(0)\,\cosh(\gamma\,x) - Z_0\,i(0)\,\sinh(\gamma\,x) \tag{3.11}$$

$$i(x) = i(0)\,\cosh(\gamma\,x) - Y_0\,u(0)\,\sinh(\gamma\,x) \tag{3.12}$$

Where x denotes the distance and "0" indicates the one terminal of the line.

If only the conditions at the terminals are of interest, as indicated in Figure 3.2, the equivalent, or corrected, equivalent Π-element may be used, Figure 3.3.

In the following l denotes the length of the line.

With $Z = \gamma\,l\sqrt{\frac{z}{y}}$ and $Y = \gamma\,l\sqrt{\frac{y}{z}}$, the connection between input and output is:

$$\begin{pmatrix} U_1 \\ I_1 \end{pmatrix} = \begin{pmatrix} \cosh(\gamma\,l) & Z\,\frac{\sinh(\gamma\,l)}{\gamma\,l} \\ Y\,\frac{\sinh(\gamma\,l)}{\gamma\,l} & \cosh(\gamma\,l) \end{pmatrix} \begin{pmatrix} U_2 \\ I_2 \end{pmatrix} \tag{3.13}$$

$$= \begin{pmatrix} \cosh(\gamma\,l) & \sqrt{\frac{z}{y}}\,\frac{\sinh(\gamma\,l)}{\gamma\,l} \\ \sqrt{\frac{y}{z}}\,\frac{\sinh(\gamma\,l)}{\gamma\,l} & \cosh(\gamma\,l) \end{pmatrix} \begin{pmatrix} U_2 \\ I_2 \end{pmatrix} \tag{3.14}$$

Z' and Y' of Figure 3.3 are found from Z and Y by the following connection:

$$Z' = Z\frac{\sinh(\gamma\, l)}{\gamma\, l} \tag{3.15}$$

$$Y' = Y\frac{\tanh\left(\frac{\gamma\, l}{2}\right)}{\frac{\gamma\, l}{2}} \tag{3.16}$$

As is seen, it is the length of the line that determines whether correction is necessary.
According to [Vørts, 1990] the correction is not necessary for cables shorter than about 125km and overhead lines shorter than about 250km for the fundamental frequency.

3.1.1 Estimation of Transfer Functions on the Basis of the Π-Equivalent

On the basis of the theory, that was rendered in Section 3.1, the transfer functions of a cable and attached load are evaluated as a function of frequency, length of cable and module of load.

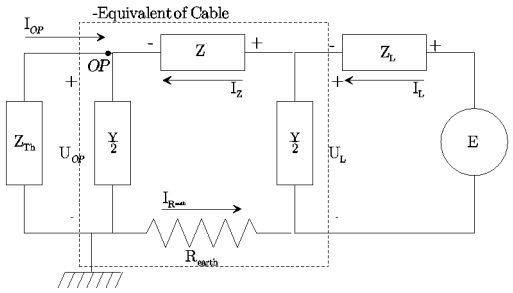

Figure 3.4: Model of Line and Load Used for the Evaluation of Transfer Functions.

In Figure 3.4 is shown the diagram of the model used in this investigation. A resistance has been applied between the legs of the Π–equivalent. This component is a model of the ground resistivity.
The elements of the Π-equivalent are found from [NKT, 1984].
Skin effect is taken into account by using the value of the resistance of the cable as it is at the fundamental frequency, without further correction as the frequency changes.
The proximity effect is neglected.
The cable was chosen to be a 95mm^2 Cu–APB-cable[4]. This type of cable is believed to be a good representative for all the kinds of cable used on **A28**.
For this kind of cable [NKT, 1984] specifies the following, (for an explanation of the symbols, refer to Section 3.1): $R = 0{,}195\frac{\Omega}{\mathrm{km}}$, $X = 0{,}076\frac{\mathrm{V}}{\mathrm{A}}$, $\left(Z(\omega,\, l) = \left(R + j\,\omega\,\frac{X}{2\,\pi\,50}\right)\, l\right)$, and $C = 0{,}36\frac{\mu\mathrm{F}}{\mathrm{km}}$, $(Y(\omega,\, l) = j\,\omega\, l\, C)$. The conductance is believed to be zero. Z_L is discussed in Section 3.2.
The total impedance seen from the generator; E, is:

$$Z_{tot} = Z_L + \left(\frac{Y}{2}\right)^{-1} \left\| \left(Z + Z_{Th} \left\| \left(\frac{Y}{2}\right)^{-1} + R_{earth} \right.\right.\right. \tag{3.17}$$

This leads to determination of I_L and U_L:

$$I_L = \frac{E}{Z_{tot}} \tag{3.18}$$

$$U_L = E - I_L\, Z_L \tag{3.19}$$

By inspection it becomes evident that $I_Z = I_{R_{earth}}$, hence;

$$U_{OP} = U_L - I_Z\, (R_{earth} + Z) \tag{3.20}$$

$$I_Z = I_L - U_L\,\frac{Y}{2} \tag{3.21}$$

[4] APB; **A**luminium, **P**last, **B**ly. *Aluminum, Plastic, Lead.*

Finally we may now determine the current at the *O*bservation *P*oint:

$$I_{OP} = -\frac{U_{OP}}{Z_{Th}} \tag{3.22}$$

In Figure 3.5 is shown the magnitude of the current–current transfer functions under various assumptions. As is seen it affects only very little the transfer function whether or not the ground resistivity is taken into account.

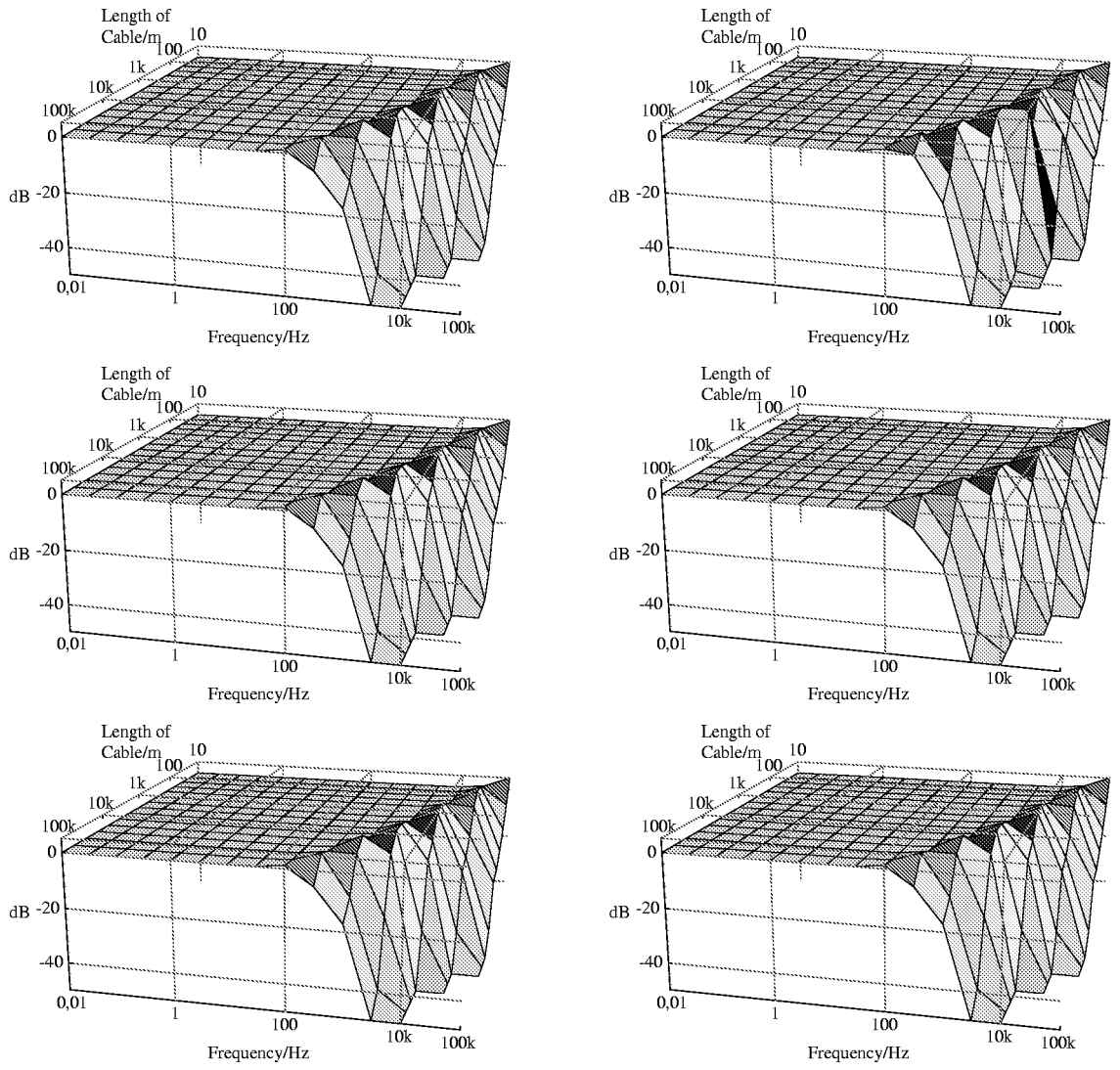

Figure 3.5: ⁘ $|Z_L| = 150\Omega$, $\cos(\varphi) = 0{,}88$. ⁘ $R_{\text{earth}} = 0$. ⁘ $|Z_L| = 150\Omega$, $\cos(\varphi) = 1$. ⁘ $|Z_L| = 150\Omega$, $\cos(\varphi) = 0$. ⁘ $|Z_L| = 10^6\Omega$, $\cos(\varphi) = 0{,}88$. ⁘ $|Z_L| = 10^{-6}\Omega$, $\cos(\varphi) = 0{,}88$.

Figure 3.5 shows that the current transfer function is quite insensitive to changes to parameters such as the ground resistivity, module and argument of the load.
This result corresponds well with the desired functionality of the distribution network; namely that customers experience their supply as a voltage source.
The current transfer "capability" deteriorates as the frequency increases. This is explained by the capacitive coupling to ground. At low frequencies this effect is almost negligible.

Figure 3.6 shows the magnitudes of the other transfer functions. The results are only shown for $|Z_L| = 150\Omega$, $\cos(\varphi) = 0{,}88$ and $R_{earth}(f, l) = 0{,}00099\frac{\Omega}{\text{Hz km}} f l$, this value is according to [Vørts, 1990] and

should be valid in Danmark.

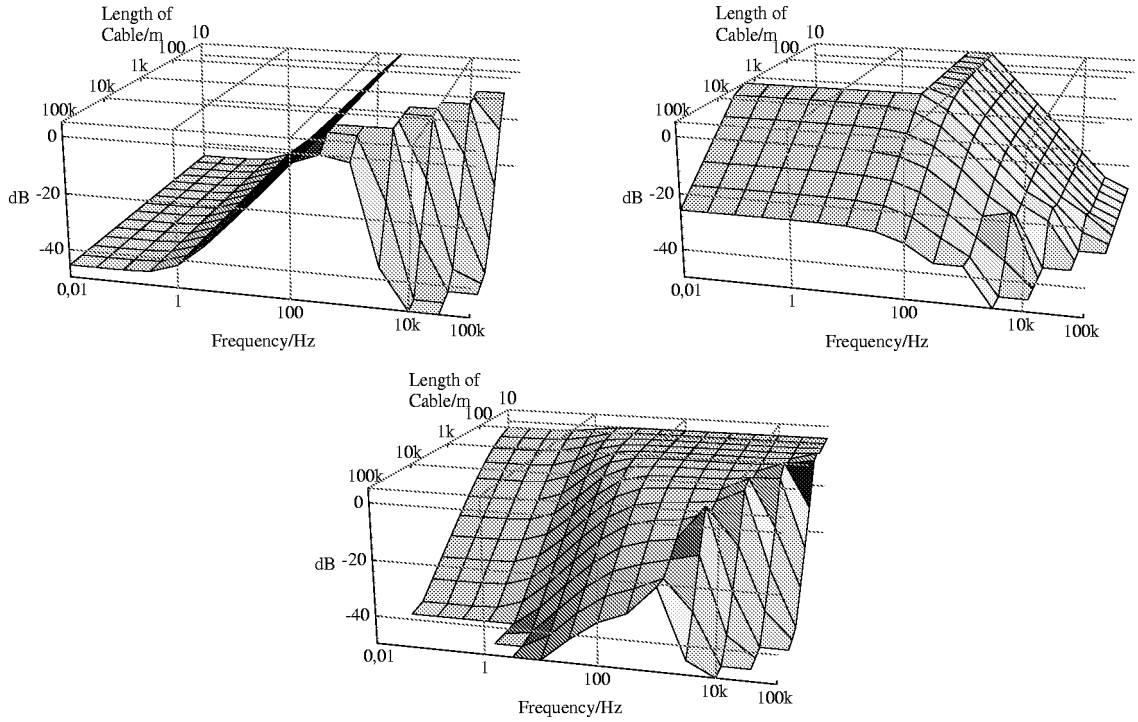

Figure 3.6: Magnitude of Transfer Functions: Current–Voltage. Voltage–Current. Voltage–Voltage.

The voltage transfer function for cables longer than some hundred meters, as expected, has quite strong attenuation at frequencies around the fundamental frequency.

The investigation thus far has been based on the assumption that the short circuit impedance at the *O*bservation *P*oint is linear and may be derived from the 50Hz value; $Z_{th} = 0{,}3\Omega\angle 89°$.
Figures 3.7–3.12, pages 16–18 show experiments with different Z_{th}. The ground resistivity and Z_L are kept unchanged.
For all the figures in the following go that on each plot is shown: Current–Current. Current–Voltage Voltage–Current. Voltage–Voltage .

The frequency and distance sensitivity of the current transfer function is seen to depend very little of the short circuit impedance. Whereas the voltage transfer function depends heavily on this impedance. This is also as should be expected, since a value of this impedance which is close to that of the load corresponds to impedance matching.

3.2 Load Modelling

When seeing how load modelling often is treated in the literature, one gets the impression that this is a neglected area of research. There are a number of reasons to this! First of all; load modelling is a very difficult task that normally requires much à-priori knowledge about the load to be modelled. Very often such information is not accessible, [Williams *et al.*, 1993].
On the other hand must be realized that for many applications, only a very "rough" model may be perfectly satisfactory.
One kind of "average load model" is the *aggregate load model.* This model is widely accepted as a good approximation, when only sparse information is available on the load(s) to be modelled. **The** model is not believed to exist. One will always have to make compromises.

There are basically two types of loads to be considered:

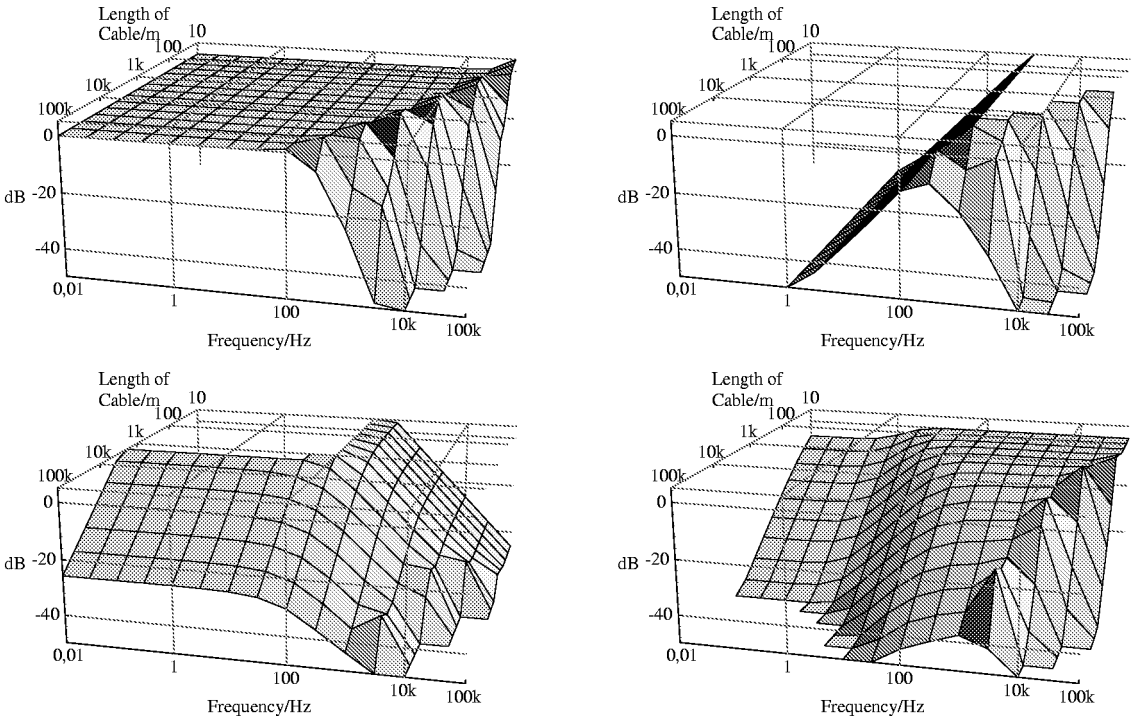

Figure 3.7: Magnitude of Transfer Functions, $Z_{th} = 0{,}3\Omega\angle 89°$.

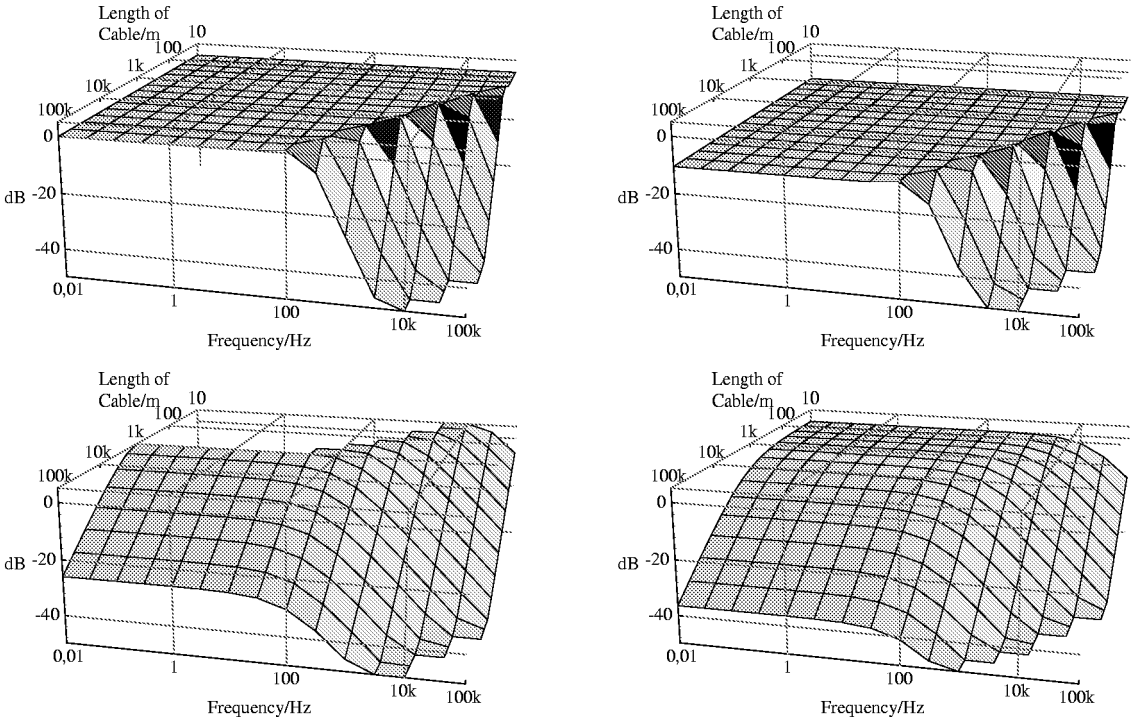

Figure 3.8: Magnitude of Transfer Functions, $Z_{th} = 0{,}3\Omega\angle 0°$.

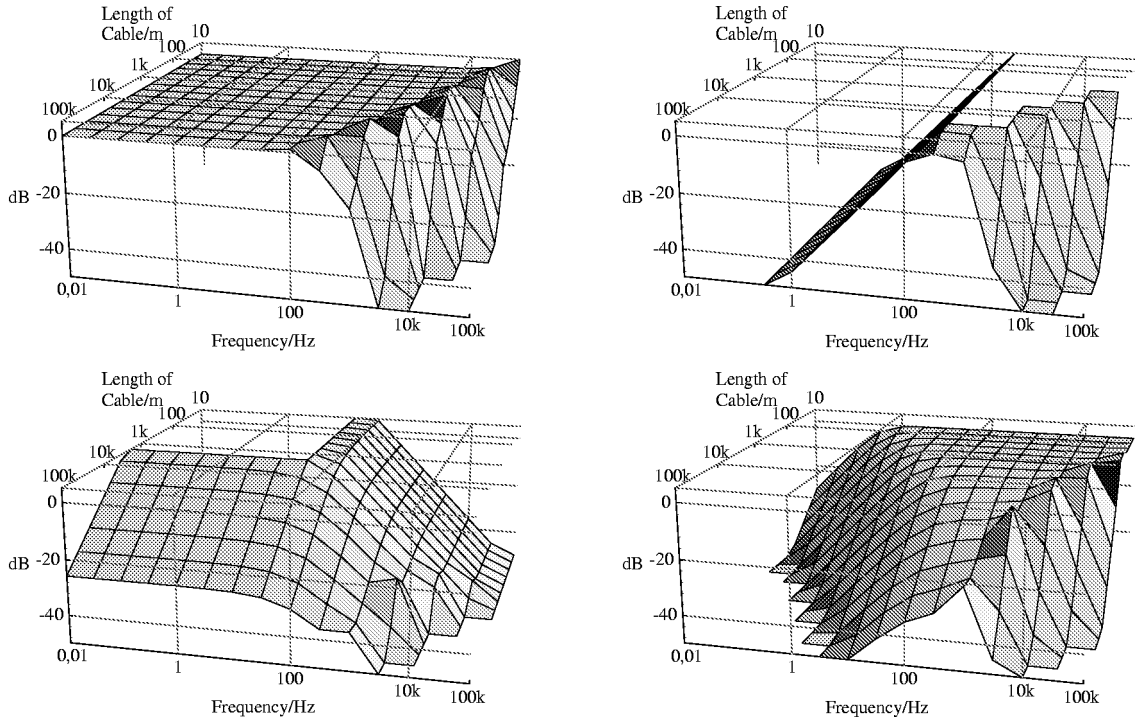

Figure 3.9: Magnitude of Transfer Functions, $Z_{th} = 0{,}3\Omega\angle 90°$.

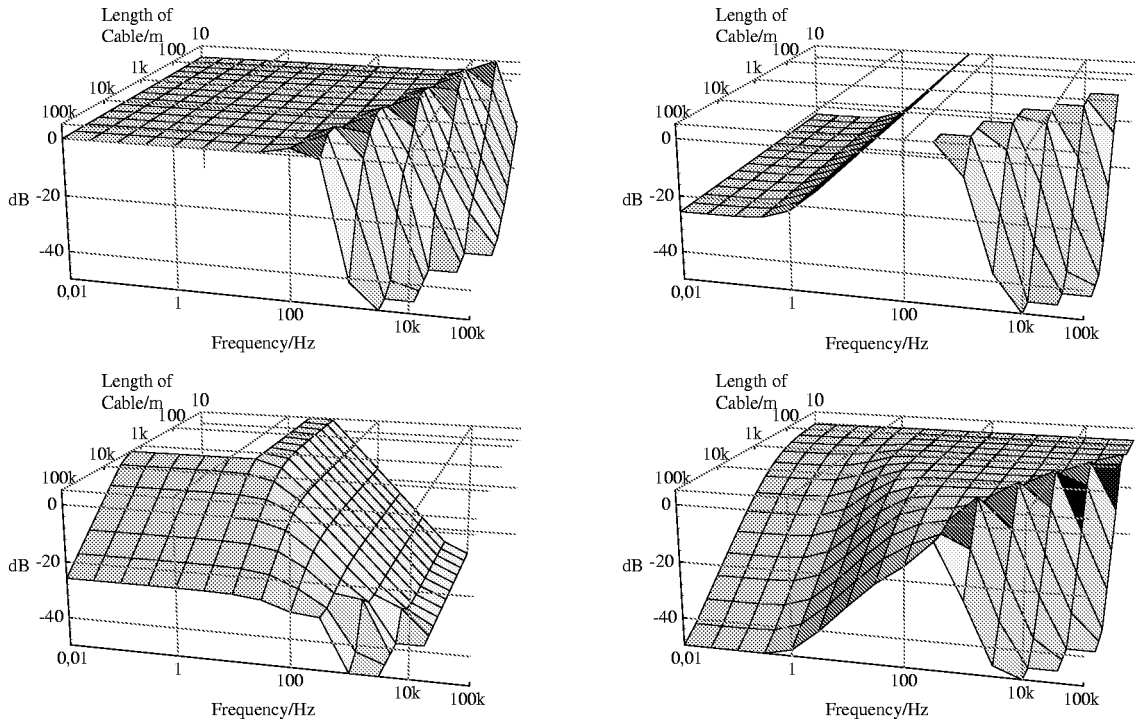

Figure 3.10: Magnitude of Transfer Functions, $Z_{th} = 3{,}0\Omega\angle 89°$.

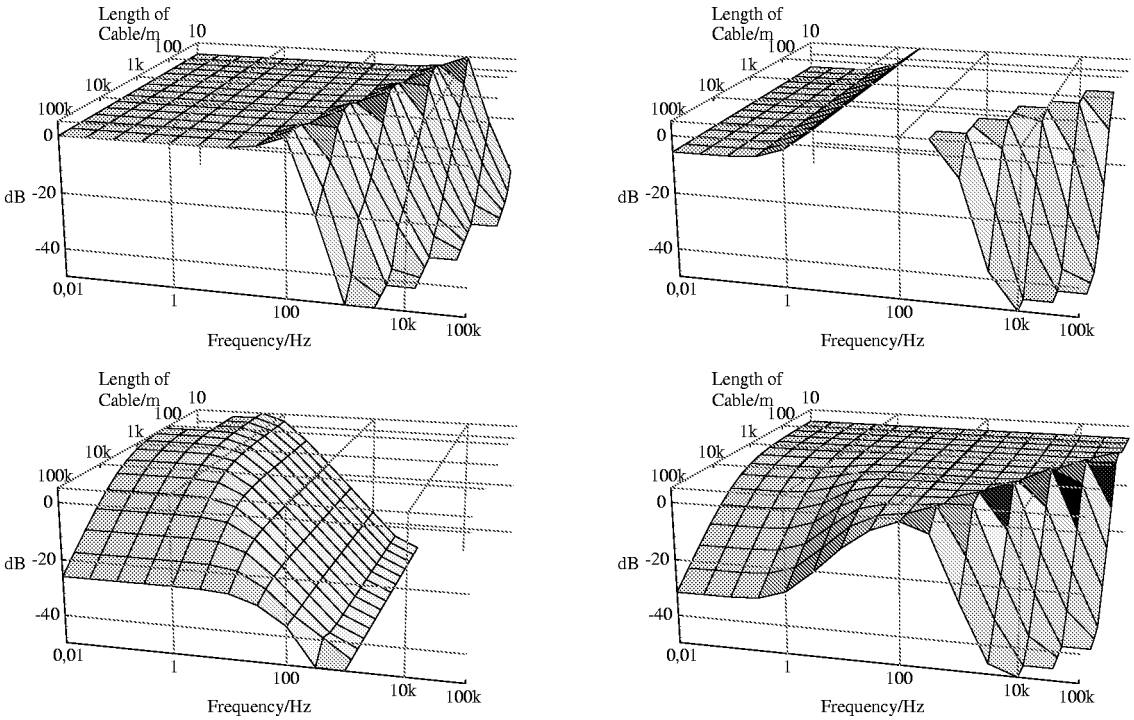

Figure 3.11: Magnitude of Transfer Functions, $Z_{th} = 30{,}0\Omega\angle 89°$.

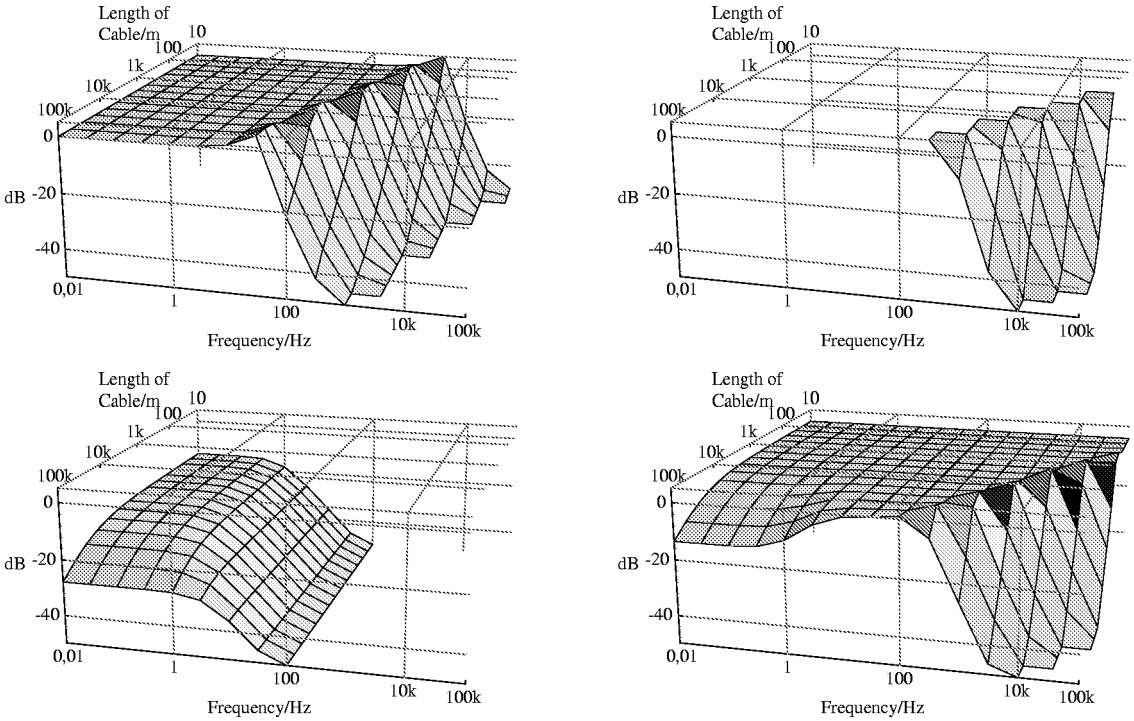

Figure 3.12: Magnitude of Transfer Functions, $Z_{th} = 300{,}0\Omega\angle 89°$.

Definition 8 Static Loads *are loads that exhibit stationarity in the mathematical sense. They may be both linear, non–linear, passive or active, but they do not give rise to transients, except at the moment they are connected to the simulation model or the simulation is initiated.*

Static loads also comprises rotating machinery that is running at a constant speed, with constant torque.

Definition 9 Dynamic Loads *covers all other cases than the ones that fit into Definition 8.*

Dynamic loads will cover the cases where the load changes its nature, e.g. the cases where a switch is operated internally in the load model.

With the above definitions it is seen that most models will fit into the group of static loads. This kind of model is adequate when one wants to investigate one particular load and its interaction with the network. However, the ensemble load of an entire feeder is only adequately modelled by a static load model over short periods of time.

The modelling that is described in this chapter has been carried out to gain insight in how the distribution network acts as a conductor of signals, i.e. how events are transmitted to the *OP*, see Figure 2.1. For this much may be learned without taking a stand on a specific choice of load model.

Power engineers talk about "cos(φ)" when they describe e.g. the nature of the load. It is easiest to make a load that exhibit a given value of cos(φ) as a series combination of a resistor and either a capacitor or an inductance.
This kind of load model was deemed adequate for the initial investigations on the signal transferring capabilities of distribution networks and their fundamental component; cables. See discussion in Section 3.2.2.
It must, however, be expected that for purposes of e.g. fine-tuning of the classification system, "accurate" models of specific loads will be needed, i.e. dynamic models that account for the behaviour of the load; turning on and off.
Such a model should be based on statistics on the load. How often is it operated. How does the consumption change with time..., see e.g. [Bergeal and Moller, 1981] and [Bergeal and Moller, 1982].

An aggregate load model will be helpful for the modelling of the state of the feeder at different times of the day. In parallel to this model is connected the model of the specific load, one wants to investigate. [Ribeiro, 1985] gives a presentation of different models and discusses their applicability.

3.2.1 Description of the Aggregate Load Model

Normally loads are described by their active and reactive powers, P and Q. This, however, is not adequate in case the load or part of it is a rotating machine, because the active power absorbed by a such does not correspond to the damping value.
According to [Ribeiro, 1985, Section 3.5.1.1] the following estimates of R and L of Figure 3.13 are valid.

$$R = \frac{V^2}{P(1-(K+K_E))} \tag{3.23}$$

$$L = \frac{V^2}{1{,}2\,K\,K_1\,P\,\omega} \tag{3.24}$$

A good approximation to Equation 3.24 is said to be $L = \frac{V^2}{5\,K\,P\,\omega}$.

3.2.2 Connection Between Series Connection and Parallel Connection of Components

Let a load impedance be described by its value at the fundamental frequency, e.g. $Z_L = 150\Omega$, $\cos(\varphi) = 0{,}88$. Under the assumption of linearity and no frequency dependence, this may be translated into a series combination of a resistor and either a capacitor or an inductance; $Z_L = 150\Omega \left(0{,}88 \pm j\,\frac{\omega}{2\,\pi\,50}\sqrt{1-0{,}88^2}\right)$
Normally the load will be inductive, hence the imaginary part will be positive.

P	is the total active power demand.
K	is the motor fraction of the total active power demand.
K_E	is the electronically controlled load fraction of the total active power demand.
K_1	is the severity of starting condition.
V	is the voltage.

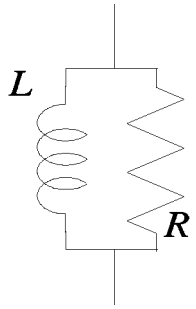

Figure 3.13: Aggregate Load Model.

If one instead wants to translate into a parallel combination of a resistor and an inductance, one gets a somewhat more complicated expression.
Let X denote the imaginary part of the impedance at the fundamental frequency, then it is desired to determine R' and X' of Equation 3.25:

$$R + j\,X \quad = \quad R' \| j\,X' = \frac{j\,R'\,X'}{R' + j\,X'} \tag{3.25}$$

Finding the solution leads to:

$$R' \quad = \quad \frac{X^2}{R} + R \tag{3.26}$$

$$X' \quad = \quad \frac{R^2}{X} + X \tag{3.27}$$

It is important to notice that either interpretation only is valid at the fundamental frequency and that, as the frequency moves away from the fundamental value, the two interpretations behave much differently.

3.3 ATP–Model of Distribution Feeder

A major effort was made to implement in the ATP a model of `A28`.
This was decided in order to have a "living room size" version of the feeder on which experiments could be performed, e.g. determination of transfer functions.

The model was also intended to be used to verify the hypothesis that the mere electrical difference between the stretches of cable that connect two nodes to the substation, where identical events occur, should be sufficient to distinguish between the two, see Section 3.3.4.1.

In Appendix G is shown the listings of some of the files making up the entire model. The line numbers are not part of the files.

3.3.1 Cable Modelling

Having chosen ATP as a tool led to the need of making compromises on how to model central parts of the entire feeder.
Today, however strange it may sound, the ATP completely lacks routines for the implementation of frequency dependent cable transmission lines.
ATP gives the user the choice of a couple of representations of the line, [Dommel and others, 1986, Chapter 5], e.g:

- Mutually coupled R, L and C elements.
- Cascaded Π.
  - Homogeneous Π-circuit modelling.

– Discrete Π-circuit modelling.

All cable stretches therefore were implemented using several mutually coupled Π–equivalents.
Each stretch of cable was modelled by cascading a number of Π–equivalents each having the same length that was chosen as closely as possible to 100m.
The Π–equivalents were calculated using the so-called **CABLE CONSTANTS**–routine. According to [Rasmussen, 1984] models calculated this way closely correspond to measured values for frequencies between 50Hz and 5kHz.
It is therefore believed that not being able to use a real frequency dependent model is not too hampering for the applicability of ATP.

The cable sections between each transformer station, see Figure 2.1 on page 6, are made up of different types of cable. Information is available on what kind of cable is used and where.
NESA also maintains a data base with detailed information on where two kinds of cable are connected. This information is important because many faults in the 10kV network occur at these joints.

To reduce the complexity of the entire model it was decided to model the stretch between two transformer stations as one cable. The model was chosen to represent the "typical" kind of cable of that section.

3.3.2 Driving Source Modelling

Driving Source actually means the ensemble overlying network inclusive the transformer that supplies the busbar at GLENTEGÅRD.

For simplicity it was decided that the overlying network should be modelled by its Thevenin equivalent. As Thevenin impedance was chosen the short-circuit impedance of the 10kV system at GLENTEGÅRD; $0{,}3\Omega\angle 89°$. This value is valid at 50Hz. It was assumed that the Thevenin impedance could be properly modelled by a linear impedance that at 50Hz attained the above value.

The other 23 feeders connected to the busbar were modelled by the input capacitance of the Π–equivalent.

The distribution network in NESA's area of operation is Petersen Coil grounded.
The coil is at GLENTEGÅRD connected to ground from the star point of the ΔY–coupled 10kV/0,4kV transformer that supplies the substation itself.
This model was implemented by Mr. Harald Wehrend, see page 107, and was kindly made available.

3.3.3 Modelling of Loads

This problem needs much attention, as explained in Section 3.2. Here is only described the fundamental implementation of loads.

Normally one would be interested in investigations that only involve conditions at the busbar and a few transformer stations on the feeder.
All transformer stations have linear loads (in most cases resistors) that correspond to the nominal load, see Figure 2.1.

A model of a 10kV/0,4kV distribution transformer was created, so events could be simulated that occur on the secondary side between phase and 0.
This model was derived from Mr. Wehrend's ΔY–model, using the **BCTRAN**–routine.

3.3.4 Experiments with the ATP–Model

Two important sets of experiments were performed using the ATP–Model, namely:

1. Investigations on the influence of cables on the phase of the current.

2. Investigations on the transfer functions from nodes on the feeder to the substation.

3.3.4.1 Phase Difference Due to Different Cables

With all nodes, except two, loaded with resistors corresponding to nominal consumption, it was investigated how the currents during an event are influenced by where in the network it occurs.

Two nodes far from the *OP* and on different branches of the feeder were selected.
The two nodes were **1090** and **5408**, see Figure 2.1 on page 6. Through the model of the distribution transformer they were both loaded by resistors between phases and 0, so that in steady state the consumption attained the nominal value of the node.

At different instants during the simulation an impedance of $(0{,}2974 + j\,0{,}0477)\Omega$ was connected and disconnected between phase R and zero first at node **5408** and then at node **1090**.

The currents and voltages at the *OP* were run through a two-state Kalman filter, see Section 6.5.

In Figure 3.14 is seen the Kalman filter estimates of the amplitudes and phases. As is seen, the amplitude level appears to be about the same during the two events.
A small difference of the phase may be noticed. A closer look reveals that the difference is about $0{,}8\text{rad} = 5°$.

This result is very encouraging, because it indicates that exact knowledge about what kind of cable is used and where may be exploited during the process of classification.

3.3.4.2 Transfer Function from a Node to the Substation, Calculated using ATP

By use of the model, current and voltage transfer functions from one node (**5408**) to the substation have been estimated.
The node corresponds to a transformer supplying a paint factory. This customer is the only one being supplied from this transformer. Heavy machinery is installed, e.g. 90kW motors.
From this point in the simulation network the transfer function to the busbar was estimated.
All other nodes in the network were loaded by resistors giving nominal consumption.

The EMTP–routine **FREQUENCY SCAN** was used.
This function only gives out node voltages. If one wishes branch voltages or currents, the introduction of measuring "transformers" is necessary. This makes it quite awkward to estimate the current transfer function.
For the curves shown in Figures 3.15 and 3.16 small resistances were placed in the network and the node voltages at each end were stored.
Because of the small voltage difference, problems with the numerical precision were encountered.

3.4 Comparison of Results from the Two Models

The two models used in the previous have some similarities but are still very different. They are both based on a Π–equivalent. The first model only used one section. The second used several cascaded Π–elements which furthermore were coupled between phases.
The ATP–model therefore is of much higher order than the simple one-section model.

These two methods of modelling should be used differently. The first model, being small, is suited for quickly gaining insight into the impact of various parameters, whereas the second model, being more complex, is suited for verifying certain cases simulated with the small model.
Seeing the impact of changing parameters is a much longer process with the ATP–model.

The results from the two investigations show the same principle: Currents are transferred to the substation almost without attenuation at frequencies into the lower tens of kiloHertz range.
In either case is also shown that the voltage at the substation is very insensitive to changes in the network. This is as expected, since the utilities make a big effort on making the network as "stiff" as possible.

In Chapter 4 is described the experiments that were made on a feeder in operation. This chapter also describes the selection of sensors.
High quality measuring equipment was chosen for both currents and voltages. It may, however, seem as

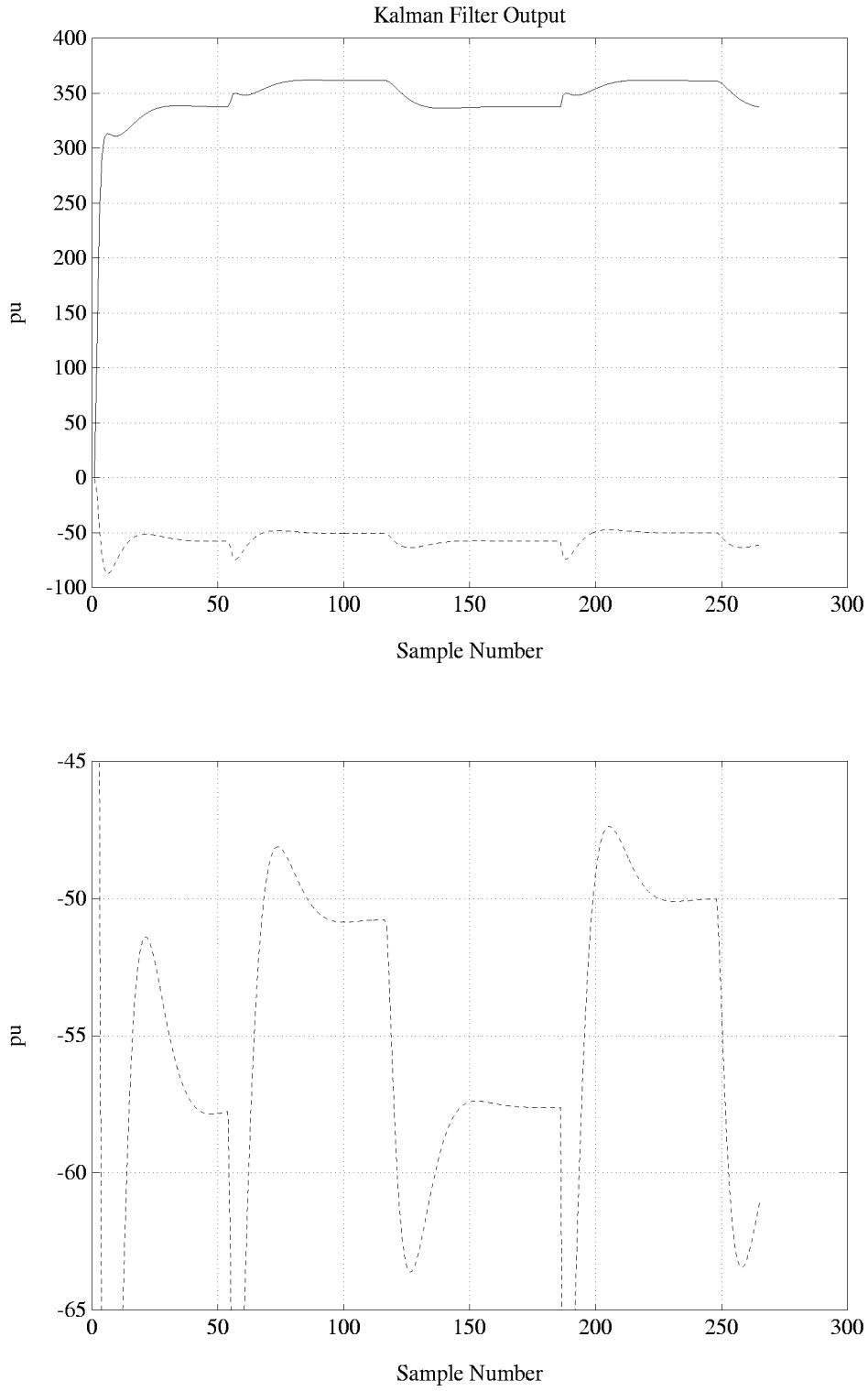

Figure 3.14: Kalman Filter Output. Solid curve; estimate of peak value of amplitude. Dashed curve; estimate of phase.

if it could be justified to measure currents and voltages in different quality. This is further discussed in Chapter 8.

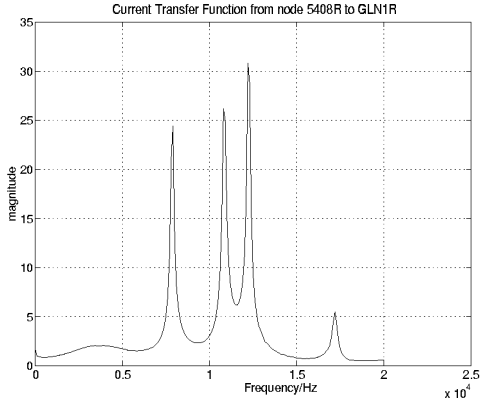

Figure 3.15: Magnitude of Current Transfer Function from Node **5408** to the Same Phase at **GLN1**.

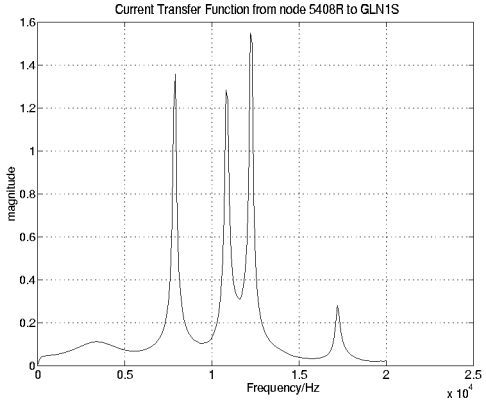

Figure 3.16: Magnitude of Current Transfer Function from Node **5408** to Another Phase at **GLN1**.

When the project was initiated it was expected that the ATP would be used extensively, as indicated in [Nielsen *et al.*, 1993]. Therefore was also taken the time to create this quite complete model of the feeder used for experiments.
Looking back it must be concluded that the ATP played a far more inferior role than originally expected. The reason for this is first of all that it is very cumbersome to implement and run a model in the ATP. Therefore one is less motivated to use this tool for the verification of smaller problems.
In the case of large systems with many nodes ATP really shows its justification. Some models may only be implemented in other tools with great effort. Some components of power systems, such as rotating machines, may be fairly easily implemented in ATP, whereas in other tools this will be enormously complicated.

The conclusion is that the use of ATP must continue for many years still, because of its many specialized features for power engineering applications.
But it is also clear that the users demand more friendly software. More and more often is seen in the literature references to both ATP/EMTP and at the same time software like MATLAB. This is taken as a clear indication of the needs for complementary software to ease simulation of power systems.

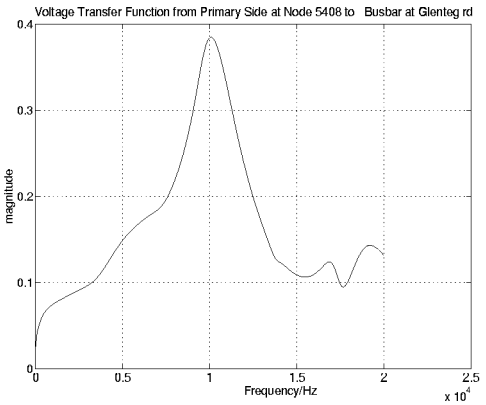

Figure 3.17: Magnitude of Voltage Transfer Function from Node **5408** to the Same Phase at **GLN1**.

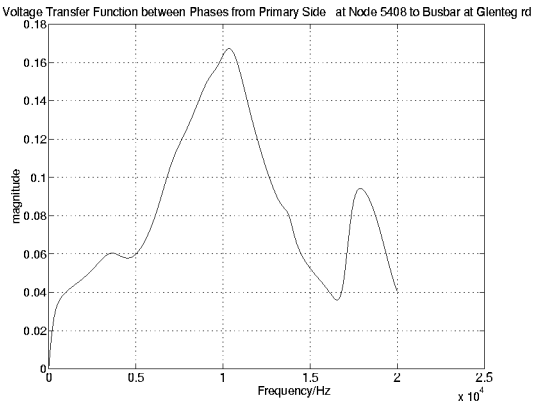

Figure 3.18: Magnitude of Voltage Transfer Function from Node **5408** to Another Phase at **GLN1**.

Chapter 4

Experiments on Feeder in Operation

The experimental part of this work has been very important. Early in the project was searched for records that describe how known events propagate through the network and on how the high frequency contents of voltages and currents of distribution networks may be used in the context of monitoring. Very little evidence was found. Therefore, a series of experiments were carried out in order to become familiar with signals of distribution networks and the signal transfer capabilities of these.

The experimental activity has progressed through three stages, starting by Stage 0, which was performed so as to get acquainted with the signals at the *OP* of **A28**.
This section gives a description of the stages one by one. The analysis of the measurements is described in Chapter 7.

4.1 Stage 0 Measurements

These measurements were taken on the 9^{th} and 10^{th} of February 1993.

As stated, the measurements were nothing but advisory measurements, that were taken in order to get to know the signals one may encounter at the *OP*.

The measurements were taken using equipment readily available in order not to spend money on equipment, for which the required specifications were unknown, and also to get measurements quickly.

As sensors were used the magnetic current and voltage sensors that were already installed, and used to monitor the RMS–values of the current into the feeder and the busbar voltage.

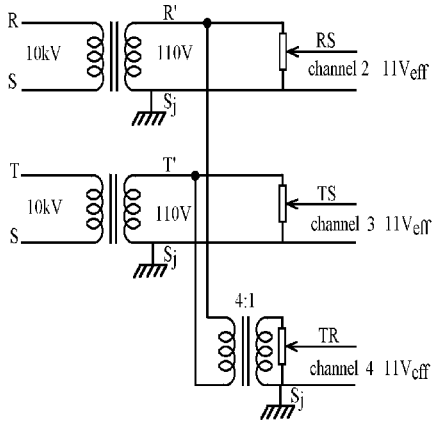

Figure 4.1: Creation of Phase TR Voltage for Stage 0 Measurements.

Limited bandwidth had to be accepted, because magnetic sensors are not believed to have a bandwidth much higher than about 1kHz.

On top of this had to be accepted that voltages could only be measured phase to phase between phase S and R and between phase S and T. The phase $T - R$ voltage had to be created using an auxiliary transformer, thus introducing yet another component with low bandwidth, see Figure 4.1.
Only being capable of measuring phase to phase voltages means that the 0–sequence system has been destroyed, see Section 6.5.3.

The measurements were stored directly at the *OP* using an analog seven track tape recorder.
On the first channel was recorded a white noise signal. On the other six were recorded the measurements.

In all were recorded four sequences of each 15min. These four sequences should supposedly cover the extremities of the operating conditions of the network.

The first sequence was taken at 10:30, when industry works at peak level.

The second sequence was taken at 19:55. At this hour a capacitor bank at 50kV level was disconnected.

The third sequence was taken at 4:20. This is about the time of the day where the activity is at its lowest.

The fourth sequence was taken at 7:20. At this hour industry starts working. Therefore many transients should be expected to occur.

Because only a two channel A/D–converter was available the six signal channels had to be converted one by one, using the second channel of the A/D–converter to convert the noise signal.
The idea was to calculate the cross correlation between the noise of two conversions to find the offset between the two. One channel was used as reference and the others were adjusted according to this channel.
This method gave fine synchronization at the beginning of the sequences. But, alas, the tape recorder did not run every time with exactly the same speed, therefore towards the end of a sequence was experienced that the six signals were completely out of synchronization.

Another problem also became apparent; there was no control over the transfer function of the entire signal acquisition chain, hence there was no clue about what the amplitude levels had been at the time of the recordings.

Due to the above mentioned problems, these measurements have mainly been used to get an idea about relative signal levels and contents of lower frequencies; below 1kHz.

4.2 Stage 1 Measurements

These measurements were taken on the 27^{th} of January 1994.

As opposed to the Stage 0 Measurements these measurements were real experiments.

At the *OP* the currents were measured using the same current sensors as during the Stage 0 Measurements. But because the already installed voltage sensors give a very incomplete measurement of the three voltages, it was decided to install new voltage sensors. Still the constraint was to use equipment already at hand. Therefore magnetic voltage sensors, that NESA had in stock, were installed between phases and ground.

To be able to excite the feeder by really significant events, the largest customer was found.
This customer is described in Chapter 2. Contact was made and access was granted, so that machinery could be operated on request at known instants.
The responsible person from the factory assigned two larger asynchronous motors; a 75kW and a 90kW, that could be turned on and off.

An auxiliary measuring point was established at the transformer **5408**. Here currents were measured on the primary side (10kV) using clamp-on transformers with a specified bandwidth of 5kHz.
Due to safety requirements voltages had to be measured on the secondary side (0,4kV) between phase and 0.

At both the *OP* and at **5408** the exact same type of tape recorder was used.
This time the seventh channel was used to record a signal that contained the absolute time.

During a period of 25min the above-mentioned two machines were in turn turned on and off several times, while the two tape recorders were recording.

A/D–conversion was made as for the Stage 0 Measurements. This time synchronization was made at all samples throughout the sequence using the clock signal as reference, hence no complete loss of synchronization is experienced towards the end of the sequences, see also page 64.

4.3 Stage 2 Measurements

These measurements were taken on the 23rd of November 1994.

The planning of these measurements started along with the planning of the Stage 1 Measurements. From the Stage 0 measurements it was already obvious that the equipment that was used was not good enough. Therefore it was decided to take the Stage 1 Measurements in order to get to know whether in the measurements one could re-find traces of the known events. If detection of such significant events as turning on and off those big machines would not be possible, creation of a measuring point for high quality measurements would be a meaningless waste of time as well as money. Luckily enough it turned out, that the events were so significant that the measurements from the auxiliary measuring point at node **5408** were not needed to find the events in the signals taken at the *OP*.
Having established this, work could proceed on defining the requirements to the equipment to be used at the *OP* of the real system.

At this stage it had been established that both the sensors and the tape recorder used to store the measurements during the Stage 0 and 1 Measurements were inadequate for high quality measurements.

4.3.1 Sensors

The sensors require the utmost attention. Since no chain is stronger than its weakest link, the signal acquisition chain will not be better than the sensors.
The A/D–card may be chosen with high resolution, (16bit), and will therefore not contribute much noise, if the dynamic range is properly used, see Section 4.3.2.
The anti-aliasing filters are basically passive, and should therefore neither distort the signal nor contribute noise, see Section 4.3.2.1 and Appendix C.

Choosing commercially available sensors is not an easy task. The reasons for this are several:

- 10kV is dangerous and many safety regulations apply.
- Distribution utilities have until now taken almost no measurements in their distribution networks (6kV – 15kV. NESA: 10kV).
- The measurements that are taken, in NESA's area of operation, are limited to the busbar voltage at the substation and the currents into each feeder.
- Until today the opinion has been that in AC-systems, for metering purposes, only the fundamental frequency is of importance.

These facts do that the supply of high voltage broad band sensors is limited.
The most readily available sensors are iron core based. Such sensors have only a very low bandwidth, at the best a few kiloHertz.
For the purposes in this project the desired bandwidth is at least 10kHz. This out rules iron core based sensors and therefore also the sensors that are already in place at NESA's 10kV substations.

In recent years much attention has been paid to optically based sensors, (Faraday Effect). Especially optical current sensors show promise.
Optical voltage sensors have also been described in the literature.

Today optical current sensors are commercially available and have the potential of becoming a low priced alternative to the inductive sensors which are widely in use. They also have the potential of having a large dynamic range and a very wide bandwidth. Finally they can be made very small and may thus fit into the little room there is in distribution transformer units, that are placed along a distribution feeder.

Though other alternatives are available, such as Rugowski coils, it was decided that high quality measurements of currents were to be taken with an optical current sensor.
NESA has been involved in the development of an optical current transducer unit that should be small enough to be used in 10kV installations. It was decided that this unit should also be used in this project. The unit, however, needed some significant modifications before it was suitable for the purposes of the project, see Section 4.3.1.2.

To measure voltages was chosen high voltage oscilloscope probes. This was mainly done because such ones were available at a reasonable price (DKK8.500 in 1994). At the same time these probes have a bandwidth which is many times higher than requested. See Section 4.3.1.1.

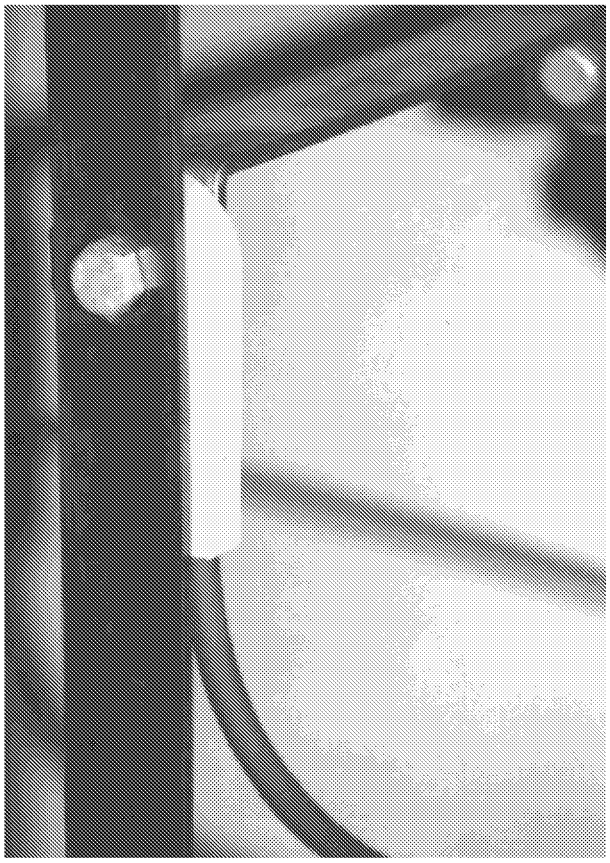

Figure 4.2: Optical Transducer Unit.

4.3.1.1 Voltage Sensor

The voltages are measured using oscilloscope probes from Tektronix. Details on the probes are given in [Tektronix, 1993]. They are believed to be linear in the frequency band of interest; < 10kHz. The voltage level is well below what is indicated as being the maximum for the probe. This, combined with the fact that the probes are passive, substantiates that no signal distortion arises from these.

The manufacturer specifies a maximum input voltage of 20kV (DC + AC). The output is a thousand times smaller.
At frequencies above 460kHz the maximum input voltage derates to 1,3kV at 100MHz.
Analysis of the voltage measurements have shown that besides the phase-to-ground voltage at 50Hz,

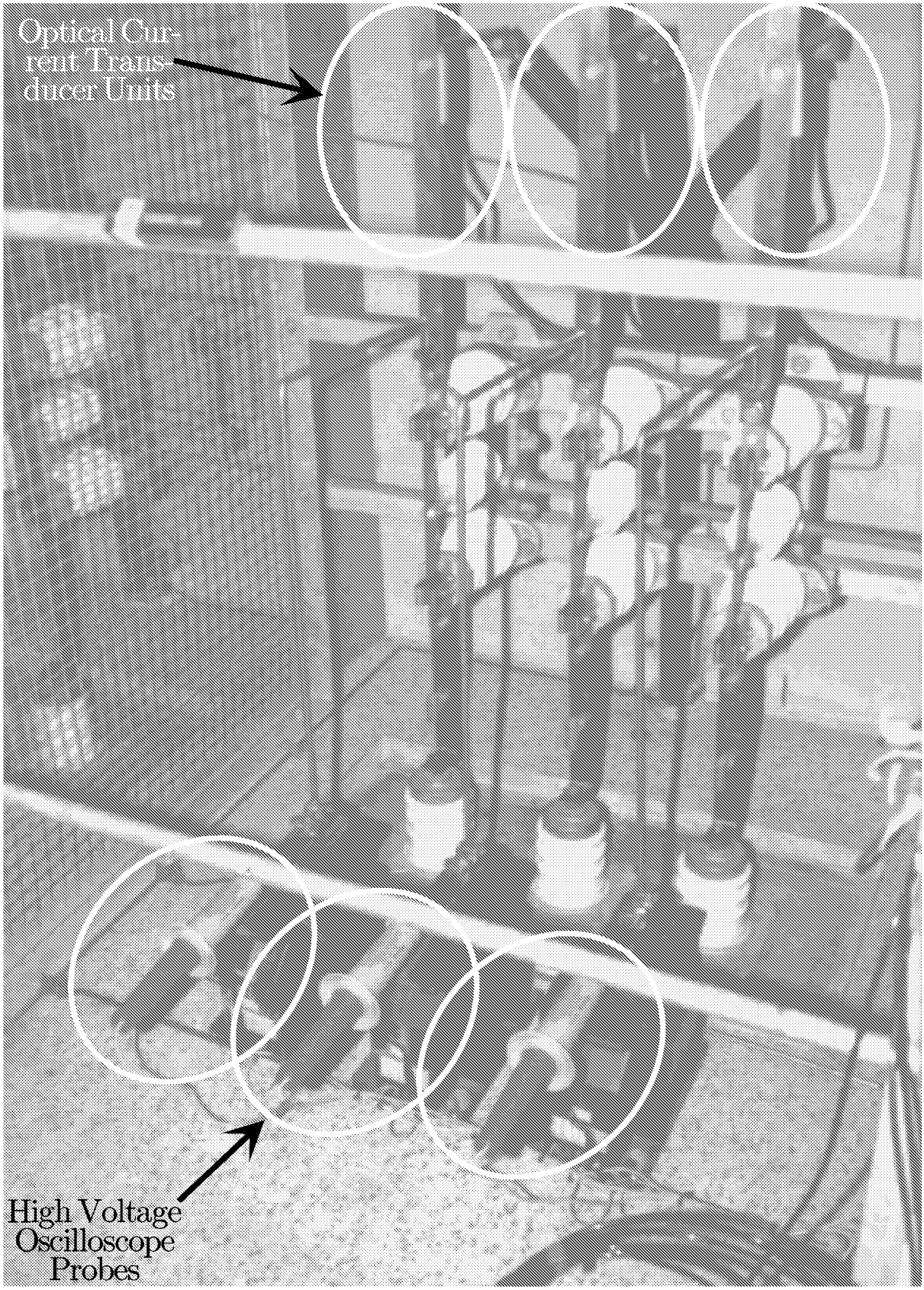

Figure 4.3: Installation of Sensors.

which is $8{,}5\text{kV}_{\text{peak}}$, the highest harmonic, which is the fifth, attains about $200\text{V}_{\text{peak}}$.
The 3dB bandwidth of the probe is specified to 75MHz.

4.3.1.2 Current Sensor

The optical current sensor consists of two components:

1. The *Optical Transducer Unit*, that is installed into the 10kV electrical circuit, is seen in Figure 4.2.

   This part was left unchanged, despite that the optical fiber is wound around a piece of metal which is of the same kind as used in transformers. Therefore the impact of this metal is an open question. It was believed that the unit was "good enough". But for future usage, it is considered necessary to analyse properly this part of the sensor.

2. An amplifier that converts the light into a voltage.
   This part of the sensor was completely redesigned.

The amplifier of the optical current sensor had to be completely changed in order to fulfil the requirements. This work was carried out by associate professor at the ELECTRONICS INSTITUTE, Mr. Allan Grukov.

The original amplifier was merely conceived for measurements of the 50Hz component, thus not much attention had been paid to higher frequency components.
With the amplifier tuned for measuring up to about 600A_{RMS}, the noise level attained about 3A_{RMS} for most of the frequency spectrum. The noise, however, was not white, but exhibited a complex amplitude characteristic.

Mr. Grukov has designed an amplifier of which the noise level attains only about $150\text{mA}_{\text{RMS}}$, when tuned to measure 200A_{RMS}.

4.3.2 Conversion and Storage of Measurements

The analysis of the measurements will be done simultaneously in all six channels. Conclusions on the ensemble analysis will be made. Therefore it is important that as few errors as possible are introduced during signal acquisition.
Instead of first storing the measurements on an analog tape recorder and subsequently convert from tape into digital format, the measurements were A/D–converted directly at the *OP*, using a multi-channel A/D–card for PC.
When choosing such a card there are two possibilities; either the channels are sampled and converted one

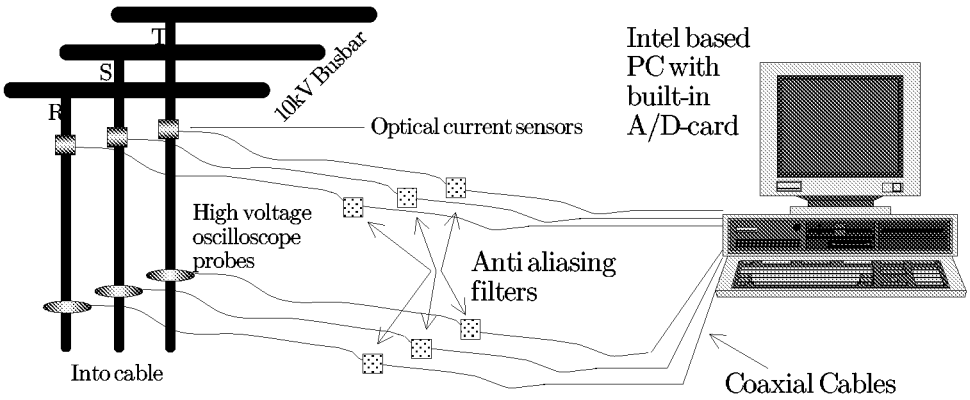

Figure 4.4: Schematic of Measuring System.

by one or converted simulatanously. This introduces a time error between two channels of one sampling

period. This is not desirable. Therefore a so-called SSH A/D–converter was chosen[1]. Where all channels are sampled at the same instant and held in buffers until they are converted one by one.

A product from DATA TRANSLATION was chosen. The company offers a 16bit 8 channel SSH A/D–card for PC's.
The card is capable of converting at a rate up to 160.000 samples/s directly to the hard disk, or 20kHz/channel in eighth channels simultaneously. This is sufficient, since only six channels at 20kHz are needed.
The card may be configured so that a different number of channels are active. When choosing six active channels and a sampling frequency of 20kHz, due to hardware constraints, one actually gets 19,84127kHz. When in the following it is stated that the sampling frequency was 20kHz is meant the above mentioned frequency.

Signal processing aspects of the A/D–converter card are described in Section 6.3

4.3.2.1 Anti-Aliasing

As always when sampling, one has to ensure that the Nyquist Theorem is obeyed.

To ensure as few noise problems as possible it was decided that the anti-aliasing filters should be realized as passive filters.

To ensure compatibility with the other equipment, the design was extended by adding operational amplifiers to the in- and outputs. Though the filters need external power supply to drive the amplifiers they are still passive.

Details on the design are given in Appendix C.

4.3.3 Establishment of Measuring Point at Substation

The optical sensor units have to be installed in the electrical circuit. This was done almost at the end of the cable, see Figure 4.3. On this figure is also shown the installation of the voltage sensors.

The boxes beneath the oscilloscope probes have nothing to do with the Stage 2 Measurements. They are the voltage transformers used during the Stage 1 Measurements.

To house the A/D–card was used a normal office PC. The hard disk of the available PC could contain 7,5min of measurements at a total of about 120.000 samples/s.
The computer was placed as close as possible to the sensors, see Figure 4.5.

4.3.4 Experiments During Stage 2 Measurements

Two sets of experiments were carried out during these measurements:

- Provoked burning out of low voltage fuses at node **1327**, see Figure 2.1 on page 6.
- Operation of the same machines as during the Stage 1 Measurements.

During the experiments contact between the 10kV system at GLENTEGÅRD and the locations in the network, where the experiments were performed, was done by a cellular telephone.
At GLENTEGÅRD the data acquisition was started and stopped after order from the site of the experiments.

In all was acquired 375s of data, corresponding to 89,3MB on the hard disk.

[1] **S**imultaneous **S**ample and **H**old.

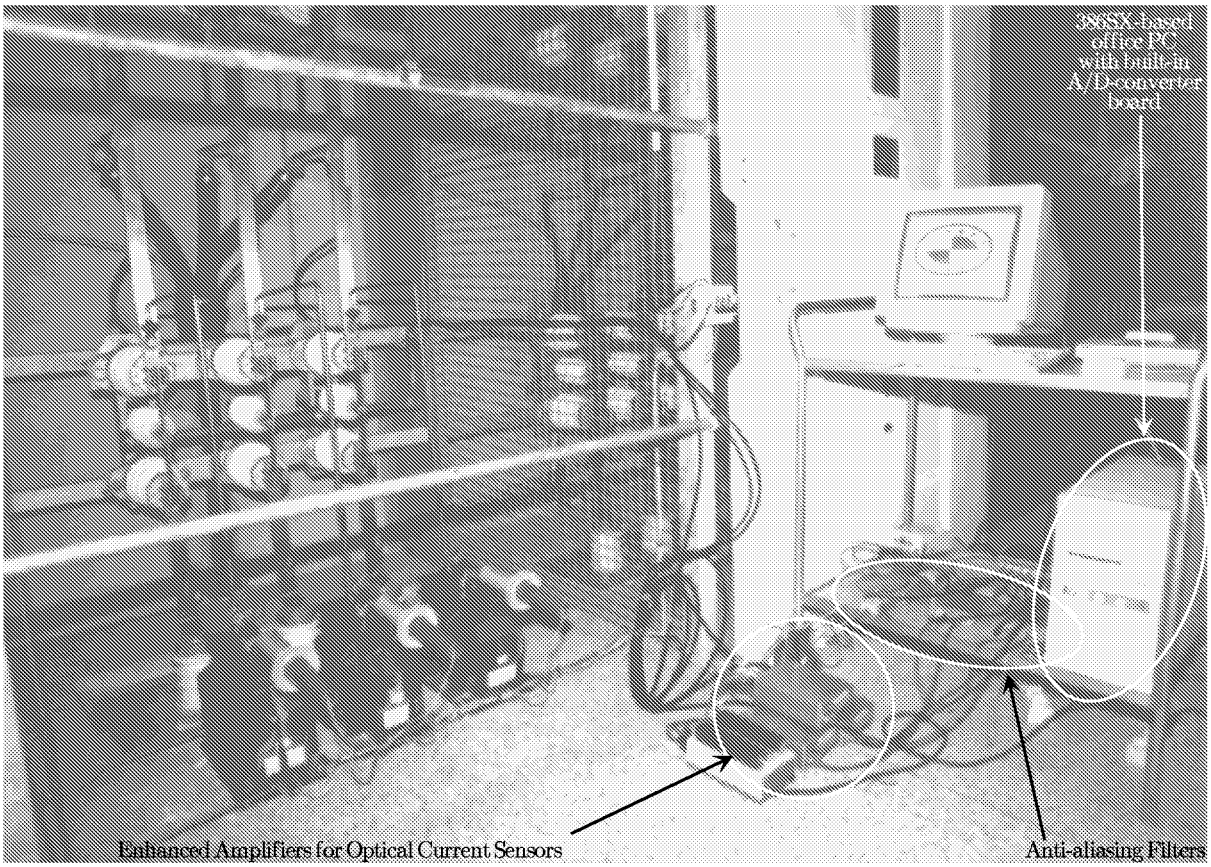

Figure 4.5: Installation of Measuring Equipment.

Figure 4.6: Mobile Power Station Used During Experiments on Burning Out of Fuses.

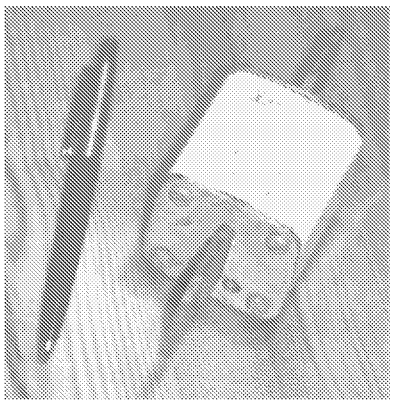

Figure 4.7: Slow 80A – 0,4kV LK-NES Fuse.

4.3.4.1 Burning Out of Fuses

Capability of detecting the burning out of fuses could be a very interesting quality of a monitoring system.
Normally, the burning out of fuses is only realized when the customers start calling the utility because they lack supply. In this case it is very easy to dispatch a repair team to the likely locations to replace the fuses.

Other situations also occur. Examples may be given on consumptions at remote locations where supply is not needed all the time, but when it is, it is urgent that everything works.
As there is nobody at the location to keep supply under surveillance, it would be very interesting to investigate if it were possible to detect that a fuse burnt out and if it were possible to give an estimate of where the event took place, so that it would be possible to dispatch the repair team before anything is damaged.

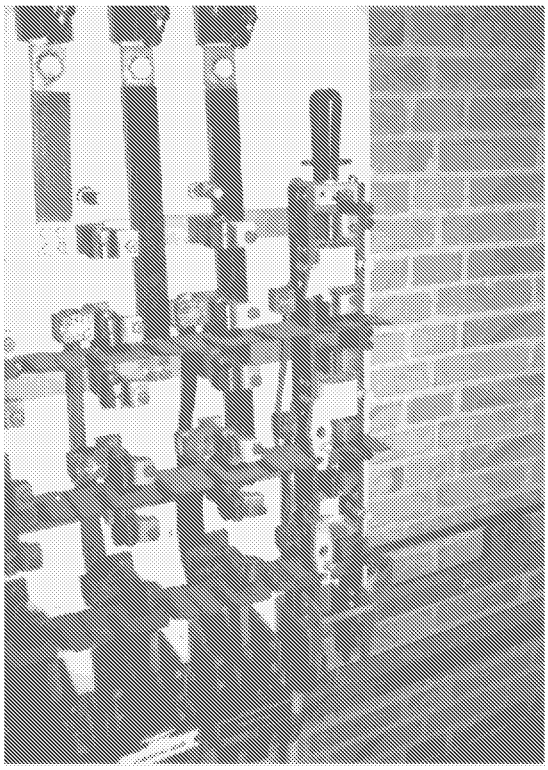

Figure 4.8: Fuses Mounted for Two-Phase Fuse Burning Out, (to the left are seen the empty slots).

Figure 4.9: Switch Used to Short Circuit Fuses, (lower left corner). On the photo is seen Mr. Torben F. Hansen, see page 107.

Fuses are used both at 10kV and 0,4kV level. It is relevant to perform experiments at both levels. But, as previously stated, 10kV is dangerous! It will also be combined with high costs to prepare for the burning out of 10kV fuses. Therefore it was decided that this investigation should start at 0,4kV level.

Still, burning out of low voltage fuses is quite a violent thing to do and many aspects need consideration during the preparation of the experiment.
The fuses were to be burnt out by a short circuit.

It would be most convenient to keep all experiments on the same system. Therefore it was investigated where on **A28** such experiments could be performed without disturbing the surroundings, i.e. the customers.
On **A28** was found one transformer station, where it would be possible to perform the experiments; **1327**.
Alas, this transformer station is located not very far from GLENTEGÅRD, only about 1.200m.
The transformer is rated 100kVA. According to the records of NESA, the short-circuit power is 2.640kVA

and the short-circuit current is 3.664A on the secondary side. The transformer is ΔY–coupled. This means that the short-circuit current on the primary side is $\frac{1}{\sqrt{3}} \frac{0{,}4\text{kV}}{10\text{kV}} 3.664\text{A} = 84{,}6\text{A}$.

The experiments were to be performed directly on the secondary side of the transformer. Therefore the customers had to be disconnected and supplied from a mobile power station, see Figure 4.6.

Disconnecting was done simply by removing the fuses between the transformer and the cables.
For the experiments a normally unused rack was used, see Figure 4.8.

Detailed information on the fuses has not been available. It is, however, known that they were manufactured by LK–NES, and that they were slow 80A fuses, see Figure 4.7. In [NESA, 1962] is shown the melting curves of slow fuses. According to this reference the 80A slow fuse should burn out in less than 10ms, with the short-circuit current of this transformer.

Three sub-experiments were performed; one- two and three phase burning out.

Data was acquired for 25s during each experiment. The switch was closed 5s into the sequence, allowing 20s for transients to die out.

4.3.4.2 Operation of Machines at Factory

Access was again granted to DYRUP A/S. The same two machines as during the Stage 1 Measurements were again operated. Unfortunately, the 75kW had to be run idle, but the 90kW machine was operated under the same conditions; fully loaded.

For each machine the data acquisition system ran for 2min30s. During this time the machines were turned either on or off every 15s.

Chapter 5

Outline of Monitoring System

In this chapter the structure of a the centralized moniotring system is presented, henceforward denoted a DISMO–system. The outline reflects the levels that have been implemented in the MATLAB-programming language as an off-line simulator, see Appendix H.

In this project simulations have been made on the signals that were acquired according to Chapter 4. Therefore the description given here of the first level; the Signal Acquisition Level, corresponds to the on-line implementation of a DISMO system.

In Figure 5.1 is shown a schematic of the elements of the system. The following sections describe further each element. Details on the signal processing are given in Chapter 6.

5.1 Data Acquisition

Signals are acquired as wave forms of the primary values at the *OP*, i.e. three phase currents and three phase to ground voltages.
The bandwidth of currents is at this stage estimated to be 10kHz and the dynamic range to be 90dB. Investigations on the Stage 2 Measurements, see Chapter 7, have revealed that it might not be required to measure the voltages in the same high quality. However, the fundamental component should be acquired with as little error as possible, since the voltages will be used as reference for phase angles.

After the analog lowpass filter the data is A/D–converted using a high-resolution converter. During the Stage 2 Measurements was used a 16bit converter, see Section 4.3.2.
To avoid delays between the separate channels, this converter must be of the SSH–kind[1].

5.2 Signal Decomposition

Presently the *signal decomposition* covers extraction of the fundamental component. One also might imagine the extraction of some of the strongest harmonics. The necessity of this is still to be proven.

All filters are implemented as FIR–filters. This is a necessity to ensure a well-defined phase delay at all frequencies.

The first lowpass filter is an anti-aliasing filter to ensure that the Nyquist Theorem is obeyed so that the decimation may take place.
Sampling is done at 20kHz[2]. Decimation by a factor of 75 yields a new sampling frequency of 266,7Hz. In the simulation system this decimation is implemented in two steps in order to reduce the filter lengths. The first step is a decimation by a factor five and the second by a factor fifteen.

The fundamental frequency component is extracted from the decimated signal by use of a bandpass filter, see Section 6.4.

[1] SSH, **S**imultaneous **S**ample and **H**old.

[2] During the Stage 2 Measurements was sampled at 19.841,27Hz, though 20kHz was desired. This was a constraint of the hardware.

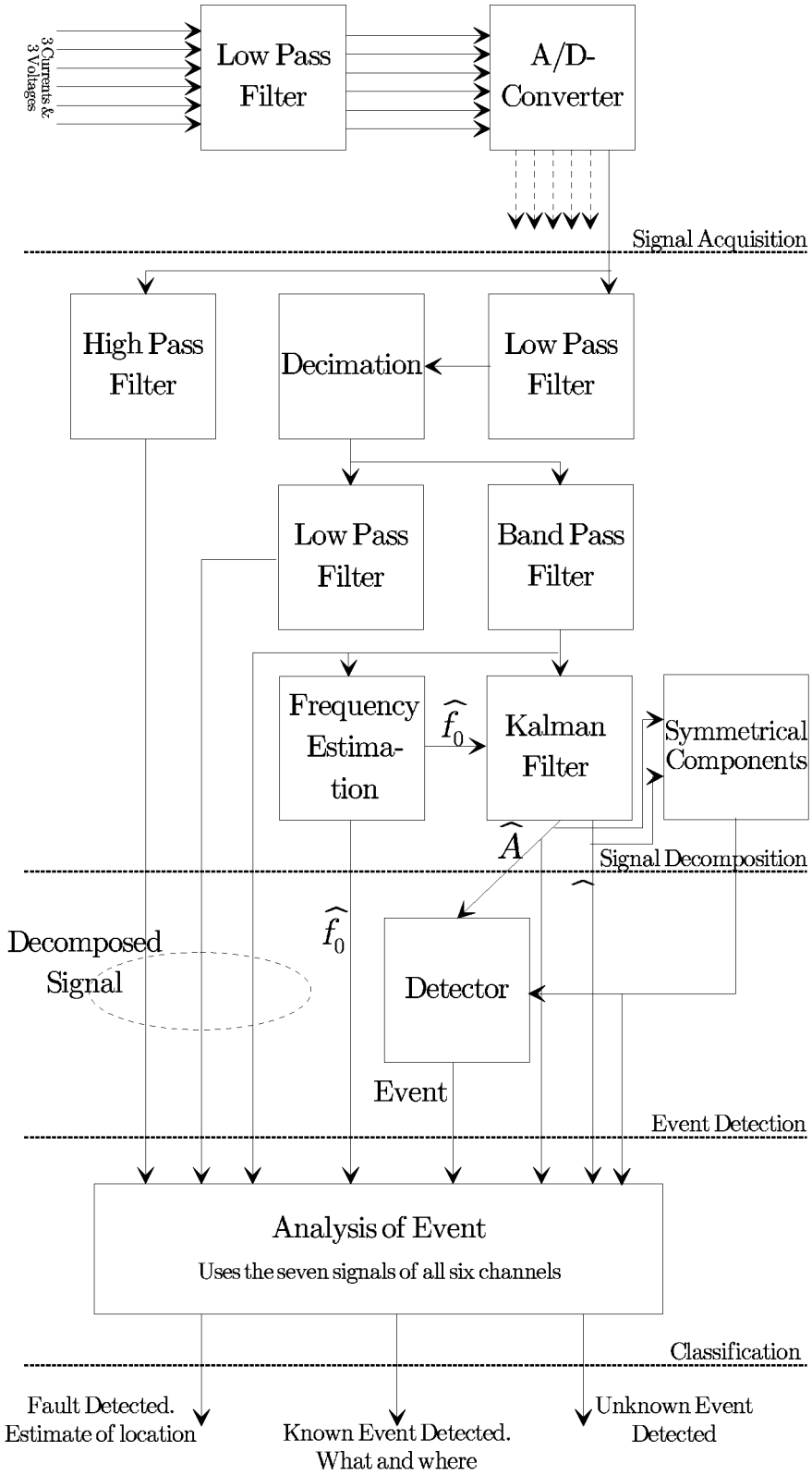

Figure 5.1: Schematic of DISMO Monitoring System.

The residual signal is divided into two components; one containing frequencies below 50Hz and the other frequencies above 50Hz, see Section 6.4.

The output from the bandpass filter is applied to both a frequency estimator, see Section 6.5.2, and to a Kalman Filter, see Section 6.5.1, to estimate amplitude and phase.

For the three currents and the three voltages the estimates of amplitude and phases are used to estimate the symmetrical components of the fundamental component.

The output from this level is for each channel five signals: The decomposed signal makes up for three signals. The estimates of the amplitude and phase from the Kalman Filter for the other two.
For the currents together is output the three complex signals of the symmetrical component representation. Likewise is output three complex signals of the symmetrical component representation of the voltages. The estimate of the instantaneous frequency is common to all six channels.

5.3 Event Detection

Detection is done on the estimates of the amplitudes of the fundamental components of the currents alone, hence all three amplitude estimates are used in the box named "Detector".

The output from the detector is either "0", for no event detected, or one of the possibilities shown in Table 6.2, on page 58 in Section 6.6.

5.4 Classification

Entering this level is now five signals from each channel, the symmetrical component representation, and the output from the detector.
The classification routines are only initiated when the output from the detector goes from 0 to one of the possibilities of Table 6.2.

This part of the monitoring system still needs very much attention. A simple classification scheme, tuned to distinguish between the two motors at DYRUP A/S, has been constructed, see Section 6.7.
That system is not intended for implementation in the DISMO–system, but has only served as a quick means for demonstration purposes.

In Appendix A classification methods are discussed. The appendix renders the outcome of the investigations that have been carried through so far.

Chapter 6

Signal Processing

This chapter describes signal processing methods as well as considerations on the system that generates the signals to be processed.

In Chapter 2 it was described the fundamental concepts of the system that is to be monitored. However, as much detailed information as accessible should be included to get as close as possible to optimal solutions.

In this chapter is also gathered the theory behind some of the analyses described in Chapter 7. Otherwise, the structure of this chapter follows the outline given in Chapter 5.

Some of the information rendered in this chapter relies on conclusions from the analysis of Chapter 7.

6.1 Model of Signals at the Observation Point

In [Jespersen, 1994] it was investigated how the amplitude of the fundamental component of the current develops over time. It was concluded that a so-called *Random Walk* is a good approximation.

$$|i|_n - |i|_{n-1} \quad = \quad \varepsilon_n, \text{ with } \varepsilon_n \in N(0, \sigma^2) \tag{6.1}$$

The random walk is an AR(1)–process. It means that it is actually unstable. Therefore, to be able to use this model on a computer, one should move the pole inside the unit circle in the z-plane.

Having established that the fundamental current amplitude is a random walk, there is no reason in not believing that this also is valid for all harmonics as well as for the fundamental, and the harmonics of the voltages.

The random walk process reflects, in fact, incessant activity on the feeder, i.e. events occur almost continuously. Most of these events, however, are so insignificant that they cannot be detected as single events.

Therefore, in Equations 2.1 and 2.2 on page 7 $\alpha(t)$ and $\beta(t)$ are assumed to be AR(1)–processes.

6.2 Data Acquisition

The sensors that were described in Section 4.3.1 were chosen to fulfil an immediate requirement, i.e. they should be readily available.

When it comes to real implementation of a DISMO–system, dedicated sensors could probably be ordered.

At this stage, there is no definite conclusion on the requirements to sensors. However, it seems as if currents and voltages need not be measured in the same quality. As expected, currents are the most sensitive to changes of the state of the feeder. Therefore, these should be measured in high quality, i.e. high bandwidth and high dynamic range.

For the Stage 2 Measurements was used a modified optical current sensor. The conclusion from the work on modifying this unit must be that optical current sensors as of today are **not** suited for high quality measurements at the voltage level of distribution networks.

Though it was proven to be possible to make the unit work satisfactory, it must be concluded that the requirements can be met with far less complicated and less expensive equipment.
It is hoped that for future installations, utilities will realize that despite the fact that their needs today are to measure the fundamental component, sensors that are capable of measuring much more than this should be installed.

As for voltage sensors goes that at most substations the voltage will be rather insensitive to changes of the state of the feeder. At this stage most of the analysis of the measurements has been performed on the currents, simply because the most is seen here.
The voltages serve at least one important purpose. They are used as reference for measures of phases. At the present, the conclusion regarding voltage measurements is that the wave form of the fundamental component must be measured in high quality. It still needs to be investigated what are the requirements at higher frequencies.

6.3 Sampling

For the Stage 2 Measurements was used an 16bit SSH A/D–converter. From the analysis of the measurements it is concluded that this was a reasonable choice. It is recommended that the future measuring system will be based on a converter of at least this quality.
The bandwidth of 10kHz of the Stage 2 Measurements seems appropriate.

The A/D–converter is described in [Data Translation, 1992]. This reference, however, does not give details on the quantization characteristics. Therefore, it is assumed that the characteristics are as in Figure 6.1. For these characteristics the signal/quantization noise ratio may be determined.

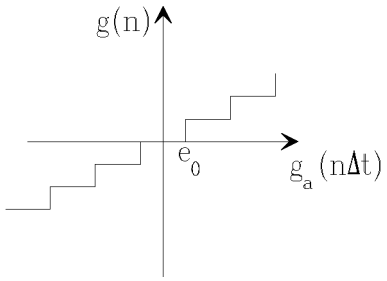

Figure 6.1: Quantization Characteristics.

The DATA TRANSLATION DT2838 A/D–converter has an input range of ±10V. The step size, e_0, therefore is:

$$e_0 = \frac{2 \cdot 10\text{V}}{2^{16}} = 305{,}18\mu\text{V} \tag{6.2}$$

The maximum RMS-value of a sinewave that may be converted by this card is: $\frac{10\text{V}}{\sqrt{2}} = 7{,}07\text{V}$.
According to [Boel Pedersen, 1987] a "*b*bit *plus sign*" converter has a S/N of:

$$\begin{aligned} \mathbf{S/N} &= 20\log\left[\frac{\text{RMS}[\textit{signal}]}{\text{RMS}[\textit{quantization noise}]}\right] && (6.3)\\ &= 20\log\left[\frac{2 \cdot 2^b \cdot e_0}{2\sqrt{2}} \cdot \frac{\sqrt{12}}{e_0}\right] && (6.4)\\ &\simeq (7{,}78 + 6{,}02 \cdot b)\,\text{dB} \end{aligned}$$

In this case, where $b = 15$, we get:

$$\text{S/N} = 98{,}09\text{dB}$$

With the above indicated maximum RMS–value, the RMS–value of the quantization noise becomes:

$$\mathrm{RMS}_{\mathrm{noise}} = \frac{7{,}07\mathrm{V}}{80.265} = 88{,}097\mu\mathrm{V}$$

6.4 Multi Rate Signal Processing

In Chapter 2 the two concepts *fundamental* and *residual* component were discussed. Without mentioning multi rate signal processing, the initial steps of a discussion of this topic were taken.
Splitting up signals into single frequencies or regions in the frequency spectrum is, indeed, multi rate signal processing. Having reduced the bandwidth of a signal one may also reduce the sampling frequency and in that way reduce the computational demands.

Another aspect of signal decomposition originates in this context.
AC electrical power systems are conceived to transfer energy at one frequency; the power system frequency or, as denoted in this thesis, the fundamental frequency.
Under normal conditions, this component will be far the most predominant. In fact, it is orders of magnitude stronger than the other components of the frequency spectrum, see Figures 6.2 and 6.3. The figures show estimates calculated over 200.000 samples using the MATLAB-function **spectrum**,

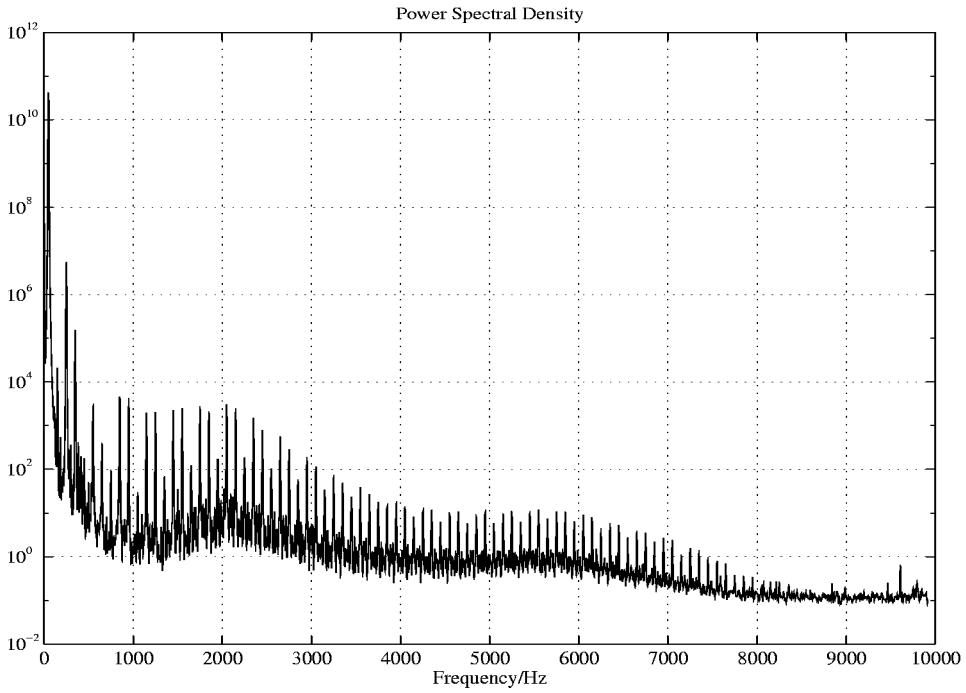

Figure 6.2: Estimate of Power Spectrum of Phase Voltage

see [Little and Shure, 1993].
spectrum calculates its result as the mean of an FFT on windowed sub-sections of the signal.

For these two reasons it seems reasonable to extract the fundamental component from the signals and process it separately. The signal without the fundamental component is the residual signal.

The straightforward approach to extracting one frequency would be to bandpass filter the signal with a narrow bandpass filter. The residual signal could then be estimated by subtracting the answer of the filter from the delayed signal, as shown in Figure 6.4. For obvious reasons, at least when looking in the rear-view mirror, this will not work.

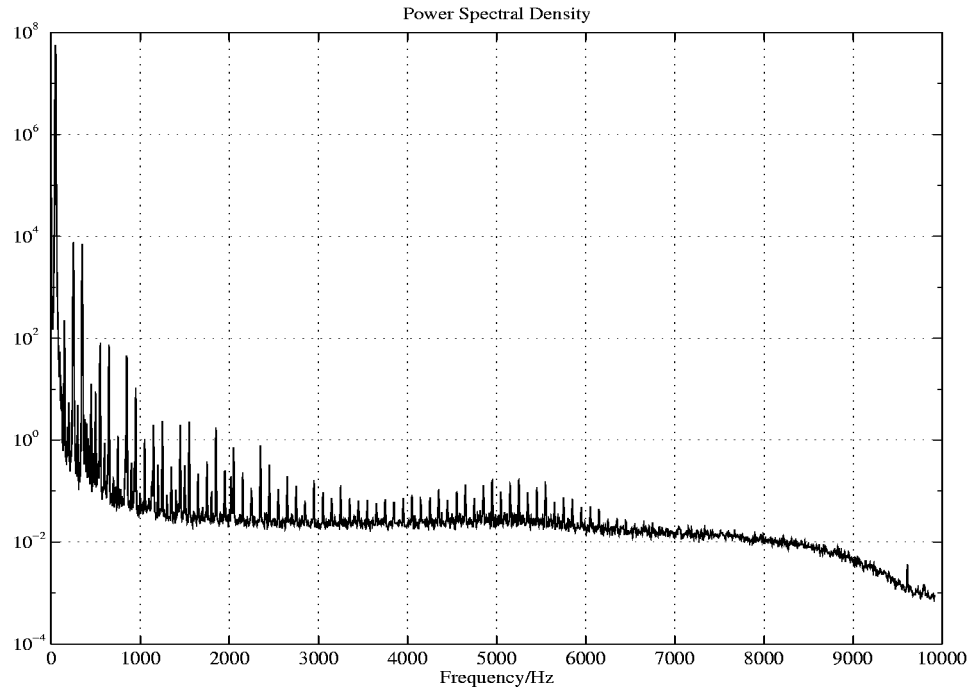

Figure 6.3: Estimate of Power Spectrum of Phase Current

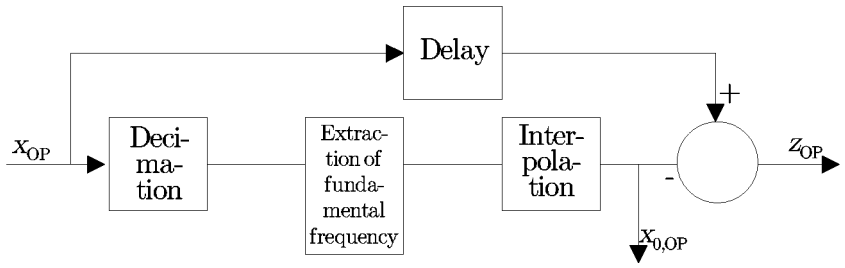

Figure 6.4: Signal Processing Chain for the Extraction of the Fundamental Frequency.

The explanation is that the bandpass filter should be narrow in comparison to the bandwidth of the input signal. Hence the Q–factor will be high. This in turn will make the filter react slowly to changes of state. Therefore events will cause part of the fundamental component to remain in the estimate of the residual signal.

Instead the structure shown in Figure 6.5 was decided on.

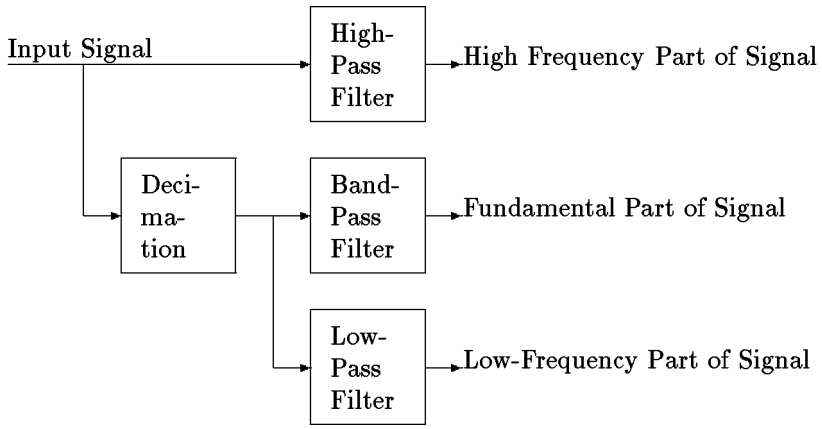

Figure 6.5: Three Track Signal Processing Chain for the Extraction of the Fundamental Frequency.

The residual signal is split into two regions; below and above the fundamental component respectively. This must be so due to the argumentation concerning the initial approach. One could imagine extracting the fundamental component from the residual signal using a notch filter. But this filter would behave much like the above mentioned bandpass filer.

All filters are implemented as FIR-filters in order to have a linear phase and a well defined delay.

The highpass filter operates directly on the sampled values, i.e. at 20kHz. It is designed so that it has a zero close to 50Hz. In order to reduce its length, the pass band starts at the fifth harmonic, i.e. 250Hz. The order is 180.

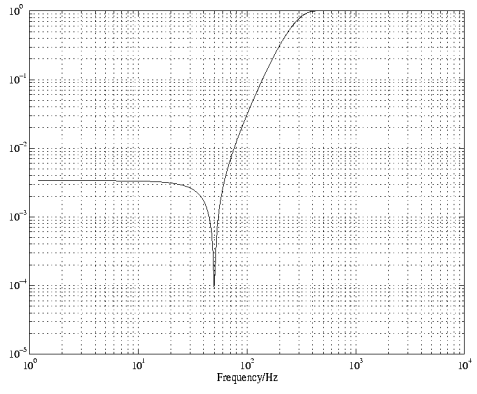

Figure 6.6: Amplitude Characteristics of Highpass Filter.

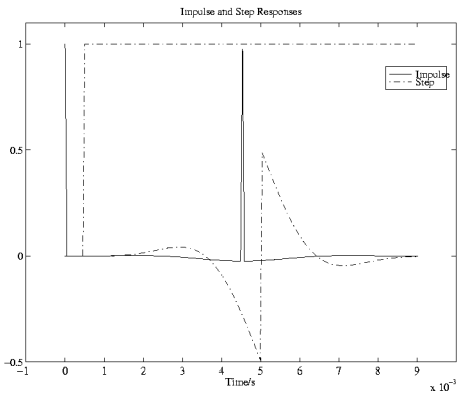

Figure 6.7: Impulse and Step Responses of Highpass Filter.

In Figure 6.7 is shown the impulse and step responses of the highpass filter.
The impulse is applied at time equal to zero and the step at time equal to 5,54μs.

The bandpass filter is applied to the signals after decimation by a factor 75, hence the sampling frequency at this stage is $\frac{20\text{kHz}}{75} = 266{,}67\text{Hz}$. The decimation is made in two steps in order to reduce the length

of the required lowpass filter. The first step is a decimation by a factor five, and the second by a factor fifteen.
For the DSP–implementation this is done in three steps.

Tests with the simulation system have revealed that the subsequent analysis of the fundamental component is not very sensitive to the presence of other frequency components close to the fundamental. The original bandpass filter, that was very narrow, was therefore changed into one having a much wider pass band, from 25Hz to 75Hz, as opposed to 49,7Hz to 50,1Hz that was chosen for the initial approach. The filter order is 128.
The new filter reacts far less violently to steps in the input.

On the same decimated signals, as uses the bandpass filter, the lowpass filter is applied.
This filter is also designed to be as short as possible. Still restricted to be of FIR-type, a satisfactory filter of order fourteen may be obtained.

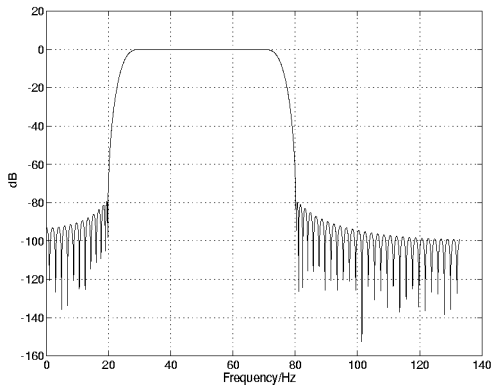

Figure 6.8: Amplitude Characteristic of Bandpass Filter

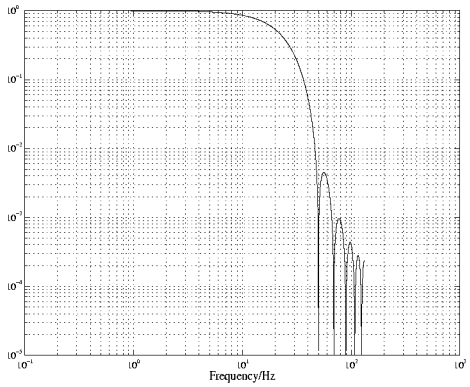

Figure 6.9: Amplitude Characteristics of Lowpass Filter

To facilitate the analysis of the entire frequency spectrum of the decimated signal, a highpass filter was designed. This filter has also a zero at the fundamental frequency.
At this stage this filter is not a part of the proposed monitoring system.

All filters were designed using the `fir1`–routine of MATLAB, see [Little and Shure, 1993].

6.4.1 Discussion of Frequency Contents of Voltages and Currents

In Chapter 3 was stated that the current was the most sensitive to changes of state of the feeder. Therefore, it may seem strange that the spectra shown in Figures 6.2 and 6.3 show that the voltage contains higher frequencies than the current.

The explanation is quite simple. The voltages were measured with a passive sensor, hence its noise contribution is very small. The currents, on the other hand, were measured using an optical sensor. This sensor works with an amplifier. Although a great effort was made to reduce the noise, it has hereby become apparent that the bandwidth of the sensor is still reduced compared to what is present on the feeder.

6.4.2 Delay Through Signal Decomposition Part of System

The input signal is now split into three components. In this section is given the delay of each channel.

Having applied FIR–filters all frequency components are delayed the same number of samples.

For FIR–filters go that the delay is determined by, (see e.g. [Bellanger, 1990, Section 5.2]):

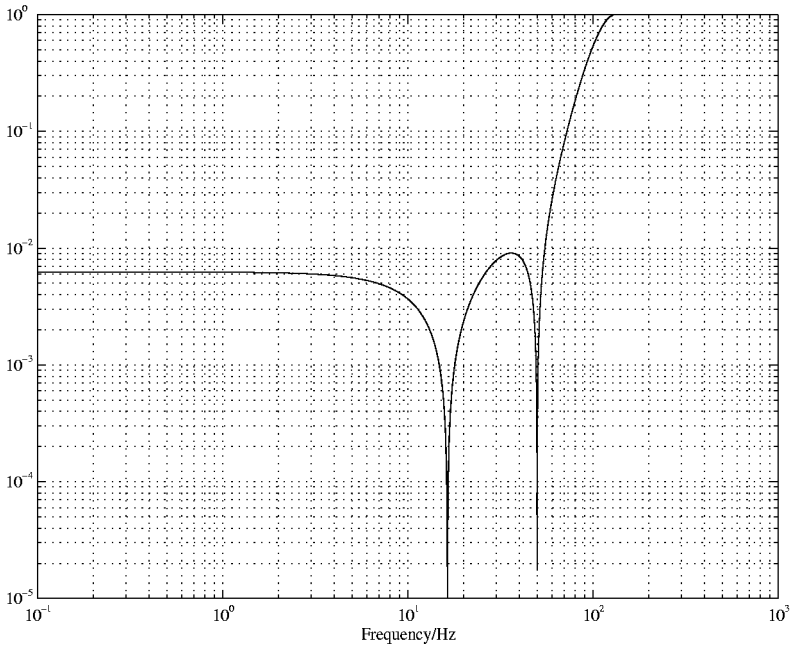

Figure 6.10: Amplitude Characteristics of Highpass Filter for Decimated Signal

N odd	N even
$\frac{N}{2}\Delta t$	$\frac{N-1}{2}\Delta t$

N is the filter order.

6.4.2.1 High Frequency Part

The highpass filter is of order 180. The sampling frequency is 20kHz, hence the delay is 4,475ms.

6.4.2.2 Fundamental Component

For both this component and the part of the residual component below 50Hz go that the delay depends on how the decimation is implemented. As mentioned previously, in the DSP–implementation the decimation is carried out in three steps. In the MATLAB–implementation it is done in two steps. The times given here are for the MATLAB–implementation.

The first lowpass filter used for the times five decimation is of order 44, the sampling frequency is 20kHz, hence the delay is: 1,075ms.
The second filter is of order 246, the sampling frequency is $\frac{20\text{kHz}}{5} = 4\text{kHz}$, hence the delay is: 6,125ms.

The bandpass filter is of order 128, the sampling frequency is $\frac{4\text{kHz}}{15} = 266{,}67\text{kHz}$, hence the delay is: 238,1ms.

All in all, the delay of the estimate of the fundamental component is: (1,075+6,125+238,1)ms = 245,3ms.

6.4.2.3 Low Frequency Part

The filter used to lowpass filter the decimated signal is of order 14, hence the delay is: 24,38ms.

With the above delay of the decimation, the total delay becomes: $(1{,}075 + 6{,}125 + 24{,}38)\text{ms} = 31{,}58\text{ms}$.

6.5 Estimation of Amplitudes and Phases

The signal is now split into basically two components. The question of what to do next then arises.

In traditional power system monitoring one would calculate the RMS–values of the voltages and currents and probably also the RMS–value of the power.
This could easily be calculated at this stage. However, it would seem a great waste, after all the efforts to get high quality measurements, only to extract so little information.

It was decided that the investigations on the frequency contents of the signals should start on known territory, so to speak. That is why much work was made on examining in detail how events on the feeder affect the fundamental component.
This section is alone concerned about the fundamental frequency components.

6.5.1 Kalman Filter

The Kalman filter is an efficient method of estimating states in a state-model.
The Kalman filter has been the target of much attention for power engineering applications, e.g. [Girgis *et al.*, 1991] and [Kamwa and Grondin, 1992].

In the first part of this section the Kalman filter is defined.
The second part defines for the application of the Kalman filter in this context a two-state model.

The Kalman filter is formulated using state-space concepts. The result yields a recursive algorithm, which is well-suited for the implementation on a digital computer.

The formulation starts by defining the *process equation*:

$$\boldsymbol{x}(n+1) \quad = \quad \boldsymbol{\Phi}(n+1,n)\,\boldsymbol{x}(n) + \boldsymbol{\nu}_1(n) \tag{6.5}$$

$\boldsymbol{\Phi}(n+1,n)$ is a **known** $M \times M$ *state transition matrix* relating the states of the system at times $n+1$ and n. $\boldsymbol{x}$ is a $M \times 1$ *state-vector.*
The *measurement equation* connects the *observation vector* $\boldsymbol{y}(n)$ to the *state transition matrix*; $\boldsymbol{\Phi}$:

$$\boldsymbol{y}(n) = \boldsymbol{C}(n)\,\boldsymbol{x}(n) + \boldsymbol{\nu}_2(n) \tag{6.6}$$

$\boldsymbol{C}$ is a **known** $N \times M$ *measurement matrix.*
Both $\boldsymbol{\nu}_1$ and $\boldsymbol{\nu}_2$ represent zero-mean, white-noise processes. The $M \times 1$ vector $\boldsymbol{\nu}_1$ is the *process noise* and the $N \times 1$ vector $\boldsymbol{\nu}_2$ is the *measurement noise.* $\boldsymbol{\nu}_1$ and $\boldsymbol{\nu}_2$ are assumed to be statistically independent, so;

$$E\left[\boldsymbol{\nu}_1(n)\,\boldsymbol{\nu}_2^H(k)\right] = \mathbf{0}, \quad \text{for all } n \text{ and } k \tag{6.7}$$

The quest is to find for each $n \geq 1$ the minimum mean-square estimates of the state $\boldsymbol{x}(i)$ using the observed data; $\boldsymbol{y}(1)$, $\boldsymbol{y}(2), \ldots, \boldsymbol{y}(n)$.

The solution to the Kalman filtering problem rendered here is the *innovations approach*, according to [Haykin, 1991].

The vector $\widehat{\boldsymbol{y}}\,(n|\mathcal{Y}_n - 1)$ denotes the minimum mean-square estimate of the observed data at time n, given all the values of the observed data starting at time $n = 1$ and extending up to and including time $n-1$, represented by the vectors; $\boldsymbol{y}(1)$, $\boldsymbol{y}(2), \ldots, \boldsymbol{y}(n)$, which span the vector space $\mathcal{Y}_{n-1}$. The *innovations process* associated with $\boldsymbol{y}(n)$ is defined as:

$$\boldsymbol{\alpha}(n) = \boldsymbol{y}(n) - \widehat{\boldsymbol{y}}\,(n|\mathcal{Y}_{n-1})\,, \quad n = 1, 2, \ldots \tag{6.8}$$

$\boldsymbol{\alpha}(n)$ represents the new information in the observed data $\boldsymbol{y}(n)$. This vector is orthogonal to all past observations:

$$E\left[\boldsymbol{\alpha}(n)\,\boldsymbol{y}^H(k)\right] = \mathbf{0}, \quad 1 \leq k \leq n-1 \tag{6.9}$$

Having either the set $\{\boldsymbol{y}(1), \boldsymbol{y}(2), \ldots, \boldsymbol{y}(n)\}$ or $\{\boldsymbol{\alpha}(1), \boldsymbol{\alpha}(2), \ldots, \boldsymbol{\alpha}(n)\}$ one may obtain the one set from the other without loss of information, since there is a one–to–one correspondence between the two.

$$\{\boldsymbol{y}(1), \boldsymbol{y}(2), \ldots, \boldsymbol{y}(n)\} \rightleftharpoons \{\boldsymbol{\alpha}(1), \boldsymbol{\alpha}(2), \ldots, \boldsymbol{\alpha}(n)\} \tag{6.10}$$

The next step is to determine the correlation matrix of the innovations process. This is thoroughly done in [Haykin, 1991, Chapter 7]. Only the results are rendered here.
The correlation matrix of the innovations process is:

$$\boldsymbol{\Sigma}(n) = E\left[\boldsymbol{\alpha}(n)\,\boldsymbol{\alpha}^H(n)\right] \tag{6.11}$$

This equation may be rewritten into:

$$\boldsymbol{\Sigma}(n) = \boldsymbol{C}(n)\,\boldsymbol{K}(n, n-1)\,\boldsymbol{C}^H(n) + \boldsymbol{Q}_2(n) \tag{6.12}$$

Where $E\left[\boldsymbol{\nu}_2(n)\,\boldsymbol{\nu}_2^H(k)\right] = \begin{cases} \boldsymbol{Q}_2(n), & n = k \\ 0, & n \neq k \end{cases}$ and;

$$\boldsymbol{K}(n, n-1) = E\left[\boldsymbol{\varepsilon}(n, n-1)\,\boldsymbol{\varepsilon}^H(n, n-1)\right] \tag{6.13}$$

Where $\boldsymbol{\varepsilon}(n, n-1) = \boldsymbol{x}(n) - \hat{\boldsymbol{x}}(n|\mathcal{Y}_{n-1})$ is the predicted state-error vector.
Next to be derived is the minimum mean-square estimate of the state $\boldsymbol{x}(i)$ from the innovations process. It may be shown that this estimate may be described as a linear combination of the innovations processes $\boldsymbol{\alpha}(1), \boldsymbol{\alpha}(2), \ldots, \boldsymbol{\alpha}(n)$:

$$\hat{\boldsymbol{x}}(i|\mathcal{Y}_n) = \sum_{k=1}^{n} \boldsymbol{B}_i(k)\,\boldsymbol{\alpha}(k) \tag{6.14}$$

$\{\boldsymbol{B}_i(k)\}$ is a set of $M \times N$ matrices to be determined:

$$\boldsymbol{B}_i(m) = E\left[\boldsymbol{x}(i)\,\boldsymbol{\alpha}^H(m)\right]\,\boldsymbol{\Sigma}^{-1}(m) \tag{6.15}$$

Now we get the mean-square estimate $\hat{\boldsymbol{x}}(i|\mathcal{Y}_n)$ as follows:

$$\hat{\boldsymbol{x}}(i|\mathcal{Y}_n) = \sum_{k=1}^{n-1} E\left[\boldsymbol{x}(n+1)\,\boldsymbol{\alpha}^H(k)\right]\,\boldsymbol{\Sigma}^{-1}(k)\,\boldsymbol{\alpha}(k) + E\left[\boldsymbol{x}(n+1)\,\boldsymbol{\alpha}^H(n)\right]\,\boldsymbol{\Sigma}^{-1}(n)\,\boldsymbol{\alpha}(n) \tag{6.16}$$

This equation may be rewritten into:

$$\hat{\boldsymbol{x}}(n+1|\mathcal{Y}_n) = \boldsymbol{\Phi}(n+1, n)\,\hat{\boldsymbol{x}}(n|\mathcal{Y}_{n-1}) + \boldsymbol{G}(n)\,\boldsymbol{\alpha}(n) \tag{6.17}$$

The $M \times N$ matrix $\boldsymbol{G}(n)$ is the Kalman gain.

$$\begin{aligned} \boldsymbol{G}(n) &= E\left[\boldsymbol{x}(n+1)\,\boldsymbol{\alpha}^H(n)\right]\,\boldsymbol{\Sigma}^{-1}(n) \\ &= \boldsymbol{\Phi}(n+1, n)\,\boldsymbol{K}(n, n-1)\,\boldsymbol{C}^H(n)\,\boldsymbol{\Sigma}^{-1}(n) \end{aligned} \tag{6.18}$$

Equation 6.18 is not very suited for the computing of the Kalman gain. It requires that the state-error correlation matrix, $\boldsymbol{K}(n, n-1)$ is known. A recursive algorithm for the calculation of $\boldsymbol{K}(n+1, n)$, ($\boldsymbol{K}$ at time $n+1$, with $\boldsymbol{K}$ and other parameters known at time n), would be desirable.
The *Riccati difference equation* gives the expression for the recursive computation of the predicted state-error correlation matrix:

$$\boldsymbol{K}(n+1, n) = \boldsymbol{\Phi}(n+1, n)\,\boldsymbol{K}(n)\,\boldsymbol{\Phi}^H(n+1, n) + \boldsymbol{Q}_1(n) \tag{6.19}$$

Where the $M \times M$ matrix $\boldsymbol{K}(n)$ is described by the recursion:

$$\boldsymbol{K}(n) = \boldsymbol{K}(n, n-1) - \boldsymbol{\Phi}(n, n+1)\,\boldsymbol{G}(n)\,\boldsymbol{C}(n)\,\boldsymbol{K}(n, n-1) \tag{6.20}$$

and $E\left[\boldsymbol{\nu}_1(n)\boldsymbol{\nu}_1^H(k)\right] = \begin{cases} \boldsymbol{Q}_1(n), & n = k \\ 0, & n \neq k \end{cases}$

Now we are about to be ready to launch the Kalman filter. We only need to consider how to start calculations. At the first step, reference to step 0 is made. One may have motives for choosing something that differs from 0, which is what one would use, having no prior knowledge about the sequence to be estimated, that is:

$$\widehat{\boldsymbol{x}}(0|\mathcal{Y}_0) = E[\widehat{\boldsymbol{x}}(0)] \tag{6.21}$$

It is seen that if $\boldsymbol{x}(n)$ has zero mean the *initial filtered estimate* becomes:

$$\widehat{\boldsymbol{x}}(0|\mathcal{Y}_0) = 0 \tag{6.22}$$

As for the correlation matrix, we may choose:

$$\boldsymbol{K}(0) = E[\boldsymbol{x}(0)\,\boldsymbol{x}^H(0)] = \boldsymbol{P}_0 \tag{6.23}$$

(The power of $\boldsymbol{x}$ at time zero.)
Given these initial conditions one gets:

$$\begin{aligned} \widehat{\boldsymbol{x}}(1|\mathcal{Y}_0) &= \boldsymbol{\Phi}(1,0)\,\widehat{\boldsymbol{x}}(0|\mathcal{Y}_0) \\ &= \boldsymbol{\Phi}(1,0)\,E[\widehat{\boldsymbol{x}}(0)] \end{aligned} \tag{6.24}$$

and:

$$\begin{aligned} \boldsymbol{K}(1,0) &= \boldsymbol{\Phi}(1,0)\,\boldsymbol{K}(0)\,\boldsymbol{\Phi}^H(1,0) + \boldsymbol{Q}_1(0) \\ &= \boldsymbol{\Phi}(1,0)\,\boldsymbol{P}_0\,\boldsymbol{\Phi}^H(1,0) + \boldsymbol{Q}_1(0) \end{aligned} \tag{6.25}$$

6.5.1.1 Two State Model for Kalman Filter Estimation of Amplitude and Phase

A two state-model is defined for the fundamental component:

$$y(n) = A(n)\,\cos(\varphi(n)) \tag{6.26}$$

Where $A(n)$ is the instantaneous amplitude and $\varphi(n)$ the instantaneous phase of the signal.
In order to have a meaningful interpretation of the phase, it must be compared to a chosen reference.
Equation 6.26 needs to be rewritten in a form that conforms with Equation 6.5 and 6.6 on page 45.
The two states describe respectively the real and imaginary parts of the signal:

$$\boldsymbol{x}(n) = \begin{pmatrix} A(n)\,\cos(\varphi(n)) \\ A(n)\,\sin(\varphi(n)) \end{pmatrix} = \begin{pmatrix} x_1(n) \\ x_2(n) \end{pmatrix} \tag{6.27}$$

Assuming that the amplitude is quasi stationary, i.e. $A(n+1) \simeq A(n)$ and assuming that the phase develops linearly, i.e. $\varphi(n+1) = \varphi(n) + \Delta\varphi$, $\Delta\varphi = 2\,\pi\,\frac{f_0}{f_s}$, $\boldsymbol{x}(n+1)$ may be expressed on the basis of $\boldsymbol{x}(n)$:

$$\begin{aligned} x_1(n+1) &= A(n+1)\,\cos(\varphi(n+1)) \\ &\simeq A(n)\,\cos(\varphi(n) + \Delta\varphi) \\ &= A(n)\,(\cos(\varphi(n))\,\cos(\Delta\varphi) - \sin(\varphi(n))\,\sin(\Delta\varphi)) \\ &= \cos(\Delta\varphi)\,x_1(n) - \sin(\Delta\varphi)\,x_2(n) \end{aligned} \tag{6.28}$$

$$\begin{aligned} x_2(n+1) &= A(n+1)\,\sin(\varphi(n+1)) \\ &\simeq A(n)\,\sin(\varphi(n) + \Delta\varphi) \\ &= A(n)\,(\sin(\varphi(n))\,\cos(\Delta\varphi) + \cos(\varphi(n))\,\sin(\Delta\varphi)) \\ &= \sin(\Delta\varphi)\,x_1(n) + \cos(\Delta\varphi)\,x_2(n) \end{aligned} \tag{6.29}$$

From Equation 6.28 and 6.29 the *state transition equation* may be immediately written:

$$\boldsymbol{x}(n+1) = \begin{pmatrix} \cos(\Delta\varphi) & -\sin(\Delta\varphi) \\ \sin(\Delta\varphi) & \cos(\Delta\varphi) \end{pmatrix} \boldsymbol{x}(n) + \boldsymbol{\nu}_1(n) \tag{6.30}$$

The signal corresponds to the state x_1, therefore the *measurement equation* becomes:

$$y(n) = \begin{pmatrix} 1 & 0 \end{pmatrix} \boldsymbol{x}(n) + \nu_2(n) \tag{6.31}$$

Both $\boldsymbol{\nu}_1$ and $\boldsymbol{\nu}_2$ are assumed to be Gaussian white noise processes:

$$\boldsymbol{\nu}_1 \in N\left(\begin{pmatrix} 0 \\ 0 \end{pmatrix}, \begin{pmatrix} \sigma_p^2 & 0 \\ 0 & \sigma_p^2 \end{pmatrix}\right) \tag{6.32}$$

$$\boldsymbol{\nu}_2 \in N(0, \sigma_m^2) \tag{6.33}$$

The above model was created under the assumption of constant frequency of the fundamental component.

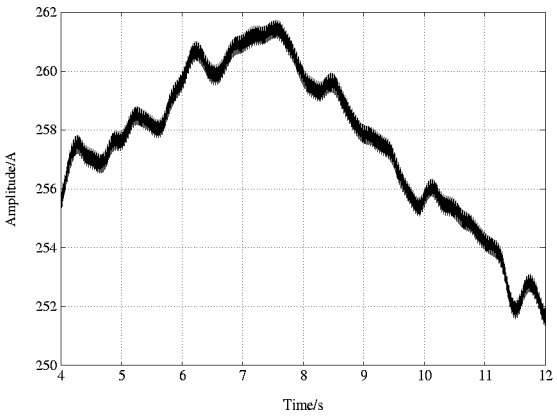

Figure 6.11: Oscillations of Amplitude Estimate from Kalman Filter using Fixed Frequency Assumption.

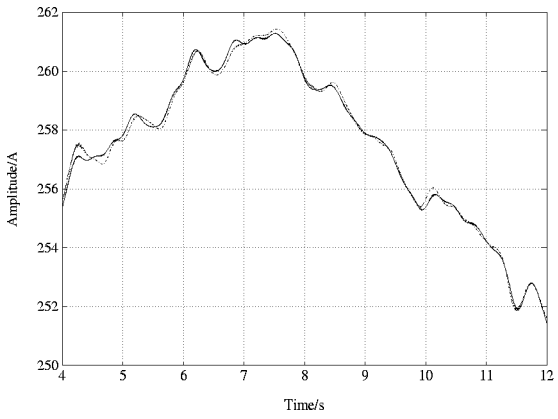

Figure 6.12: Amplitude Estimate from Kalman Filter using Frequency Estimate in State Transition Matrix. Solid Line True Course. Dashed Line Estimate.

However, during the work described in [Høg, 1994] it was realized that the small frequency deviations in the measurements had to be accounted for. Otherwise oscillations of the estimates occurred, see Figure 6.11.
The approach was to modify the state transition matrix. Instead of using a constant matrix, an estimate of the instantaneous frequency is applied, so that Equation 6.30 instead becomes:

$$\boldsymbol{x}(n+1) = \begin{pmatrix} \cos(\Delta\varphi(n)) & -\sin(\Delta\varphi(n)) \\ \sin(\Delta\varphi(n)) & \cos(\Delta\varphi(n)) \end{pmatrix} \boldsymbol{x}(n) + \boldsymbol{\nu}_1(n) \tag{6.34}$$

Where $\Delta\varphi(n) = 2\,\pi\,\frac{\widehat{f_0}(n)}{f_s}$.
During the work described in [Jespersen, 1994] more work with other state models than the one described here was carried out.
Two other models were tried. One where the amplitude was assumed to be stochastic and one where both the amplitude and frequency were assumed stochastic.
The conclusion was that only in some special cases anything could be gained from such a description. It was concluded that in this context it was appropriate to proceed using the description corresponding to Equation 6.34.

6.5.2 Estimation of Instantaneous Frequency

In order to use the Kalman filter with the state transition matrix of Equation 6.34, an estimate of the instantaneous frequency is required.

Before starting an investigation on suitable methods for the estimation of the fundamental frequency, it must be investigated how the frequency behaves. As was indicated in Chapter 2, the only reference that was found, dealing with the network frequency on Sjælland is [NESA, 1978]. The reference relies on measurements dating as far back as 1970 and 1974!
The reference states that the frequency deviations shown in Table 6.1 were valid in 1978. The paper

$\Delta f \leq \pm 0{,}02$Hz for 49,0% of the time
$\Delta f \leq \pm 0{,}04$Hz for 84,0% of the time
$\Delta f \leq \pm 0{,}06$Hz for 96,0% of the time
$\Delta f \leq \pm 0{,}08$Hz for 99,4% of the time

Table 6.1: Deviations of Network Frequency.

reports on two characteristic changes of the frequency:

1. A variation of $\pm 10-20$mHz with a period of about half a minute.
2. A variation of ± 5mHz with a period of about 2s.

A suitable algorithm will be capable of tracking these deviations. Larger deviations will be exceptional. Therefore it will be satisfactory if the algorithm may track those with a longer convergence time.

As there is only one frequency of interest, the algorithm should work on the estimate of the fundamental component. Thereby computational savings will become possible.
A pure sinusoidal will correspond to a δ–function in the frequency spectrum. The quest is to locate the peak in the frequency spectrum corresponding to the δ–function of the fundamental component.

Some kind of representation of the frequency spectrum is needed. For obvious reasons this cannot/should not be arrived at by Fourier transformation. First of all, stationarity cannot be assumed and secondly it would also require a very big computational effort.

Because the signals cannot be assumed to behave stationarily, an algorithm to estimate the frequency must be based on an assumption of non-stationarity.

[Griffiths, 1975] starts by an introduction that almost describes the problem we face here. Therefore it was decided to try out the recommendations of that reference.
The reference is oriented towards speech processing, but the conditions for using the described methods are the same.
In speech processing linear prediction is a well-known topic. It has been used extensively in speech coding, where it is desired to extract as much as possible of the deterministic contents of a signal, so that the signal may be represented with fewer parameters.

In forward linear prediction is assumed that the signal, u, at time n may be described by a linear combination of previous (observed) values of u.

$$\widehat{u}(n|\mathcal{U}_{n-1}) = \sum_{k=1}^{M} w_{o,k}^{*}\, u(n-k) \tag{6.35}$$

$w_{o,k}$ denotes the prediction filter coefficients. The optimal set of coefficients results in a minimum mean-square-error, $P_M = E[\varepsilon^2(n)]$.

$$\varepsilon(n) = u(n) - \widehat{u}(n|\mathcal{U}_{n-1}) \tag{6.36}$$

$\mathcal{U}_{n-1}$ denotes the M–dimensional space spanned by the samples $u(n-1), u(n-2), \ldots, u(n-M)$.
The optimum set of prediction filter coefficients may be expressed in matrix notation as:

$$\boldsymbol{w}_o = \boldsymbol{R}^{-1}\boldsymbol{r} \tag{6.37}$$

Where: (6.38)

$$\boldsymbol{w}_o = \begin{pmatrix} w_{o,1} \\ w_{o,2} \\ \vdots \\ w_{o,M} \end{pmatrix} \tag{6.39}$$

$$\boldsymbol{r} = \begin{pmatrix} r^*(1) \\ r^*(2) \\ \vdots \\ r^*(M) \end{pmatrix} = E[\boldsymbol{u}(n-1)\,\boldsymbol{u}^*(n)] \tag{6.40}$$

$$\boldsymbol{R} = \begin{pmatrix} r(0) & r(1) & \cdots & r(M-1) \\ r^*(1) & r(0) & \cdots & r(M-2) \\ \vdots & \vdots & \ddots & \vdots \\ r^*(M-1) & r^*(M-2) & \cdots & r(0) \end{pmatrix} = E[\boldsymbol{u}(n-1)\,\boldsymbol{u}^H(n-1)] \tag{6.41}$$

The linear prediction spectrum may be expressed using the optimum prediction filter coefficients.

$$SM(\omega) = \frac{r(0) - \sum_{k=1}^{M} w_{o,k}\, r(k)}{\left|1 - \sum_{k=1}^{M} w_{o,k}\, \mathrm{e}^{-j\,2\omega,k}\right|^2} \tag{6.42}$$

The numerator may be recognized as $P_M = r(0) - \boldsymbol{r}^H \boldsymbol{w}_o$ for the optimum set of coefficients, hence Equation 6.42 may be written as:

$$SM(\omega) = \frac{P_M}{\left|1 - \sum_{k=1}^{M} w_{o,k}\, \mathrm{e}^{-j\,\omega,k}\right|^2} \tag{6.43}$$

Now the linear prediction spectrum has been found. Its maximum will be for the value of ω that minimizes the denominator of Equation 6.43, since the numerator is a constant.

In this context is known that there is only one frequency component in the interval of interest. Finding this value could be done by simply searching the interval from one end to the other. This was the approach that was initially tried. But, as one may expect, this will be a very slow process. Instead could be exploited that, in fact, there is only one maximum. In [Jespersen, 1994] was assumed that for a narrow interval, the frequency spectrum could be described by a second order model. Hence from three points of the estimate of the spectrum, the maximum could be calculated.
This approach was implemented and substantial calculational savings were achieved.

At this point the frequency estimation algorithm did not perform satisfactory. Around changes of state of the input signal, the estimate gave a start, so to speak.
The problem was located to the way the filter coefficients were updated. The estimation was carried out by use of an LMS–estimator.
LMS–estimation is thoroughly treated in the literature, e.g. [Haykin, 1991], and will not be described here.

The modification to the LMS–algorithm, developed during the work that is documented in [Jespersen, 1994], leads to an algorithm that could be called the *Truncated LMS–Algorithm*.

In the LMS–algorithm the filter coefficients are updated according to Equation 6.44.

$$\begin{aligned} \widehat{\boldsymbol{w}}(n+1) &= \widehat{\boldsymbol{w}}(n) + \mu\,\boldsymbol{u}(n)\,\varepsilon(n) \\ &= \widehat{\boldsymbol{w}}(n) + \Delta\boldsymbol{w}(n) \end{aligned} \tag{6.44}$$

The modification lies in imposing a limit to $\Delta\boldsymbol{w}(n)$ of the *Normalized LMS*–algorithm.

$$\Delta\boldsymbol{w}(n) = \mathrm{sign}(\varepsilon(n))\, \min\left(|\varepsilon(n)|\,\mu, \Delta w_{max}\right) \frac{\boldsymbol{u}(n)}{\|\,\boldsymbol{u}(n)\,\|_2} \tag{6.45}$$

The initial implementation of the frequency estimator and the estimator based on the truncated normalized LMS–algorithm were run on the signal in Figure 6.13. In Figures 6.14 and 6.15 are seen the estimates of the frequencies.

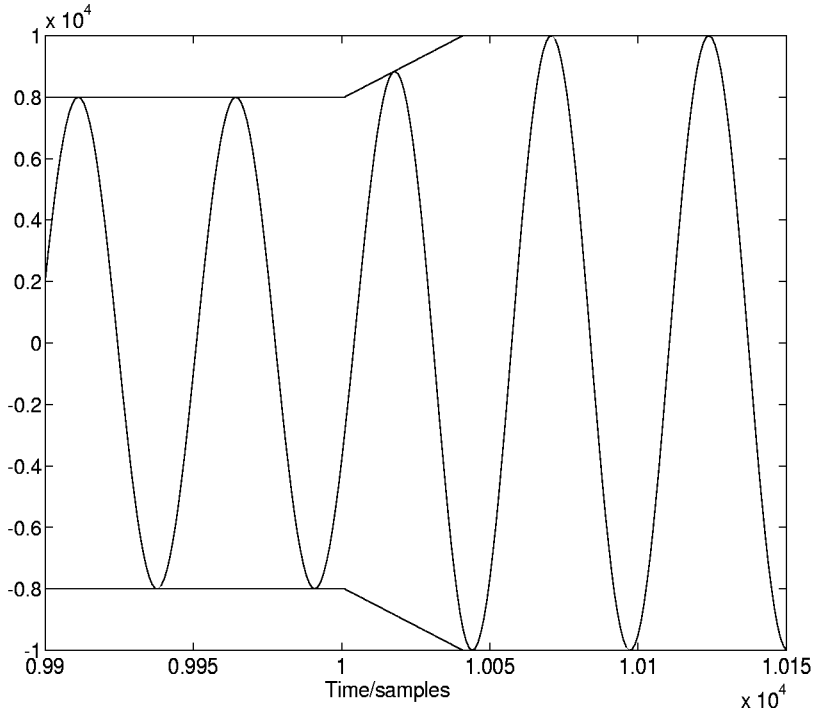

Figure 6.13: Test Signal Used to Evaluate the Frequency Estimation Algorithms. See Figures 6.14 and 6.15.

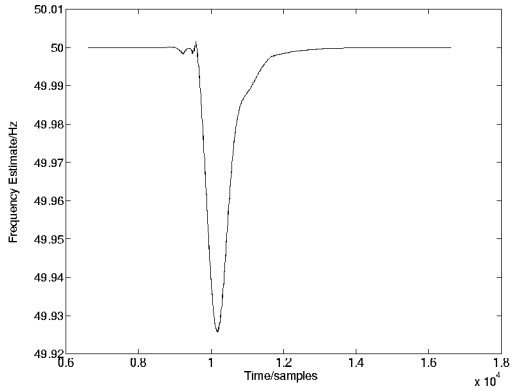

Figure 6.14: Frequency Estimate Based on the LMS–Algorithm.

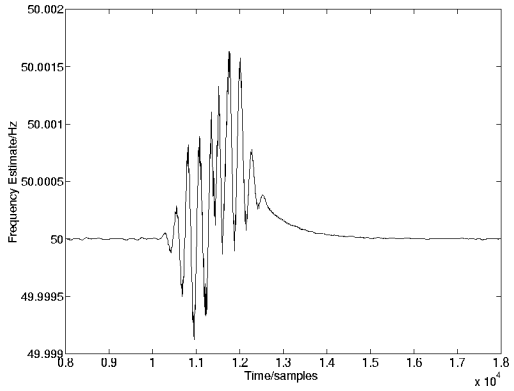

Figure 6.15: Frequency Estimate Based on the Truncated Normalized LMS–Algorithm. $M = 4$, $\mu = 2 \cdot 10^{-6}$ and $\Delta w_{max} = 10^{-5}$.

The truncated algorithm clearly yields a better result than the initial approach.

So far, the frequency of the fundamental component has been the target. For future use of the system it may become important to be able to track other frequencies, e.g. the frequencies of harmonics.

It may be considered to enhance the way the maximum is located. Instead of using only three points, it could be considered to calculate the estimate as a **L**east **S**quares, estimate, based on more points, see Appendix D.

A least squares estimator has been implemented in the DSP–implementation project that is described in [Lauritsen, 1995]. The experience from that work is that for the fundamental component nothing is gained, compared to the estimate based on three points of the linear prediction spectrum.
It is still to be shown whether LS–estimates give better results for other frequency components.

6.5.3 Symmetrical Components

When loaded symmetrically, voltages and currents of the three phase electrical system, will also be symmetrical. Thus knowledge about the current of one phase gives precise knowledge about the currents in the two other phases. There will only be a phase difference of 120°:

$$\begin{pmatrix} U_R \\ U_S \\ U_T \end{pmatrix} = \begin{pmatrix} Z & Z_m & Z_m \\ Z_m & Z & Z_m \\ Z_m & Z_m & Z \end{pmatrix} \cdot \begin{pmatrix} e^{j\,\omega\,t} \\ e^{j(\omega\,t-120°)} \\ e^{j(\omega\,t+120°)} \end{pmatrix} \cdot I_R \tag{6.46}$$

Z_m is the mutual impedance.

The system being perfectly symmetrical is the ideal case.

At transmission level the system may be almost symmetrical, but moving closer and closer to the customers, the load may become more and more unsymmetrical.
Large consumptions must be symmetrical. But the average of small loads is not necessarily symmetrical. Faults may cause temporary unsymmetry.

Symmetrical Components is the name of another representation of the primary quantities. As the name suggests, the representation is symmetrical. The idea is to provide a representation so that again one may perform calculations as is if the system were symmetrical.
In this context symmetrical components are believed to be of interest because they may be straightforwardly calculated from the output of the Kalman filter.

It is believed that the symmetrical components may be an aid for detection and classification, see Section 6.6. Changes to the zero system may be used to verify that an event was a ground fault.

Three new systems are introduced:

0. The *Zero System.*

   This system may be interpreted as a representation of currents and voltages that arise due to connection to ground.

   An example of such a connection is the capacitive coupling to ground.

1. The *Synchronous System.* This system represents the symmetrical fraction of currents and voltages.

   This system will be identical to the currents and voltages one may measure if the system were perfectly symmetrical.

2. The *Inverse System.*

   This system may be interpreted as a representation of currents and voltages that arise due to unsymmetries in the network.

   An example is a load connected between two phases only.

The transformation between phase values and symmetrical components is done according to Equation 6.47:

$$\boldsymbol{x} = \begin{pmatrix} \boldsymbol{S} & \boldsymbol{0} \\ \boldsymbol{0} & \boldsymbol{S} \end{pmatrix} \boldsymbol{x}_{symm.} \tag{6.47}$$

$\boldsymbol{x}$ is the complex representation of the measurements described on page 8.
The matrix $\boldsymbol{S}$ is the transformation matrix:

$$\boldsymbol{S} = \begin{pmatrix} 1 & 1 & 1 \\ a^2 & a & 1 \\ a & a^2 & 1 \end{pmatrix} \tag{6.48}$$

$$a = e^{j\frac{2}{3}\pi} \tag{6.49}$$

The inverse transformation is:

$$\boldsymbol{x}_{symm.} = \begin{pmatrix} \boldsymbol{S}^{-1} & \boldsymbol{0} \\ \boldsymbol{0} & \boldsymbol{S}^{-1} \end{pmatrix} \boldsymbol{x} \tag{6.50}$$

$$\boldsymbol{S}^{-1} = \frac{1}{3}\boldsymbol{S}^{H} = \frac{1}{3}\begin{pmatrix} 1 & a & a^2 \\ 1 & a^2 & a \\ 1 & 1 & 1 \end{pmatrix} \tag{6.51}$$

H denotes Hermitian transposition.

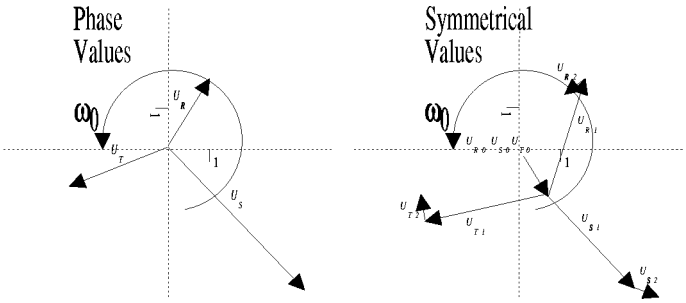

Figure 6.16: Decomposition into Symmetrical Components.

It is customary only to show the symmetrical representation of one phase. The other two only differ by the phase difference of 120°.
The full representation of Equation 6.50 would be:

$$\begin{pmatrix} \boldsymbol{x}_{symm.,R} & \boldsymbol{x}_{symm.,S} & \boldsymbol{x}_{symm.,T} \end{pmatrix} = \begin{pmatrix} \boldsymbol{S}^{-1} & \boldsymbol{0} \\ \boldsymbol{0} & \boldsymbol{S}^{-1} \end{pmatrix} \boldsymbol{x} \begin{pmatrix} 1 & a & a^2 \end{pmatrix} \tag{6.52}$$

6.6 Detection of Events

The detection of a signal basically covers the testing of two hypotheses against each other:

0. Signal absent.
1. Signal present.

In this context *signal present* covers the term *event*.
A well-know signal detector is a simple test against a threshold:

$$\begin{array}{lcl} d(n) & \overset{\text{yes}}{>} & threshold \\ & \vee & \\ d(n) & \overset{\text{no}}{<} & threshold \end{array} \tag{6.53}$$

Detection of signals in noise is a well-treated subject in the literature, e.g. [Lee and Messerschmitt, 1988] and [Gardner, 1988].

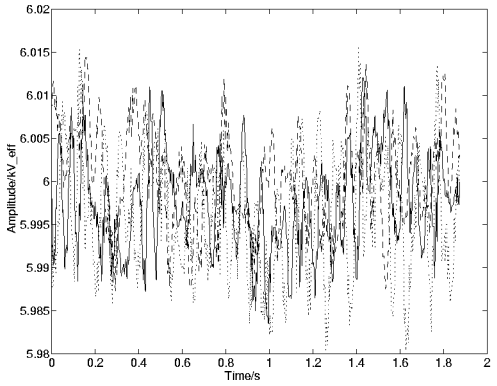

Figure 6.17: Kalman Filter Amplitude Estimate of Voltages During the Starting of the 90kW Machine at the Factory.

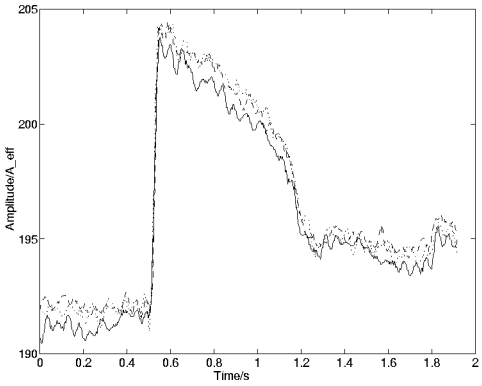

Figure 6.18: Kalman Filter Amplitude Estimate of Currents During the Starting of the 90kW Machine at the Factory.

The signal-in-noise model is only appropriate in this context after some abstraction from what ordinarily is thought of, when talking about noise.

It has been shown that the bandwidth of currents of the Stage 2 Measurements is about 6,5kHz. For voltages it is has been shown that higher frequency components are present, see the discussion on page 43.

As seen on Figures 6.2 and 6.3 the spectrum does not resemble noise, but rather the spectrum is a line spectrum. The contents are gathered around discrete frequencies, namely the harmonics.
As previously discussed, the fundamental component is significantly stronger than the rest of the components, at the same time it is also this component that will be most significantly affected by a change of state. The fundamental component exhibits two characteristics; it contains both the signal to be detected, and at the same time it acts as "noise".

With the Kalman filter in place it would seem sensible to investigate how events may be detected on the basis of the estimated amplitudes.
The symmetrical components may offer important additional information that could substantiate the detection. At the end of this section it is investigated how the symmetrical components behave around the event.

The amplitude estimate may look as shown in Figures 6.17 and 6.18.
Obviously, it will be difficult to detect using the voltages. Therefore is focused on the the fundamental component of the currents as the source of information on the occurrence of events.

On Figure 6.18 it looks as if the amplitude jumps to the peak value almost instantaneously. Taking a closer look, one realizes that the slope is finitely steep. On the basis of this a detection scheme according to Equation 6.54 seems reasonable.

$$d(n) = A(n) - A(n-p) \tag{6.54}$$

$A(n)$ is the amplitude estimate of a phase current.

The span defined by p must be tuned according to the nature of the events that may be encountered on the feeder.
In [Jespersen, 1994] a detector, according to Equation 6.54, was used on the events originating from the operation of the aforementioned 90kW machine.
To detect the starting of the machine $p = 8$ was found to be a good value[1].

On Figure 6.18 is seen fluctuations of the amplitude estimate. It was found that for weaker events these might cause malfunction of the detector, i.e. *no alarm*, when, in fact, an event has occurred.

To suppress these fluctuations one might consider filtering the amplitude estimate with a lowpass filter. This would indeed be a means of getting rid of the fluctuations. Unfortunately, this approach would

[1]Detection is done on the decimated signal. $p = 8$ therefore corresponds to a time span of 8 $\left(\frac{20\text{kHz}}{75}\right)^{-1} = 30\text{ms}$.

also make less apparent changes to the amplitude estimate as the result of an event. Therefore without trying, one may out rule lowpass filters.

Another group of filters, the so-called *median filters*, is well-suited for this problem, see Section 6.6.2.

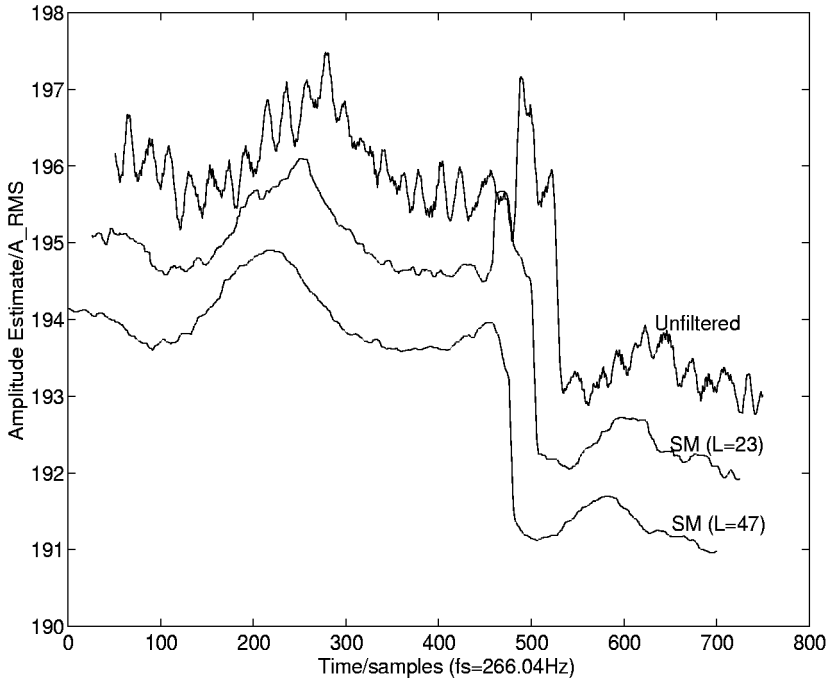

Figure 6.19: Estimate of Current Amplitude before and After Median Filtering. The Curves of the Two Filtered Versions are moved $1A_{RMS}$ and $2A_{RMS}$ Respectively and 25samples and 50samples Respectively.

In Figure 6.19 the input and the output from two median filters are seen.

The event is the turning off of the machine. This event is much weaker than the turning on. This leads to the assumption that the test quantity $d(n)$ of Equation 6.54 should be compared against two thresholds. One for events that increase the current and another for events that decrease it:

$$d(n) \in [A_-; A_+] \Rightarrow \text{no detection of event} \tag{6.55}$$

$$d(n) \notin [A_-; A_+] \Rightarrow \text{detection of event} \tag{6.56}$$

Now a detector having three parameters, p, A_- and A_+, is defined. In order to use properly this detector it must be investigated how it works as a function of these.

The investigation was based on simulations, where sinusoidals having the envelope, shown in Figure 6.20, were to be detected in a sinusoidal signal with constant amplitude. The amplitude of the "background" signal was $200A_{RMS}$. During one 50Hz period, the event was started at 50 different instants with ΔA and Δt held constant. This was repeated for various values of ΔA and Δt. An estimate of the probability density function for correct result, $P_D(\Delta A, \Delta t)$, was calculated as the number of times the correct result was obtained divided by the number of simulations.

On each of the Figures, 6.21–6.24, is also indicated the probability of false alarm, P_{FA}.

The simulations were performed with $p = 8$ and on *standard median filtered* input signals. The filter length was 23. In [Jespersen, 1994] the choice of these values was investigated, and the above mentioned were found to be adequate, at least for the 90kW motor.

Figures 6.21–6.24 clearly show the tradeoff between obtainable P_D and acceptable P_{FA}.

$d(n)$ calculated from a part of the measurements that contain the start and stop of the 90kW motor is shown in Figure 6.25.

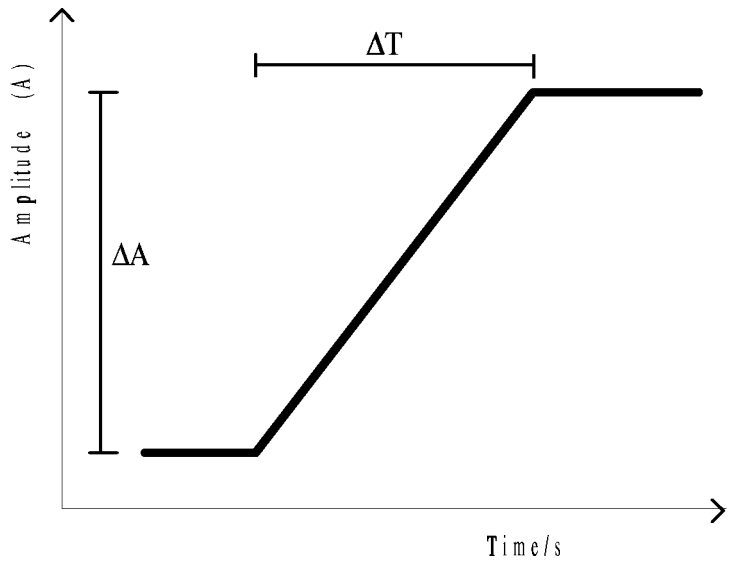

Figure 6.20: Envelope of Event Used for Verification of Detector. The Two Parameters are the Amplitude Difference; ΔA and the Rise Time; Δt.

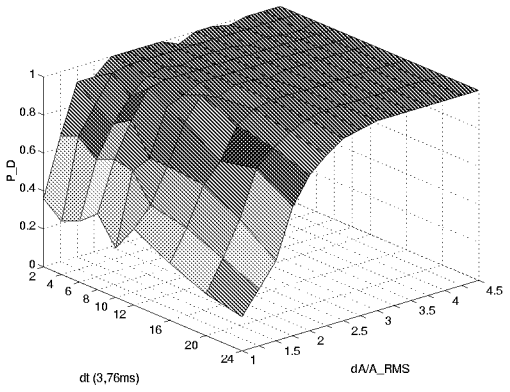

Figure 6.21: $P_D(\Delta A, \Delta t)$ for $\Delta A_+ = 0{,}8\mathrm{A_{RMS}}$. $P_{FA} = 3{,}0 \cdot 10^{-4}$.

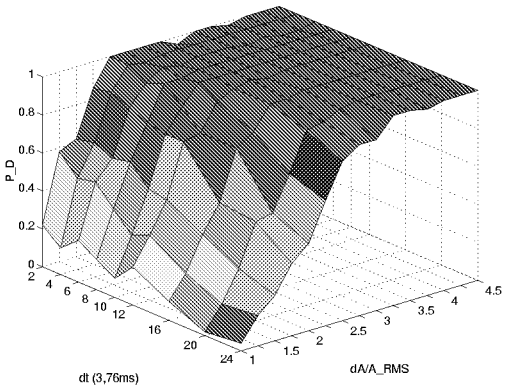

Figure 6.22: $P_D(\Delta A, \Delta t)$ for $\Delta A_+ = 1{,}0\mathrm{A_{RMS}}$. $P_{FA} = 3{,}8 \cdot 10^{-4}$.

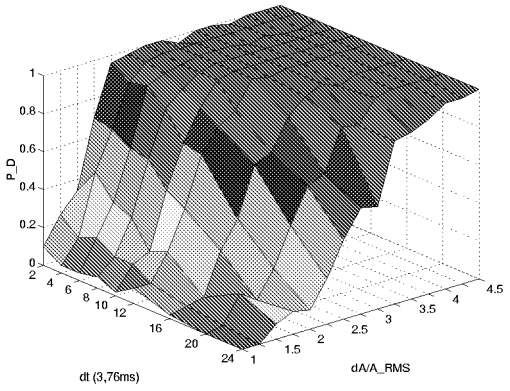

Figure 6.23: $P_D(\Delta A, \Delta t)$ for $\Delta A_+ = 1{,}25\mathrm{A_{RMS}}$. $P_{FA} = 3{,}2 \cdot 10^{-4}$.

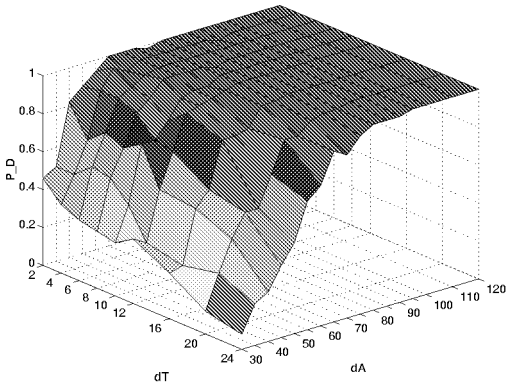

Figure 6.24: $P_D(\Delta A, \Delta t)$ for $\Delta A_+ = 2{,}5\mathrm{A_{RMS}}$. $P_{FA} = 3{,}4 \cdot 10^{-4}$.

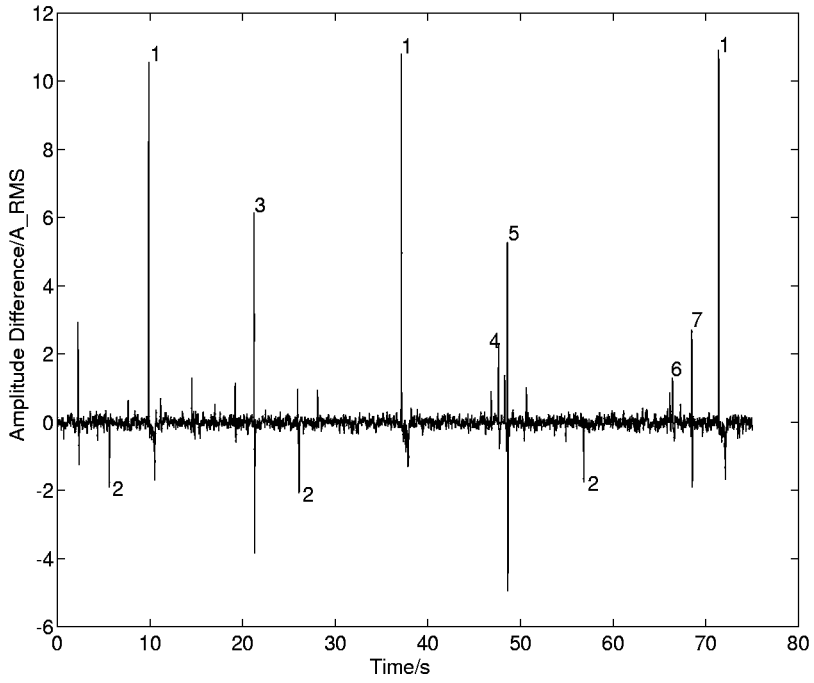

Figure 6.25: Test Quantities During Operation of 90 kW Machine at Factory. Event 1 is Starting of Machine. Event 2 is Stopping. Other Events are Unknown. The Median Filter Length 23 samples. p of Equation 6.54 is 8.

Events in the distribution network may be categorized into three types:

- Events affecting only one phase.
- Events affecting two phases.
- Events affecting all three phases.

This categorization does consider the nature of the event. Also it does not take into account whether or not there is connection to ground.

In Table 6.2 is shown the test quantities in the three categories events may be classified into.

The signal termed "Event" in Figure 5.1 on page 36 actually covers the distinction between these three subcases.

6.6.1 Detection Using the Symmetrical Components

Detection might also be carried out on the basis of the symmetrical components.
For normal events must be expected that only the synchronous and inverse systems will be affected. Faults to ground directly on the feeder will give rise to components in the zero system, whereas faults in the low voltage network cannot cause changes to the zero system, due to the transformers.

In Figure 6.26 is seen the synchronous component of the current during the starting of the 90kW motor. The curve resembles very much that of the phase value, Figure 6.18. In Figure 6.27 is seen that the impact on the inverse and zero systems is very small, though some reaction in the inverse system may be seen.

Type of Event	Test Quantity
Three Phase	$A_{RST}(k) = \frac{1}{3}\left(\text{MED}(\widehat{A_R}(k)) + \text{MED}(\widehat{A_S}(k)) + \text{MED}(\widehat{A_T}(k))\right)$
Two Phase	$A_{RS}(k) = \frac{1}{2}\left(\text{MED}(\widehat{A_R}(k)) + \text{MED}(\widehat{A_S}(k))\right)$ $A_{ST}(k) = \frac{1}{2}\left(\text{MED}(\widehat{A_S}(k)) + \text{MED}(\widehat{A_T}(k))\right)$ $A_{TR}(k) = \frac{1}{2}\left(\text{MED}(\widehat{A_T}(k)) + \text{MED}(\widehat{A_R}(k))\right)$
One Phase	$A_R(k) = \text{MED}(\widehat{A_R}(k))$ $A_S(k) = \text{MED}(\widehat{A_S}(k))$ $A_T(k) = \text{MED}(\widehat{A_T}(k))$

Table 6.2: Test Quantities in the Three Sub Cases. The $\widehat{A}$ Denotes the Amplitude Estimate from the Kalman Filter.

The 90kW motor is such a large load that it must be symmetrical, i.e. load the network equally on all three phases. Therefore it should also be expected that almost nothing should be seen, except in the synchronous system.

Smaller loads are often only connected between phase and zero. On the 10kV side, this will be seen as a load between two phases. In this case the impact on the inverse system should be bigger.

It seems as if detection may be done on the phase values of the currents alone. Instead it is expected that the symmetrical components may contribute important information for classification.

In Section 7.2 is described the result of fitting the models to the events of the two machines.

6.6.2 Median Filtering

Figure 6.19 illustrates what median filters do. They may be designed to track slow changes to the input and at the same time let through steep changes.

The theory of median filters will not be rendered here. Details may be found in [Haavisto *et al.*, 1988], [Gallagher and Wise, 1975], [Heinonen and Neuvo, 1988] and [Öistämö *et al.*, 1992].

These references deal with various methods of finding the median of a given input sequence. Roughly speaking, the desired functionality is to have a filter, that as output, $y(n)$, calculates the median, MED,

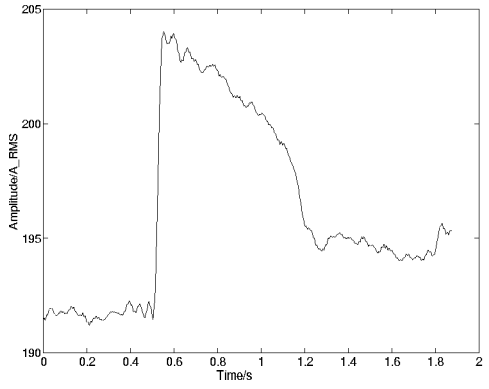

Figure 6.26: Amplitude of Synchronous Sequence Current During the Starting of Motor.

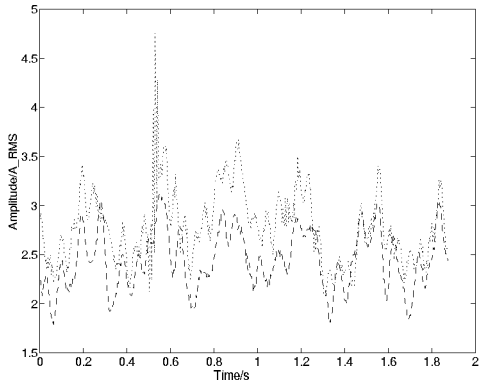

Figure 6.27: Amplitudes of Inverse, $(\cdots)$, and Zero, $(- - -)$, Sequence Currents During Starting of Motor.

from past and future elements of the input, $x(n)$:

$$y(n) = \text{MED}(x(n-k), x(n-k+1), \ldots, x(n), \ldots, x(n+k-1), x(n+k)) \quad (6.57)$$

$$N = 2k+1 \quad (6.58)$$

N is the filter length.

6.7 Classification

Classification will be initiated when an event has been detected.

The DISMO–project is presently at the threshold of entering this problem. So far, only very rudimentary investigations have been made, see Appendix A.

In this section, on the basis of a very simple model, will be shown that it is possible to develop methods that will be able to distinguish events that are much alike.

6.7.1 Simple Method for the Classification of the Two Motors at Dyrup

Besides the 90kW motor, that has already been referred to several times, the 75kW motor is taken into consideration.

These two motors are connected to the same transformer. They are both asynchronous machines. Therefore, they are expected to be very similar.

In Figures 6.18 and 6.19 are shown the amplitude estimates of the currents at the turning on and off of the 90kW machine. This looks almost the same for the 75kW machine.

By inspection the following model of the Kalman filter estimates of the amplitudes is obtained:

The model for start of asynchronous machines at factory:

$$\boldsymbol{\theta}_{on}^T = \begin{pmatrix} t_{1_{on}} & t_{2_{on}} & t_{3_{on}} & \alpha_{1_{on}} & \alpha_{2_{on}} & \alpha_{3_{on}} & \alpha_{4_{on}} \end{pmatrix} \quad (6.59)$$

$$f(t, \boldsymbol{\theta}_{on}) = \begin{cases} \alpha_1 & \text{for } t_{min} \le t < t_1 \\ \alpha_1 + \alpha_2 \frac{t-t_1}{t_2} & \text{for } t_1 \le t < t_1 + t_2 \\ \alpha_1 + \alpha_2 + \alpha_3 \frac{t-(t_1+t_2)}{t_3} + \alpha_4 \left(\frac{t-(t_1+t_2)}{t_3}\right)^2 & \text{for } t_1 + t_2 \le t < t_1 + t_2 + t_3 \\ \alpha_1 + \alpha_2 + \alpha_3 + \alpha_4 & \text{for } t_1 + t_2 + t_3 \le t \le t_{max} \end{cases} \quad (6.60)$$

t_1 denotes the start of the event. t_2 and t_3 do not denote absolute time, but time differences to t_1. The parameter $\alpha_{1_{on}}$ describes the level of the current prior to the event.

The first part of the event is modelled by a straight line. The second part by a second order polynomial.

Model for stop of asynchronous machines at factory:

$$\boldsymbol{\theta}_{off}^T = \begin{pmatrix} t_{1_{off}} & t_{2_{off}} & \alpha_{1_{off}} & \alpha_{2_{off}} \end{pmatrix} \quad (6.61)$$

$$f(t, \boldsymbol{\theta}_{off}) = \begin{cases} \alpha_{1_{off}} & \text{for } t_{min} \le t < t_{1_{off}} \\ \alpha_{1_{off}} + \alpha_{2_{off}} \frac{t-t_{1_{off}}}{t_{2_{off}}} & \text{for } t_{1_{off}} \le t < t_{1_{off}} + t_{2_{off}} \\ \alpha_{1_{off}} + \alpha_{2_{off}} & \text{for } t_{1_{off}} + t_{2_{off}} \le t \le t_{max} \end{cases} \quad (6.62)$$

By a straight line this model connects the level before the event to the level after it.

During the initial investigations, the parameters were LS–estimated, minimizing Equation 6.63, see also page 137.

$$J(\boldsymbol{\theta}_{min}) = \min_{\boldsymbol{\theta}} \sum_{k=1}^{k_{max}} (f(k, \boldsymbol{\theta}) - \boldsymbol{y}_k)\, (f(k, \boldsymbol{\theta}) - \boldsymbol{y}_k)^* \quad (6.63)$$

[Jespersen, 1994] describes this model in detail. An important result was that it makes a big difference whether it is assumed that the parameters are real or complex.

For real parameters it is difficult to distinguish the two machines, whereas they are clearly distinguishable using complex parameters. See Section 7.2.

6.8 Time-Frequency Signal Analysis

Throughout this text it has been stated several times that currents and voltages in the distribution network are not stationary. This fact more or less stamps out the Fast Fourier Transformation as a means of analysis.

Still, analyses in the frequency domain are believed to be crucial for the understanding of distribution networks as a means for the transfer of signals.

In this section is rendered the theory of the *time-frequency*-analysis methods; the STFT and Wavelets transformation.

The **S**hort **T**erm **F**ourier **T**ransform is, as the name indicates, based on the **Fourier Transformation**, see Section 6.8.1.

On the basis of the STFT the fundamentals of Wavelet transformation are rendered, see Section 6.8.2.

6.8.1 Short Term Fast Fourier Transformation

The principle behind its calculation is rather simple. The time-series that one wishes to analyse is divided into subsections by applying a window. Finding the proper window is, in fact, the first one needs to do. Regarding this, the literature gives different recommendations. One may find mention of the *Rectangular Window*, the *Hamming Window*, the *Hanning Window*, the *Gaussian Window* and numerous others. They all exhibit different characteristics. E.g. the main lobe of the *Rectangular Window* is narrower than that of the *Hamming Window*, but the side lobes attain a higher value.

Let $f(t)$ denote the time-series to be analysed, then the standard Fourier transform of this is, (e.g. [Boel Pedersen, 1986]):

$$G(f) = \int_{-\infty}^{\infty} g(t)\, \mathrm{e}^{-j\,2\,\pi\,f\,t} dt \leftrightarrow g(t) = \frac{1}{2\,\pi} \int_{-\infty}^{\infty} G(f)\, \mathrm{e}^{j\,2\,\pi\,f\,t} df \tag{6.64}$$

The transformation would render a kind of "mean" over the entire time axis, thus local deviations from stationarity would be leveled out.

The STFT applies a window to the signal, makes the FT on that window, moves the window and repeats the process until the time-series is exhausted:

$$G(f,\tau) = \int_{-\infty}^{\infty} g(t)\, h^*(t-\tau)\, \mathrm{e}^{-j\,2\,\pi\,f\,t} dt \tag{6.65}$$

Where $h(t)$ is the window function.

In case one uses a *Gaussian Window* the STFT develops into the *Gabor Transformation*.

The Gabor Transformation, when used on real signals, forces a modification of the Gaussian Window. Outside the window on which the FT is calculated, it is assumed that the signal is zero.

This leads to the following pair:

$$h(t) = \begin{cases} \frac{1}{\sigma\sqrt{2\,\pi}}\, \mathrm{e}^{-\frac{1}{2\,\sigma^2}\,t^2}, & |t| \leq \frac{T}{2} \\ 0, & |t| > \frac{T}{2} \end{cases} \tag{6.66}$$

$$\updownarrow \tag{6.67}$$

$$H(f) = 2\,\mathrm{e}^{-2\,f^2\,\pi^2\,\sigma^2} \left(\mathrm{erf}\left(\frac{2\,j\,f\,\pi\,\sigma^2 + \frac{T}{2}}{\sqrt{2}\,\sigma} \right) - \mathrm{erf}\left(\frac{2\,j\,f\,\pi\,\sigma^2 - \frac{T}{2}}{\sqrt{2}\,\sigma} \right) \right) \tag{6.68}$$

erf is the *Error Function*. The Error Function is defined as:

$$\mathrm{erf}(x) = \frac{2}{\sqrt{\pi}} \int_0^x \mathrm{e}^{-u^2} du \tag{6.69}$$

Regardless of the type of window used, a drawback of the STFT using a fixed length window is that as the frequency increases, more and more cycles are included inside the window. Therefore, not all frequencies are treated in the same way.

Name	Time Domain Properties
Rectangular	$h(t) = \begin{cases} 1, & \lvert t\rvert \leq \frac{T}{2} \\ 0, & \lvert t\rvert > \frac{T}{2} \end{cases}$
Hamming	$h(t) = \begin{cases} 0{,}54 - 0{,}46\cos\left(\frac{2\pi t}{T}\right), & \lvert t\rvert \leq \frac{T}{2} \\ 0, & \lvert t\rvert > \frac{T}{2} \end{cases}$
Hanning	$h(t) = \begin{cases} \frac{1}{2}\left(1 - \cos\left(\frac{2\pi t}{T}\right)\right), & \lvert t\rvert \leq \frac{T}{2} \\ 0, & \lvert t\rvert > \frac{T}{2} \end{cases}$
Gaussian	$h(t) = \frac{1}{\sigma\sqrt{2\pi}} e^{-\frac{1}{2\sigma^2}t^2}$

Name	Frequency Domain Properties
Rectangular	$\lvert H(f)\rvert = \frac{\sin(\pi f T)}{\sin(\pi f)}, \quad \lvert f\rvert \leq \frac{1}{2}$
Hamming	$\begin{aligned} \lvert H(f)\rvert = {} & 0{,}54\frac{\sin(\pi f T)}{\sin(\pi f)} + \cdots \\ & \cdots + 0{,}23\frac{\sin\left(\pi T\left(f-\frac{1}{T}\right)\right)}{\sin\left(\pi\left(f-\frac{1}{T}\right)\right)} + \cdots \\ & \cdots + 0{,}23\frac{\sin\left(\pi T\left(f+\frac{1}{T}\right)\right)}{\sin\left(\pi\left(f+\frac{1}{T}\right)\right)}, \qquad \lvert f\rvert \leq \frac{1}{2} \end{aligned}$
Hanning	$\begin{aligned} \lvert H(f)\rvert = {} & \frac{1}{2}\frac{\sin(\pi f T)}{\sin(\pi f)} + \cdots \\ & \cdots + \frac{1}{4}\frac{\sin\left(\pi T\left(f-\frac{1}{T}\right)\right)}{\sin\left(\pi\left(f-\frac{1}{T}\right)\right)} + \cdots \\ & \cdots + \frac{1}{4}\frac{\sin\left(\pi T\left(f+\frac{1}{T}\right)\right)}{\sin\left(\pi\left(f+\frac{1}{T}\right)\right)}, \qquad \lvert f\rvert \leq \frac{1}{2} \end{aligned}$
Gaussian	$H(f) = e^{-2f^2\pi^2\sigma^2}$

Table 6.3: Example of Some Window Functions.

The STFT will not give good time– and frequency resolution simultaneously. This is a consequence of the uncertainty principle:

$$\Delta t\,\Delta f \geq \frac{1}{4\pi} \tag{6.70}$$

Applying the Gaussian Window makes Equation 6.70 assume equality.

An expansion of the STFT in order to exploit better the available resolution is the so-called *Wavelet Transformation*. For more on *Wavelets* see Section 6.8.2.

The initial analysis shown in Chapter 7 was performed using the STFT with the *Hanning Window*. On the plots on pages 75–93 are indicated both the length of the window, in points, and the number of samples the window was moved between FFT's.

6.8.2 Wavelet Transformation

The *Wavelet Transformation* may be regarded as another kind of STFT. The difference lies in the use of a another kernel than the one used for the Fourier Transform. Instead of the "normal" $e^{-j\,2\pi f\,t}$ one might use something like:

$$e^{-\frac{t^2}{2}+j(2\pi f+m)\,t} \tag{6.71}$$

Hence the modification lies in the use of a complex valued window.

The Wavelet Transformation exhibits constant relative bandwidth, as opposed to Fourier Transformation that exhibits constant bandwidth.

For a window to be used in *Wavelet Transformation*, some requirements must/should be fulfilled:

- $\int \frac{H(f)}{|f|} df < \infty$
  This implies that if $H(f)$ is smooth in the neighbourhood of the frequency origin then $H(0) = 0$, i.e. there is no DC component in $h(t)$.
- $h(t)$ should be concentrated in time.
- $H(f)$ should be concentrated in frequency.

The two latter items show that the time-bandwidth product should be as small as possible. As stated, the smallest time-bandwidth product is achieved by the Gaussian function:

$$h_1(t) = \mathrm{e}^{-\frac{t^2}{2} + j\,\omega\,t} \tag{6.72}$$

This function is used to give the kernel shown in Equation 6.71. Other references assign the second derivative of a Gaussian:

$$h_2(t) = \left(1 - t^2\right) \mathrm{e}^{\frac{t^2}{2}} \tag{6.73}$$

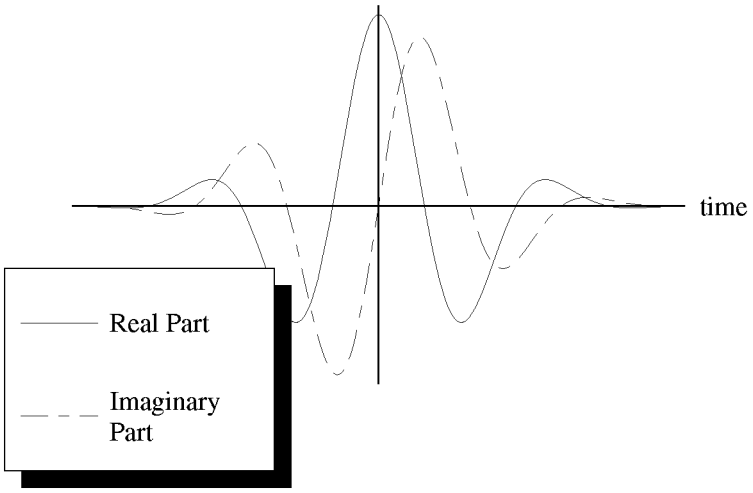

Figure 6.28: Real and Imaginary Parts of Gaussian Mother Wavelet of Equation 6.72.

The choice of "window function" is called the *Mother Wavelet*. This window function is shifted and scaled into *Daughter Wavelets*:

$$h'(t, a, b) = \frac{1}{\sqrt{a}}\, h\left(\frac{t - b}{a}\right) \tag{6.74}$$

Using this window function we get:

$$W(a, b) = \int h'^{*}(t, a, b)\, g(t)\, dt \tag{6.75}$$

W denotes the STFT using a window that fulfils the Wavelet requirements.
The inverse transformation is:

$$g(t) = \frac{1}{\int \frac{1}{|w|} |h(w)|^2\, dw} \iint W(a, b)\, \frac{1}{\sqrt{a}}\, h\left(\frac{t - b}{a}\right) \frac{da\, db}{a^2} \tag{6.76}$$

The Wavelet Transformation is characterized by applying different resolution at different frequencies, hence it does not suffer from some of the "inconveniencies" of the STFT.

For the Wavelet Transformation to be used on a digital computer, it is necessary to expand the transformation further. [Rioul and Vetterli, 1991] discusses two discrete time approaches; the *subband coding analysis* and the *pyramidal coding analysis.*

Details about the *Wavelet Transformation* and some of its applications in power engineering may also be found in the following references:

> [Tuteur, 1992], [Ribeiro, 1994a, Ribeiro, 1994b], [Akansu and Haddad, 1992], [Young, 1993], [Daubechies, 1987], [Cody, 1992], [Chui, 1992], [Ruskai *et al.*, 1992], [Robertson *et al.*, 1994].

Work on Wavelets used in the context of centralized monitoring is a topic of on-going research, see e.g. [Nielsen, 1995].

6.9 Future Elements of Monitoring System

In this chapter different signal processing methods are descibed that have either been implemented in the system simulator, or that have been used to gain insight into the nature of the physical system, the distribution network, that is to be monitored.

It was claimed that a method for the detection of events may be created. It was also claimed that models may be defined, and parameters extracted, so that two similar events may be distinguished. The results from using these methods are shown in Chapter 7.

At this stage of the work on centralized monitoring, very little work has been made on investigating methods for classifying events, once they have been detected.
The work has been carried to the brink of investigations on the Wavelet transformation as part of the classification system. It is believed that Wavelet analysis may contribute important information to the classifying system.

Wavelet transformation or similar approaches will be the first line of the classification system. Their results will be sent further into the system, where interpretation is to take place.
Methods like *Fuzzy Logic* or *Neural Networks* could be used as part of the classification system. It would have been very interesting, had it been possible to try out some of these methods at this stage, see also the discussion in Section 8.3.1.

Intuitively it seems clear that methods belonging to the above-mentioned could be suitable for this purpose. When an event is detected, it will probably be possible to classify it into several possibilities. Combining these possibilities with other known information such as; the time of the day or year, temperature, *instantaneous topology* of the network, current level before, during, and after the event, and so on, may be used to determine which of the possibilities that are more likely than others.

The DISMO–project has only been concerned with the monitoring of one feeder. It must be investigated how many feeders may be monitored by one computer. To this end comes also investigations on the asset by being able to look into several feeders at the same time.
One could imagine that a fault that causes very high currents at the substation that may cause the relays to interrupt all the supply to the feeders, could be classified into affecting only one feeder, so that supply quickly could be reestablished to the unaffected feeders.

This latter problem opens for a completely new line of investigations that breaks fundamentally with the ideas that have been worked with so far. Namely the DISMO–concept as a method for distribution network **protection**.
Until now it has been assumed that plenty of time was available to analyse events. But if instead it is assumed that the DISMO–system should **also** trip circuit breakers, much will be different.

Chapter 7

Analysis of Measurements

In this chapter the results of the three sets of measurements are analysed.

The analysis is based on the theory that is rendered in Chapter 6.

Since this was the first time analysis of this kind was performed, the principle of analysis has been based on an "eyes-wide-open" approach. I.e. poking about in the measurements has drawn the attention towards aspects that were unknown as the investigation started.
This chapter is intended to give a kind of verbatim account on what may be seen in the measurements.

As the analysis progresses it is emphasized what the impact one set of measurements had on the preparations for the next.

Not much is to be said about the Stage 0–Measurements. No real analysis was made. But the measurements made it clear what where the weak points of the existing measuring system. E.g. the necessity of installing new voltage sensors that could measure the phase to ground values.
Still some wee attempts were made to have closer looks at the residual signal after having removed the fundamental component, see Section 7.1.

During the post-processing of the Stage 0–Measurements it became clear that MATLAB version 3.5 not really was suited for the analysis of data in such amounts as had been recorded. Even with a sampling frequency of only 2,66kHz one could not load and perform calculations on anything but small subsections of the signals.
The program `SH-GR` was written to have an efficient means for browsing through the measurements, see Appendix I.
Later on came version 4 of MATLAB that offers the possibility of random file access.

`SH-GR` was used to go through all the signals. The number of significant events was not very big. This, combined with the fact that all events were unknown, lead to that two measuring points were established for the Stage 1 Measurements, as well as events were made to happen at known instants.
In Chapter 4 was explained the choice of equipment.

From the processing of the Stage 0 Measurements was learned that something had to be done to counteract the drifting of the signals of the six A/D–conversions. But at the time of the Stage 1 Measurements only the same A/D–equipment was available. Instead the signals were post-synchronized using the time signal that was recorded on the one channel.
The work is described in [Jespersen, 1994]. It turned out that the process was extremely time consuming. Therefore only the measurements taken at the substation were synchronized.

It must be realized that the process of synchronization is in fact filtering of the signals. Therefore the wave forms of the signals may have been altered.

These measurements were still with low bandwidth. Therefore it was decided that until the Stage 2 Measurements had been taken, analysis should be restricted to the low frequencies, around 50Hz. However, this is only one side of the motivation for doing so. As has previously been mentioned, the electricity distribution system is conceived to transfer energy at 50Hz. Therefore it seems reasonable to start analyses around this frequency and later, based on the experiences from this work, the analyses may be extended to other frequencies.

In Section 6.6 is described a detection scheme that was developed on the basis of events from the two asynchronous machines at the factory.

The detector was run on the entire sequence, measured at the *OP*, containing starts and stops of the two motors. Comparing the time stamps to the instants where it was known that events should occur, the provoked events were found in the measurements.

Figure 6.2 on page 58 shows other significant events that are unknown. These were avoided and the analysis was focused on the known events.

Both start and stop are transmitted to the *OP* as significant events.

Figure 6.18 on page 54 and Figure 6.19 on page 55 show the Kalman filter estimates of the amplitudes around the two main events connected to the operation of the machines at the factory.

7.1 Auto- and Cross-Correlations of Residual Signals from Stage 0 Measurements

On the residual signal from the measurements taken at 10:30 on the 9^{th} of February 1993, the cross- and auto-correlation functions were estimated using the `xcorr` of the MATLAB SIGNAL PROCESSING TOOLBOX, see [Little and Shure, 1993]. This function calculates the estimate as:

$$c(k) = \eta(k) \sum_{n=0}^{N-|k|-1} x(n)\, y^*(n+k) \tag{7.1}$$

Where $\eta(n)$ may be chosen to be one of the following three possibilities:

$$\eta_1(k) = 1, \text{ no normalization.} \tag{7.2}$$

$$\eta_2(k) = \frac{1}{N}, \text{ biased estimate.} \tag{7.3}$$

$$\eta_3(k) = \frac{1}{N-|k|}, \text{ unbiased estimate.} \tag{7.4}$$

The investigation was carried through using the *unbiased estimate*.

No significant events occurred during the sequences used for this investigation.

It turned out that this investigation was very little informative, so only a few examples are rendered here.

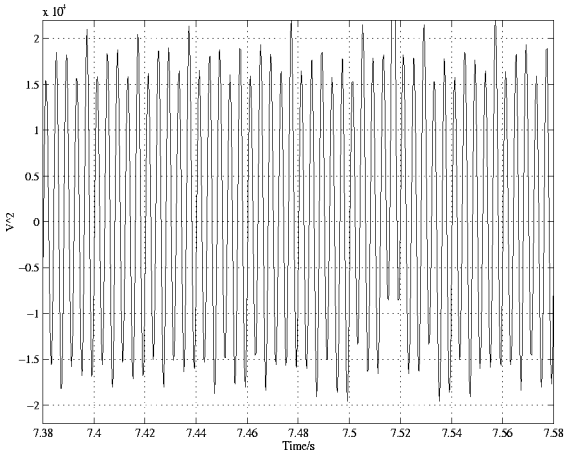

Figure 7.1: Auto-Correlation Function of Residual Part of Phase to Phase Voltage.

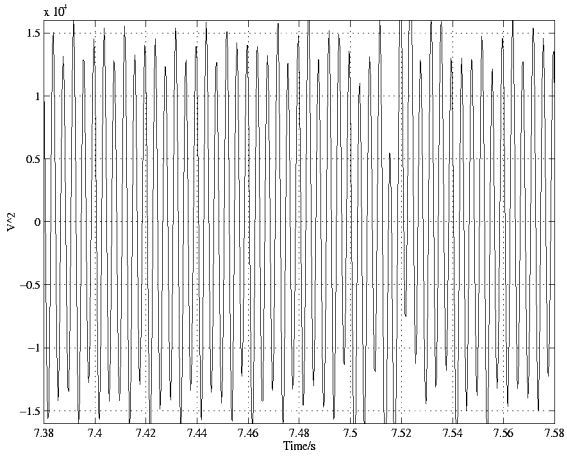

Figure 7.2: Cross-Correlation Function of Residual Part of Phase to Phase Voltage.

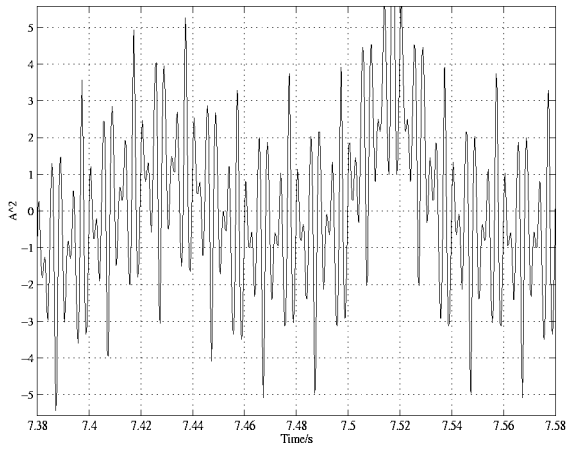

Figure 7.3: Auto-Correlation Function of Residual Part of Current.

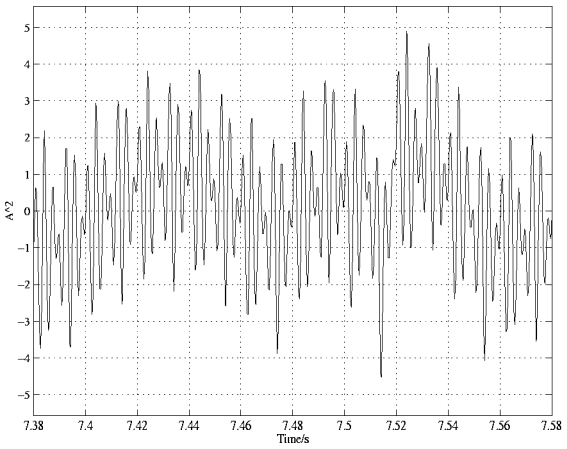

Figure 7.4: Cross-Correlation Function of Residual Part of Current.

Harmonics account, in part, for the uselessness of this investigation.
In order to make such an analysis interesting, it must therefore be concluded that the stronger harmonics must be suppressed.

7.2 Classification of Events Using Fundamental Frequency Information

With the Stage 1 Measurements came signals originating from known events. The first question was if it were possible to find these in the measurements.
In Figure 7.5 and 7.6 is shown the voltage and current of one phase during the starting of the 90kW motor.

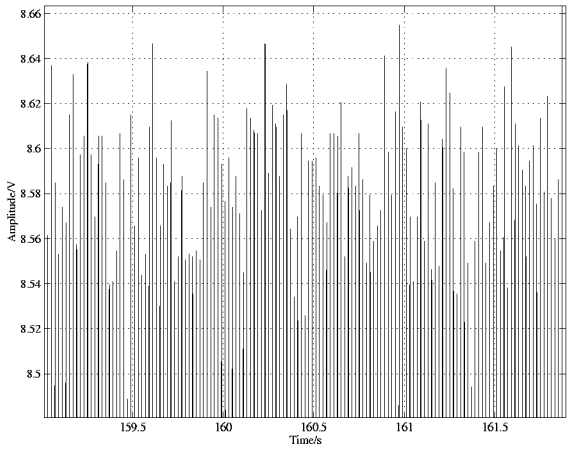

Figure 7.5: Voltage During Turning On of 90kW Machine.

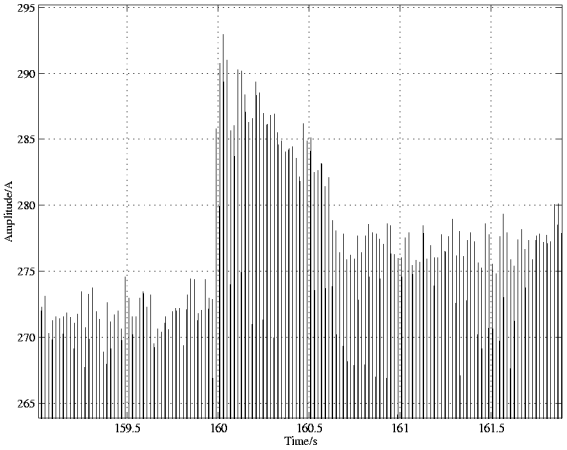

Figure 7.6: Current During Turning On of 90kW Machine.

Based on the models shown in Equation 6.60 on page 59 and Equation 6.62 the parameters were estimated for a number of events.

As these events were known to be symmetrical, the average of the currents of the three phases was calculated. This approach should suppress noise in the signals.

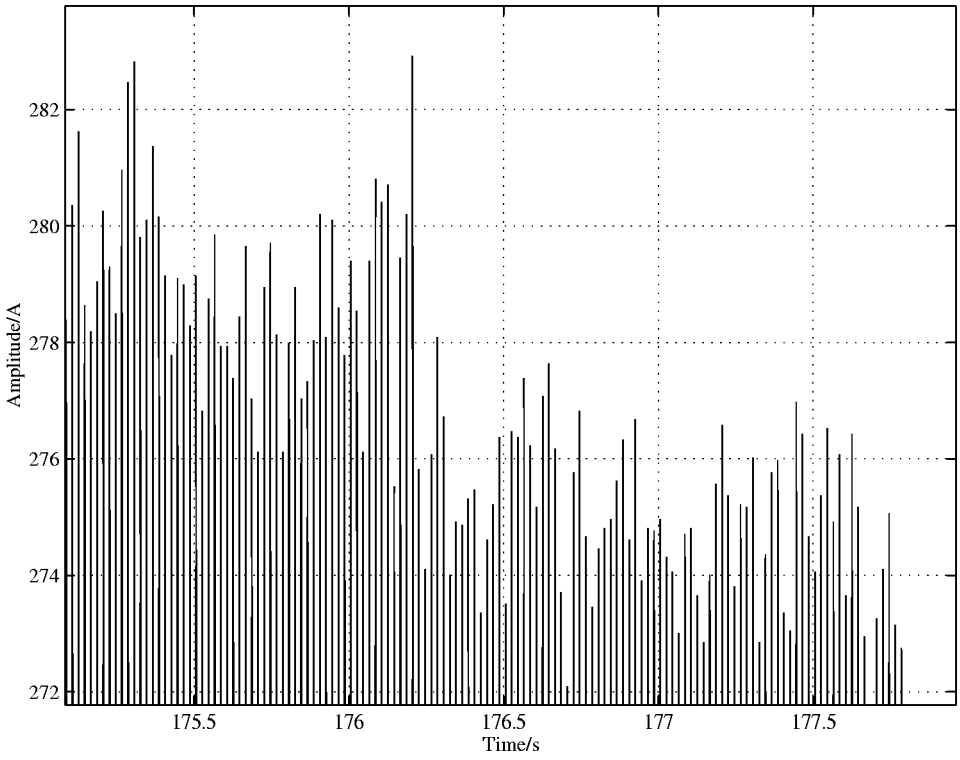

Figure 7.7: Current During Turning Off of 90kW Machine.

However, for non-symmetrical events, parameter sets for each phase must be defined, whereby the number of parameters will increase.

The method that was used to estimate the parameters was based on the `constr` routine of the MATLAB OPTIMIZATION TOOLBOX, see [Grace, 1993]. This function finds the minimum of constrained multivariable functions.

In Section 6.7 was mentioned that complex parameters made the two events more distinguishable than real parameters. Here a closer look is taken on the differences between the two ways of modelling the events.

The model based on real parameters only uses information contained in the amplitude estimates from the Kalman filter, whereas the model based on complex parameters also uses the phase information.
The complex parameter model is also more *complex*, i.e. moving from the real description to the complex, does in fact correspond to increasing the number of parameters.

What must be expected from a satisfactory model, is that it may be able to distinguish events that are much alike, without being identical. The two motors at the factory is a good example of this. The result of the investigation is therefore an indication of whether it would be possible to arrive at a method that exhibit this quality.
At this stage it is not expected to assign the "final" method.

Estimating parameters of multi dimensional spaces lead to the problem of finding the global minimum. Frequently one may experience that the method converges to local minima. Suitable methods therefore must be capable of continuing the search of minima, even though one minimum has been found.
This investigation has accommodated this requirement by human interaction. This is acceptable at this stage but it is not satisfactory for methods to be implemented into an automated monitoring system.

Table 7.1 shows the parameters assuming a real model.

In Table 7.2 the same parameters are shown, but under the assumption of a complex model.

The real parameter model distinguishes nicely between turning on of the two motors. But for the turning off there is no significant difference. Using the complex parameters, α_2 is clearly different.

	t_2	t_3	α_2	α_3	α_4
90kW (on)	6,27	197,13	11,535	-1,872	-0,300
	5,35	217,94	10,646	-2,017	-0,346
	6,21	223,49	11,859	-2,122	-0,303
75kW (on)	6,34	76,02	35,078	-7,243	-0,981
	6,47	72,75	36,392	-7,430	-0,957
	6,26	74,74	34,752	-7,470	-0,965
	6,47	74,36	36,235	-7,622	-0,998
	6,17	67,17	33,318	-7,038	-0,887
	6,43	73,40	35,693	-7,786	-0,905
	5,93	77,26	35,012	-7,531	-1,037
	6,86	73,77	39,071	-7,658	-1,006
90kW (off)	7,80	—	-2,350	—	—
	7,07	—	-2,551	—	—
	9,24	—	-2,513	—	—
75kW (off)	11,91	—	-2,818	—	—
	8,43	—	-2,858	—	—
	6,68	—	-2,127	—	—

Table 7.1: Estimated Real Parameters of Known Events.

	t_2	t_3	α_2	α_3	α_4
90kW (on)	6,12	201,65	12,675∠5,114°	2,205∠−179,813°	0,406∠160,895°
	5,20	211,24	11,358∠5,599°	2,076∠−174,401°	0,554∠161,610°
	6,02	219,51	12,814∠6,373°	2,253∠−173,374°	0,493∠159,331°
75kW (on)	6,27	79,92	39,247∠4,807°	8,144∠−169,219°	1,086∠160,755°
	6,37	77,23	40,590∠4,959°	8,446∠−170,264°	1,000∠159,466°
	6,62	76,70	38,666∠4,125°	8,245∠−170,514°	0,956∠174,027°
	6,52	76,94	40,260∠3,413°	8,493∠−172,688°	0,992∠172,696°
	6,69	73,35	37,604∠6,522°	8,251∠−167,333°	0,717∠156,841°
	6,80	85,92	41,236∠6,564°	9,860∠−169,982°	0,749∠128,827°
	6,33	80,21	39,659∠3,815°	8,600∠−172,068°	0,950∠177,023°
	6,97	76,77	43,405∠5,955°	8,776∠−172,749°	0,951∠172,912°
90kW (off)	20,00	—	2,714∠179,585°	—	—
	7,02	—	2,630∠−165,502°	—	—
	9,75	—	2,604∠−165,632°	—	—
75kW (off)	17,82	—	3,844∠166,913°	—	—
	8,81	—	4,040∠163,801°	—	—
	12,33	—	4,040∠151,465°	—	—

Table 7.2: Estimated Complex Parameters of Known Events.

In [Jespersen, 1994] the two models were fitted to almost about every event that could be detected with the detection limits fixed at $A_- = 1{,}0\text{A}$ and $A_+ = 1{,}5\text{A}$. Here this investigation will not be rendered. It is sufficient to notice that it was possible to assign a method that could extract parameters that are clearly different for different events.
This result is of the utmost importance for the future work on the DISMO–idea. This is discussed in Chapter 8.

Because the Stage 1 Measurements had limited bandwidth no real attempt to see the impact of events on the higher frequencies was made. Such investigations were performed on the Stage 2 Measurements only, see Section 7.3.2.

7.3 Waveforms of Stage 2 Measurements During the Burning Out of Fuses

The events of the experiments performed during the Stage 1 Measurements may be regarded as being slow, compared to the burning out of fuses due to a short circuit.

Quite as expected, at the substation, the impact of burning out of low-voltage fuses was very significant.

By visual inspection, only the currents seem to be affected by these events.

The increase of the currents corresponds quite well to the estimates that were calculated on page 33.

It is interesting to notice that all three currents seem more affected during the two phase burning out than during the three phase burning out.
The explanation to this is believed to be that the short circuit was established at different instants during the 50Hz period.

No attempt was made to create a model, as the ones described on page 59, due to the unfitness for automated analysis of that method.
Instead was performed time-frequency analyses of both the fundamental- and the residual components.

The components were separated according to Figure 6.5 on page 42.

7.3.1 Fundamental Component Analysis of Measurements from Burning Out of Fuses

The fundamental frequency analysis was carried through on the estimates from the Kalman filter. The voltage of phase R was chosen as the reference for phase measures.
The complex phase impedance was estimated as the ratio between the complex voltage and the complex current.

This investigation reveals a very interesting result. The voltages are affected by these events.
A voltage drop of some Volts, compared to tens of kiloVolts, does not sound of much. But it is so much that it can be seen! See Figures 7.14–7.16.

For the one phase burning out, is noticed that one phase is completely unaffected. Whereas for both two and three phase burning out, all phases are affected. This must be so due to the transformer. It is a ΔY–coupled transformer.

Comparing the amplitudes of all six fundamental components of the two and three phase burning out, shows that no significant difference can be observed, that would make one capable on this basis to distinguish between the to kinds of events.

7.3.2 Residual Component Analysis of Measurements from Burning Out of Fuses

It was expected that these events would cause high frequencies, even though the signals first had to pass the distribution transformer.

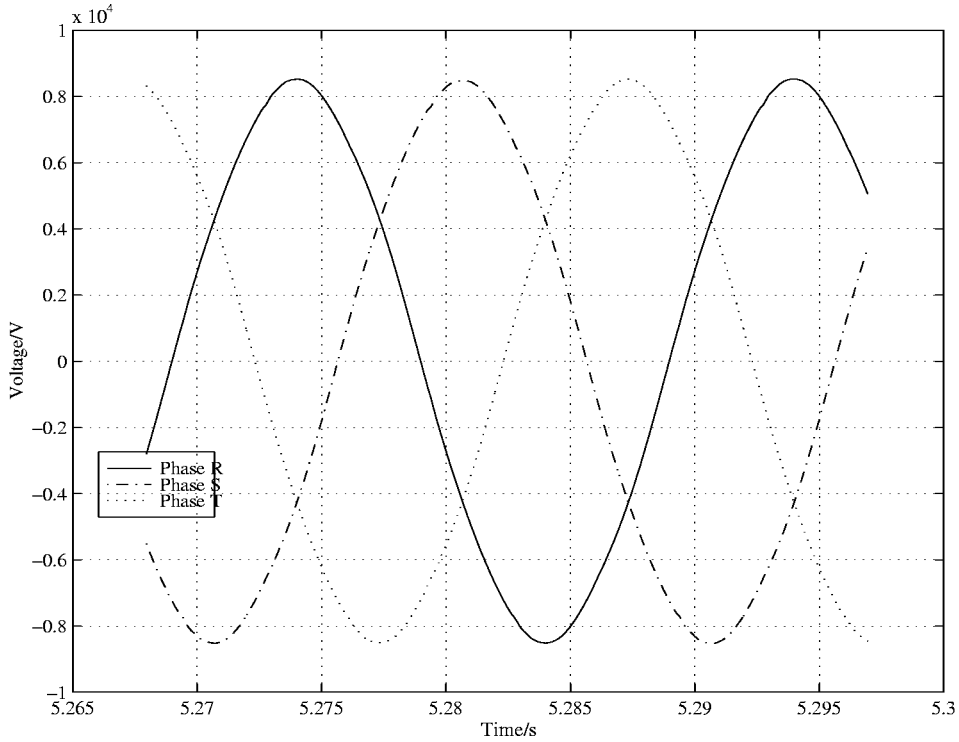

Figure 7.8: Voltages During One Phase Fuse Burning Out.

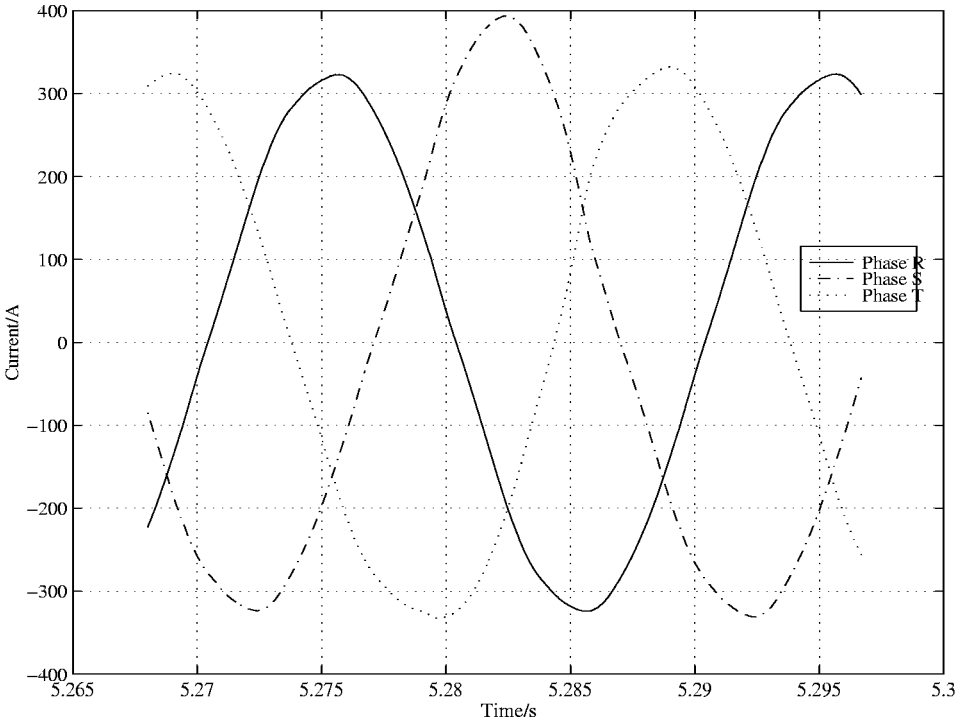

Figure 7.9: Currents During One Phase Fuse Burning Out.

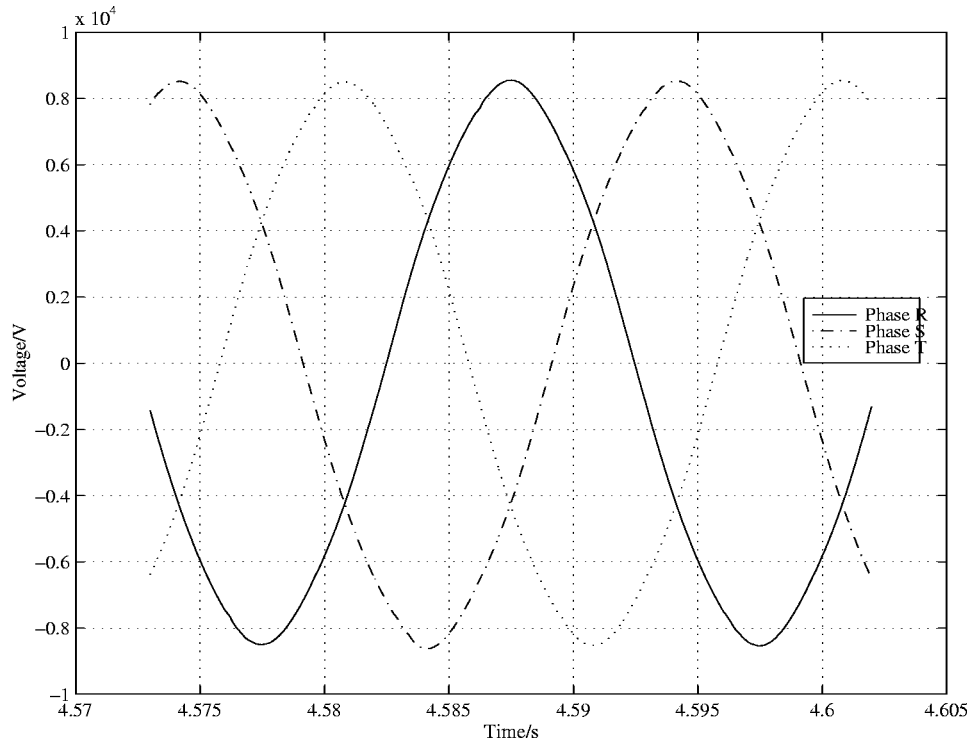

Figure 7.10: Voltages During Two Phase Fuse Burning Out.

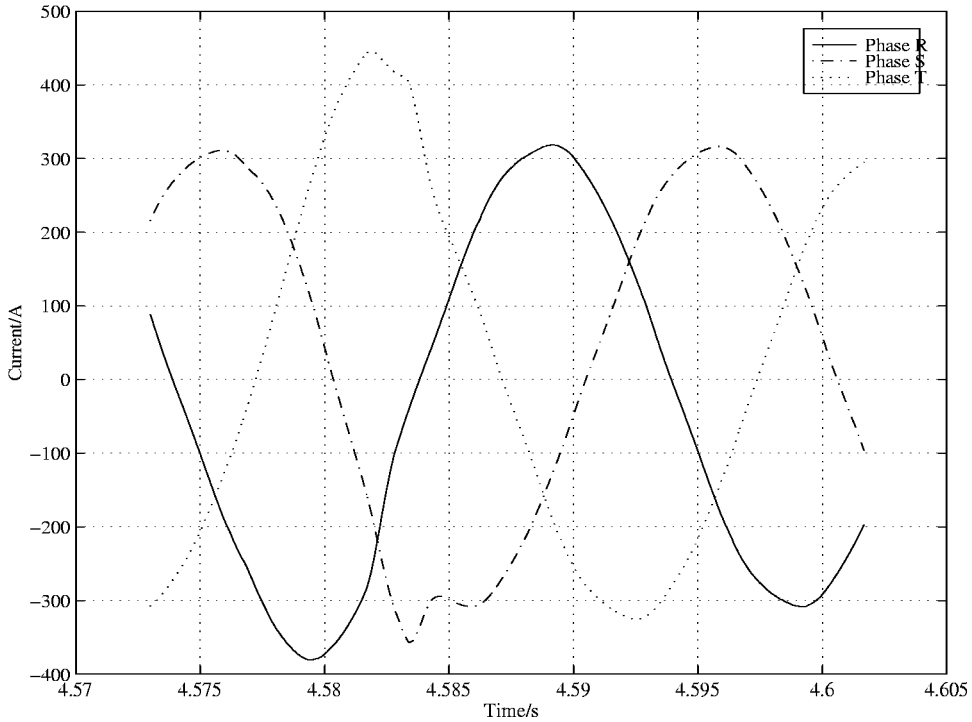

Figure 7.11: Currents During Two Phase Fuse Burning Out.

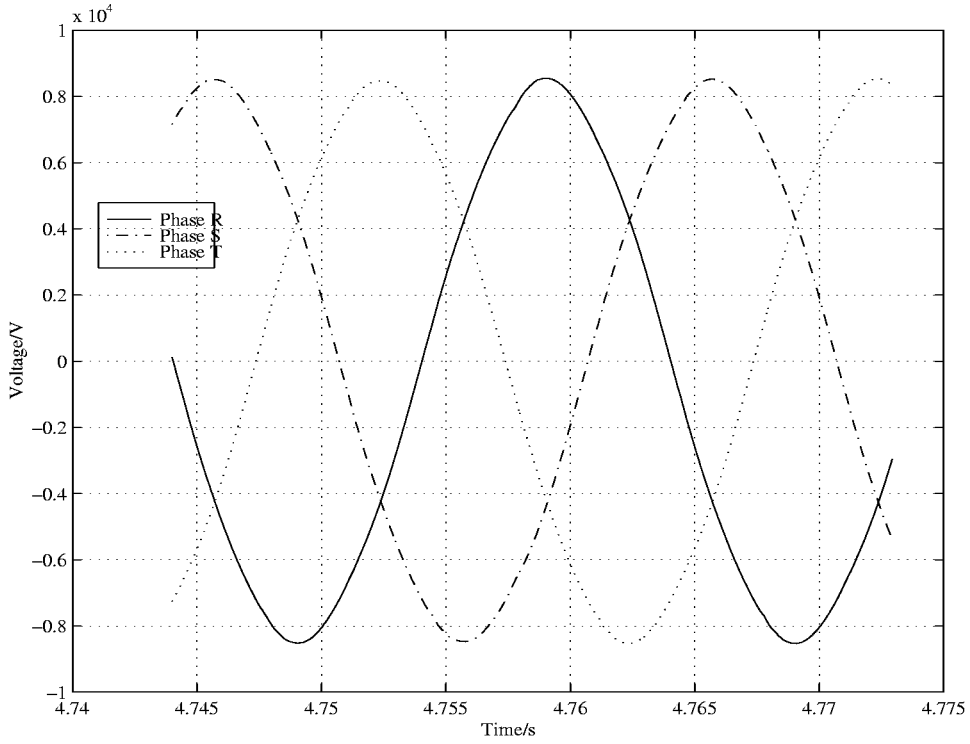

Figure 7.12: Voltages During Three Phase Fuse Burning Out.

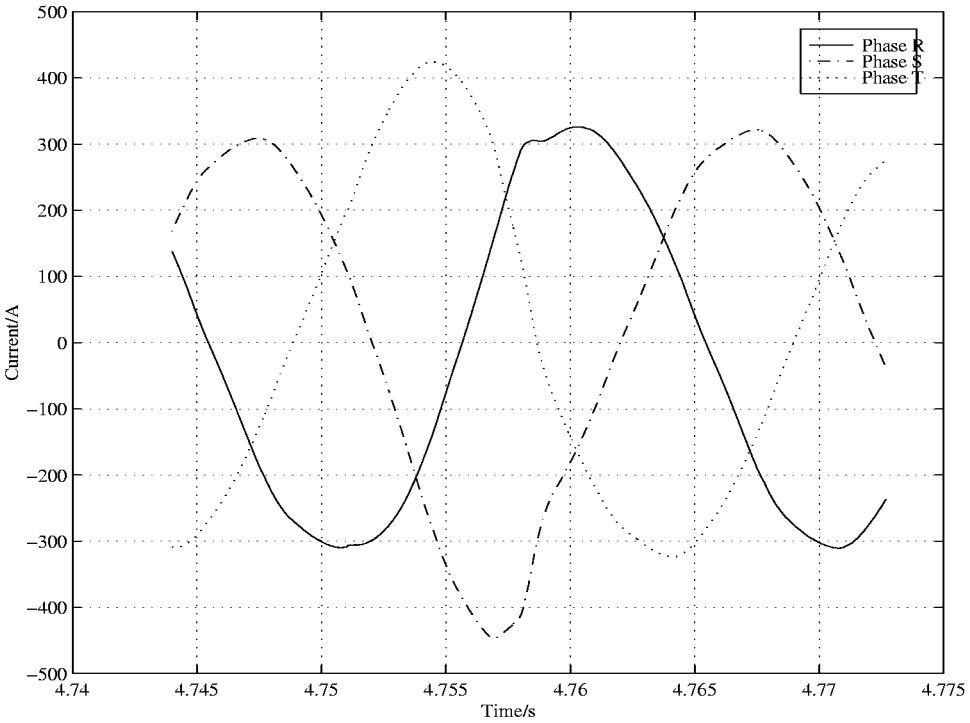

Figure 7.13: Currents During Three Phase Fuse Burning Out.

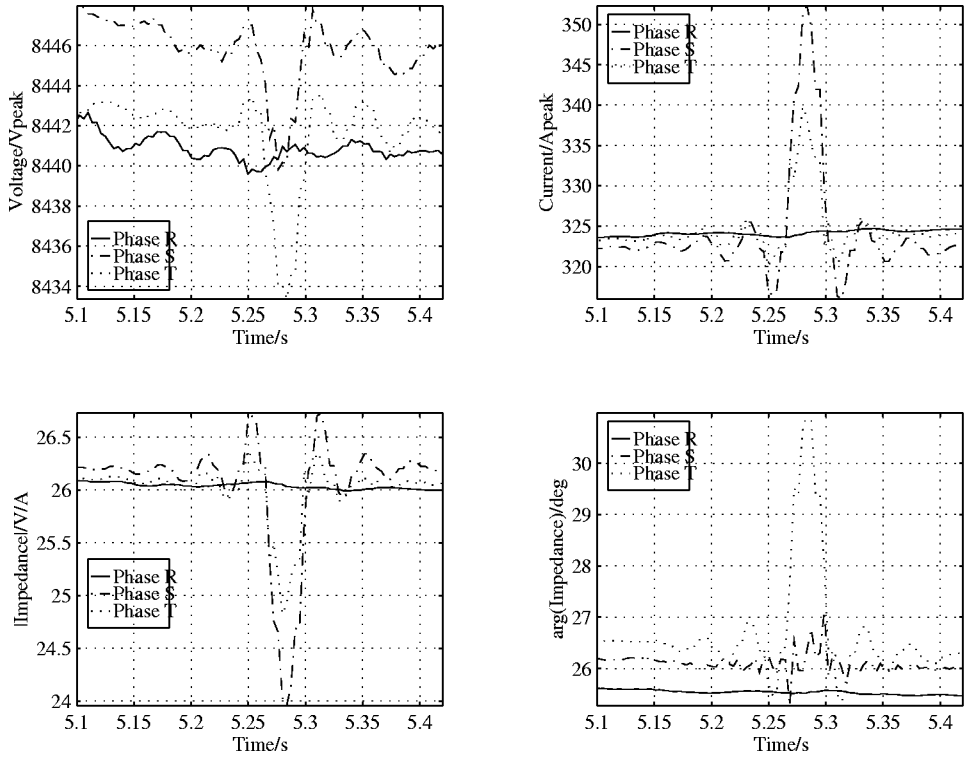

Figure 7.14: Fundamental Frequency Analysis of Currents and Voltages During One Phase Fuse Burning Out.

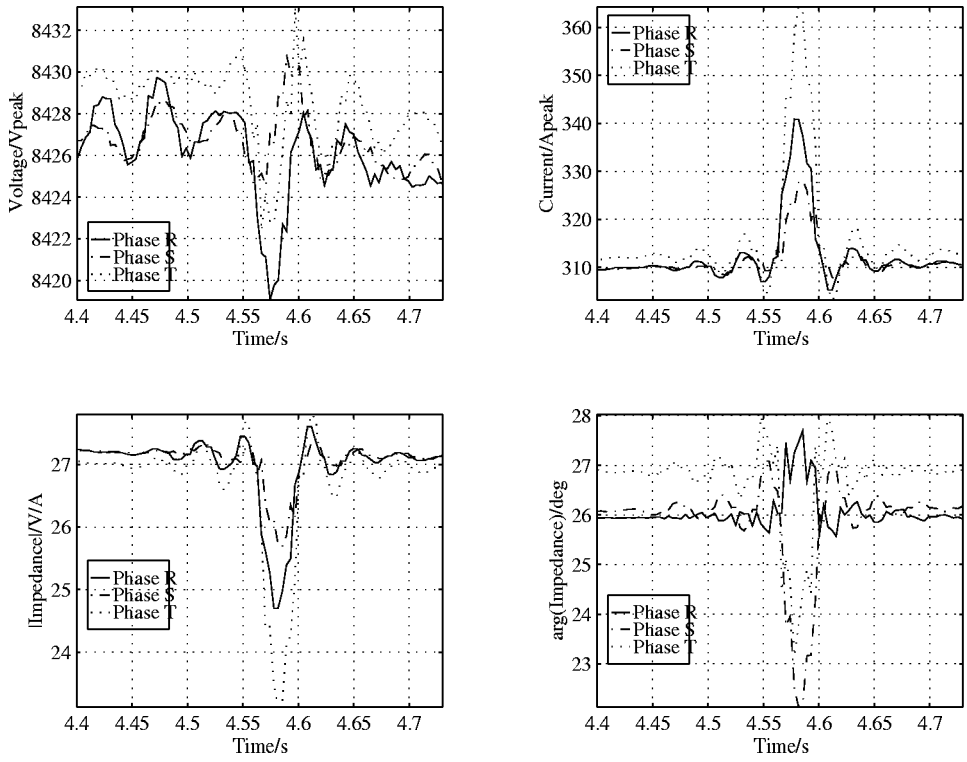

Figure 7.15: Fundamental Frequency Analysis of Currents and Voltages During Two Phase Fuse Burning Out.

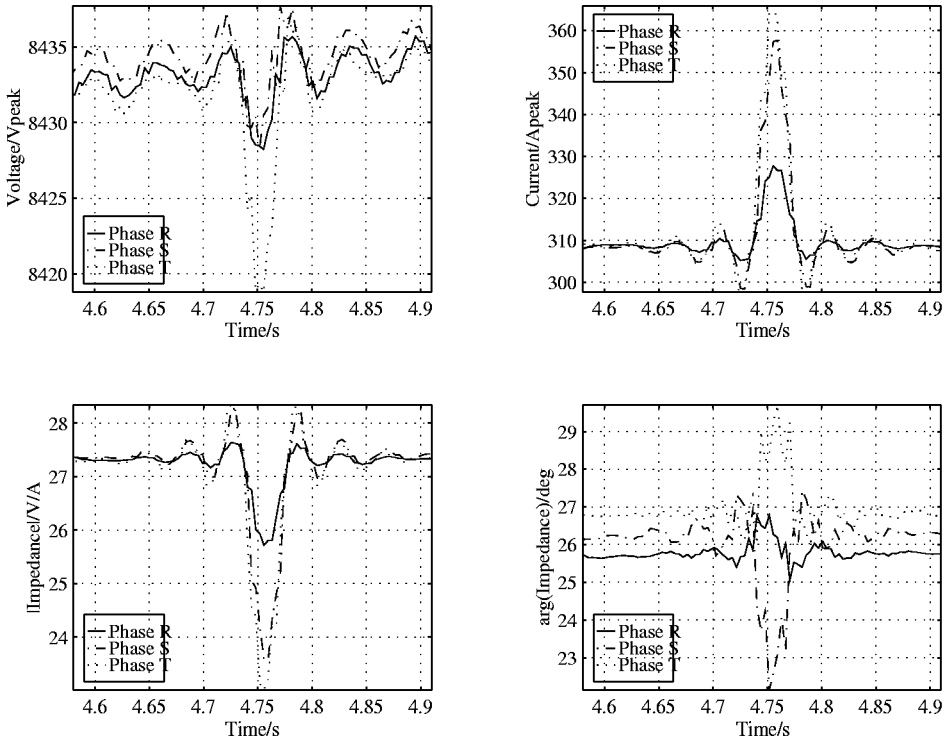

Figure 7.16: Fundamental Frequency Analysis of Currents and Voltages During Three Phase Fuse Burning Out.

The residual signals were analysed using the *Short Term Fourier Transform*, see Section 6.8.1.
On each of the plots in the following it is indicated what was the window length and what was the offset between FFT's.
To get an idea about the magnitude of the frequency components, each plot is accompanied by sections taken at different times.

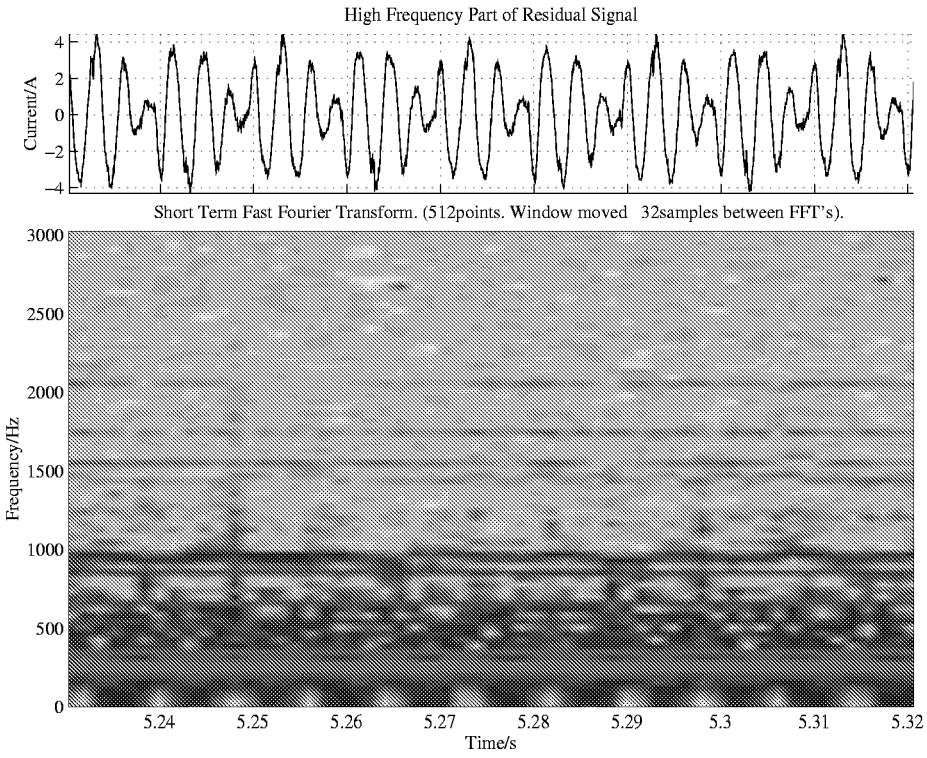

Figure 7.17: High Frequency Analysis of Phase R Current During One Phase Fuse Burning Out.

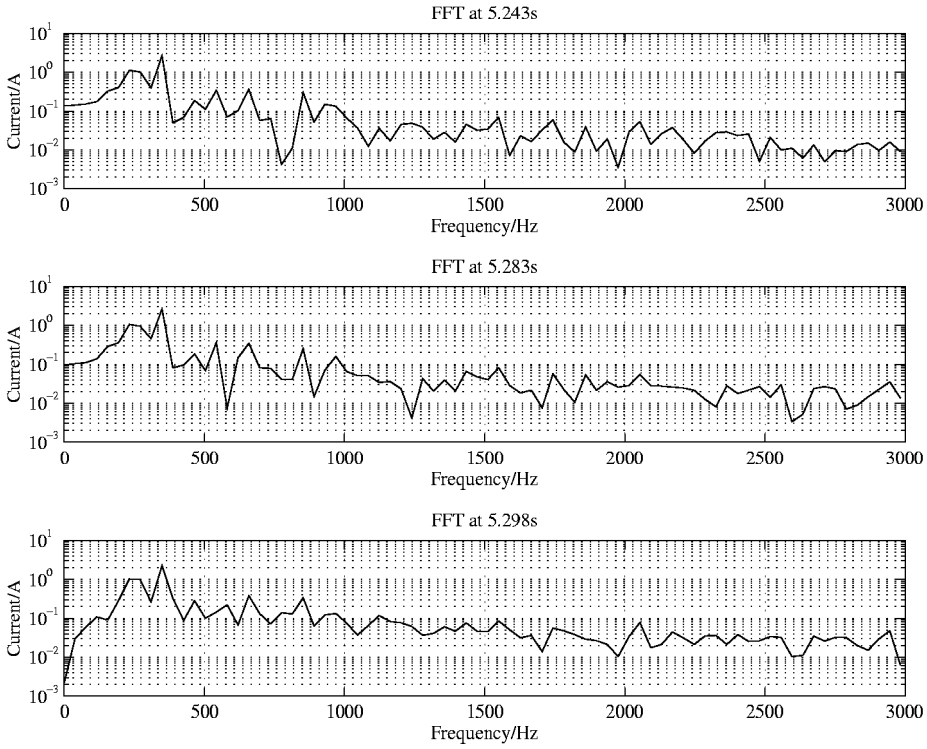

Figure 7.18: High Frequency Analysis of Phase R Current During One Phase Fuse Burning Out — Cross Sections of STFT.

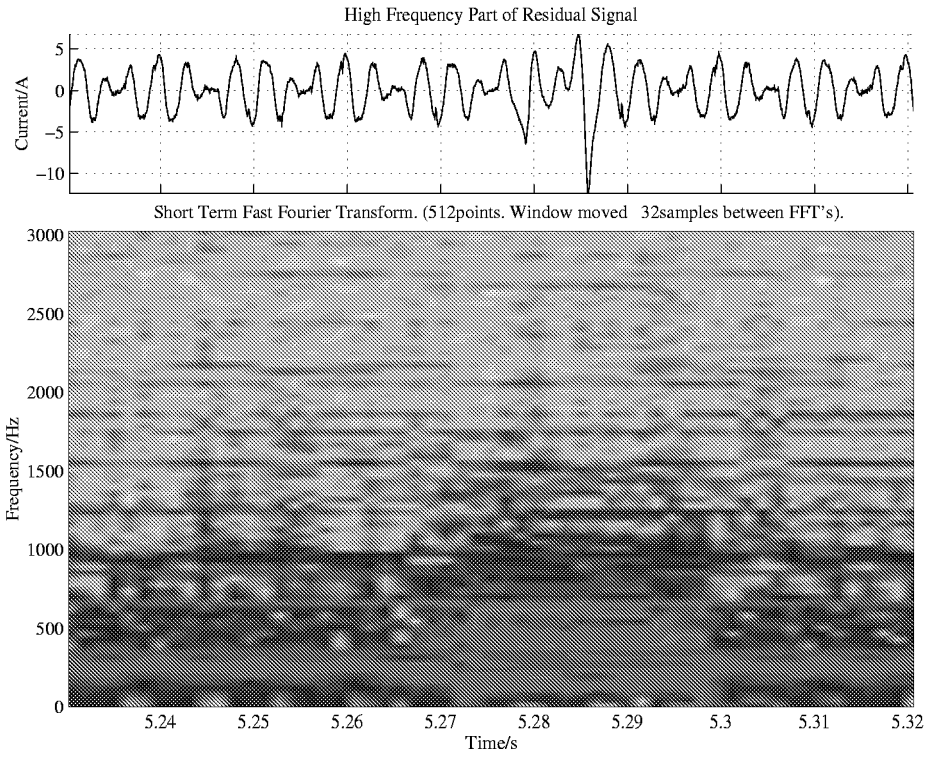

Figure 7.19: High Frequency Analysis of Phase S Current During One Phase Fuse Burning Out.

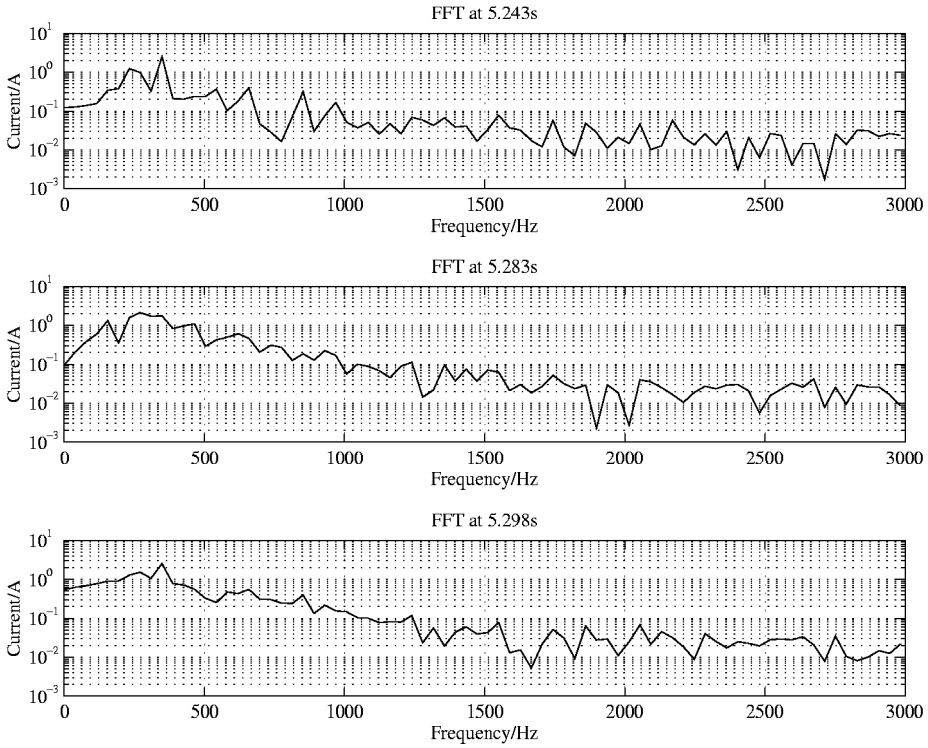

Figure 7.20: High Frequency Analysis of Phase S Current During One Phase Fuse Burning Out — Cross Sections of STFT.

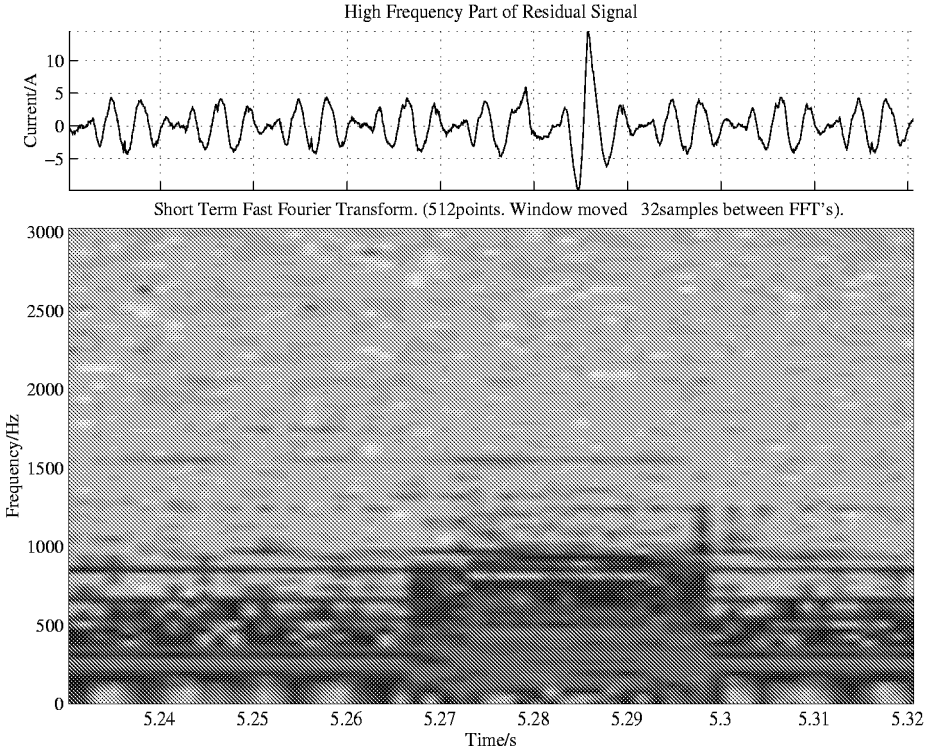

Figure 7.21: High Frequency Analysis of Phase T Current During One Phase Fuse Burning Out.

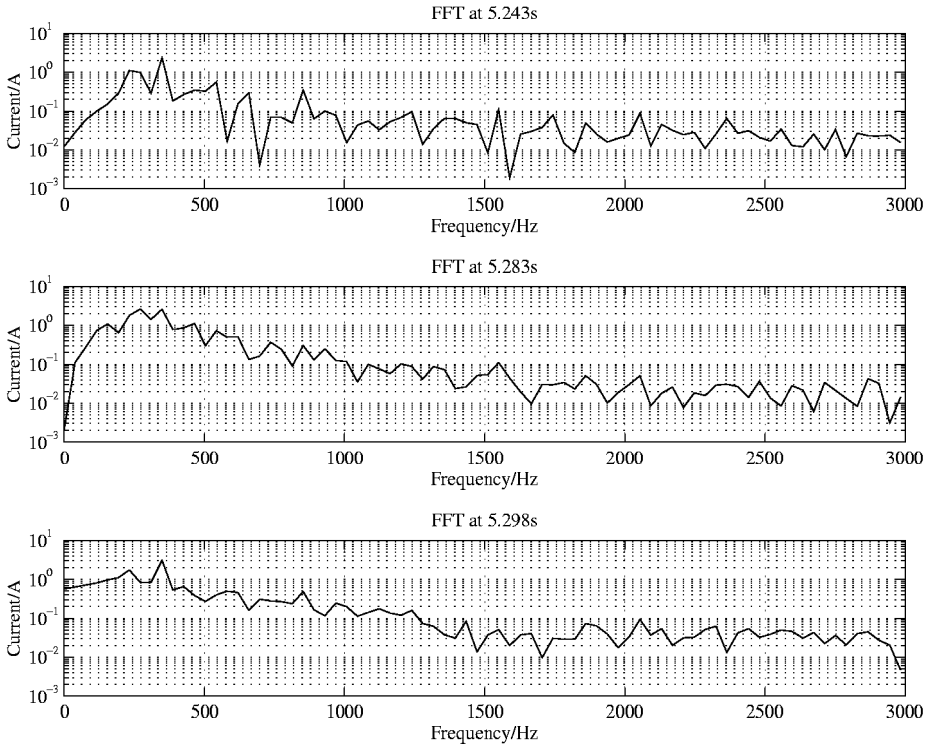

Figure 7.22: High Frequency Analysis of Phase T Current During One Phase Fuse Burning Out — Cross Sections of STFT.

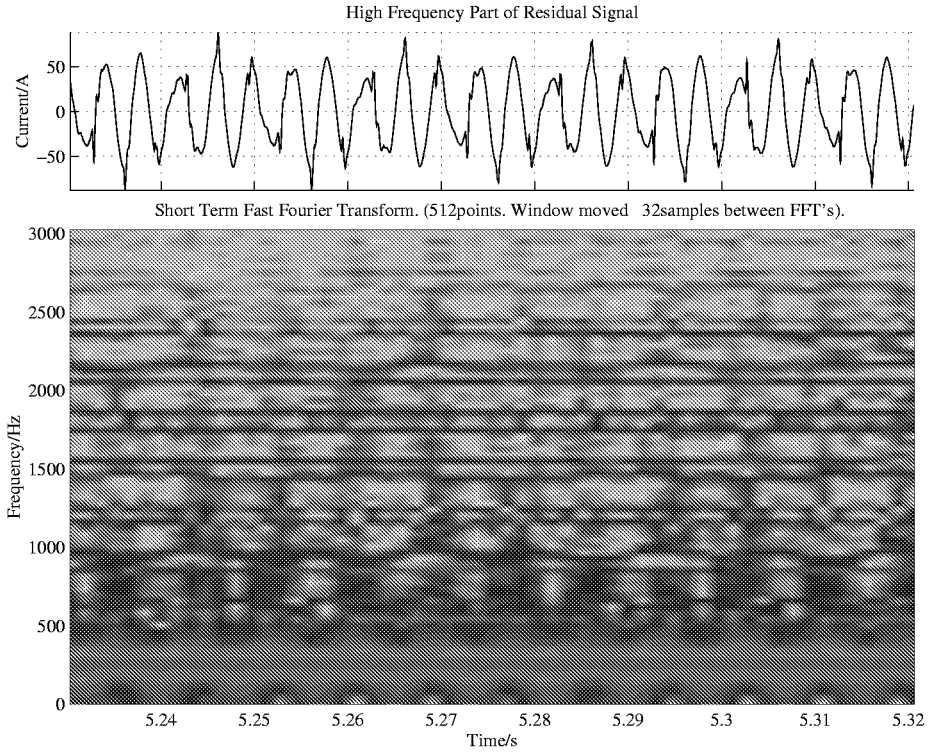

Figure 7.23: High Frequency Analysis of Phase R Voltage During One Phase Fuse Burning Out.

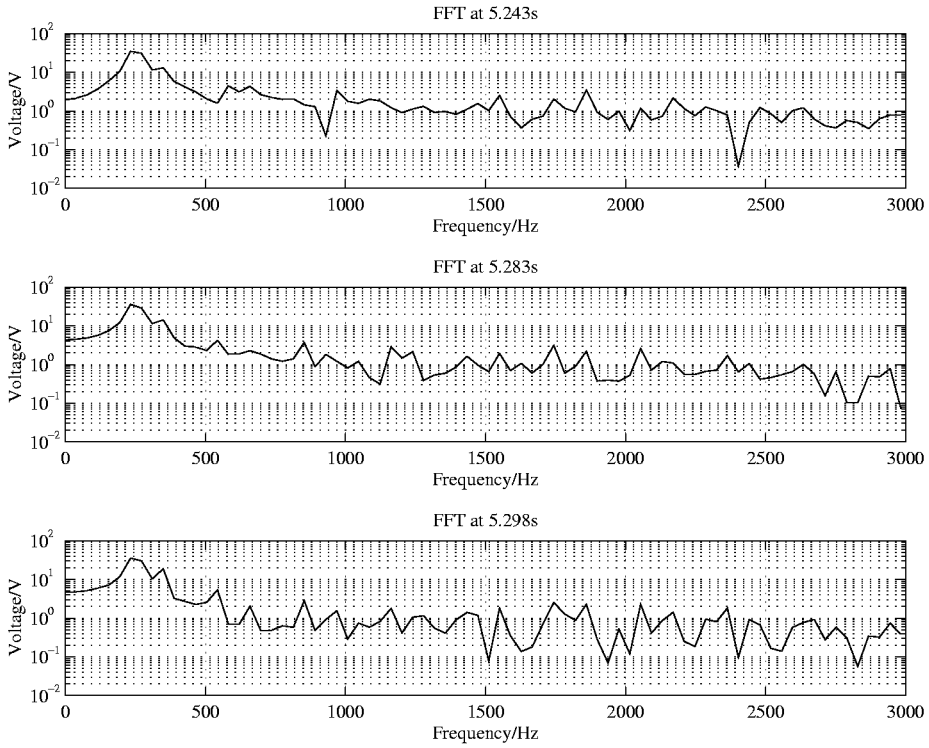

Figure 7.24: High Frequency Analysis of Phase R Voltage During One Phase Fuse Burning Out — Cross Sections of STFT.

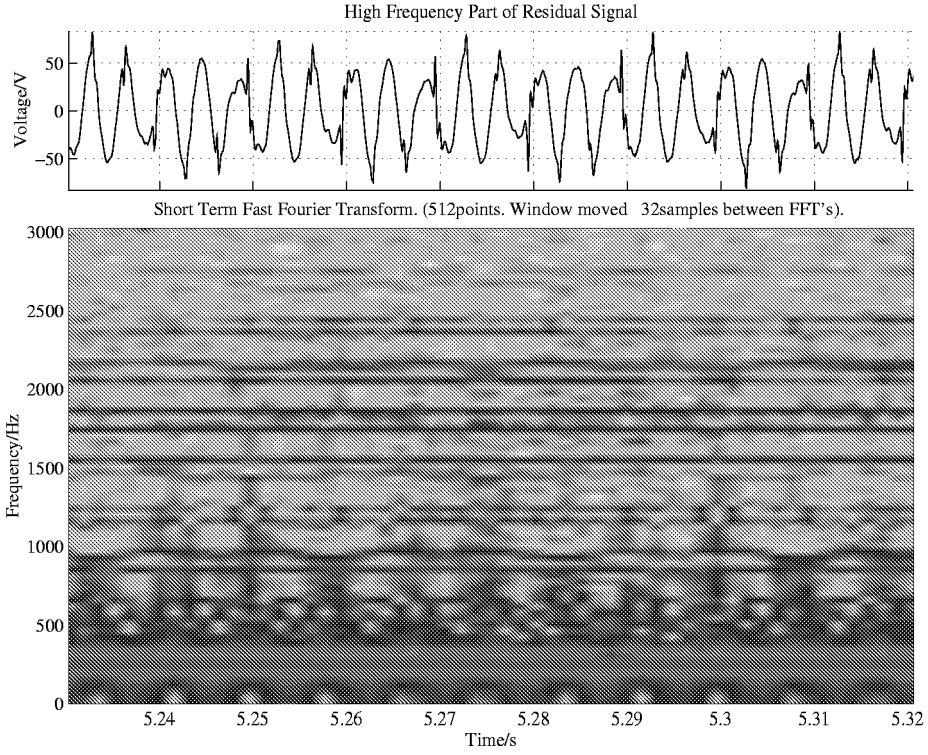

Figure 7.25: High Frequency Analysis of Phase S Voltage During One Phase Fuse Burning Out.

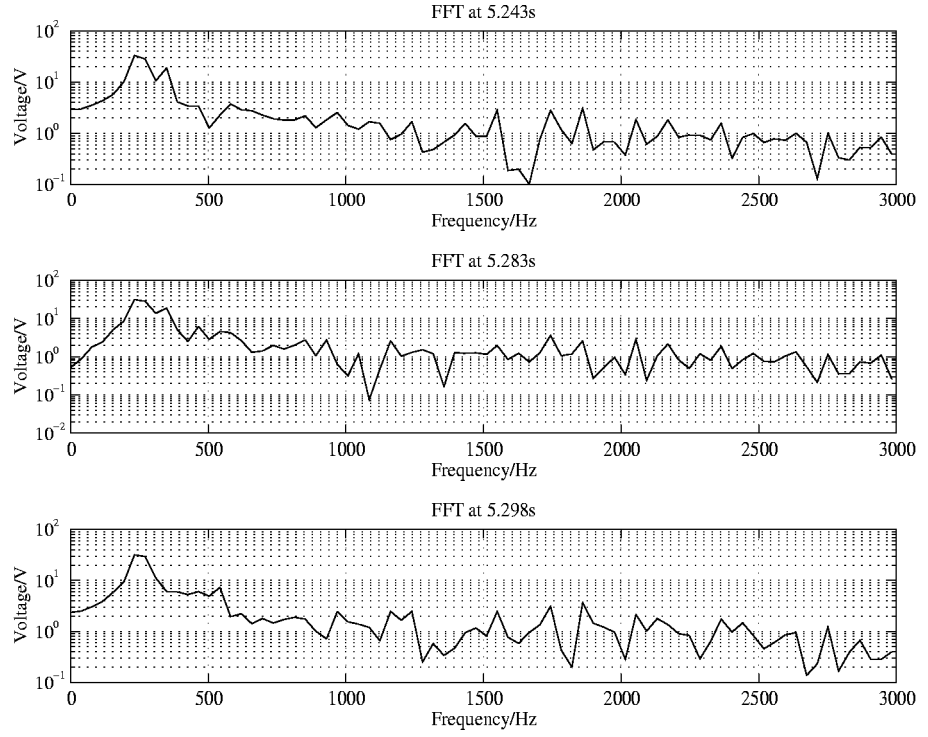

Figure 7.26: High Frequency Analysis of Phase S Voltage During One Phase Fuse Burning Out — Cross Sections of STFT.

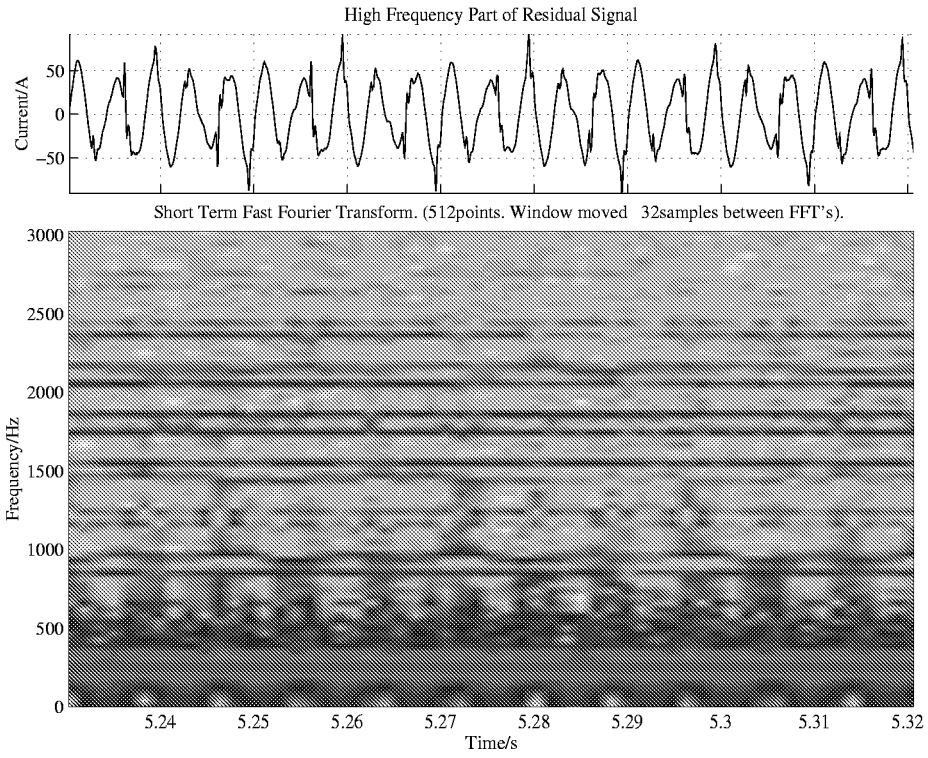

Figure 7.27: High Frequency Analysis of Phase T Voltage During One Phase Fuse Burning Out.

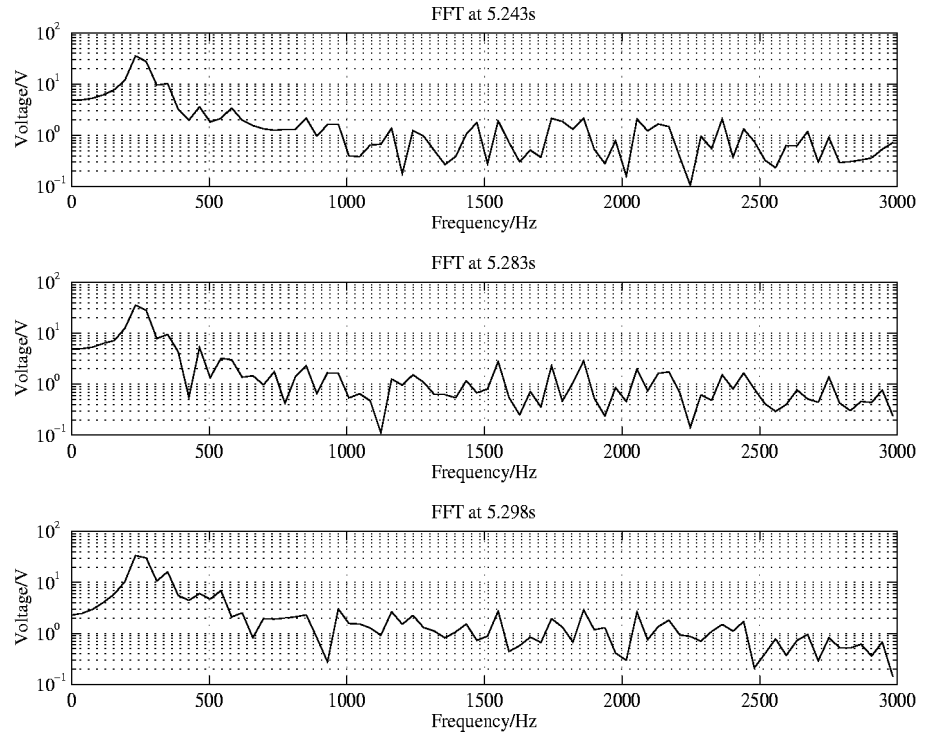

Figure 7.28: High Frequency Analysis of Phase T Voltage During One Phase Fuse Burning Out — Cross Sections of STFT.

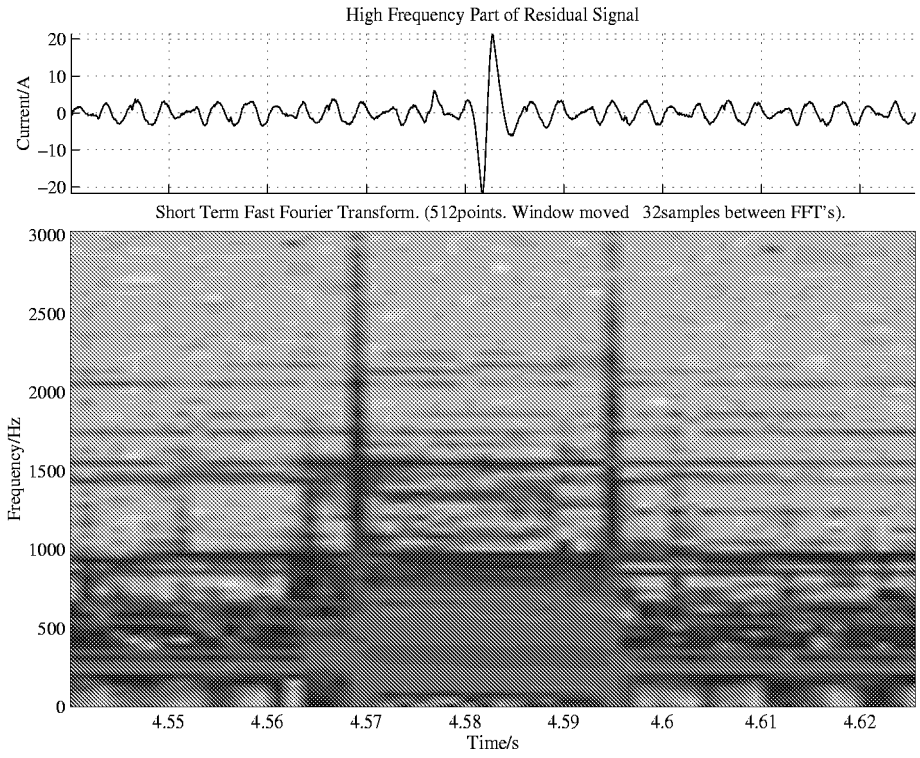

Figure 7.29: High Frequency Analysis of Phase R Current During Two Phase Fuse Burning Out.

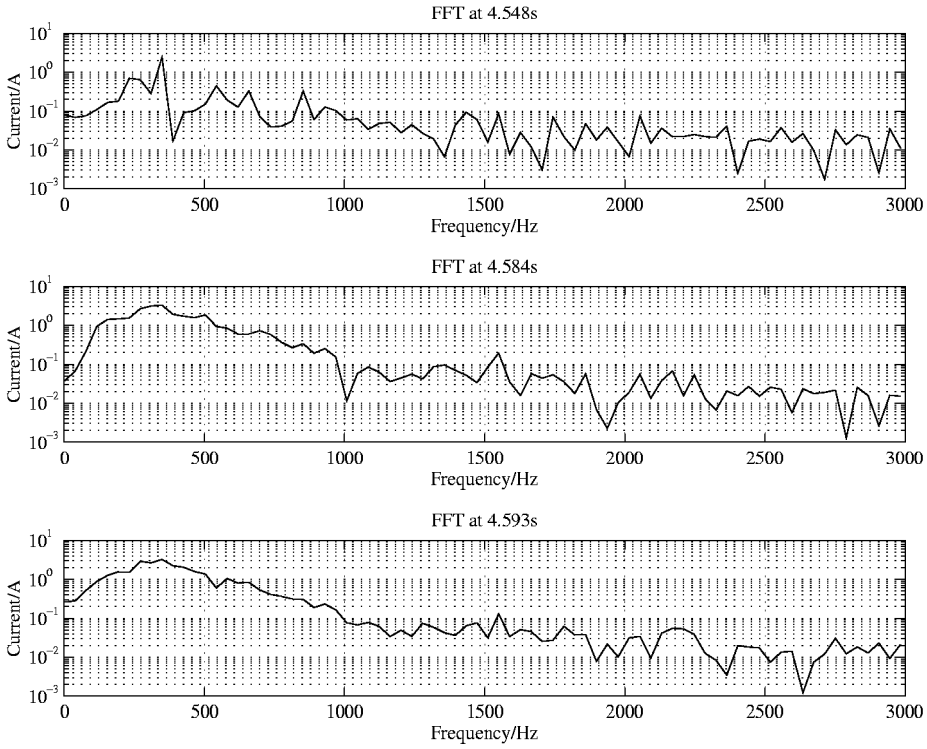

Figure 7.30: High Frequency Analysis of Phase R Current During Two Phase Fuse Burning Out — Cross Sections of STFT.

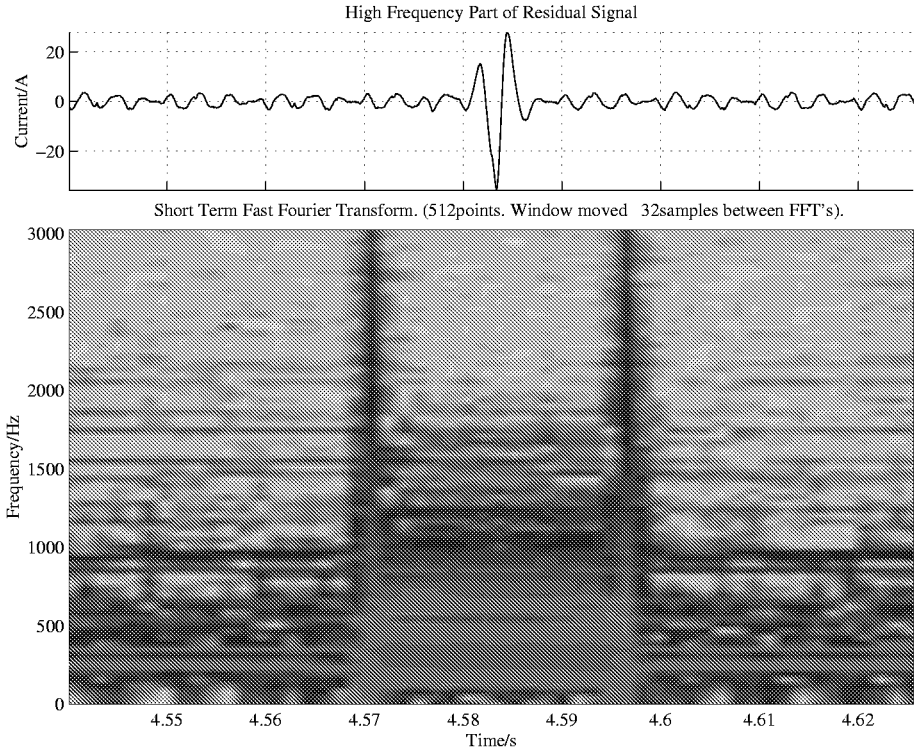

Figure 7.31: High Frequency Analysis of Phase S Current During Two Phase Fuse Burning Out.

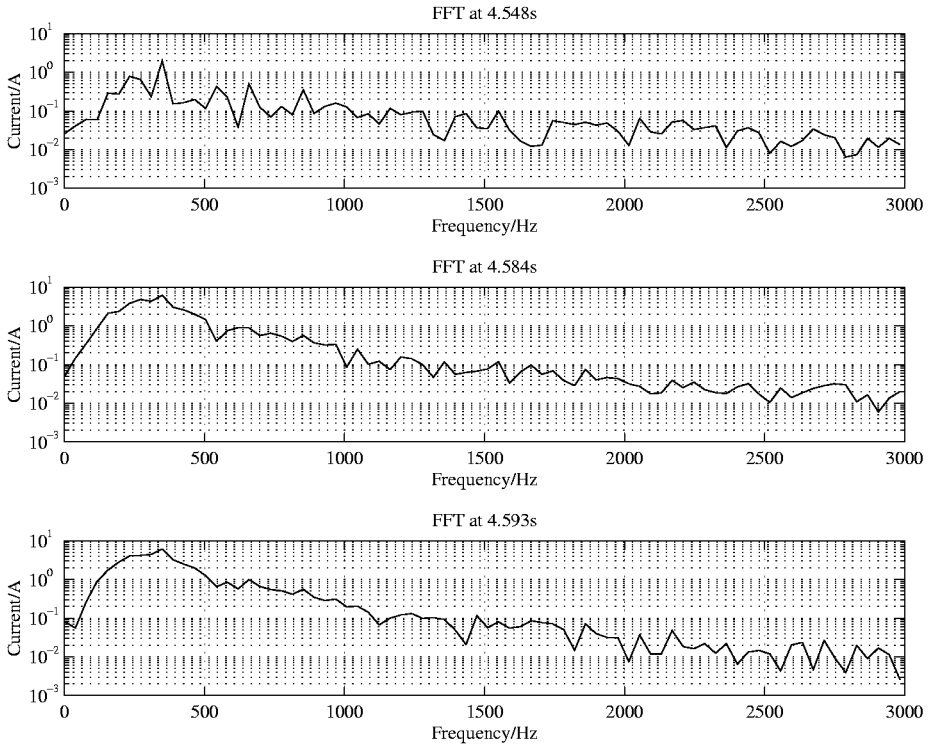

Figure 7.32: High Frequency Analysis of Phase S Current During Two Phase Fuse Burning Out — Cross Sections of STFT.

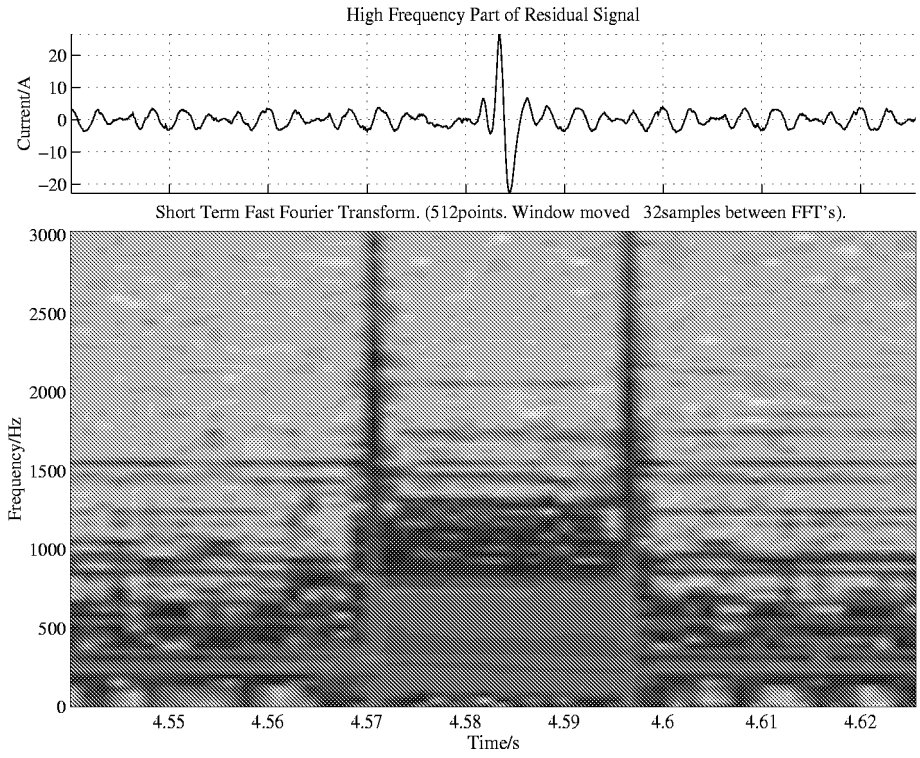

Figure 7.33: High Frequency Analysis of Phase T Current During Two Phase Fuse Burning Out.

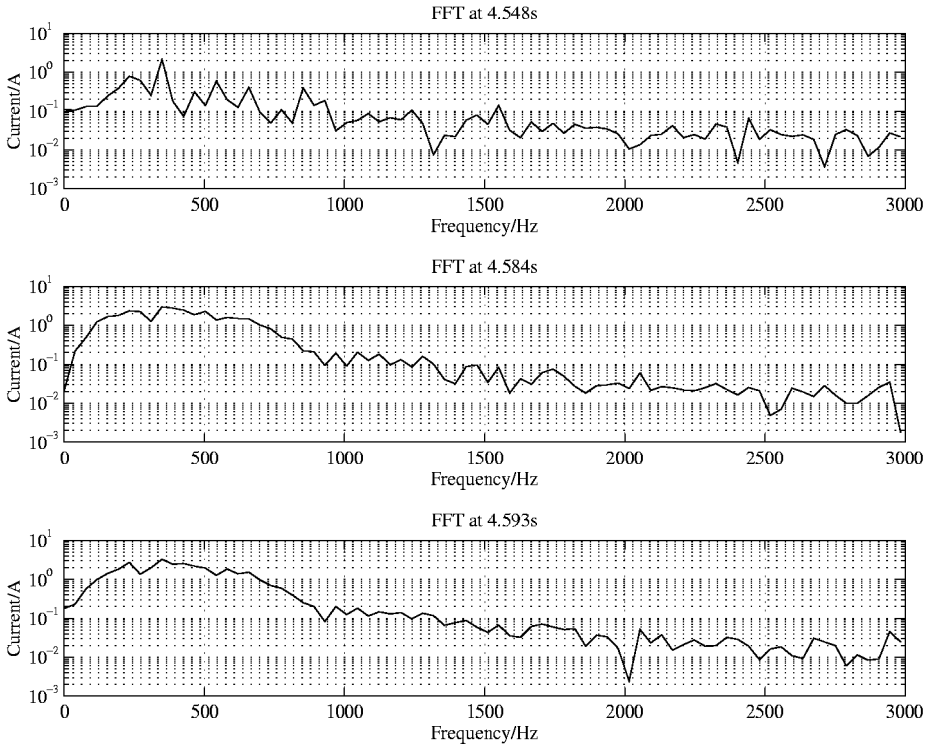

Figure 7.34: High Frequency Analysis of Phase T Current During Two Phase Fuse Burning Out — Cross Sections of STFT.

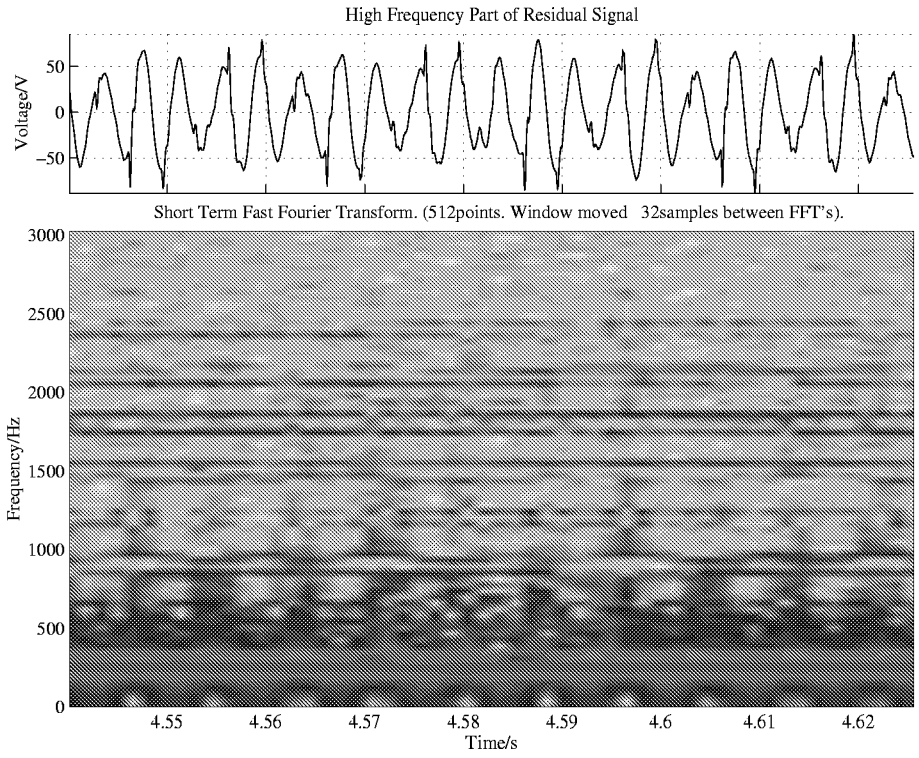

Figure 7.35: High Frequency Analysis of Phase R Voltage During Two Phase Fuse Burning Out.

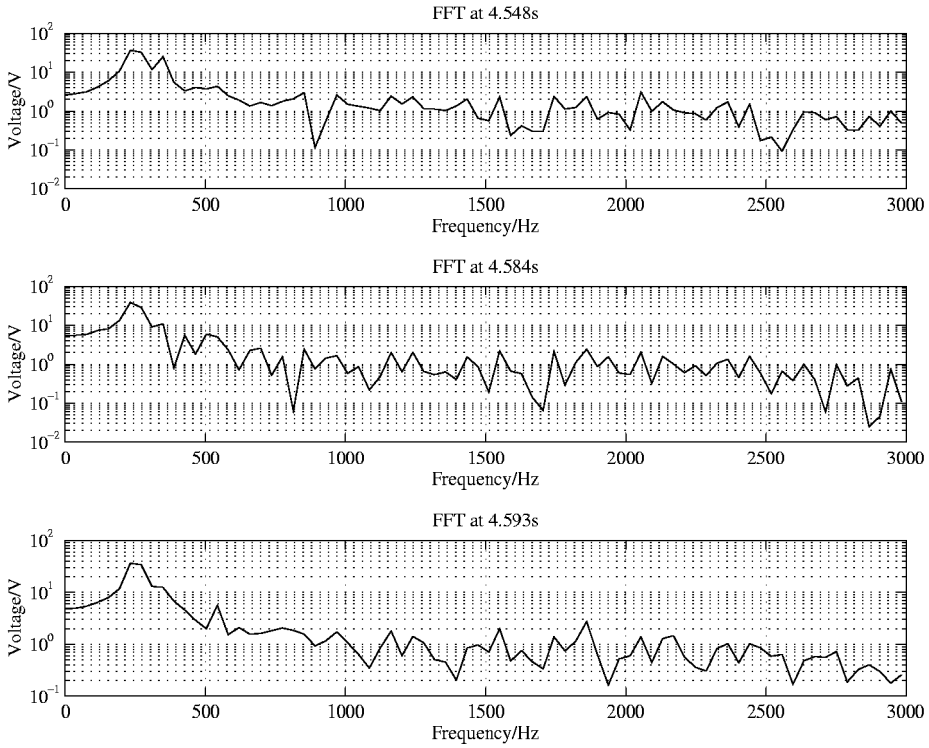

Figure 7.36: High Frequency Analysis of Phase R Voltage During Two Phase Fuse Burning Out — Cross Sections of STFT.

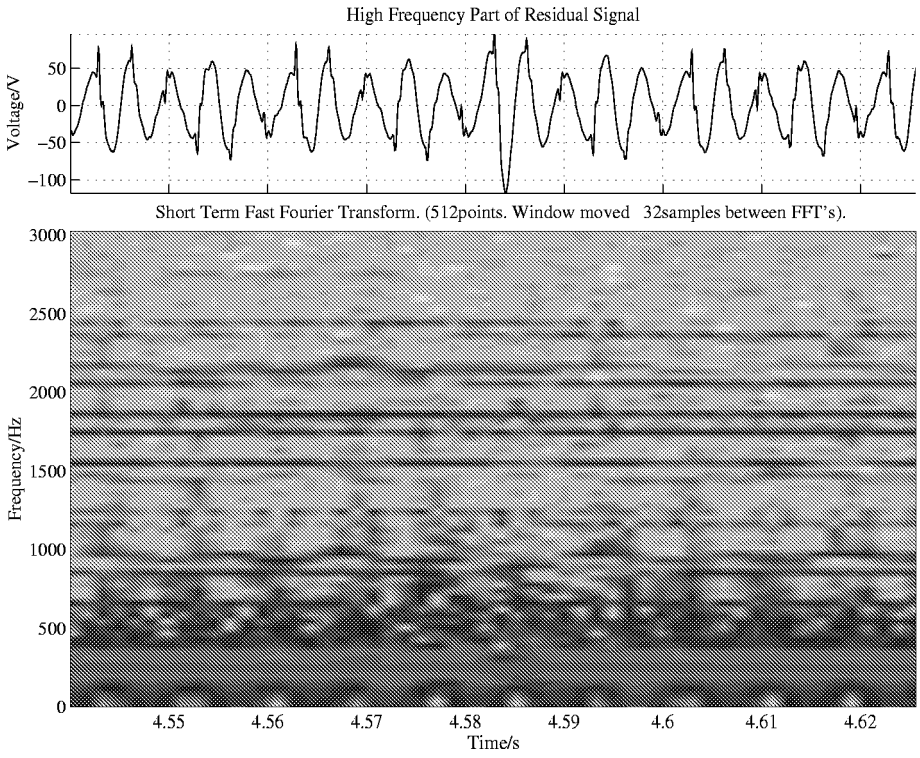

Figure 7.37: High Frequency Analysis of Phase S Voltage During Two Phase Fuse Burning Out.

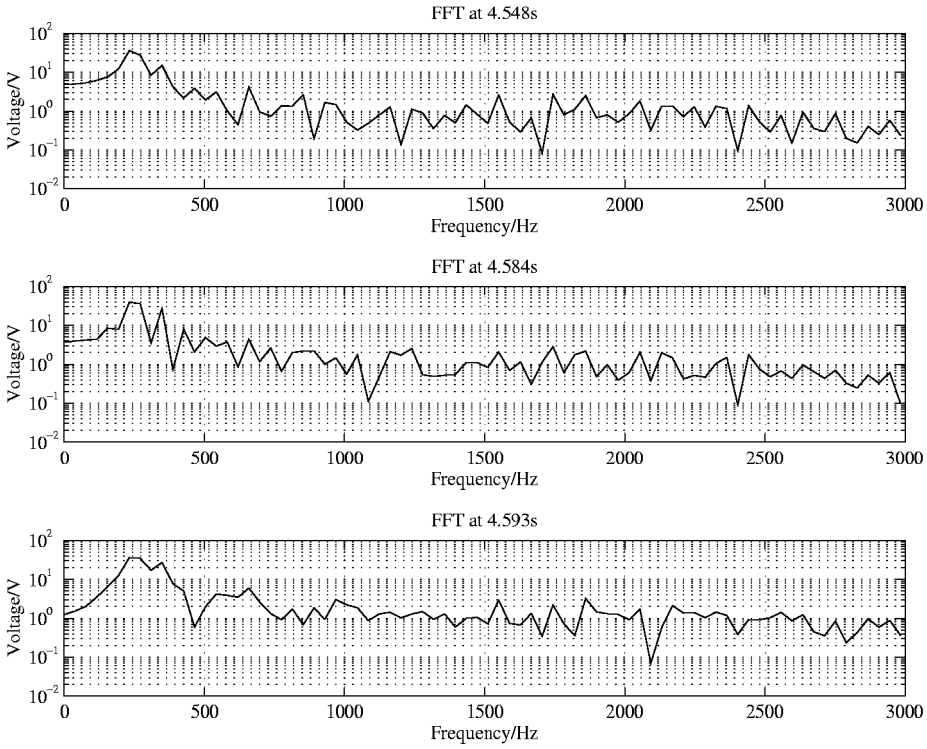

Figure 7.38: High Frequency Analysis of Phase S Voltage During Two Phase Fuse Burning Out — Cross Sections of STFT.

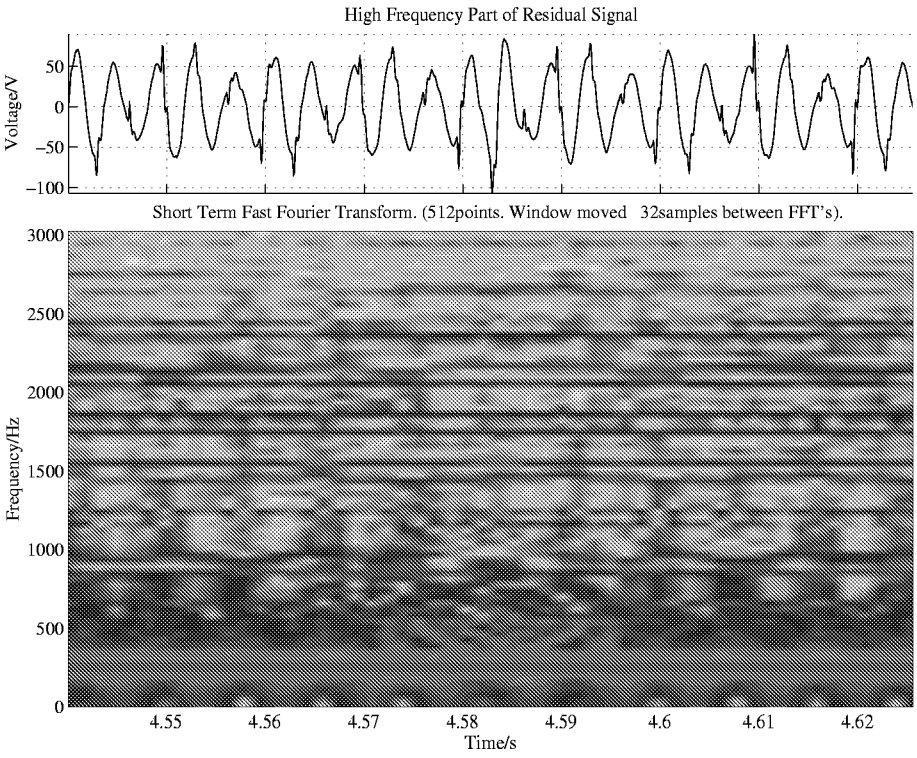

Figure 7.39: High Frequency Analysis of Phase T Voltage During Two Phase Fuse Burning Out.

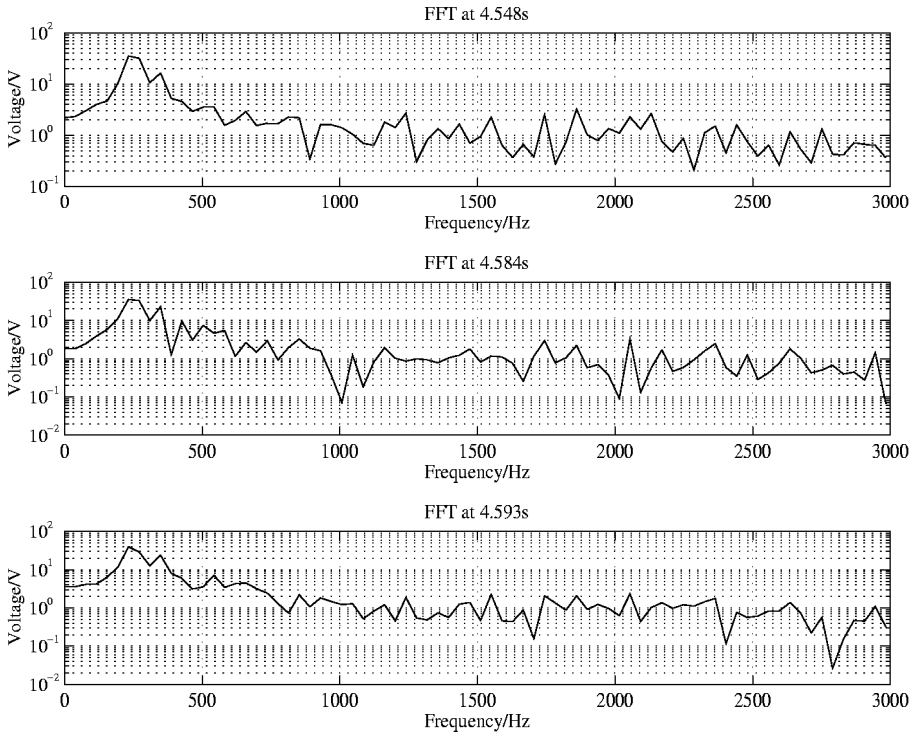

Figure 7.40: High Frequency Analysis of Phase T Voltage During Two Phase Fuse Burning Out — Cross Sections of STFT.

The STFT gives a rather blurred impression of what goes on. Despite this, this investigation has yielded very important results.
Depending on the event, frequencies as high as 2,5kHz are seen. The flanks caused by the windowing must be disregarded.

Generally not much is seen at higher frequencies in the voltages. Though in some cases these also show traces of high frequency components.
The phase R voltages of both the two and three phase burning out show weak traces of components extending into the kiloHertz range.
However, the impact is so small that it seems as if the voltages should be considered as insensitive to such events, except for the fundamental component.

7.3.3 Residual Component Analysis of Measurements from Operation of Machine at Factory

Opposite the events that were described in the previous section, these events are "slow", in the way that they last seconds and not only some milliseconds. It must therefore be expected that much of the high frequency components will attain a very low level. This implies that it must be expected that the high frequency contents injected into the feeder are low. Combined with the long distance, this substantiates that not much should be expected at the substation in the high part of the frequency spectrum.

The first analysis was to use the Kalman filter on the currents of the entire sequence of the experiment with the 90kW machine, see Figure 7.53 on page 94.
In the first place it was not deemed necessary to investigate the voltages. This was based on the analysis of the Stage 1 Measurements. However, the voltages recorded during the Stage 2 Measurements seem to show stronger traces of the events. Still the impact is small. If, however, an investigation of the currents reveals significant high frequency contents, an investigation of the high frequency contents of the voltages will become relevant.
Because the event is very long; 16s from the starting of the machine until the turning off, it has been necessary to analyse the sequence in smaller parts.
The first part starts at about 59s and lasts three seconds. The second starts at about 64s and lasts also three seconds. The third part starts at about 75s.

For these three parts of the total event, a Short Term FFT is made.
The size of the result was considerable; taking up more than 4MB of memory. Plotting the result was an even tougher task to the computer — an Intel–486DX2 based desktop, with 16MB RAM and 340MB harddisk. It took about 10min to show the result of one STFT on the screen — a QVision driven SVGA screen.

After numerous trials it was realized that it was necessary to abandon the PC for a work-station.
On the work-station of ELECTRONICS INSTITUTE it took only about four minutes to plot the same results.
On-screen analysis of the STFT's revealed, however, that nothing was seen in the spectra at that resolution, except for the harmonics.
This investigation opened up for a closer look at the contents at lower frequencies.

Only the analysis of the currents of phase R is shown, since the picture is the same for the two other phases.

Though being "blurred" the plots reveal that the starting of the motor at DYRUP only injects frequencies up to about the third harmonic, i.e. 150Hz, see Figure 7.54 on page 95.

7.3.4 Wavelet Analysis of Measurements

The time frequency analysis that has been performed, has clearly shown that the frequency contents vary significantly over time — which is indeed what was expected.

The results of the investigation are very important. With simple methods an indication was given of the frequency contents of the measurements.
On this basis it may be motivated to start working on the creation of methods that may exploit this

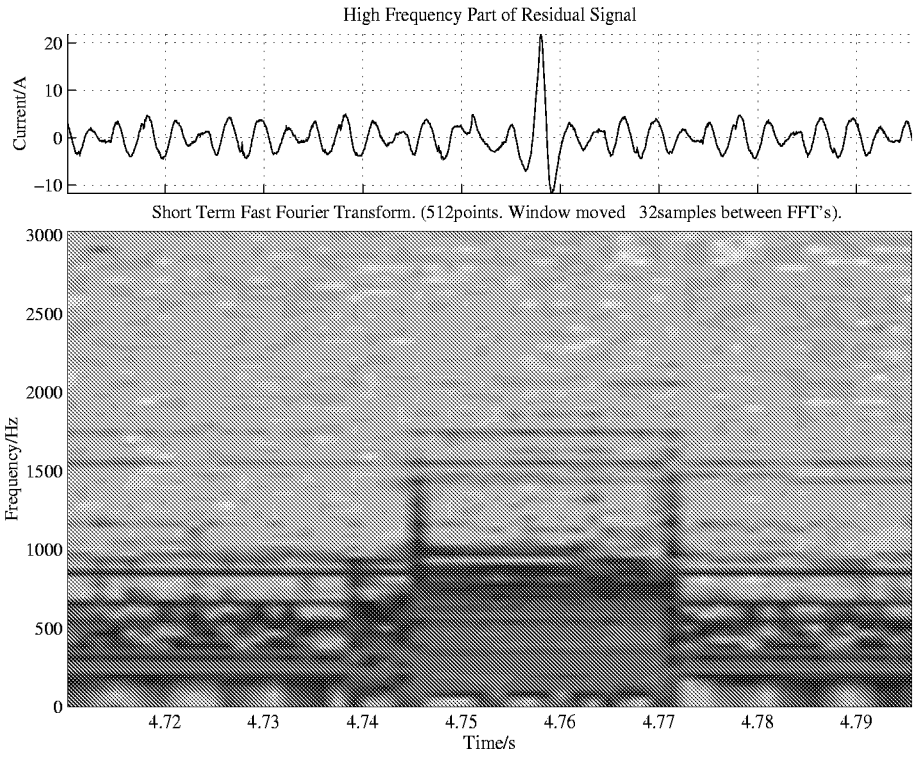

Figure 7.41: High Frequency Analysis of Phase R Current During Three Phase Fuse Burning Out.

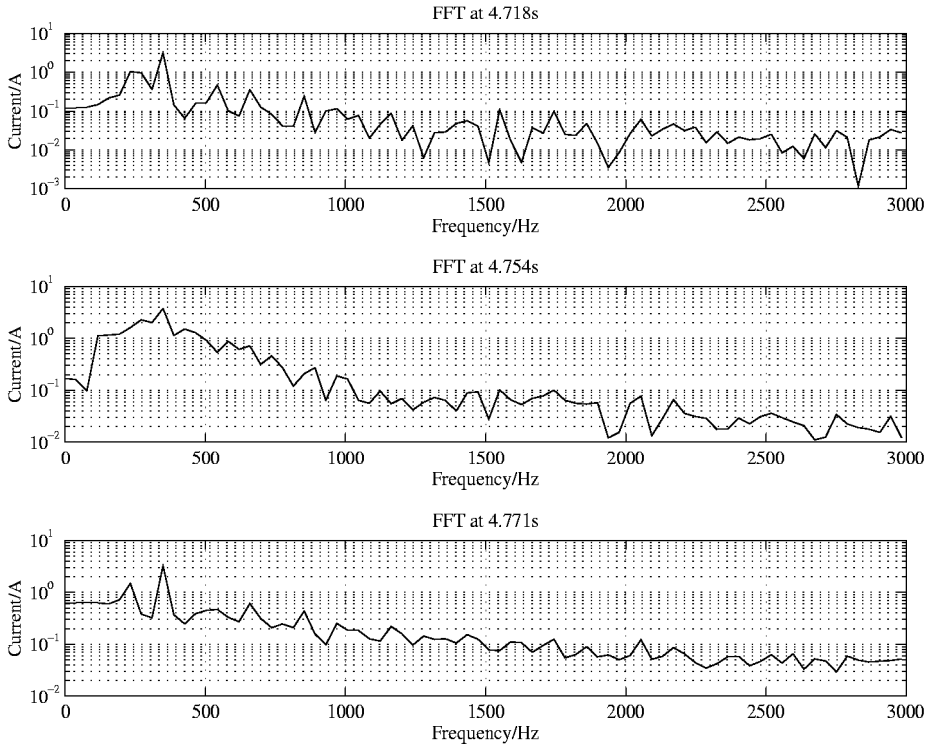

Figure 7.42: High Frequency Analysis of Phase R Current During Three Phase Fuse Burning Out — Cross Sections of STFT.

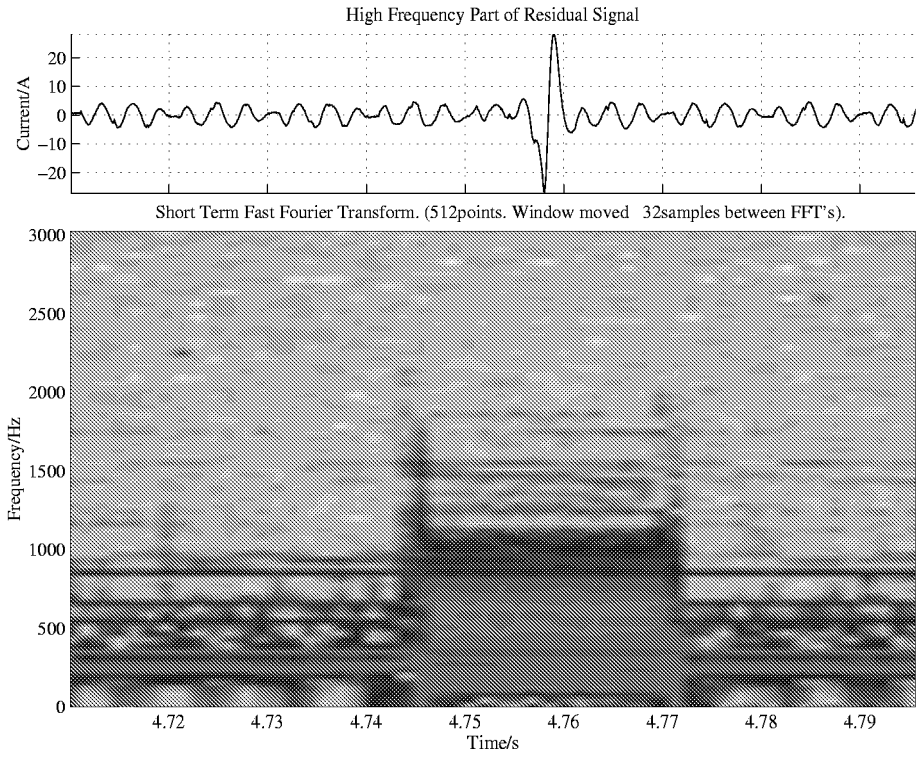

Figure 7.43: High Frequency Analysis of Phase S Current During Three Phase Fuse Burning Out.

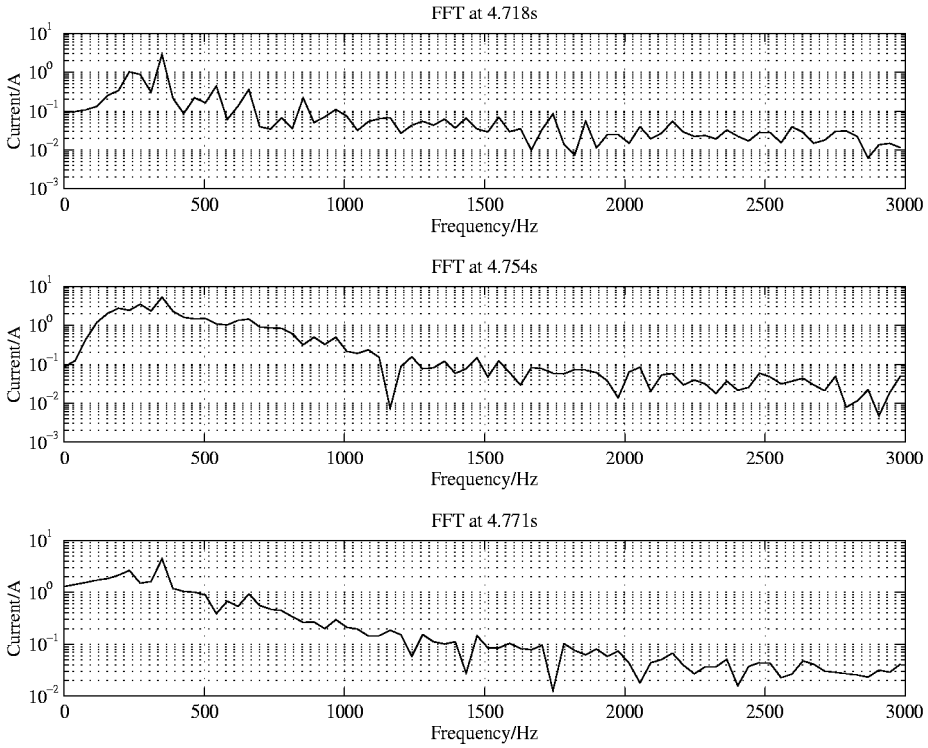

Figure 7.44: High Frequency Analysis of Phase S Current During Three Phase Fuse Burning Out — Cross Sections of STFT.

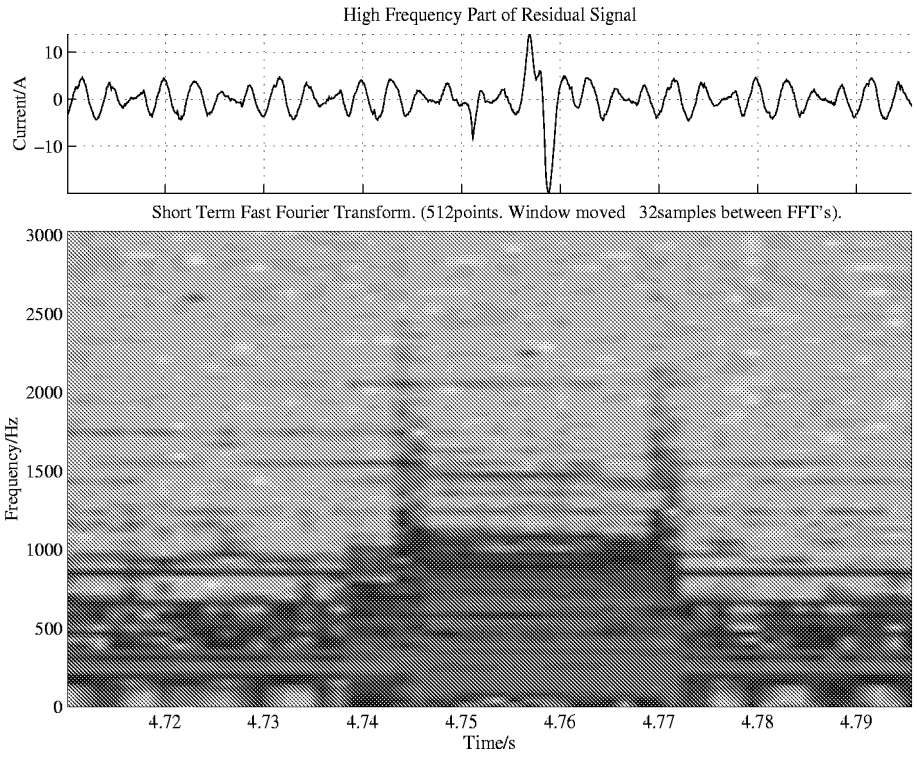

Figure 7.45: High Frequency Analysis of Phase T Current During Three Phase Fuse Burning Out.

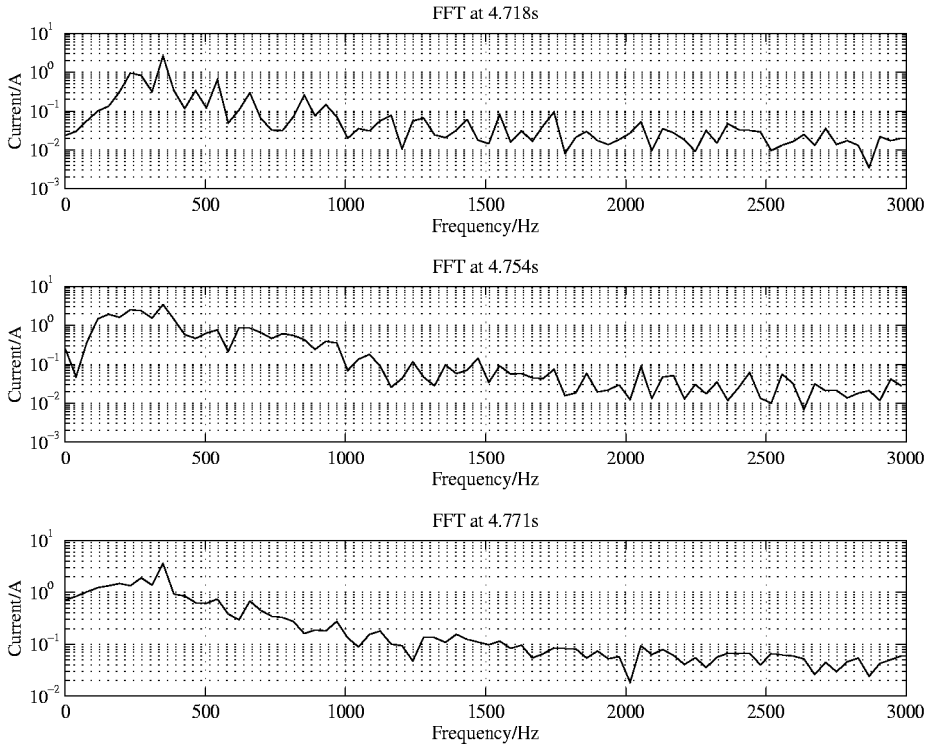

Figure 7.46: High Frequency Analysis of Phase T Current During Three Phase Fuse Burning Out — Cross Sections of STFT.

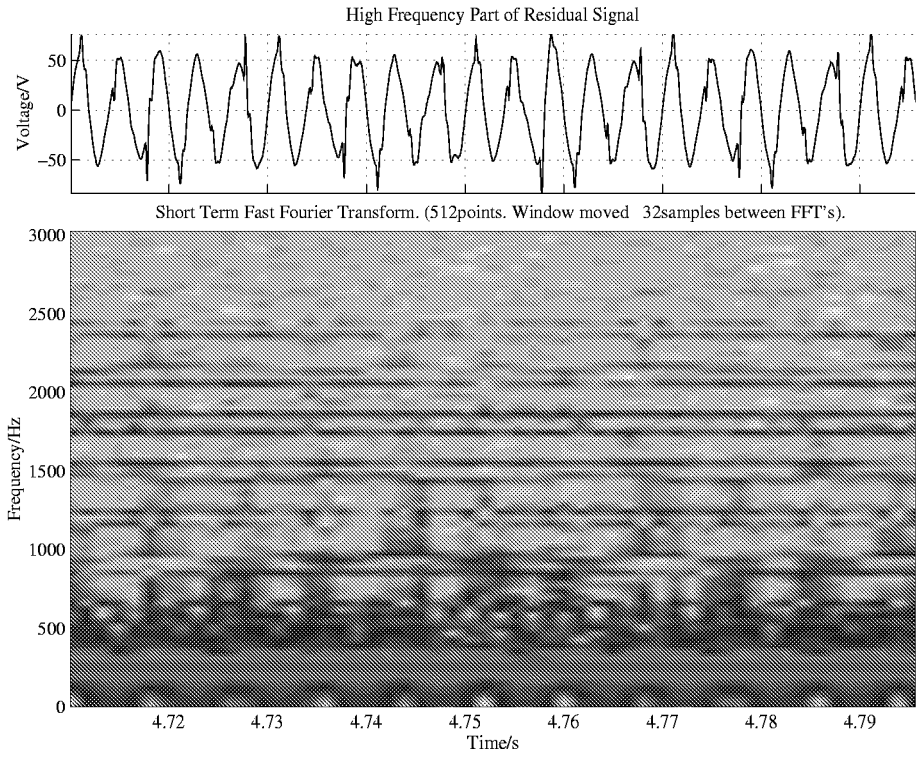

Figure 7.47: High Frequency Analysis of Phase R Voltage During Three Phase Fuse Burning Out.

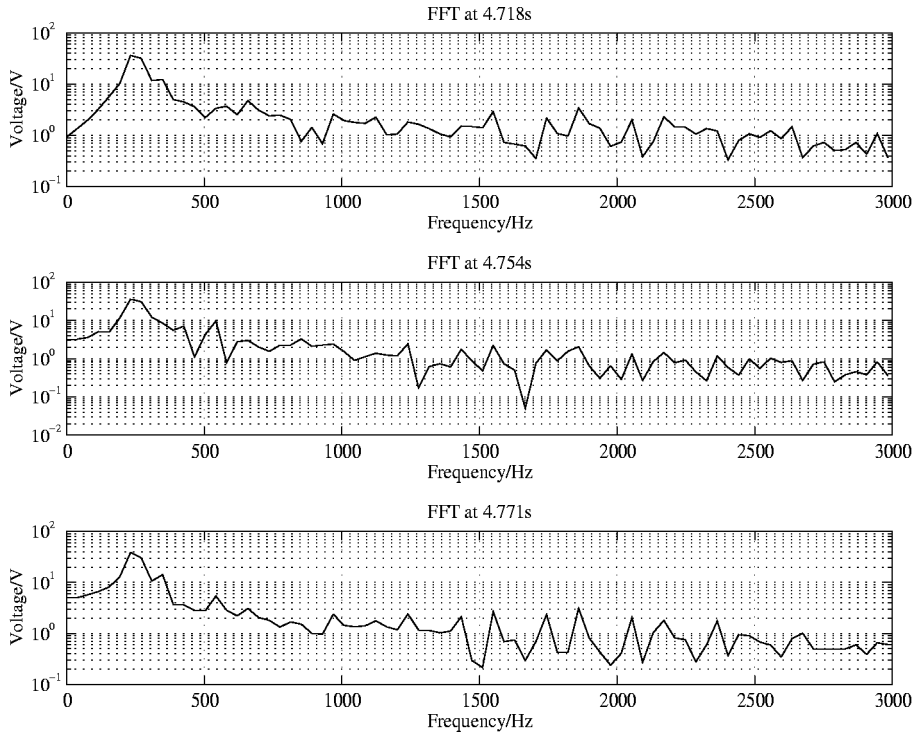

Figure 7.48: High Frequency Analysis of Phase R Voltage During Three Phase Fuse Burning Out — Cross Sections of STFT.

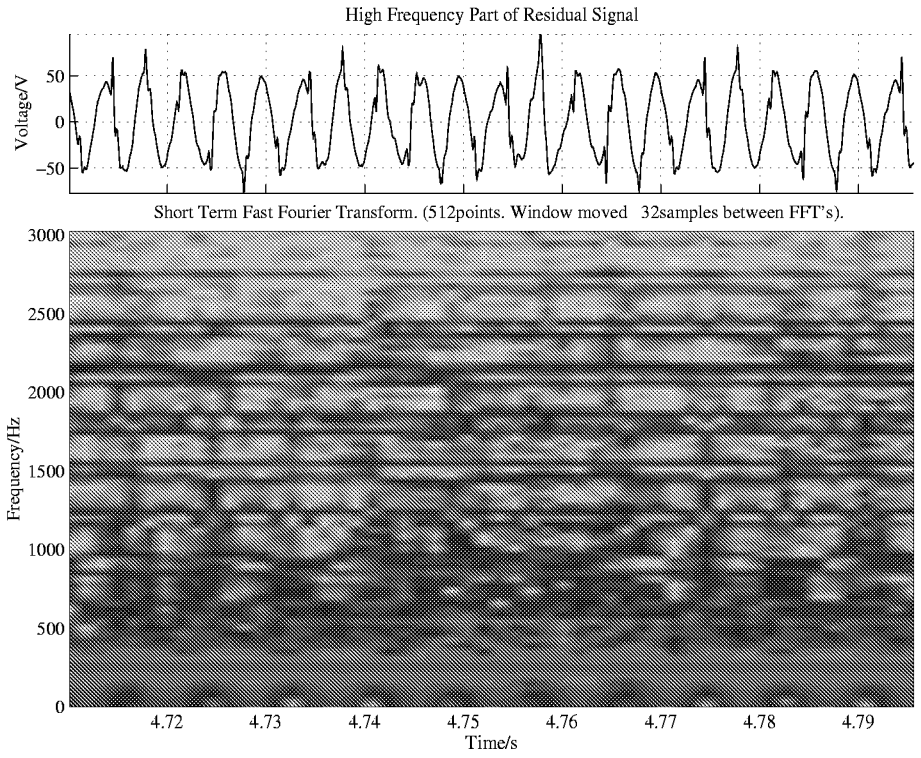

Figure 7.49: High Frequency Analysis of Phase S Voltage During Three Phase Fuse Burning Out.

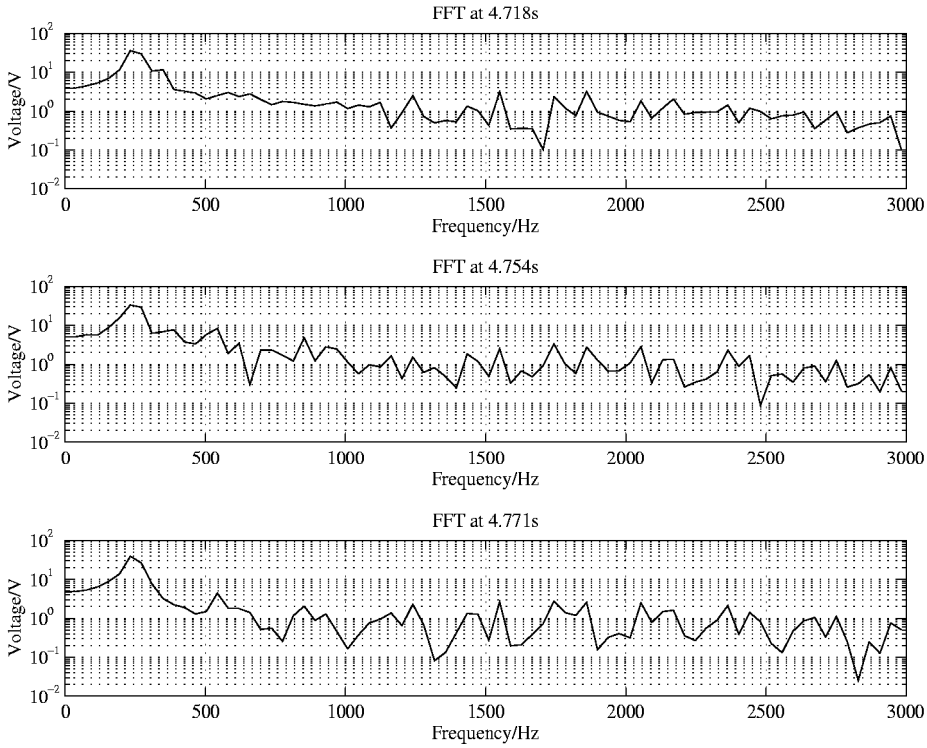

Figure 7.50: High Frequency Analysis of Phase S Voltage During Three Phase Fuse Burning Out — Cross Sections of STFT.

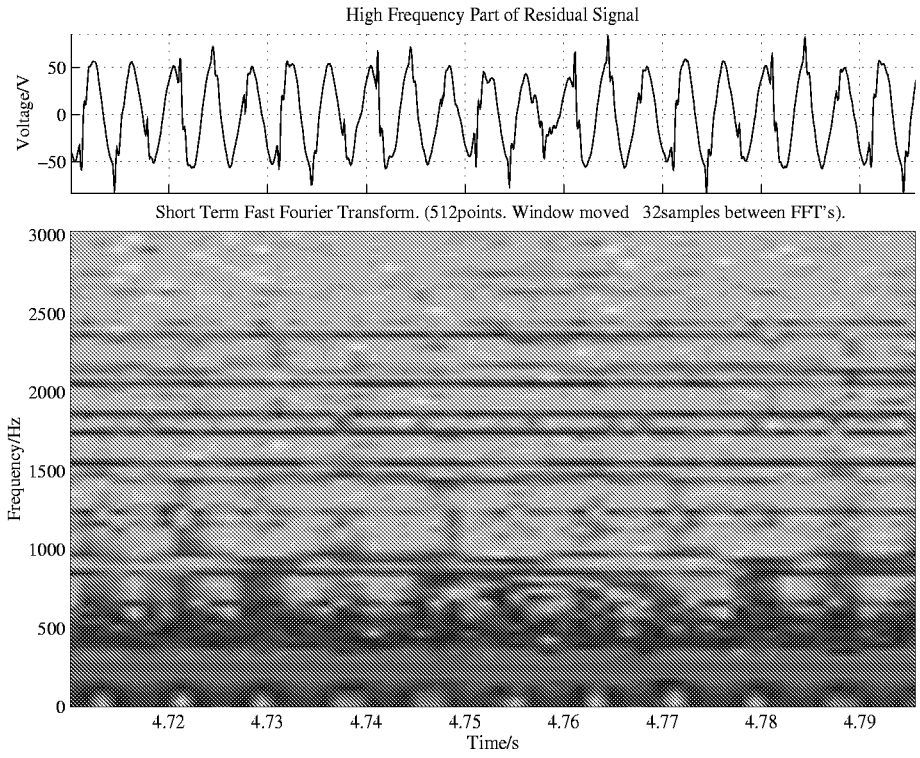

Figure 7.51: High Frequency Analysis of Phase T Voltage During Three Phase Fuse Burning Out.

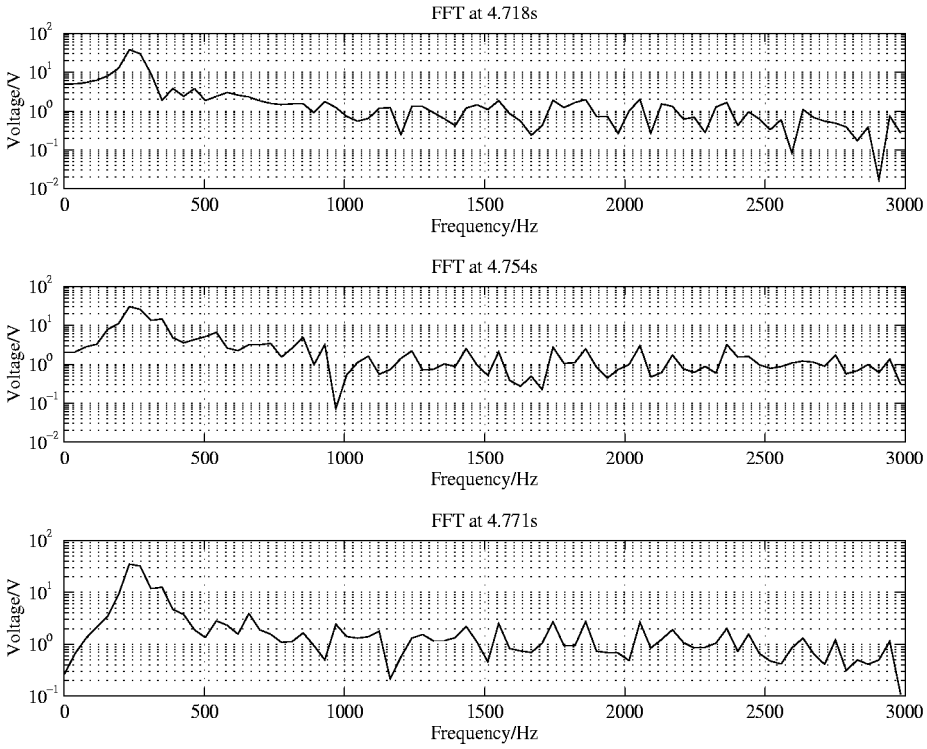

Figure 7.52: High Frequency Analysis of Phase T Voltage During Three Phase Fuse Burning Out — Cross Sections of STFT.

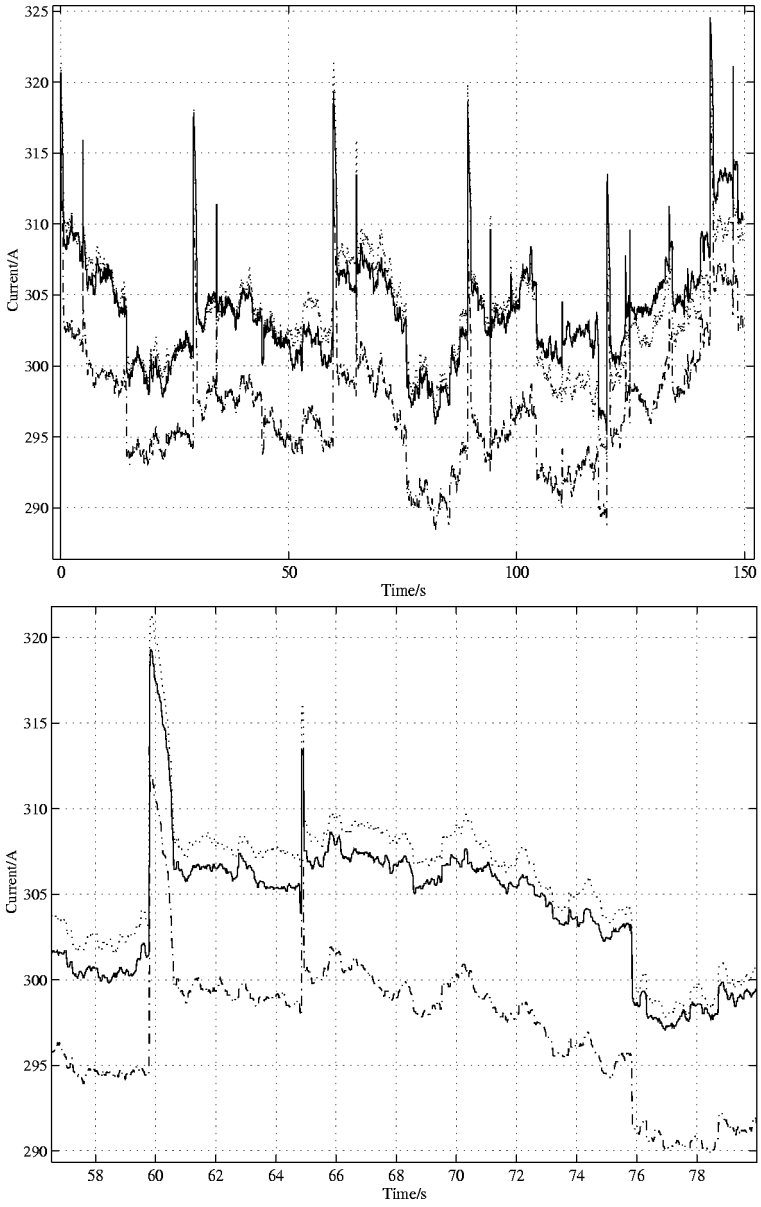

Figure 7.53: Kalman Estimate of the Amplitude of the Currents During Operation of Machines at DYRUP, (median filtered).

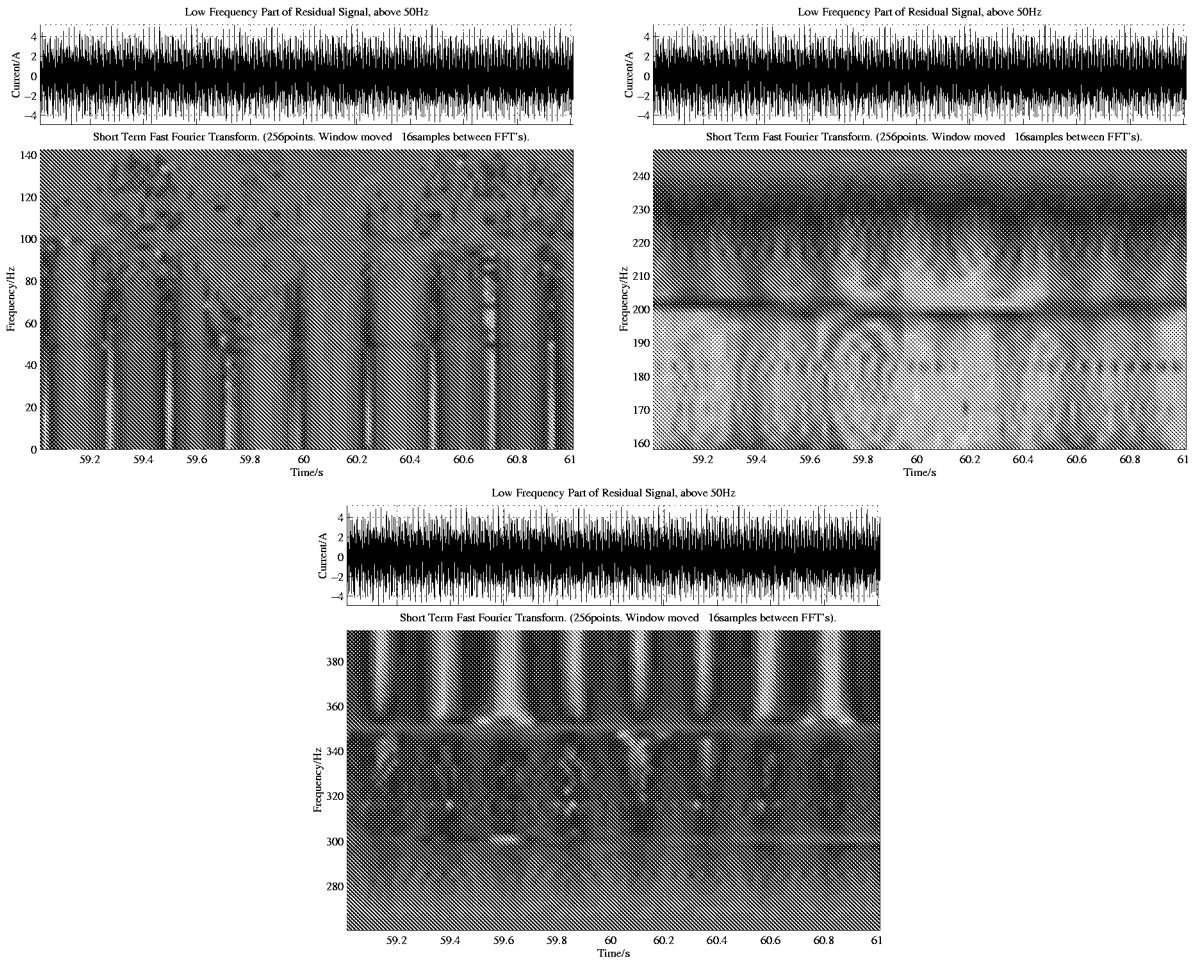

Figure 7.54: STFT of Phase R Current, First Part of Event, according to description on page 87. Notice that that frequencies around 150Hz have been omitted. This is due to the strong third harmonic.

information. This means, in the first place, "that the magnifying glass should be polished", so that the details are more clearly seen.

The drawback of the STFT is that it uses the same resolution all over. I.e. if one wants good resolution at the lower frequencies, one has to adjust the window length accordingly. This causes, however, that the higher frequencies are not optimally processed — and visa versa.

The Wavelet Transformation exhibits the quality of being a multi-resolution methods, i.e. the resolution Δt and Δf vary in the time-frequency plane, as explained in Section 6.8.2.

On the plots of the currents during the burning out of fuses, it is seen that the residual signal during the event resembles very much the *Mother Wavelet* shown in Figure 6.28 on page 62.

Work on time-frequency analysis using Wavelet Transformation in this context has been initiated as a student-project; the fourth project mentioned in the Preface on page iii.

It is intended to investigate the applicability of Wavelet-based methods to extract features of events.

Chapter 8

Discussion

Elements of a centralized monitoring system have been investigated and it has been shown possible to assign methods that may extract information from the measurements.

With these methods, the measurements of the three stages have been analysed.

At a very early stage, it was decided that the measurements were to be split into the fundamental- and residual components. All filters were implemented as FIR-filters. This was adequate for investigations. However, it may be considered instead to implement filters as IIR–filters, if it turns out that there is a problem with the implementation into hardware.
FIR–filters are convenient because they offer linear phase and because they are always stable. The latter requirement is less important as long as the filters are used in an environment with high precision, such as MATLAB that uses 64bit precision.
On the other hand, IIR–filters may be considered because filtering by such ones requires far less operations. But because of the above mentioned inconveniences, it is believed that IIR–filters are only to be used in the event that it will not otherwise be possible to implement the system into hardware.
During the work that is described in [Lauritsen, 1995] it was investigated whether the monitoring system, without the classification part, could be implemented into a floating point DSP from ANALOG DEVICES. No real problems were encountered in implementing these parts, though some parts of the system connected to, in fact, filtering, must be written in Assembler in order to make the system run real-time.

There seems to be no reason to doubt that the splitting up of the measurements should be the first module in an implementation of a centralized monitoring system.

Subsequent analysis will therefore be performed basically in two tracks.

The fundamental component has been processed by use of a Kalman filter that was developed around a two-state model, hence the amplitude and phase are the outputs of this module.
Tests on early implementations showed some sensitivity of the estimates to changes of the fundamental frequency.
Since larger changes of the fundamental frequency is an almost certain sign that something is severely wrong in the overlying electrical network, it was thought that calculation of an estimate of the fundamental component frequency would serve not only to enhance the estimates of the Kalman filter, but could also be used by the system to put itself in a waiting state during extreme situations.

However, the frequency estimation part of the system requires many operations and is by far the most demanding module of the system at this stage.
So far, it has not been proven feasible to detect extreme situations using deviations of the fundamental frequency. If it turns out that such ones may be detected by other means, it may be acceptable to abandon the frequency estimation. This is a question that must be investigated further. Removing the frequency estimation will cause oscillations to arise in the estimates from the Kalman filter. But this might be acceptable — considering the computational savings.

The Kalman filter has only been applied to the fundamental frequency. However, it seems intuitively reasonable that it could be beneficial also to estimate phases and amplitudes of some of the stronger

harmonics.
Because of the magnitude of the fundamental component, it causes a very distinctive peak in the linear prediction spectrum. But for harmonics, that are known to be significantly weaker, this may not be the case. Therefore, during the work described in [Lauritsen, 1995] an attempt was made to include more information into the estimation of the location of the maximum. In the DSP–implementation the maximum is found by LS–estimation, as opposed to the implementation that was tried during the work that is described in [Jespersen, 1994], where the spectrum around its maximum was modelled by a second order polynomial of which the maximum may be determined from three points only. However, nothing seems to be won by using LS–estimation, when estimating the fundamental frequency.

Having the first modules of a centralized monitoring system in place, the path was paved for having a closer look at the measurements.

8.1 Modelling

Thus far the work has been based on an assumption that activity in the network would cause high frequency components at the substation. Everybody seemed to agree that it had to be so, but nobody had any "evidence". A theoretical investigation of the signal transferring capabilities therefore was in its place.
As was discussed in Section 3.2 one faces a complicated problem when initiating modelling of distribution networks.
When regarding a stretch of cable as a transmission line, in the electro-magnetic sense, one must also consider what the terminations should be. By doing so, one takes a stand on the nature of the load.
In order to be satisfactory in this context, it was assumed that a passive, linear load was sufficient.
The cable was modelled in two ways; both as a three phase mutually coupled model and as a single phase model.
The three phase model was implemented in the ATP. Here it was made up of several Π–equivalents. The single phase model was made as a one section Π–equivalent.
Though both models are linear they are very different. First of all, the ATP–implementation exhibits a much higher order than the single phase model does. The two models should also be regarded as complementary, i.e. two different points of view of the same problem.

Using the two models gave, of course, different results. But the tendency was clear in both cases; cables may transmit rather high frequencies; into the tens of kiloHertz range.
Originally the hypothesis was that the bandwidth of the measurements should be at least 10kHz. The investigations of this has shown that the transferring capabilities of cables reach beyond that, though only frequencies up to about 7kHz have been seen in the Stage 2 Measurements. For the first time these measurements gave an image of the higher frequencies caused by events.
When evaluating the outcome of these measurements it is very important to bear in mind that the events were restricted to take place in the low-voltage network. The signals have therefore passed through a distribution transformer.
Though the signal transferring capabilities of distribution transformers are poorly investigated, the general view is that they behave like lowpass filters. The "cutoff frequency" is said to lie slightly above 1kHz.
It is therefore believed that had it been possible to make events happen directly on the 10kV cable, much higher frequencies would have arisen.

Modelling is an area where there is still a need for much more work.

This theoretical investigation has also opened up for new ideas. In Chapter 1 was mentioned that one of the questions that originally it was expected to clarify in this project, was what the impact would be of auxiliary measuring points placed along the feeder, see also Section 8.4.1.
One of the results of the DSO–project was that the communication channel that is required with every measuring point is very expensive. If it were possible to develop an inexpensive sensor that could inject back the measurements into the cable, the extra signal transferring capabilities of the cable would be utilized.
If it is assumed that "natural" frequencies up to 10kHz may be distinguished from the background noise,

then the higher frequencies could be used to transfer measurements. By doing so, the natural frequency contents are not polluted by communication signals.

8.2 State-Space Description of Load Composition

It is to be expected that the performance of a centralized monitoring system will depend on the activity on the feeder. This is a question that needs attention. One could think of all possible configurations (number of loads turned on, their location...) as states of a state-space description.

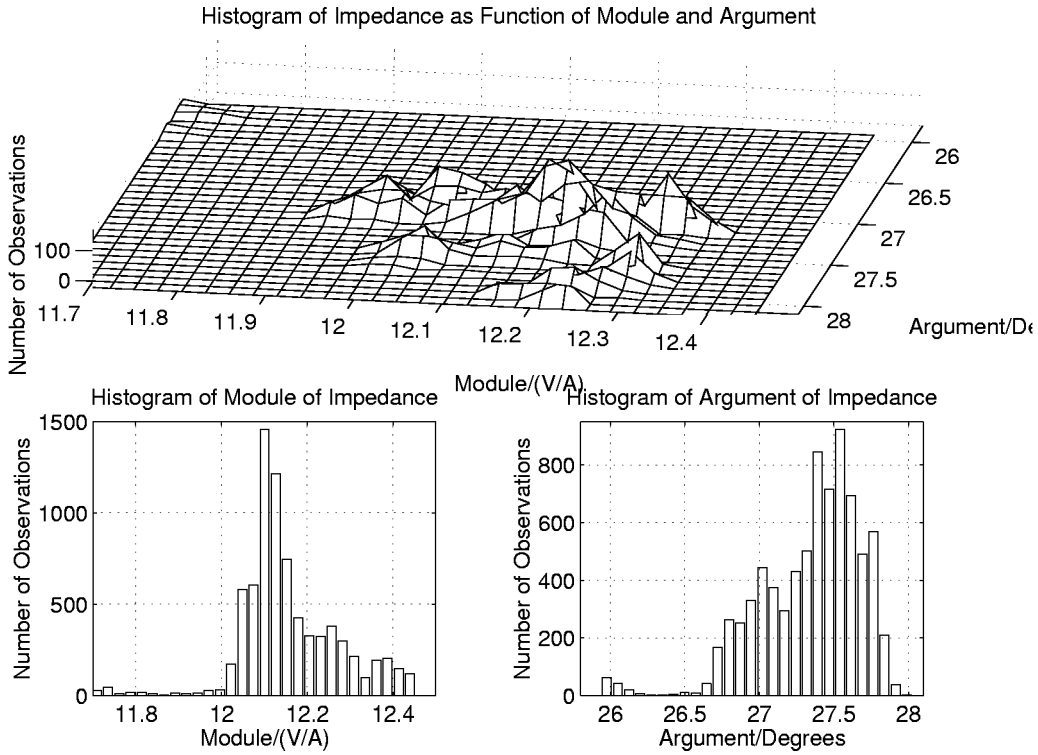

Figure 8.1: Histogram of Total Impedance as Function of Module and Argument Calculated from the Stage 2 Measurements.

As is more clearly seen in Figure 8.1, it is as if the impedance moves between a finite number of values, seen as "hills". This substantiates that some of the various states, the network may be in, may be distinguished.
Figure 8.1 was calculated on the basis of the Kalman filter estimates of a sequence from the Stage 2 Measurements.

Over a short period of time, these states explicitly correspond to a certain combination of loads connected to the feeder.
Again, over short periods of time, the transition between states may be described by a state-space model. The transition from one state to another implies what kind of operation caused the detected event.
Over longer periods of time transitions from these *micro state-spaces* to others will occur.
Figure 8.1 may be regarded as a visualization of one micro state space. This state space is a (small) part of the *total state-space* for the entire feeder. So, as the states move away from this "zoom", other regions of the total state-space will become the present micro state-space.
Let Figure 8.2 be a model of a micro state space. The dashed lines leaving the figure indicate connection to other parts of the total state space.

Monitoring current and voltage over long periods of time, the states and also the *state probabilities*, see [Jørsboe, 1984, Chapter 26], may be estimated.

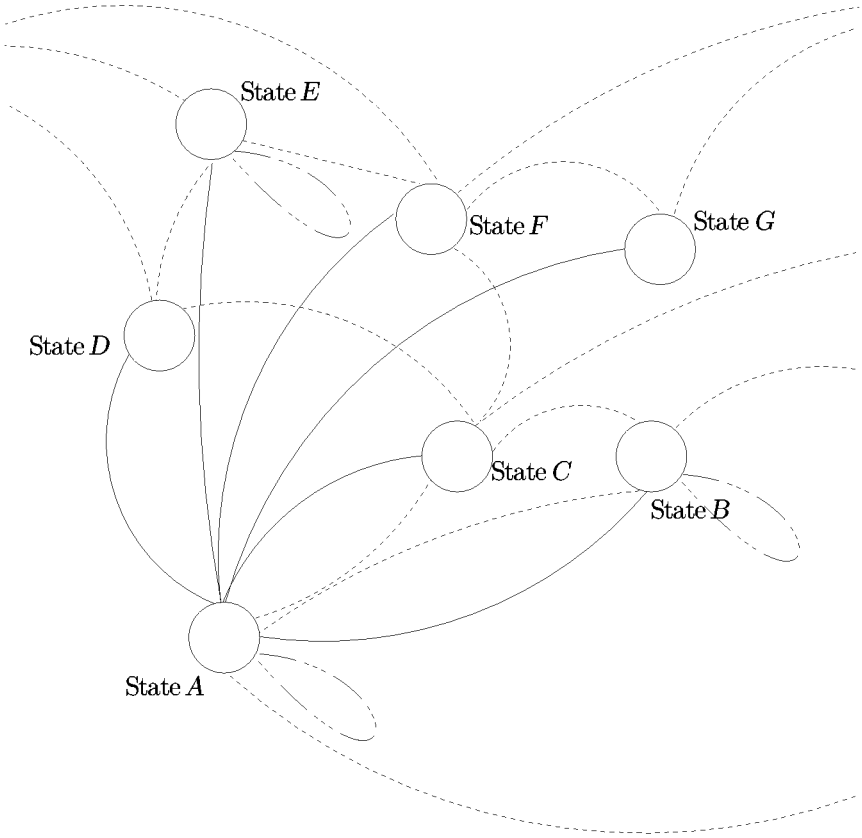

Figure 8.2: State Space Model with Indication of Possible Transitions.

Such a state space description will also accommodate that it may be more difficult to detect and classify some events at some times of the day, whereas at other times it may be fairly easy.
In the state space description this will be reflected by being in a state where the activity on the feeder is high.

8.3 Classification

On the basis of the information contained in the fundamental frequency, it has been shown that it is possible to define models and estimate the parameters so that two similar events may be distinguished.

At this stage of the project, the classification has been performed as "hands-on", i.e. human interaction has been required.
This is also perfectly satisfactory, because it has hereby been shown that it is possible to extract distinguishable parameters from different events. For the final use, it must be required that the algorithms may act "on their own", i.e. they do not need human interaction.

Based on the results from the initial work on classification, it seems very likely that methods may be developed that will at least be capable of processing events as strong as the operation of the motors at the factory.
An important open question arises at this point. 'How strong must events be, before they can be detected and classified'?
It is expected that the answer to this question will be based on insight in the nature of the activity on the feeder.
The events that have been treated during this project were intentionally very strong ones. Because, if it had not been possible to detect these, it would seem rather pointless to try with weaker ones.
It may also be argued that the types of events that have been tried are very limited. However, both high

and low frequency events have been investigated; namely very fast events and rather slow ones.
It has not been shown that this is sufficient to state that other events that could be said to lie in between, may also be detected and classified. But it does seem reasonable that it is so.

Burning out of fuses is a many-sided kind of event. Only one of the sides has been investigated; namely the burning out as the result of a short circuit. This led to a very high powered kind of event. However, fuses may also burn out in much less violent ways.
If a fuse is only slightly overloaded, it may hold the current for quite a while before it melts. In this case no sudden increase of the current will be seen and therefore the higher frequencies that were seen as the results of the experiments on short circuits will not occur.

The high frequency components that have been shown to arise during the burning out of fuses are believed to be a source of additional information.
Therefore, as a means of enhancing the performance of the classification scheme, classification must be based on using all available information.

The time-frequency analyses that were performed on the residual signals from the operation of the 90kW motor did not show significant traces of high frequency components.
Whether these events really are characterized by the absence of higher frequencies, is a result that needs to be confirmed, e.g. by Wavelet analyses, .
Assuming that higher frequencies practically do not arise, then the classification that was described in Section 6.7.1 was, in fact, based on all available information.

It is expected that one of the first steps of the classification system will be a Wavelet analysis of the input signals. The results will be passed on further into the classification module.

An important concept to be defined is the so-called *Equivalent Geometric Distance*. It covers the process of estimating where geographically an event occurred in the network.
In Appendix B is discussed a method to estimate the equivalent geometric distance. This method may be used in the transmission system, where the relay is intended to protect a small part of the transmission network that does not branch out.
Also, the task in relaying is to interrupt supply in the event of a fault, i.e. the current will attain a very high level.
These two facts make it fairly simple to develop methods that are capable of estimating the distance from the relaying point to the event (fault).
In a radial distribution network, where the feeders also branch out, several geometric distances will correspond to the same electrical distance. This fact complicates the problem enormously. Information from auxiliary measuring points placed at certain locations along a feeder may help to reduce the complexity of the problem, see Section 8.4.1.

In Appendix A.4 is reproduced the initial steps of investigations of this question. It is believed that solving this problem will be essential to the performance of the centralized monitoring system.

8.3.1 Fuzzy Logic and Neural Networks

Neither Fuzzy Logic nor Neural Networks have been tried out during the project. However, it does not seem reasonable that such methods could be applied to the problems that are faced in the context of centralized monitoring.

By intuition it seems clear that with an event at hand, it could be discussed how well it resembles one of the already known events. Situations like; 'it does look like this event, but it could also be that event', are expected to occur.

The neural network will be suited to adapt the system to one feeder. It is not likely that the system may be developed from knowledge of one feeder alone and afterwards carried to another and optimally function there.
Adaptivity to the feeder is believed to be a must. This could be accommodated by applying neural network techniques.
Unfortunately, such methods suffer today from being computationally very demanding.

[Kreiss, 1994] describes a Fuzzy Logic-based system to be used as a tool for determining the cause of abnormalities.
This reference confirms the above mentioned combination of adaptivity and Fuzzy Logic.

Regarding both Fuzzy Logic and Neural Networks it must be understood that they both represent ways of solving problems that one does not fully understand the nature of. Therefore, it is believed that resorting to these methods should be seen as the last solution. A solution that should only be used after having exhausted all other possibilities.

8.4 Sensors

Being the first link of the many that make up the centralized monitoring system, it is obvious that the obtainable quality of the ensemble system cannot exceed the quality of the sensors.

To be able to take measurements, it was necessary to make some compromises and choose equipment that was maybe not the most optimal.
Especially the choice of the current sensor was much influenced by considerations other than just finding the best one suitable.
That the choice of current sensor could/should have been better is indicated in Figures 6.2 and 6.3 on page 40. These figures show that the voltages contain higher frequencies than the currents — or rather that the spectrum of the current reaches the background noise sooner than the spectrum of the voltage. The voltage sensors were passive. It seems therefore reasonable to assume that they are capable of giving a correct image of the noise on the busbar.
On the other hand, the current sensors are active. Though a very big effort was made to design a better amplifier than the one was delivered with the sensors, it is very difficult to make an active sensor as noiseless as a passive.

It took a complete redesign of the amplifier part of the sensor and much work remains before that sensor is ideal for DISMO–application. Furthermore goes that the optical fiber is wound around a piece of normal transformer sheet metal. Such material is known not to be ideal for transferring high frequencies. Therefore, it appears to be more reasonable to apply other sensor principles, such as Rugowski Coils.
Though in its un-modified form, the sensor could serve the purposes of utilities as they are today, it is believed that utilities should realize that in future, it will be required of sensors that they are capable of measuring other frequency components than the fundamental. Therefore, already today utilities must prepare for purchasing current sensors that can measure with high quality — despite that it may still last some years before their potential may be fully exploited.

Voltage probes as the ones used during the Stage 2 Measurements are of sufficiently good quality. But maybe they are not the most ideally suited for en-masse installation. After all, they are conceived as oscilloscope probes.

On the other hand, the time-frequency analyses have shown that only very weak traces of events are found in the higher frequencies of voltages. Therefore differentiated quality criteria for voltage and current sensors could be defined.
There is little doubt that currents should be measured with very high quality.
Regarding the voltages, it could be considered to ensure high quality over a narrower frequency band. Maybe a good image of the 50Hz component alone would be sufficient.
Work on the development of a classification scheme will show if it really is necessary to measure voltages in as good a quality as currents.

8.4.1 Auxiliary Measuring Points

Until now, the project has shown that strong events are easily seen from the *OP*. The problem of distinguishing events that occur in the same electrical distance from the *OP*, but on different branches of the feeder is one that needs further attention.
It must be investigated if the installation of auxiliary sensors, so-called *slave measuring points*, at locations on the feeder may contribute sufficient information to motivate the extra expenses.

Such an investigation will have many sides. First of all these extra sensors must be very cheap. This imposes some limits to what may be achieved.

It would seem obvious for communication purposes to exploit the extra signal transferring capabilities of cables. This will result in a limitation of the bandwidth; at the best some tens of kiloHertz.
This capacity must be divided between all the auxiliary sensors, further limiting the actual available bandwidth of one sensor.

It is also very important to investigate how slave measuring points should be located in the network.

Chapter 9

Conclusion

This Ph.D.–project has demonstrated that centralized monitoring will be possible.

The perspectives of this result to electricity utilities are far-reaching. If, as expected, utilities will decide on detailed monitoring of their distribution networks, the DISMO–concept will certainly be worth considering. Because, by taking the step from transmission network monitoring to distribution network monitoring, the number of nodes becomes orders of magnitude larger. Therefore, the "money-density" will become small, i.e. the equipment must be cheap, because so many units are needed.

A so-called DISMO–*O*bservation *P*oint is equipped with high quality sensors.
In this project the current sensors were optically based.
Much work was made to enhance an existing model. However, the conclusion from that work and the subsequent analysis of the measurements taken with the enhanced sensor, is that it must be advised against relying on sensors based on this principle in the future. To be used in distribution networks other, simpler sensor principles should be applied — contrary to the voltage levels of transmission networks, where it is easier to motivate going through all the difficulties of applying optical current sensors.

At this stage the results indicate that currents and voltages need not be measured in the same quality.
Currents should be measured in a bandwidth of about 10kHz. The dynamic range should be better than the about 90dB that was obtainable with the enhanced optical current sensor.
The voltages are rather insensitive to events in the network. But, as they serve an important role as reference for measures of phase, at least the fundamental frequency component must be measured in high quality. Measuring the fundamental component solely, vastly reduces the requirements to voltage sensors.
First of all, the required dynamic range of measuring busbar voltages will be low. Only in extreme situations will the voltage deviate much from its nominal value.

It must be realized that the complexity of the electrical network is very high. Therefore, as was discussed in Chapter 8, the influence on a centralized monitoring system of many parameters are still to be investigated before the goal; a working centralized monitoring system, is reached.
In this project it has been shown that on the basis of measurements taken only at the substation, it is possible to extract parameters, so that two similar events, that occur at the same location in the network, may be distinguished.
This is a very important result, as it shows that details about events are transmitted to the substation. Despite so few events, of all possible, have been investigated, the results lead to the conclusion that it is only a question of allocating sufficient resources to the development of a centralized monitoring system, before such one could be seen in action, monitoring a feeder.

As was indicated in Chapter 1 and discussed in Chapter 8 it must be clarified what will be the outcome of providing additional information to the centralized monitoring system from some locations in the network.
This will require sensors. As was stated, all equipment to be used as part of a monitoring system for the distribution network must be cheap.
In Chapter 3 the signal transferring capabilities of cables were investigated. The conclusion of that investigation is that the bandwidth of cables is higher than the bandwidth of the signals that were measured

at the substation.
If sensors could be developed that send their measurements back on the cable, it should be no problem to add to the centralized monitoring system algorithms that extract that information from the measurements, see Section 9.1.

9.1 Future Work

Research should be initiated in methods for protocol-free communication on the electrical network.
Such a communication scheme should be part of a sensor that does not need ground reference, but may be clamped on the cable.
To keep the price low, it must be investigated if such a unit could be made power "self-sufficient", i.e. taking the required energy from the cable.

Along with the on-going research in centralized monitoring methods, work on making a commercial product available could be initiated.

Classification is a many-sided problem that still needs much attention.
The development of classification methods will be influenced by the availability of auxiliary measuring points. Therefore, it is believed that it should be given high priority to investigate the possibilities of having reported back to the *OP* measurements from some nodes along the feeder.

As has been stated, research in the use of Wavelet Transformation as a means of extracting information is an interesting topic. Therefore work within this area should proceed. See e.g. [Nielsen, 1995].

More information is needed to form the basis of a statistical description on the nature of the activity on a real feeder.
Therefore it is required to acquire more measurements. To do so, a system that may perform some kind of data reduction right at the *OP* is needed.

Higher order spectra analysis could be an interesting tool to investigate, see e.g. [Nikias and Mendel, 1993] and [Swami *et al.*, 1993].

Acknowledgements

Besides the members of the steering committee, whom I am greatly obliged to for their support, I wish to thank specifically the following people for their assistance and interest in this work.
The ordering is alphabetical and does by no means express any kind of priority.

Mr. Flemming Bo Christiansen of NESA A/S for preparing the two measuring points of the Stage 1 Measurements and assisting while the experiments were performed.

Mr. Laurent Dubé for his kind assistance on using `MODELS` under ATP.

Mr. Allan Grukov of the ELECTRONICS INSTITUTE at the TECHNICAL UNIVERSITY for his extremely valuable work on improving the optical current sensor used during the Stage 2 Measurements.

Mr. Erling Hansen of NESA A/S for interesting and inspiring discussions during the initial stages of the project.

Mr. Mogens Hansen of NESA A/S for planning the burning out of fuses during the Stage 2 Measurements and for many educative conversations.

Mr. Torben F. Hansen of NESA A/S for preparation of the site for fuse burning out during the Stage 2 Measurements, and for operating the switch to provoke the short circuit.

Mr. Per Herager of NESA A/S for making it possible to establish the *OP* at GLENTEGÅRD.

Mr. Gunner Isbrandt of NESA A/S for helping with finding a suitable feeder for the experiments.

Ms. Inger Lise Munk for proofreading this thesis.

Mr. Gunner Nissen of DYRUP A/S for letting us use machines at the factory during the experiments.

Ms. Anja Degn-Petersen of NESA A/S for assistance with the Stage 0 Measurements.

Dr. Paulo F. Ribeiro for educative discussions on modelling and Wavelet Transformation both via E-mail and during my stay in the U.S.A.

Paulo also had arranged everything nicely for my stay in San Jose. I warmly thank him for making that trip a success.

Mr. Frey Ulman of NESA A/S for his sincere interest in the project and kind assistance during all three stages af the measurements.

Mr. Niels Weber of NESA A/S for assisting in taking the Stage 0 Measurements in the middle of the night.

Mr. Harald Wehrend of the University in Hannover for assistance on EMTP–modelling.

Bibliography

[Akansu and Haddad, 1992] Ali N. Akansu and Richard A. Haddad. *Multiresolution Signal Decomposition, Transforms □ Subbands □ Wavelets.* Academic Press, Inc., 1992.

[ATV, 1994] Erhvervsforskerudvalget, Akademiet for de Tekniske Videnskaber, Lundtoftevej 266, DK–2800 Lyngby. *Erhvervsforskeruddannelsen, vejledning til erhvervsforskeruddannelsen*, Mar. 1994.

[Aucoin and Russel, 1987] Mike Aucoin and B. Don Russel. Detection of distribution high impedance faults using burst noise signals near 60Hz. *IEEE Transactions on Power Delivery*, 2(2):342–348, Apr. 1987.

[Bastard *et al.*, 1992] Patrick Bastard, Pierre Bertrand, Tokuo Emura, and Michel Meunier. The technique of finite-impulse-response filtering applied to digital protection and control of medium voltage power system. *IEEE Transactions on Power Delivery*, 7(2):620–626, Apr. 1992.

[Begović *et al.*, 1993] Miroslav M. Begović, Petar M. Djurić, Sean Dunlap, and Arun G. Phadke. Frequency tracking in power networks in the presence of harmonics. *IEEE Transactions on Power Delivery*, 8(2):480–486, Apr. 1993.

[Beides and Heydt, 1991] Husam M. Beides and G. T. Heydt. Dynamic state estimation of power system harmonics using Kalman filter methodology. *IEEE Transactions on Power Delivery*, 6(4):1663–1669, Oct. 1991.

[Bellanger, 1990] Maurice Bellanger. *Digital Processing of Signals, Theory and Practice.* John Wiley & Sons, 2nd edition, 1990.

[Benmouyal, 1992] Gabriel Benmouyal. Frequency-domain characterization of Kalman filters as applied to power system protection. *IEEE Transactions on Power Delivery*, 7(3):1129–1138, Jul. 1992.

[Bergeal and Moller, 1981] J. Bergeal and L. Moller. Influence des charges sur la propagation des perturbations de type harmoniques. Principales consequences. Technical report, Direction des Études et Recherches – EDF Clamart, 1, av. du Général de Gaulle, F-92141 Clamart, France, 1981.

[Bergeal and Moller, 1982] J. Bergeal and L. Moller. Étude analytique de l'impédance spectrale d'un réseau. Utilisation de métodes numériques. Technical report, Direction des Études et Recherches – EDF Clamart, France, 1982.

[Bernard and Durocher, 1994] J.-P. Bernard and D. Durocher. An expert system for fault diagnosis integrated in existing SCADA systems. *IEEE Transactions on Power Systems*, 9(1):548–554, Feb. 1994.

[Bickford *et al.*, 1980] J.P. Bickford, N. Mullineux, and J.R. Reed. *Computation of Power System Transients.* Peter Peregrinus Ltd., 1980.

[Boel Pedersen, 1986] Simon Boel Pedersen. *Signalanalyse I & II.* Laboratoriet for Akustik, Danmarks Tekniske Højskole, 1986.

[Boel Pedersen, 1987] Simon Boel Pedersen. *Anvendt Digital Signalbehandling. 1. Sampling & Kvantisering.* Laboratoriet for Akustik, Danmarks Tekniske Højskole, 1987.

[Bose, 1985] N. K. Bose. *Digital Filters, Theory and Applications.* Elsevier Science Publishing Co. Inc. 1985.

[Brown and Hwang, 1992] Robert G. Brown and Patrick Y. C. Hwang. *Introduction to Random Signals and Applied Kalman Filtering.* John Wiley & Sons, Inc., 1992.

[Chang *et al.*, 1994] Yu Lo Cyrus Chang, Leslie C. Lander, Horng-Shing Lu, and Martin T. Wells. Bayes analysis for fault location in distributed systems. *IEEE Transactions on Reliability*, 43(3):457–465, Sep. 1994.

[Chui, 1992] Charles K. Chui. *Wavelets Analysis and its Applications, An Introduction to Wavelets*, volume I. Kluwer Academic Publishers, 1992.

[Clarke, 1943] Edith Clarke. *Circuit Analysis of A-C Power Systems*, volume I. John Wiley & Sons, Inc., 1943.

[Cody, 1992] Mac A. Cody. The fast wavelet transform. Beyond Fourier transforms. *Dr. Dobb's Journal*, pages pp. 16–28 and 100–101, Apr. 1992.

[Data Translation, 1992] Data Translation, Inc., 100 Locke Drive, Marlboro, MA-01752-1191, U.S.A. *DT2832 Series*, Sept. 1992.

[Daubechies, 1987] I. Daubechies. Orthonormal bases of wavelets with finite support – connection with discrete filters. In J. M. Combes, A. Grossmann, and Ph. Tchamitchian, editors, *Wavelets: Time-Frequency Methods and Phase Space. Proceedings of the International Conference, Marseille, France*, pages 38–65, 1987.

[Denys *et al.*, 1991] Ph. Denys, C. Counan, L. Hossenlopp, and C. Holweck. Measurement of voltage phase for the French future defence plan against losses of synchronism. *IEEE Transactions on Power Delivery*, 1991.

[Derin and Kelly, 1989] Haluk Derin and Patrick A. Kelly. Discrete-index Markov-type random processes. In *Proceedings of the IEEE*, volume 77, pages 1485–1510, 1989.

[Dommel and others, 1986] Hermann W. Dommel et al. *Electromagnetic Transients Program Reference Manual, EMTP Theory Book.* Bonneville Power Administration, Portland, U.S.A., 1986.

[Eichhorn and Łobos, 1991] K.-Fr. Eichhorn and T. Łobos. Recursive real-time calculation of basic waveforms of signals. *IEE Proceedings*, 138, Pt. C(6):469–470, Nov. 1991.

[Emanuel *et al.*, 1994] A.E. Emanuel, J. Janczak, D.J. Pileggi, E.M. Gulachenski, C.E. Root, M. Breen, and T.J. Gentile. Voltage distortion in distribution feeders with nonlinear loads. *IEEE Transactions on Power Delivery*, 9(1):79–87, Jan. 1994.

[Emanuel, 1990] Alexander Eigeles Emanuel. Powers in nonsinusoidal situations a review of definitions and physical meaning. *IEEE Transactions on Power Delivery*, 5(3):1377–1389, Jul. 1990.

[Gallagher and Wise, 1975] N.C. Gallagher and G.L. Wise. A theoretical analysis of the properties of median filters. *IEEE Transactions on Acoustics, Speech and Signal Processing*, 29(6):207–221, Apr. 1975.

[Gardner, 1963] Murray F. Gardner. *Transients in Linear Systems*, volume I. John Wiley & Sons, Inc., 16^{th} edition, 1963.

[Gardner, 1988] William A. Gardner. *Statistical Spectral Analysis.* Prentice Hall, 1988.

[Gaunholt, 1988] Hans Gaunholt. *Konvertering af Samplinghastighed.* Instituttet for Teleteknik, Danmarks Tekniske Højskole, 1988.

[GEC Measurements, 1987] The General Electric Company p.l.c. GEC Measurements. *Protective Relays. Application Guide.* GEC Measurements, The General Electric Company p.l.c., St. Leonards Works, Stafford, ST174LX, England, 1987.

[Girgis and Brown, 1981] Adly A. Girgis and R. Grover Brown. Application of Kalman filtering in computer relaying. *IEEE Transactions on Power Apparatus and Systems*, 100(7):3387–3395, Jul. 1981.

[Girgis and Brown, 1985] Adly A. Girgis and R. Grower Brown. Adaptive kalman filtering in computer relaying: Fault classification using voltage models. *IEEE Transactions on Power Apparatus and Systems*, 104:1168–1177, May. 1985.

[Girgis and Hwang, 1984] Adly A. Girgis and T. L. Daniel Hwang. Optimal estimation of voltage phasors and frequency deviation using linear and non-linear Kalman filtering: Theory and limitations. *IEEE Transactions on Power Apparatus and Systems*, 103(10):2943–2951, Oct. 1984.

[Girgis and McManis, 1989] Adly A. Girgis and R. Brent McManis. Frequency domain techniques for modeling distribution or transmission networks using capacitor switching induced transients. *IEEE Transactions on Power Delivery*, 4(3):1882–1890, Jul. 1989.

[Girgis *et al.*, 1991] Adly A. Girgis, W. Bin Chang, and Elham B. Makram. A digital recursive measurement scheme for on-line tracking of power system harmonics. *IEEE Transactions on Power Delivery*, 6(3):1153–1160, Jul. 1991.

[Golub and van Loan, 1989] Gene Golub and Charles F. van Loan. *Matrix Computations.* The John Hopkins University Press, 2 edition, 1989.

[Gooi and Sebo, 1985] H. B. Gooi and S. A. Sebo. Distribution of ground fault currents along transmission lines – an improved algorithm. *IEEE Transactions on Power Apparatus and Systems*, 104(3):663–669, Mar. 1985.

[Gorman and Granger, 1992] Michael J. Gorman and John J. Granger. Transformer modelling for distribution system studies. Part I: Linear modelling basics. *IEEE Transactions on Power Delivery*, 7(2):567–580, Apr. 1992.

[Grace, 1993] Andrew Grace. *OPTIMIZATION TOOLBOX, for use with* MATLAB™. The MathWorks, Inc., Jun. 1993. See also [MATLAB, 1992].

[Greenfield, 1984] E. W. Greenfield. Transient behaviour of short and long cables. *IEEE Transactions on Power Apparatus and Systems*, 103(11):3193–3203, Nov. 1984.

[Griffiths, 1975] Lloyd J. Griffiths. Rapid measurement of digital instantanous frequency. *IEEE Transactions on Acoustics, Speech and Signal Processing*, 23(2):207–221, Apr. 1975.

[Haavisto *et al.*, 1988] P. Haavisto, Pekka Heinonen, and Yrjö Neuvo. Vector FIR-median hybrid filters for multispectral signals. *Electronics Letters*, 24(1):7–8, Jan. 1988.

[Hansen, 1985] Per Christian Hansen. *Hæfte 53 – Kurvetilpasning.* Numerisk Institut, Danmarks Tekniske Højskole, 1985. Notes used in the course Numerical Methods.

[Hart, 1992] George W. Hart. Nonintrusive appliance load monitoring. In *Proceedings of the IEEE*, volume 80, pages 1870–1891, Dec. 1992.

[Hatziargyriou and Papadopoulos, 1989] N. D. Hatziargyriou and M. Papadopoulos. Transient analysis of extended distribution networks. *IEEE Transactions on Power Delivery*, 4(2):1290–1296, Apr. 1989.

[Haykin, 1991] Simon Haykin. *Adaptive Filter Theory.* Prentice-Hall, 1991.

[Heinonen and Neuvo, 1988] Pekka Heinonen and Yrjö Neuvo. FIR-median hybrid filter with predictive FIR substructures. *IEEE Transactions on Acoustics, Speech and Signal Processing*, 36(6):892–899, Jun. 1988.

[Hemminger *et al.*, 1987] R. C. Hemminger, L. J. Gale, and J. B. O'Neal. Signal propagation on single phase distribution lines at power line carrier frequencies. *IEEE Transactions on Power Delivery*, 2(1):28–33, Jan. 1987.

[Heydt, 1989a] G. T. Heydt. Identification of harmonic sources by a state estimation technique. *IEEE Transactions on Power Delivery*, 4(1):569–576, Jan. 1989.

[Heydt, 1989b] G. T. Heydt. A new method for the calculation of subtransmission and distribution system transients based on the FFT. *IEEE Transactions on Power Delivery*, 4(3):1869–1875, Jul. 1989.

[Hiyama *et al.*, 1989] T. Hiyama, M. S. A. A. Hammam, and Thomas H. Ortmeyer. Distribution system modeling with distributed harmonic sources. *IEEE Transactions on Power Delivery*, 4(2):1297–1304, Apr. 1989.

[Høg, 1994] Rasmus Høg. Analyse af transienter i el-distributionsnetværk. Master's thesis, Danmarks Tekniske Universitet, Elektronisk Institut, 1994.

[Høholdt *et al.*, 1984] Tom Høholdt, Helge Elbrønd Jensen, and Frank Nielsen. *Lineære Differential Ligninger.* Matematisk Institut, Danmarks Tekniske Højskole, 1984.

[Horowitz *et al.*, 1988] S.H. Horowitz, A.G. Phadke, and J.S. Thorp. Adaptive transmission system relaying. *IEEE Transactions on Power Delivery*, 3(4):1436–1445, Oct. 1988.

[Huelsman and Allen, 1980] L. P. Huelsman and P. E. Allen. *Introduction to the Theory and Design of Active Filters.* McGraw-Hill Book Company, 1980.

[Jenkins and Watts, 1968] Gwilym M. Jenkins and Donald G. Watts. *Spectral Analysis and its applications.* Holden-Day, 1968.

[Jensen, 1977] A. Frank Jensen. *Netværksteori I.* Instituttet for Teleteknik, Den Polytekniske Læreanstalt, 1977.

[Jespersen, 1994] Jesper Kring Jespersen. Analyse af transienter i el-distributionsnetværk, detektion. Master's thesis, Danmars Tekniske Universitet, Elektronisk Institut, 1994.

[Jeyasurya and Smolinski, 1983] B. Jeyasurya and W.J. Smolinski. Identification of a best algorithm for digital distance protection of transmission lines. *IEEE Transactions on Power Apparatus and Systems*, 102(10):3358–3370, Oct. 1983.

[Johnson *et al.*, 1992] David E. Johnson, Johnny R. Johnson, and John L. Hilburn. *Electric Circuit Analysis.* Prentice-Hall, 1992.

[Jørsboe, 1984] Ole Groth Jørsboe. *Sandsynlighedsregning.* Matematisk Institut, Danmarks Teksniske Højskole, 1984.

[Kamwa and Grondin, 1992] I. Kamwa and R. Grondin. Fast adaptive schemes for tracking voltage phasor and local frequency in power transmission and distribution systems. *IEEE Transactions on Power Delivery*, 7(2):789–795, Apr. 1992.

[Karlsson and Gjendal, 1986] P.W. Karlsson and S.J. Gjendal. *Indledende Teknisk Elektromagnetisme, forelæsningsnoter.* Fysisk Laboratorium II, Den Polytekniske Læreanstalt, 3 edition, 1986.

[Karlsson and Hill, 1994] Daniel Karlsson and David J. Hill. Modelling and identification of nonlinear dynamic loads in power systems. *IEEE Transactions on Power Systems*, 9(1):157–166, Feb. 1994.

[Koefoed Møller *et al.*, 1988] Peter Koefoed Møller, Simon Boel Pedersen, and John Aasted Sørensen. Anvendt digital signalbehandling, bd. 1– 8. Elektronisk Institut, Danmarks Tekniske Højskole, 1988.

[Kolcio *et al.*, 1992] N. Kolcio, J.A. Halladay, G.D. Allen, and E.N. Fromholtz. Transient overvoltages and overcurrents on 12.47kV distribution lines: Field test results. *IEEE Transactions on Power Delivery*, 7(3):1359–1365, Jul. 1992.

[Kolcio *et al.*, 1993] N. Kolcio, J.A. Halladay, G.D. Allen, and E.N. Fromholtz. Transient overvoltages and overcurrents on 12.47kV distribution lines: Computer modelling results. *IEEE Transactions on Power Delivery*, 8(1):359–366, Jan. 1993.

[Krebs, 1989] Rainer Krebs. Richtungsbestimmung von oberschwingungsquellen und anisotropien in drehstromnetzen. *etzArchiv*, Bd. 11 (H. 9):291–294, 1989.

[Kreiss, 1994] David G. Kreiss. Analyzing voltage disturbances using a fuzzy logic based expert system. In *Third International Conference on Power Quality: End-Use Applications and Perspectives*, 1994.

[Larsen *et al.*, 1987] P. Martin Larsen, T. Leisner, J. Rønne-Hansen, B. Svarrer Hansen, and O. Tønnesen. *Stærkstrømsteknik.* Stækstrømsafdelingen, Danmarks Tekniske Højskole, 1987.

[Lauritsen, 1995] Thomas Kjær Lauritsen. Analyse af transienter i el-distributionsnetværk, implementering i hardware. (*DSP implementering af overvågningssystem til 10kV distributionsnetværk*). Master's thesis, The Technical University of Denmark, DTU, Elektronisk Institut, 1995.

[LEC, 1992] Leuven EMTP Center. *Alternative Transients Program Rule Book*, June 1992.

[Lee and Messerschmitt, 1988] Edward A. Lee and David G. Messerschmitt. *Digital Communication.* Kluwer Academic Publishers, P.O. Box 322, NL-3300 AH Dordrecht, The Netherlands, 1988.

[Lehtonen, 1992] Matti Lehtonen. *Transient Analysis for Ground Fault Distance Estimation in Electrical Distribution Networks.* PhD thesis, VTT Technical Research Centre of Finland, Esbo, 1992.

[Little and Shure, 1993] John N. Little and Loren Shure. *SIGNAL PROCESSING TOOLBOX, for use with* MATLAB^{TM}. The MathWorks, Inc., May. 1993. See also [MATLAB, 1992].

[Liu, 1992] Chen-Ching Liu, editor. *Proceedings of the IEEE, Special Issue on Knowledge-Based Systems in Electric Power Systems*, 1992.

[Ljung, 1987] Lennart Ljung. *System Identification: Theory for the User.* Prentice-Hall, 1987.

[Ljung, 1993] Lennart Ljung. *SYSTEM IDENTIFICATION TOOLBOX, for use with* MATLAB^{TM}. The MathWorks, Inc., May 1993. See also [MATLAB, 1992].

[Lobos, 1989] T. Lobos. Nonrecursive methods for real-time determination of basic waveforms of voltage and currents. *IEE Proceedings*, 136, Pt. C(6):347–351, Nov. 1989.

[Madsen, 1989] Henrik Madsen. *Tidsrækkeanalyse.* Institutet for Matematisk Statestik og Operationsanalyse, Danmarks Tekniske Højskole, 1989.

[Mak, 1993] Sioe T. Mak. Propagation of transients in a distribution network. *IEEE Transactions on Power Delivery*, 8(1):337–343, Jan. 1993.

[MATLAB, 1992] The MathWorks, Inc.. *MATLAB, High-Performance Numeric Computation and Visualization Software, Reference Guide*, Aug. 1992.

[McGrananghan *et al.*, 1981] M. F. McGrananghan, J. H. Shaw, and R. E. Owen. Measuring voltage and current harmonics on distribution systems. *IEEE Transactions on Power Apparatus and Systems*, 100(7):3599–3608, Jul. 1981.

[McLaren and Redfern, 1975] P. G. McLaren and M. A. Redfern. Fourier-series techniques applied to distance protection. *IEE Proceesings*, 122(11):1301–1305, Nov. 1975.

[Mejlbro, 1985] Leif Mejlbro. *Kompleks Funktionsteori.* Matematisk Institut, Danmarks Tekniske Højskole, 1985.

[Morched and Kundur, 1987] A. S. Morched and P. Kundur. Identificaton and modelling of load characteristics at high frequencies. *IEEE Transactions on Power Systems*, 2(1):153–160, Feb. 1987.

[Munk and Aasted Sørensen, 1995] Steen M. Munk and John Aasted Sørensen. Distribution network monitoring. In *Fourth International Conference on Power Quality: End-Use Applications and Perspectives*, 1995. See Appendix J.

[Nayak *et al.*, 1995] Omprakash Nayak, Garth Irwin, and Arthur Neufeld. GUI enhances electromagnetic transients simulation tools. *IEEE Computer Applications in Power*, 8(1):17–22, Jan. 1995.

[NESA, 1962] Lavspændingssikringer, L.K. patronsikringer, træge, 1962. NESA ref. H 3d 51.

[NESA, 1978] Analyse af den sjællandske netfrekvens. Technical Report R 1978-94, NESA/IFV's netudvalg. EK's netudvalg, NESA A/S, Strandvejen 102, DK-2900 Hellerup, Nov. 1978.

[Nielsen *et al.*, 1993] Arne Hejde Nielsen, Knud Ole Helgesen Pedersen, Torben Rahbek, John Aasted Sørensen, and Steen Michael Munk. Optimal udnyttelse af strøm- og spændingsmålinger i distributionsnet, endelig uddannelsesplan/syllabus for Ph.D. project EF467. Published as requested by the Academy of Technical Sciences to fulfil the obligation to have the syllabus approved within six months of the start of the project. Reference: EF467-93.011, May 1993. In English.

[Nielsen, 1995] Jacob Thymann Nielsen. Analyse af transienter i el-distributionsnetværk, Waveletanalyse. Master's thesis, Danmars Tekniske Universitet, Elektronisk Institut, 1995. In English.

[Nikias and Mendel, 1993] Chrysostomos L. Nikias and Jerry M. Mendel. Signal processing with higher-order spectra. *IEEE Signal Processing Magazine*, pages 10–37, Jul. 1993.

[NKT, 1984] NKT. *Kabelteknisk håndbog, Stærkstrøm.* København, 1984.

[Öistämö *et al.*, 1992] Kai Öistämö, Petri Jarske, Jaakko Astola, and Yrjö Neuvo. Vector median filters for complex signal. In *International Conference on Acoustics, Speech and Signal Processing*, volume 2, pages 813–816, 1992.

[Olesen, 1975] Ole Jan Olesen. *En systematisk behandling af tilstandsestimering for elforsyningsnet.* PhD thesis, Danmarks Tekniske Højskole, Stærkstrømsafdelingen, 1975.

[Oppenheim and Schafer, 1975] Alan V. Oppenheim and Ronald W. Schafer. *Digital Signal Processing.* Prentice-Hall, Inc., 1975.

[Phadke and Thorp, 1988] Arun G. Phadke and James S. Thorp. *Computer Relaying for Power Systems.* John Wiley & Sons, Inc., 1988.

[Pinto de Sá, 1992] J. L. Pinto de Sá. A new Kalman filtering approach to digital relaying. *IEEE Transactions on Power Delivery*, 7(3):1652–1660, Jul. 1992.

[Porat and Friedlander, 1992a] Boaz Porat and Benjamin Friedlander. Performance analysis of a class of transient detection algorithms – a unified framework. *IEEE Transactions on Signal Processing*, 40(10):2536–2546, Oct. 1992.

[Porat and Friedlander, 1992b] Boaz Porat and Benjamin Friedlander. Performance analysis of transient detectors based on a class of linear data transforms. *IEEE Transactions on Information Theory*, 38(2):665–673, Mar. 1992.

[Proakis *et al.*, 1992] John G. Proakis, Charles M. Rader, Fuyun Ling, and Chrysostomos L. Nikias. *Advanced Digital Signal Processing.* MacMillan Publishing Company, 1992.

[PSC Enertec, 1990] PSC Protections et systèmes de contrôle. *Sessions Techniques de Formation — Protection des réseaux de transport d'énergie électrique à haute tension*, 1990. PSC Enertec is now named GEC–ALSTHOM P&C. In French.

[Rabiner, 1989] Lawrence R. Rabiner. A tutorial on hidden Markov models and selected applications in speech recognition. In *Proceedings of the IEEE*, volume 77, pages 257–286, Feb. 1989.

[Rasmussen, 1984] Frank Rasmussen. Electromagnetic transients in electrical power transmission systems. Technical report, The Academy of Technical Sciences, The Technical University of Denmark & Elkraft a.m.b.a., Aug. 1984. Industrial Research Education Programme Thesis.

[Ribeiro, 1985] Paulo F. Ribeiro. *Investigations of Harmonic Penetration in Transmission Systems.* PhD thesis, The Victoria University of Manchester, July 1985.

[Ribeiro, 1993] Paulo F. Ribeiro. Modeling general transmission and distribution loads for harmonic studies: A complete representation. CRS Sirrine Engineers, Inc. Suite 300, 95 South Market Street, San Jose, California 95113, 1993.

[Ribeiro, 1994a] Paulo F. Ribeiro. Application of wavelets to determine motor drive performance during power systems switching transients. CRS Sirrine Engineers, Inc. Suite 300, 95 South Market Street, San Jose, California 95113, 1994.

[Ribeiro, 1994b] Paulo F. Ribeiro. Wavelet transform: An advanced tool for analyzing non-stationary harmonic distortions in power systems. In *International Conference on Harmonics in Power Systems*, Sep. 1994.

[Rioul and Vetterli, 1991] Olivier Rioul and Martin Vetterli. Wavelets and signal processing. *IEEE SP Magazine*, pages 14–38, Oct. 1991.

[Robertson *et al.*, 1994] Dave Robertson, Octavia I. Camps, and Jeffrey Mayer. Wavelets and power system transients: Feature detection and classification. In Harold H. Szu, editor, *Wavelet Applications*, pages 474–487, Apr. 1994.

[Rønne-Hansen, 1993] Jan Rønne-Hansen. *Elforsyningssystemer.* Stærkstrømsafdelingen, Danmarks Tekniske Højskole, elf.nr 89–14 edition, Jan. 1993.

[Rüdenberg, 1950] Reinhold Rüdenberg. *Transient Performance of Electric Power Systems, Phenomena in Lumped Networks.* McGraw–Hill Book Company, Inc., 1950.

[Ruskai *et al.*, 1992] Mary Beth Ruskai, Gregory Beylkin, Ronald Coifman, Ingrid Daubechies, Stephane Mallat, Yves Meyer, and Loise Raphael. *Wavelets and thier Applications.* Jones and Bartlett Publishers, 1992.

[Sachdev and Nagpal, 1991] M. S. Sachdev and M. Nagpal. A recursive least error squares algorithm for power system relaying and measurement applications. *IEEE Transactions on Power Delivery*, 6(3):1008–1013, Jul. 1991.

[Sachdev *et al.*, 1985] M. S. Sachdev, H. C. Wood, and N. G. Johnson. Kalman filtering applied to power system measurements for relaying. *IEEE Transactions on Power Apparatus and Systems*, 104(12):3565–3573, Dec. 1985.

[Scharf, 1991] Louis L. Scharf. *Statistical Signal Processing Detection, Estimation and Time Series Analysis.* Addison-Wesley Publishing Company, Inc., 1991.

[Schaumann *et al.*, 1990] Rolf Schaumann, Mohammed S. Ghausi, and Kenneth R. Laker. *Design of Analog Filters.* Prentice Hall, Englewood Cliffs, New Jersey 07632, 1990.

[Schweppe and Wildes, 1970] Fred C. Schweppe and J. Wildes. Power system static-state estimation, part I, II and III. *IEEE Transactions on Power Apparatus and Systems*, 89(1):120–135, Jan. 1970.

[Shao and Nikias, 1993] Min Shao and Chrysostomos L. Nikias. Signal processing with fractional lower order moments: Stable processes and their applications. In *Proceedings of the IEEE*, volume 81, pages 986–1010, Jul. 1993.

[Shultz *et al.*, 1983] R.D. Shultz, R.A. Smith, and G.L. Hickey. Calculation of maximum harmonic currents and voltages on transmission lines. *IEEE Transactions on Power Apparatus and Systems*, 102(4):14–37, Apr. 1983.

[Shynk, 1989] John J. Shynk. Adaptive IIR filtering. *IEEE ASSP Magazine*, pages 4–21, Apr. 1989.

[Shynk, 1992] John J. Shynk. Frequency-domain and multirate adaptive filtering. *IEEE Signal Processing Magazine*, pages 14–37, Jan. 1992.

[Sørensen *et al.*, 1984] E.V. Sørensen, B. Guldbrandsen, and N. Tovborg Jensen. *Elementær Kredsløbsteori, del 1, 2 & 3.* Den Private Ingeniørfond ved Danmarks Tekniske Højskole, 3. edition, 1984.

[Steiner *et al.*, 1992] J.P. Steiner, W.L. Weeks, and H.W. Ng. An automated fault locating system. *IEEE Transactions on Power Delivery*, 7(2):967–978, Apr. 1992.

[Swami *et al.*, 1993] Ananthram Swami, Jerry M. Mendel, and C. L. Nikias. *Hi Spec™ TOOLBOX, for use with* MATLAB™. The MathWorks, Inc., Jun. 1993. See [MATLAB, 1992].

[Tektronix, 1993] Tektronix, Inc. *P6015A 1000X High Voltage Probe, 070-8223-02*, 1993.

[Thorp *et al.*, 1985] J. S. Thorp, A. G. Phadke, and K. J. Karimi. Real time voltage-phasor measurements for static state estimation. *IEEE Transactions on Power Apparatus and Systems*, 104(11):3098–3104, Nov. 1985.

[Tuteur, 1992] F.B. Tuteur. Wavelet transformations in signal detection. In Charles K. Chui, editor, *Wavelets: A Tutorial in Theory and Applications*, pages 132–138. Academic Press, Inc, 1992.

[Vaidyanathan, 1990] P.P. Vaidyanathan. Multirate digital filters, filter banks, polyphase networks, and applications: A tutorial. In *Proceedings of the IEEE*, volume 78, pages 56–93, Jan. 1990.

[Vørts, 1990] S. Vørts. *Elektriske Fordelingsanlæg.* Polyteknisk Forlag, Anker Engelundsvej 1, DK-2800 Lyngby, 4. edition, 1990.

[Widrow and Stearns, 1985] Bernard Widrow and Samuel D. Stearns. *Adaptive Signal Processing.* Prentice-Hall, Inc., 1985.

[Williams *et al.*, 1993] Stephen M. Williams, Gary T. Brownfield, and Justin W. Duffus. Harmonic propagation of an electric distribution system: Field measurements compared with computer simulation. *IEEE Transactions on Power Delivery*, 8(2):547–552, Apr. 1993.

[Wolfram, 1992] Stephen Wolfram. *Mathematica, A System for Doing Mathematics by Computer.* Addison-Wesley Publishing Company, second edition, 1992.

[Young, 1993] Randy K. Young. *Wavelet Theory and its Applications.* Kluwer Academic Publishers, 1993.

[Zeidler, 1990] James R. Zeidler. Performance analysis of LMS adaptive prediction filters. In *Proceedings of the IEEE*, volume 78, pages 1780–1806, Dec. 1990.

Appendices

Appendix A

Classification Methods

The general purpose of the work that is described here has been to learn how much information there is in the signals at the *OP*. The work is in its initial stage, so it is not possible to make any definite conclusions yet.

A.1 Classification Principle

The overall structure of a possible classification scheme is outlined in Figure A.1. The first step towards classification will be to detect the event.
It is believed that *detection* and *classification* should be regarded as two separate tasks. The classification scheme will not be initiated unless the detection scheme has decided that an event occurred.

The first step of the classification scheme is proposed to be an estimation of the **direction** of the event. This is not an attempt to estimate the **distance** to the event, see Section A.4.
If the event is estimated not to be on the feeder, only this should be reported. Otherwise, if the event is on the feeder, it is desired to estimate which event it was.

A.2 Backward Calculation after Detection of an Event

On the basis of the diagram in Figure A.2, which is a model af a feeder, the transfer functions from the *OP* to each load are calculated. Note that the loads which on the diagram are indicated by vertical "rectangles" may also be active, i.e. containing a generator.

Though this section is concentrated around a specific model, the calculations are general and will apply to any network problem. Also mutual impedances will not change the way the problem is handled.
For reasons of simplicity only a one-phase system, with no mutual impedances, is used.

After detection of an event it is assumed that there is enough time before the occurrence of a new event to extract the portion of the current and voltage respectively that arose from the event.
On the basis of these signals, that have been transferred by the network from the point where the event took place, one calculates backwards to all nodes of the network to see what action caused an event to be detected.
It is assumed that the topology is known in detail, i.e. that also all loads are known.

Even a network as simple as the one in Figure A.2 becomes enormously cumbersome to analyze if one does not apply proper tools.
To handle this problem *node matrices* will be used. For more on this see [Sørensen *et al.*, 1984], [Jensen, 1977] and [Rønne-Hansen, 1993].

The *admittance matrix*, $\boldsymbol{Y}$, is a diagonal matrix, because there are no mutual impedances in this model:

$$\boldsymbol{Y} = \text{diag}\left(\frac{1}{Z_1}, \frac{1}{Z_2}, \frac{1}{Z_3}, \frac{1}{Z_4}, s\,C_5, \frac{1}{Z_6}, s\,C_7, s\,C_8, \frac{1}{Z_9}, s\,C_{10}, s\,C_{11}, \frac{1}{Z_{12}}, s\,C_{13}\right) \tag{A.1}$$

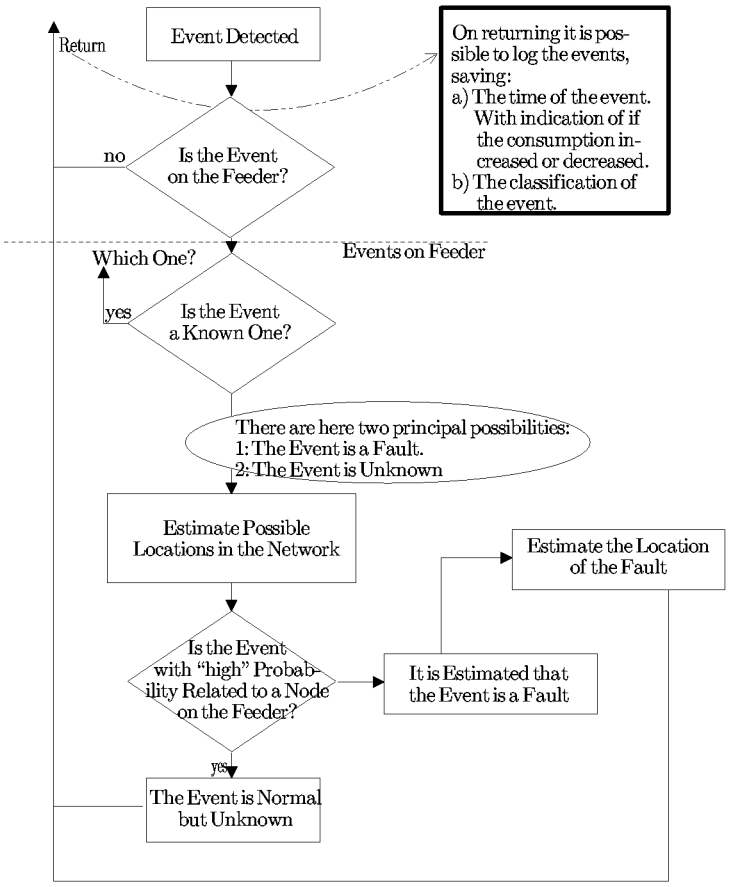

Figure A.1: Overall Classification Scheme.

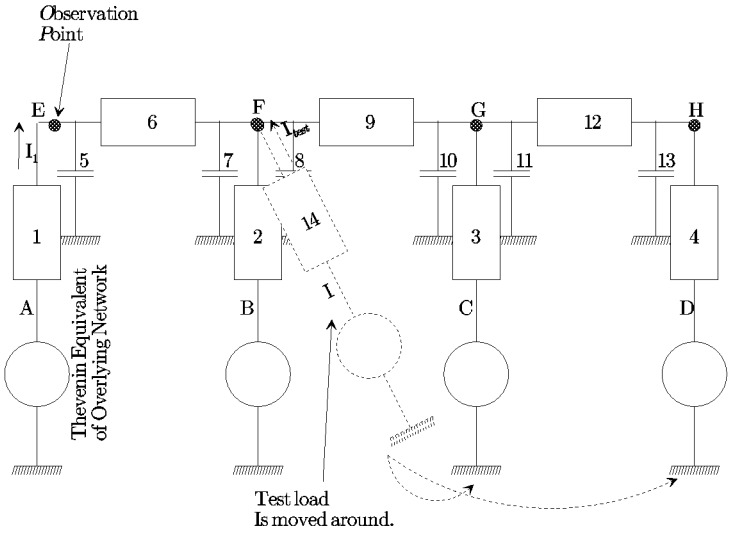

Figure A.2: Diagram of Network.

For this diagram the *node incidence matrix* becomes:

$$\boldsymbol{A} = \begin{array}{c} \\ 1 \\ 2 \\ 3 \\ 4 \\ 5 \\ 6 \\ 7 \\ 8 \\ 9 \\ 10 \\ 11 \\ 12 \\ 13 \end{array} \begin{array}{c} \begin{array}{cccccccc} A & B & C & D & E & F & G & H \end{array} \\ \left(\begin{array}{cccccccc} 1 & 0 & 0 & 0 & -1 & 0 & 0 & 0 \\ 0 & 1 & 0 & 0 & 0 & -1 & 0 & 0 \\ 0 & 0 & 1 & 0 & 0 & 0 & -1 & 0 \\ 0 & 0 & 0 & 1 & 0 & 0 & 0 & 1 \\ 0 & 0 & 0 & 0 & 1 & 0 & 0 & 0 \\ 0 & 0 & 0 & 0 & 1 & -1 & 0 & 0 \\ 0 & 0 & 0 & 0 & 0 & 1 & 0 & 0 \\ 0 & 0 & 0 & 0 & 0 & 1 & 0 & 0 \\ 0 & 0 & 0 & 0 & 0 & 1 & -1 & 0 \\ 0 & 0 & 0 & 0 & 0 & 0 & 1 & 0 \\ 0 & 0 & 0 & 0 & 0 & 0 & 1 & 0 \\ 0 & 0 & 0 & 0 & 0 & 0 & 1 & -1 \\ 0 & 0 & 0 & 0 & 0 & 0 & 0 & 1 \end{array} \right) \end{array} \tag{A.2}$$

With these two matrices defined it is now possible to calculate the *node admittance matrix*, $\boldsymbol{A}^T \boldsymbol{Y} \boldsymbol{A}$. The *node impedance matrix* is $\left(\boldsymbol{A}^T \boldsymbol{Y} \boldsymbol{A}\right)^{-1}$.

Now Ohm's Law in matrix form may be expressed:

$$\boldsymbol{u}' = \left(\boldsymbol{A}^T \boldsymbol{Y} \boldsymbol{A}\right)^{-1} \boldsymbol{i}' \tag{A.3}$$

The vectors $\boldsymbol{u}'$ and $\boldsymbol{i}'$ are the node voltage vector and the node current vector respectively:

$$\boldsymbol{u}' = (u_A, u_B, u_C, u_D, u_E, u_F, u_G, u_H)^T \tag{A.4}$$

$$\boldsymbol{i}' = (i_A, i_B, i_C, i_D, i_E, i_F, i_G, i_H)^T \tag{A.5}$$

E, F, G and H are nodes with no connection out of the diagram, therefore i_E, i_F, i_G and i_H are all zero.

The voltages at A, B, C and D are known because they are fixed by the generators.

If a new current vector $\boldsymbol{i}_1$ is introduced, Equation A.5 may be written as: $\boldsymbol{i}' = \left(\boldsymbol{i}_1^T, \boldsymbol{0}\right)^T$. $\boldsymbol{i}_1 = (i_A, i_B, i_C, i_D)^T$.

The vector $\boldsymbol{u}_1^T = (u_A, u_B, u_C, u_D)$ may likewise be introduced: $\boldsymbol{u}' = \left(\boldsymbol{u}_1^T, \boldsymbol{u}_n^T\right)^T$. $\boldsymbol{u}_n$ is unknown.

To solve Equation A.3 it is useful to rewrite the expression a little:

$$\begin{pmatrix} \boldsymbol{i}_1 \\ \boldsymbol{0} \end{pmatrix} = \begin{pmatrix} \boldsymbol{Y}_{11} & \boldsymbol{Y}_{12} \\ \boldsymbol{Y}_{21} & \boldsymbol{Y}_{22} \end{pmatrix} \cdot \begin{pmatrix} \boldsymbol{u}_1 \\ \boldsymbol{u}_n \end{pmatrix} \tag{A.6}$$

Equation A.6 is solved first for $\boldsymbol{u}_n$:

$$\begin{aligned} \boldsymbol{Y}_{21}\,\boldsymbol{u}_1 + \boldsymbol{Y}_{22}\,\boldsymbol{u}_u &= \boldsymbol{0} \\ \boldsymbol{u}_n &= -\boldsymbol{Y}_{22}^{-1}\,\boldsymbol{Y}_{21}\,\boldsymbol{u}_1 \end{aligned} \tag{A.7}$$

Using this result in the upper part of the equation gives:

$$\boldsymbol{i}_1 = \boldsymbol{Y}_{11}\,\boldsymbol{u}_1 + \boldsymbol{Y}_{12}\,\boldsymbol{u}_n \tag{A.8}$$

$$= \left(\boldsymbol{Y}_{11} - \boldsymbol{Y}_{12}\boldsymbol{Y}_{22}^{-1}\boldsymbol{Y}_{21}\right)\boldsymbol{u}_1 \tag{A.9}$$

With these equations in place it is possible to calculate the transfer function between nodes in the network.

However desirable it may be to get an analytical expression as the result, it will be a quite considerable task to manipulate the expressions into something meaningful. With tools like MATHEMATICA or MATLAB with it's SYMBOLIC TOOLBOX, one might be able to find a way through?

No matter how useful this result could be, it was decided not to spend the required amount of time and instead do with numeric calculations only.
With the above equations the means for calculating the transfer function of single frequencies was also provided — which may be done with almost any software that performs calculations with complex numbers.

A.3 Direction of the Event

Though the network at substations is very stiff, situations may occur where an "upstream" event causes current to flow **from** the feeder back to the busbar.
In future it may be expected that power produced on decentralized units will attain such a level, that a feeder may in fact supply electrical energy to the busbar at the substation to be used on neighbouring feeders.
The first case shall only be classified as *not related to the feeder*, no further actions should be taken. In the latter case only what is connected to supplying energy to the feeder shall be classified as *related to the feeder*. The event, supposedly on another feeder, that caused energy to be drawn from the feeder must be classified as *not related to the feeder*.

In distance relays, digital as well as analog, is usually implemented a directional estimation algorithm. This algorithm is used to tell whether an event is within or outside the zones of protection. For more on relaying practices see Appendix B.

In Section B.2 is shown how the distance to a low impedance event may be estimated.
It is quite clear that precisely the fact that the different kinds of events that are of interest in a distribution network monitoring system are not only low impedance, will cause that current still flows past the point in the network where the event takes place, hence the algorithm in Section B.2 will yield still poorer estimates as the impedance of the event increases.
Furthermore the algorithm is also based on the assumption of a homogeneous transmission line, i.e. that the impedance of the line is directly proportional to the length. This does not apply for distribution networks, especially not if they are cable based. In this case it is common that the line between two points is pieced together by pieces of different electrical nature. Therefore, there is no direct connection between the impedance of the cable and its length.

It is a fundamental assumption, however, that the topology of the feeder to be monitored is known in detail, i.e. knowledge exists on where different types of cable are connected, and on the types of the cables.
This assumption is valid, though not all distribution companies possess such data.

After having detected an event, the first step is, as previously stated, to determine if, in fact, the event is one that the system should care about.
In Section B.1 is presented an algorithm that may determine the direction of the flow of power. It is stated that knowledge on the phase characteristics of both the voltage and current sensor is required in order to rely on the phase comparison estimate of the direction. Such knowledge may easily be provided.
It has been established that the Kalman filter efficiently may be used for the estimation of amplitude and phase of sinusoidals, see Section 6.5.1. The Kalman filter has been incorporated into the monitoring system simulator. For details on the implemented algorithms and their implementation in the MATLAB–language see [Jespersen, 1994]. Therefore, both amplitude and phase of all currents and voltages are available on a sample to sample basis. It therefore seems more appropriate, on the basis of these, to calculate an estimate of the direction.

Let $A_{I_R}(t)$ denote the estimate of the amplitude of the current of phase R, and let $\varphi_{I_R}(t)$ denote the estimate of the phase relative to a chosen reference. Likewise for the other phases.
For reasons of simplicity the single phase case is considered. The detection scheme has detected an event and shown in which phases it took place. With signals from the affected phases the amplitude and phase of each current are compared to the corresponding voltage.
At this stage there are eight situations to be taken into account, see Figure A.3. Half of these situations must be immediately ignored, because they are not related to the feeder. Anyway, all eight situations must be analysed so as to learn about their impact on the estimation of the direction. **The terms**

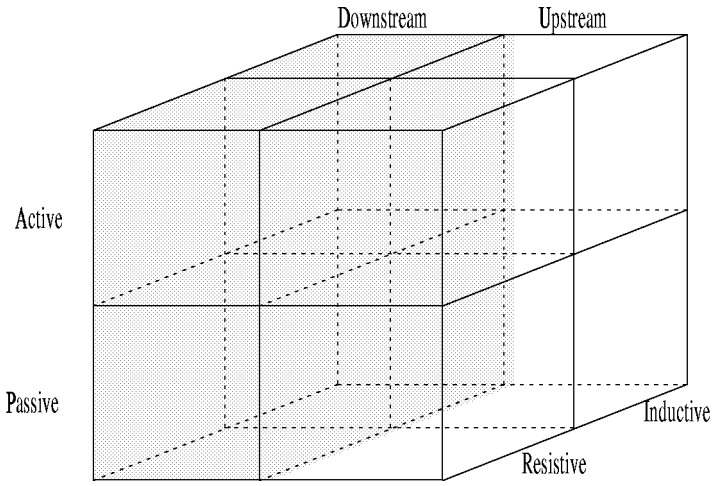

Figure A.3: Eight Possibilities for Classification of Event.

"resistive" and "inductive" refer solely to the angle of the load, i.e. if the current is in phase or lacking. By definition both resistive and inductive loads are passive. A resistive, active load will be modelled by an ideal source (current or voltage) in series with a resistance.
Note that capacitive loads are not mentioned. Most loads are almost purely Ohmic or slightly inductive. Cables appear as capacitive loads, but only very little. For low voltage cables this is negligible.

In Figure A.4 is shown both the amplitude of the current, and its phase relative to the corresponding phase voltage around the start and stop of a known machine at a known location in the network.

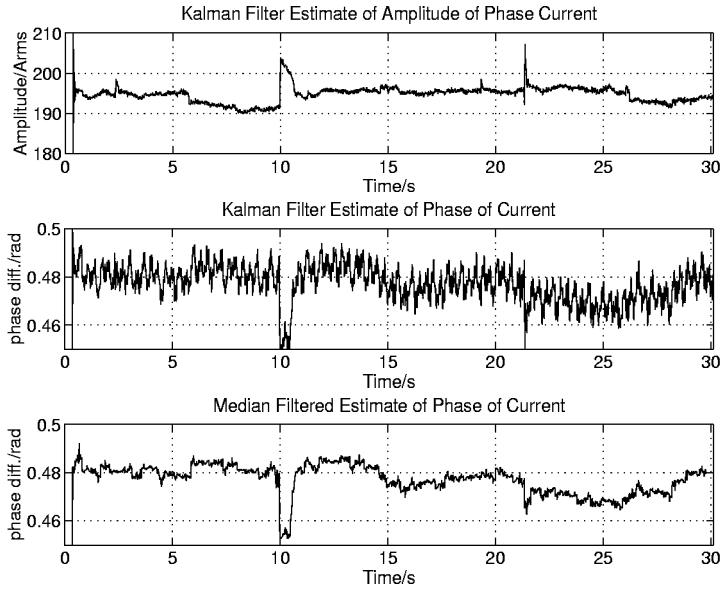

Figure A.4: Amplitude and Phase Estimates of Current When Known Load is Switched.

In Figure A.5 is shown the estimate of the residual signal from the same period as Figure A.4. Only a small start may be distinguished at around 10s, when the motor is started. However, it is believed that this is caused by the time it takes the bandpass filter to converge to a new state. During the transition it also attenuates frequencies in the passband region.
Taking this into account it is not evident by visual inspection that information should be available in

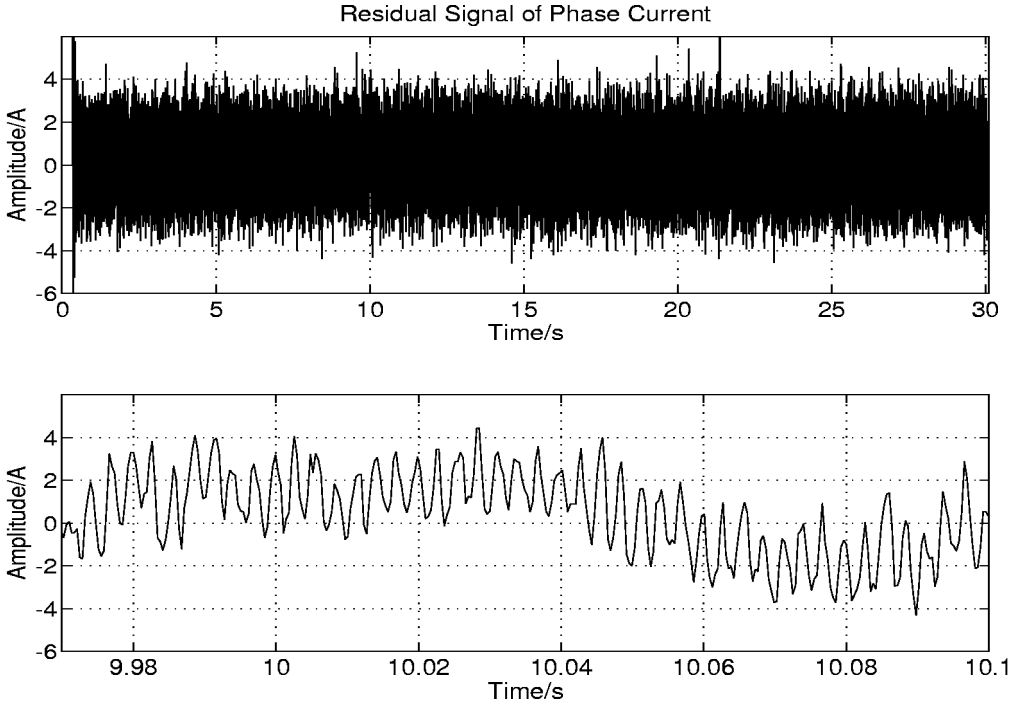

Figure A.5: Residual Signal from the Same Period as in Figure A.4.

the residual signal.

A.3.1 A Closer Look at the Phase of the Currents from the Stage 1 Measurements

On the basis of the complex estimates from the Kalman filter, implemented in the system simulator, the phase of the current of phase R was estimated relative to the phase of the voltage of the same phase.

In Figure A.6 is shown an estimate of the angle, after having extracted the mean.
The mean is estimated as a moving average, with a memory of 500 samples, see Appendix F, Expression F.1.

For this particular extract of the measurements it is assumed that only passive events on the feeder have been recorded.
Bearing in mind that most loads are either purely Ohmic or slightly inductive and that the cable network, apart from the capacitive coupling to ground, is inductive every decrease of the phase most likely corresponds to the connection of a load, and every increase to the disconnection of one.

After connecting the 90kW machine, at 10s into the example, it is seen that the phase attains positive values. This is due to the time it takes the algorithm to converge. The machine is disconnected at about 26s. This may be recognized in Figure A.6 also.

Figure A.8 shows the development of the module and argument of the total impedance of the feeder as a function of time.
The phase of the current was modified, so that the power factor was approximately $0{,}9_{\text{inductive}}$.
It is interesting to notice that the impedance appears quantified, in the way that "lumps" may be distinguished, see figure on page 99.
On the basis of about 7700 samples, corresponding to about 30s of signal, in Figure 8.1 histograms of the magnitude and phase of the total argument were drawn.

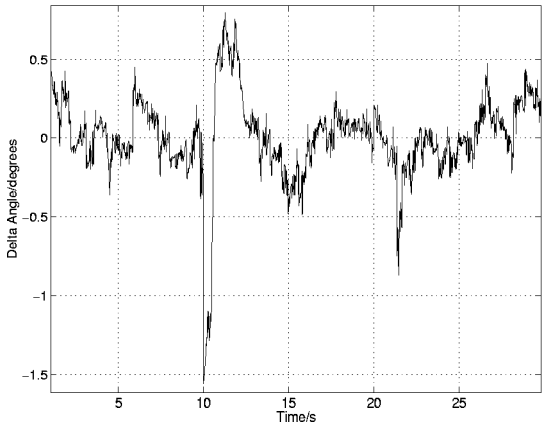

Figure A.6: Development of phase after extraction of mean value, $m = 500$.

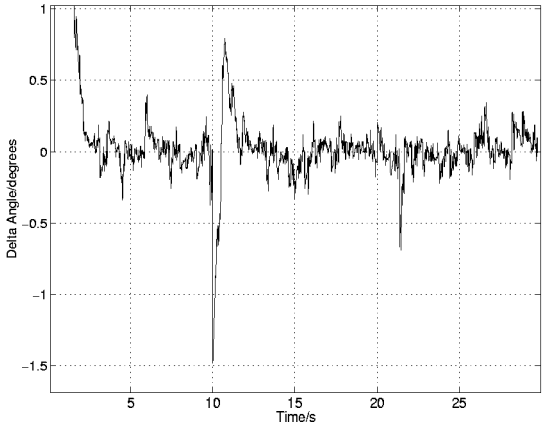

Figure A.7: Development of phase after extraction of mean value, $\lambda = 0{,}99$.

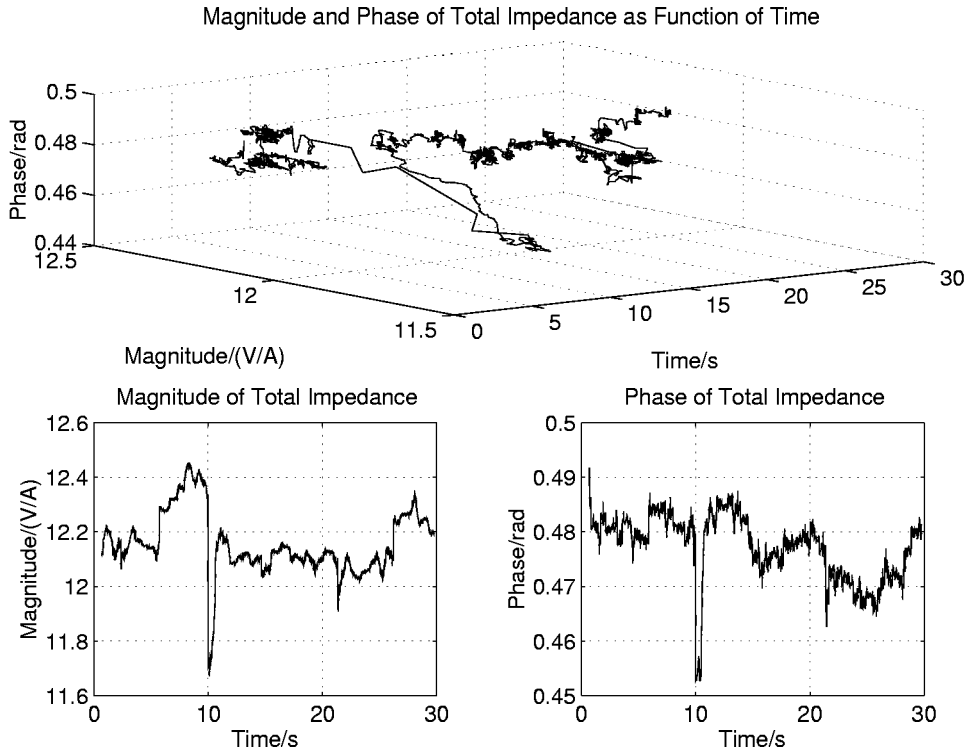

Figure A.8: Magnitude and Phase of Total Impedance.

A.3.2 ATP Simulation of Up- and Downstream Events

The model shown in Figure A.9, page 126, was implemented in the ATP. The connections to ground of the line elements indicate the ground connection of the Π-equivalents.

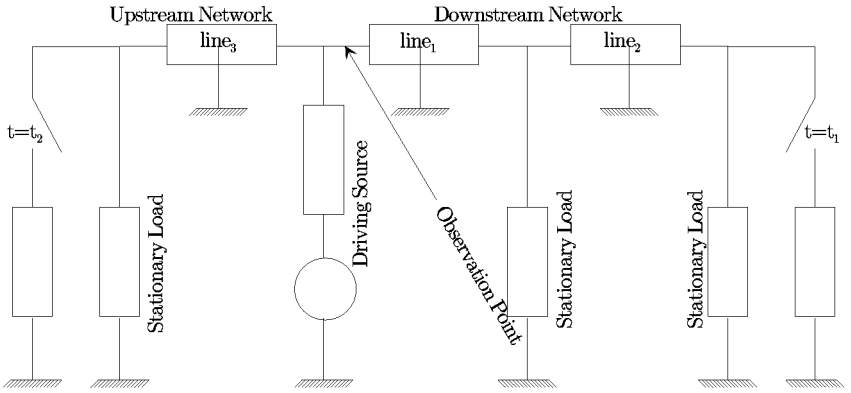

Figure A.9: Model Implemented in the EMTP for Simulations of Up- and Downstream Events.

Subsequently the Kalman filter was applied to give estimates of the amplitudes and phases.

The downstream load was lumped into two impedances each of $20\text{MW}_{\text{p.f.}=0,9}$. At 3,02s into the simulation a purely resistive load of 90kW was connected. It was disconnected at 3,1s.

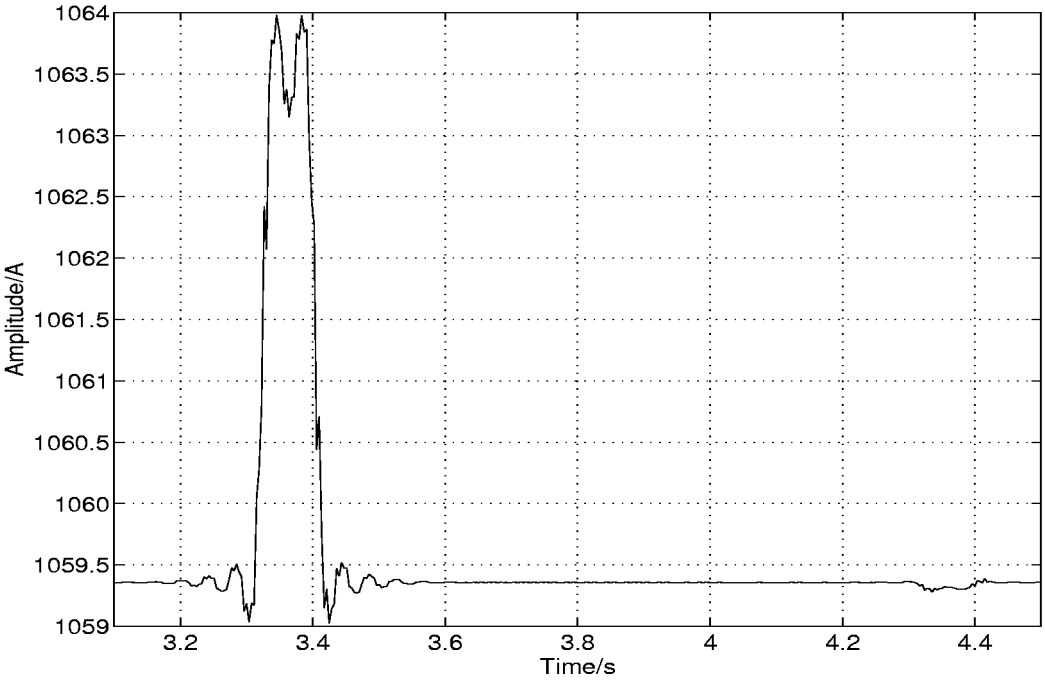

Figure A.10: Current during Switching of both Downstream and Upstream Loads.

The upstream load was lumped into one impedance of $50\text{MW}_{\text{p.f.}=0,95}$. At 4,02s into the simulation a purely resistive load of 90kW was connected. It was disconnected at 4,1s.

The downstream event gives rise to an additional current of about 5,5A.
Seen from the *OP* the upstream event causes a reduction of the current of about 0,1A.

A.4 Equivalent Geometric Distance

The investigation described here represents the results of the initial research into the definition of the so-called *Equivalent Geometric Distance*.
The investigation is far from being complete. Therefore, the following material is included only to be used as inspiration for future work on the subject.

Equivalent Geometric Distance is an estimate of the distance to the location where the event occurred, calculated from an estimate of ΔZ, which is the increase/decrease of the impedance seen from the *OP*.

For the assumptions behind this investigation it is fundamental that full information on the network is available, i.e. the lengths of the cable sections, their type, their physical dimensions...
All this information may be processed into a complete electrical description of the monitored feeder.
The mere difference in the network connecting two different nodes to the substation is expected to yield sufficient information to distinguish identical kinds of loads from each other.

Starting such an investigation on a simple model is beneficial. Thus the first model should be one only describing the network as being single-phased (with return through ground). The two capacities of the

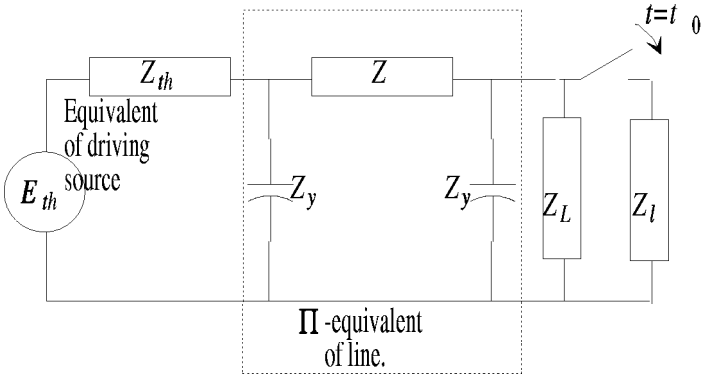

Figure A.11: Simple network model for initial studies.

Π-equivalent of the line are neglected. In this case the current just prior to $t = 0$ is found using Laplace transformation:

$$I(s) = \frac{E_{th}\frac{s}{s^2+\omega_0^2}}{R_{th}+R+R_L+s\,(L_{th}+L+L_L)} \qquad t<0 \tag{A.10}$$

The steady state solution to this is:

$$i(t) = E_{th}\,\frac{(R_{th}+R+R_L)\cos(\omega_0 t)+(L_{th}+L+L_L)\,\omega_0\sin(\omega_0 t)}{(L_{th}+L+L_L)^2\omega_0^2+(R_{th}+R+R_L)^2} \tag{A.11}$$

The initial condition on the current at $t = 0$ then becomes:

$$i(0) = \frac{R_{th}+R+R_L}{(L_{th}+L+L_L)^2\omega_0^2+(R_{th}+R+R_L)^2}\,E_{th} \tag{A.12}$$

After the event the network is basically the same as before. The load may be described in terms of a real and an imaginary part:

$$R' = \frac{R_L^2\,R_l+R_L\,R_l^2+\omega_0^2\,(L_L+L_l)\,(R_L\,L_l+R_l\,L_L)}{(R_L+R_l)^2+\omega_0^2\,(L_L+L_l)^2} \tag{A.13}$$

$$X' = \omega_0\,\frac{R_L^2\,L_l+R_l^2\,L_L}{(R_L+R_l)^2+\omega_0^2\,(L_L+L_l)^2} \tag{A.14}$$

E_{th}	describes the magnitude of a sinusoidal generator: $E_{th}\cos(\omega_0 t)$. $E_{th} = \frac{\sqrt{2}}{\sqrt{3}}10{,}4\text{kV}$, $\omega_0 = 2\pi\,50\text{Hz}$.
Z_{th}	describes the equivalent impedance of the network supplying the feeder: $Z_{th} \simeq 0{,}3\Omega\angle 89°$.
Z	describes the impedance of the line/cable. For a cable 4km of length these values are used: $R = 0{,}5\Omega$ and $X = 0{,}3\Omega$.
Z_L	describes the ensemble load prior to the event. To get consumption in the order as has been measured, $\lvert Z_L\rvert = 32\Omega$ is used. At GLENTEGÅRD has been measured that $\cos(\varphi) = 0{,}95$. This corresponds to a time constant, $\tau \simeq 1\text{ms}$. In order to get approximately this time constant of the model prior to an event it is necessary to use this model for Z_L: $Z_L = 32\Omega\angle 17{,}46°$.
Z_l	describes the impedance of the new load that caused the event. To get an increase in the current of about 1A_{RMS}, $\lvert Z_l\rvert = 5\text{k}\Omega$ is used.

Table A.1: Notation

Equations A.13 and A.14 come from solving Equations A.15 and A.16:

$$R' = \Re(R_L \parallel Z_l) \tag{A.15}$$

$$L' = \frac{\Im(R_L \parallel Z_l)}{\omega_0} = \frac{X'}{\omega_0} \tag{A.16}$$

The current of Equation A.12 will die out with a time constant of $\tau = \frac{L_{th}+L+L'}{R_{th}+R+R'}$

$$i(t) = \frac{E_{th}}{L''^2\omega_0^2 + R''^2}\left(-R''\,\mathrm{e}^{-\frac{R''}{L''}t} + R''\cos(\omega_0 t) + L''\omega_0\sin(\omega_0 t)\right) \tag{A.17}$$

$R'' = R_{th} + R + R'$ and $L'' = L_{th} + L + L'$.
Taking into account the initial condition, the total solution to the current is:

$$\begin{aligned} i(t) = {} & E_{th}\left(\frac{R_{th}+R+R_L}{(L_{th}+L+L_L)^2\omega_0^2 + (R_{th}+R+R_L)^2} - \right. \\ & \left.\frac{R_{th}+R+R'}{(L_{th}+L+L')^2\omega_0^2 + (R_{th}+R+R')^2}\right)\mathrm{e}^{-\frac{R_{th}+R+R'}{L_{th}+L+L'}t} + \\ & Eth\,\frac{(R_{th}+R+R')\cos(\omega_0 t) + (L_{th}+L+L')\sin(\omega_0 t)}{(L_{th}+L+L')^2\omega_0^2 + (R_{th}+R+R')^2} \end{aligned} \tag{A.18}$$

Entering the values indicated in Table A.1 and assuming that $\cos(\angle Z_l) = 0{,}9$ one gets:

$$i(0) = 246{,}959\text{A}_{\text{peak}} = 174{,}626\text{A}_{\text{RMS}} \tag{A.19}$$

$$\tau = 1{,}04991\text{ms} \tag{A.20}$$

$$i(t) = -1{,}44799\,\mathrm{e}^{-\frac{t}{\tau}} + 248{,}41\cos(\omega_0 t) + 81{,}9344\sin(\omega_0 t), \quad t \geq 0 \tag{A.21}$$

$$= -1{,}44799\,\mathrm{e}^{-\frac{t}{\tau}} + 261{,}57\cos(\omega_0 t + 18{,}254°), \quad t \geq 0 \tag{A.22}$$

$$i(t) = 246{,}959\cos(\omega_0 t) + 81{,}1865\sin(\omega_0 t), \quad t < 0 \tag{A.23}$$

$$= 259{,}96\cos(\omega_0 t + 18{,}20°), \quad t < 0 \tag{A.24}$$

The next obvious case to consider is the simple line model, but with the load change taking place at an arbitrary fraction of the line. The entire post-event load is not placed at the end of the line, as is indicated in Figure A.12. The impedance denoted Z_{L1} attains the same value as Z_L in Figure A.11. Z_{L2} is ten times the value of Z_{L1}.

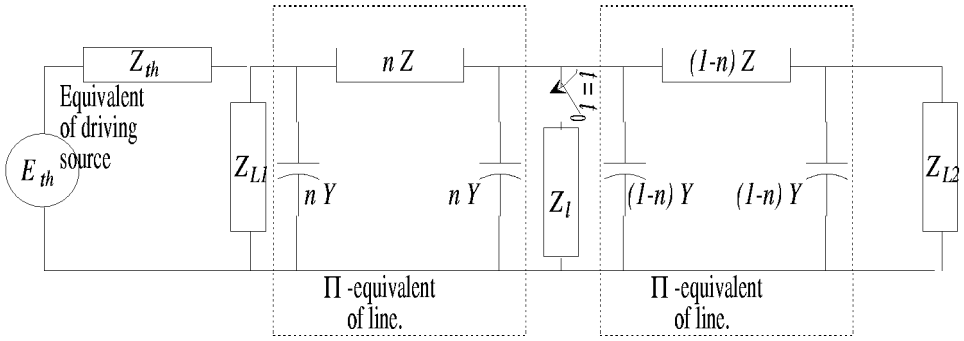

Figure A.12: Simple network model for initial studies. Load change at the middle of the line.

The steady state prior to the event remains almost the same. Despite the simplifications of the model (omitting the capacitances), it is enormously cumbersome to give a tractable symbolic expression for the current as a function of all the parameters, hence the quantities of interest are shown graphically in Figures A.13 and A.14.

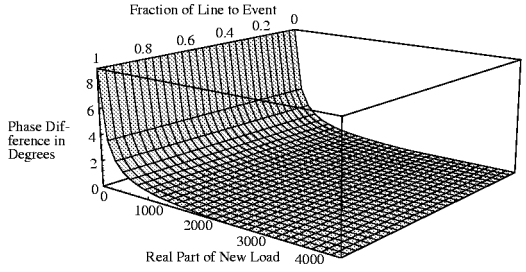

Figure A.13: Phase difference of current before and after en event. The event is moved along the cable. It's real part is changed from 0Ω to 4500Ω, $\cos(\varphi) = 0{,}95$.
Fraction of Line to Event corresponds to n of Figure A.12.

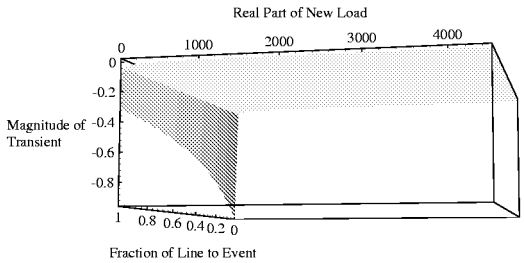

Figure A.14: Magnitude of transient in current after event. **Magnitude of Transient** is in p.u. Hence "−1" corresponds to the highest possible amplitude of the transient. See remark in caption of Figure A.13.

On the basis of this simple model one gets an indication of the levels upon a change of state one should expect for the amplitude of the transient.
The transient does not attain a very high amplitude for values of the new impedance above about 200Ω. On the other hand, the phase change is more easily influenced. This is a confirmation of the result of the simulation with the ATP–model of the distribution feeder **A28**, SØBORGHAVE. See Section 3.3.4.1.

A.5 Phase Difference as Function of Location in the Network

It must be required, of methods to identify a specific event, that they can distinguish the occurrence of an event at one node from the occurrence of the same event, but at another node.

For normal switching events one already knows one thing for certain; they take place at known positions in the network. Namely at the transformers[1]. If an event is found that cannot be traced back to a

[1] There is, of course, the underlying 0,4kV network, that will affect events on the way to the 10kV network. But as the template of a load to be monitored will be taken at 10kV level, the part of the 0,4kV network between the load and the primary side of the distribution transformer may be regarded as part of the load.

distance from the *OP* that corresponds to the known distances to the transformers of the feeder, there is a reason to believe that a fault has occurred. This may further be substantiated by comparing the development of the symmetrical components. I.e. the rise of zero-system quantities indicate that a path to ground has been established. Calculating backwards an estimate of the location of this fault may be given[2].

In Figure A.15 is given the initial model for the investigation of the development of the phase difference before and after the occurrence of an event as function of the cable type and distance to the node at which it takes place.

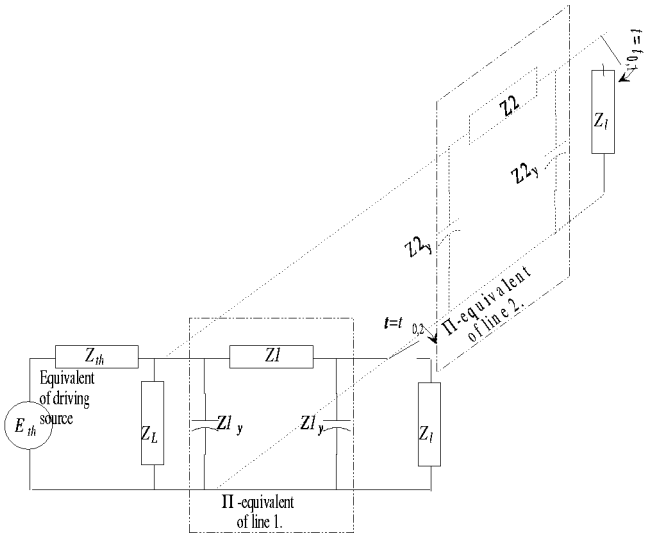

Figure A.15: Model of the Switching of an Identical Load at Two Locations in the Network.

In this investigation the capacitors $Z_{1,y}$ and $Z_{2,y}$ are taken into account.
A one section Π-equivalent is used. Data is taken from [NKT, 1984] and corresponds to a 10kV 95mm^2 Cu.–APB[3]–cable, see Table A.2.

Reactance	0,076Ω/km
Capacitance	0,35μF/km
DC-resistance	0,194Ω/km

Table A.2: Data for 10kV 95mm^2 Cu.–APB–Cable. The reactance is given at 50Hz. Skin-effect is not taken into account.

The same type of cable is used for the *Π-equivalent of line 1* as for *Π-equivalent of line 2*. Only the lengths are different.

[2]Ground faults in the 0,4kV network will not contribute to changes in the zero-system of the symmetrical components. This is because ΔY-coupled transformers will not let through any zero-system information.

[3]APB; **A**luminium, **P**last, **B**ly. *Aluminum, Plastic, Lead.*

Appendix B

Distance Relaying Techniques

This appendix is intended to establish some fundamentals of relaying techniques. It is assumed that the term "event" covers low impedance faults, either between phases or to ground. It is even assumed that the fault impedance is so low that a good approximation to its magnitude is 0.

Many relaying principles exist, e.g:

- Over Current Relays.
- Traveling Wave Relays.
- Distance Relays.

Yet other principles may be used, see [Phadke and Thorp, 1988] and [GEC Measurements, 1987].

The principles that apply best for gaining more insight into *centralized monitoring* are the principles of traveling wave relays and distance relays.

Here only some principles of distance relays will be explained, since this gives good insight in the terminology.

Distance relays are normally only applied to the transmission network. This is due to the cost. A modern (1995) digital distance relay costs DKK200.000–300.000. This is substantially higher than what may be spent in distribution networks.

Also the topology of the transmission network is fundamentally different from the distribution network.

Relays are normally placed in substations. Each line connected to that substation has relays, (and backup relays). At the other end of a line, at another substation, is also a relay. These two relays that are assigned to one line, are both assigned to look **into** the line. They both interpret events somewhere on the line as "downstream". An event found to be located downstream is an event that is in the **zone of protection**.

The zone of protection is normally divided into three zones according to [PSC Enertec, 1990]:

Zone 1 extends to 80% of the length of the line (between the two relays).

Zone 2 extends to 120% of the length of the line.

Zone 3 extends to 150% of the length of the line.

A fourth zone is also defined. This zone covers all of the upstream network, i.e. the network behind the relay.

Zone 2, 3 and 4 serve as backup zones for other relays. The relay is so adjusted, that if it detects an event in one of those zones, it "hesitates" before it gives the opening command to the circuit breakers. If the other relays fail to react within a given period of time, the relay will open the breakers.

Especially for Zone 4 the relay will have a long delay before it takes action. It is essential to be able to distinguish events in this zone from events in the three downstream zones. Therefore there is implemented an algorithm that estimates the direction in which an event took place.

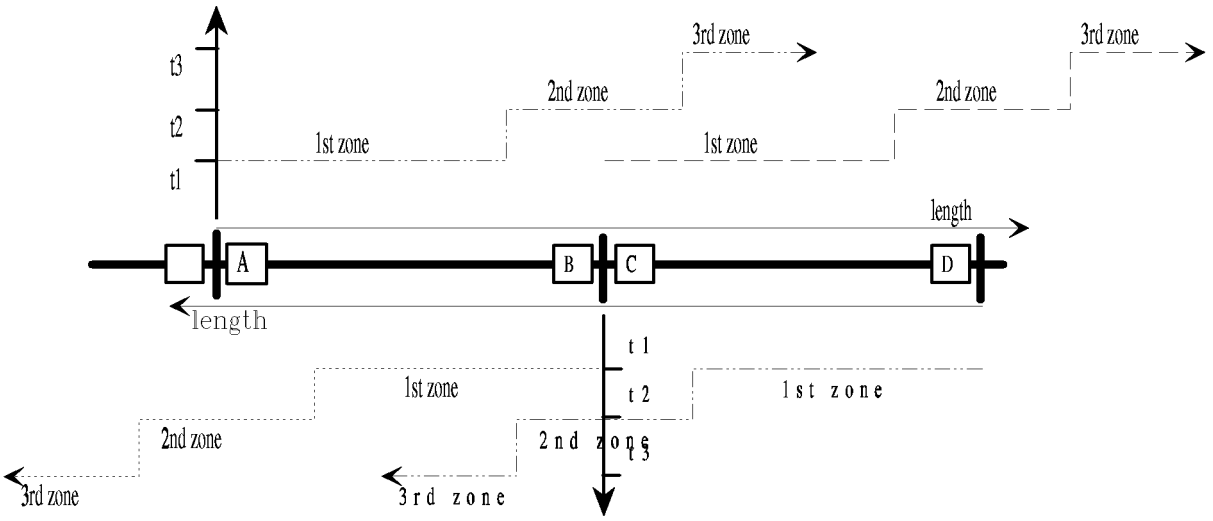

Figure B.1: Division of Transmission Line into Protection Zones.

B.1 Phase Comparison

Phase comparison is the comparison of the sign of the phase between two sinusoidals to a threshold (normally 0).
Let $u(t) = a\cos(\omega_0 t)$ denote the phase to ground voltage measured at the relaying point and $i(t) = b\cos(\omega_0 t + \varphi_0)$ the phase current. The expression in Equation B.1 then may be easily evaluated into yielding the sign.

$$\begin{aligned} P(t) &= -\frac{u(t)\frac{di(t)}{dt} - \frac{du(t)}{dt}i(t)}{\omega_0} \\ &= a\,b\sin(\varphi_0) \end{aligned} \tag{B.1}$$

A condition for this to work is that there is no difference in the phase delay of the current and voltage sensors. This is not likely to be so, therefore must instead be determined this phase delay difference. Let us assume that this phase delay difference is an additional φ_{delay}rad. Then we get:

$$P(t) = a\,b\sin(\varphi_0 + \varphi_{delay}) \tag{B.2}$$

In this case, to be able to use Equation B.1, it is necessary to get to know this difference and compensate for it.

B.2 Distance Relaying

To estimate in which of the zones an event is, it is necessary to estimate the distance to the event.
The following algorithm is one that is used in a commercially available digital distance relay.
The algorithm is inspired by the *Gauss–Seidel LMS* algorithm.

Having a homogeneous system, as are overhead lines, there is proportionality between the distance to the fault and the line impedance.
If furthermore it is assumed that during a fault the current into the fault is predominant, one has a well defined system, see Figure B.2. The following equation forms the basis of the distance estimation algorithm of the relay:

$$U_N = x\,V_N + y\,W_N \tag{B.3}$$

Where:

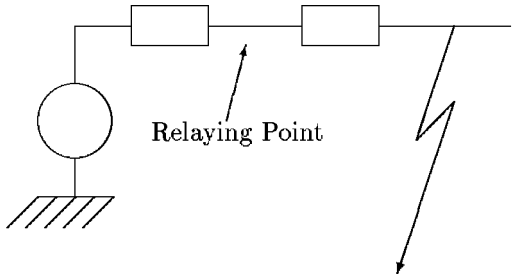

Figure B.2: Simple Network Model for the Estimation of Fault Resistance and Distance.

x is the distance to the fault.

y is the fault resistance, (including ground resistance).

U_N is the N^{th} sample of the measured voltage.

V_N is the N^{th} sample of the normalized voltage drop of the line:

$$V_N = \frac{X}{\omega_0}\frac{dI}{dt} + RI \tag{B.4}$$

Where:

$\frac{X}{\omega_0}$ is the inductance corresponding to the maximum fault distance.
R is the corresponding line resistance.
ω_0 is the fundamental frequency.

W_N is the N^{th} value of the current into the fault.

$$W_N = R_{dm}\, I \tag{B.5}$$

Where:

R_{dm} is the maximum measurable fault resistance.

As is seen the derivative of the current is used. In the relay in question this is calculated using a fifth order FIR–filter.
To estimate the parameters of Equation B.3 the following set of equations could be used:

$$X_N = \frac{\sum_{n=1}^{N} u_n\, v_n - Y_{N-1}\sum_{n=1}^{N} v_n\, w_n}{\sum_{n=1}^{N} v_n^2} \tag{B.6}$$

$$Y_N = \frac{\sum_{n=1}^{N} u_n\, w_n - Y_{N-1}\sum_{n=1}^{N} v_n\, w_n}{\sum_{n=1}^{N} w_n^2} \tag{B.7}$$

In the relay in question the sums are approximated by:

$$\sum_{n=1}^{N} a_n\, b_n \simeq S_{a\,b}(N) = a_N\, b_N + k\, S_{a\,b}(N-1), \quad \text{with } |k| \leq 1 \tag{B.8}$$

The LMS is simple and converges rapidly under ideal conditions. This algorithm is known to be capable of converging to the exact value of the parameters within eight samples, **if** the input signals are pure stationary sinusoidals.
This condition is very demanding to an algorithm that has to operate reliably in an environment such as a protection relay.

The algorithm is extremely sensitive to "outliers", i.e. samples that do not match a given pure sinusoidal. Do such samples occur the process of convergence has to start anew.

One example of a situation that will generate outliers is the case of faults where the fault currents attain such levels that the current transformers saturate that supply the relay with images of the line current. In this case the algorithm does not work properly.

Appendix C

Design of Anti-Aliasing Filters

The anti-aliasing filter is designed as an *M–Derived* filter.
In Figures C.1 and C.2 are shown the amplitude transfer function and corresponding phase.

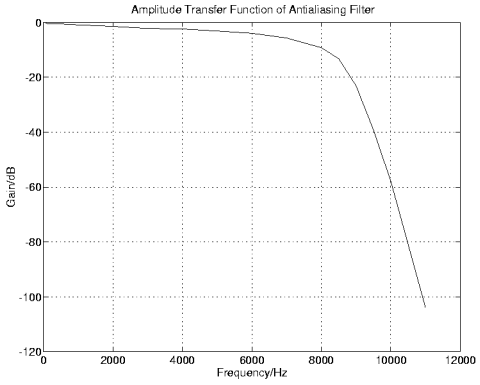

Figure C.1: Amplitude Transfer Function of Anti-aliasing Filter.

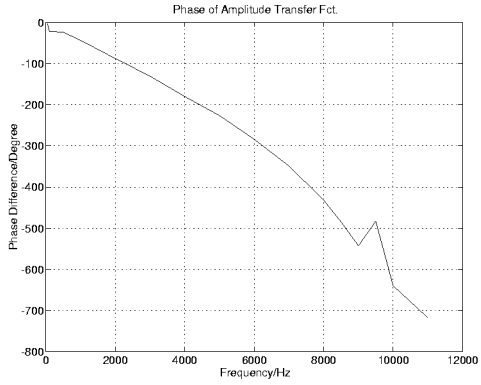

Figure C.2: Phase of Amplitude Transfer Function of Anti-aliasing Filter.

The amplitude has been normalized so that the gain at 50Hz corresponds to 0dB.
In practice, however, it may be desirable to adjust the filter gain, so that the filter in fact amplifies the input.

The power supply is symmetric $-15V{:}0{:}+15V$. The transfer function was evaluated using as input a pure sinusoidal with a peak value of 11,4V.
This value is a good deal higher than the maximum value of the measurements that will ever be encoun-

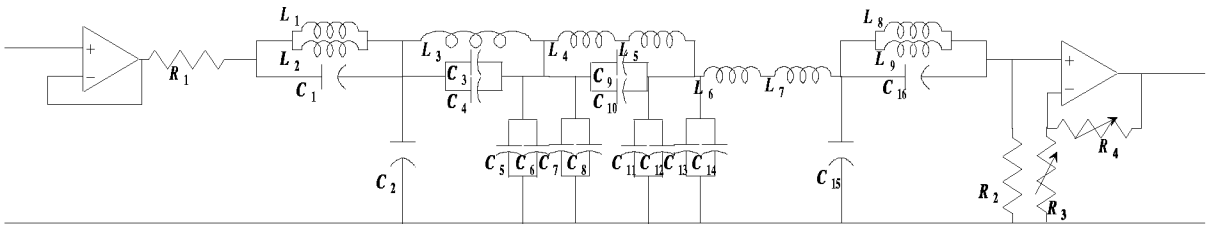

Figure C.3: M-derived Lowpass Filter.

tered.
Choosing a peak value this high was done to ensure that the amplifiers of the filter will not be driven into saturation under normal operating conditions.

In Figure C.3 is shown the diagram for the filters. The list of components is shown in Table C.1.

Capacitors			Coils	
C_1	22,0	nF	L_1	15,0mH
C_2	30,0	nF	L_2	15,0mH
C_3	1,0	nF	L_3	22,0mH
C_4	2,0	nF	L_4	15,0mH
C_5	18,0	nF	L_5	15,0mH
C_6	18,0	nF	L_6	15,0mH
C_7	1,0	nF	L_7	15,0mH
C_8	1,0	nF	L_8	15,0mH
C_9	0,056	nF	L_9	15,0mH
C_{10}	0,620	nF	Resistors	
C_{11}	18,0	nF	R_1	1kΩ
C_{12}	18,0	nF	R_2	1kΩ
C_{13}	2,4	nF	R_3	1kΩ
C_{14}	2,4	nF	R_4	1kΩ
C_{15}	33,0	nF		
C_{16}	22,0	nF		

Table C.1: List of Components.

Filter #	Min./V	Max./V	Mean/mV	Mean of |Min| and Max/V
0	-9,6176	9,6274	4,9	9,6225
1	-9,6274	9,6280	0,3	9,6277
2	-9,6356	9,6552	9,8	9,6454
3	-9,6228	9,6378	7,5	9,6303
4	-9,6402	9,6310	-4,6	9,6356
5	-9,6216	9,6378	8,1	9,6297
6	-9,6515	9,5874	-32,05	9,6195
7	-9,6259	9,6103	-7,8	9,6181

Table C.2: Minimum and maximum values of the filter outputs.

C.1 Calibration of Filters

All in all eight anti-aliasing filters were made.

The filters were all calibrated by applying the signal from one of the oscilloscope probes attached to the 10kV busbar at GLENTEGÅRD. The output of these probes is 1000:1 of the input, hence with $10{,}4\text{kV}_{\text{phase to phase}}$ the output was: $\sqrt{\frac{2}{3}}\,10{,}4\text{V} = 8{,}49\text{V}_{\text{peak}}$, or $6{,}00\text{V}_{\text{RMS}}$.

The filter gain was adjusted so that the output was measured to $6{,}70\text{V}_{\text{RMS}}$.

Subsequent analysis using the STATPACK–utility of GLOBAL LAB showed the peak values indicated in Table C.2.

If 6,7V were true RMS, then the peak value should be around 9,48V.

Later analysis of the measurements has revealed that what the meter indicates is very close to the RMS of the fundamental alone, hence it is assumed that the input to the filters in fact was 9,48V. This gives the following amplification factors for the filters, normalizing using the first element of the last column of Table C.2 as reference, see Table C.3:

Filter #	Ampl.
0	1,1167
1	1,1173
2	1,1193
3	1,1176
4	1,1182
5	1,1175
6	1,1163
7	1,1162

Table C.3: Amplification Factors for Anti-aliasing Filters.

Appendix D

Least Squares

Given m datapoints: $\{(x_i, y_i)\}_{i=1}^{m}$, and n developing functions: $\{f_j(x)\}_{j=1}^{n}$, determine the linear combination;

$$F(x) = \sum_{j=1}^{n} c_j \, f_j(x) \tag{D.1}$$

that minimizes the distance measure:

$$\rho_p = \rho_p(c_1, c_2, \ldots, c_n) \equiv \left[\sum_{i=1}^{m} |y_i - F(x_i)|^p \right]^{\frac{1}{p}} \tag{D.2}$$

$\boldsymbol{c}$ is the set of unknown parameters, that is to be estimated.
The difference between the measured values and $F(x_i)$ is called the residues:

$$r_i \equiv y_i - F(x_i) = y_i - \sum_{j=1}^{n} c_j \, f_j(x_i) \tag{D.3}$$

Equation D.2 may now be written as:

$$\rho_p = \left[\sum_{i=1}^{m} |r_i|^p \right]^{\frac{1}{p}} \tag{D.4}$$

Commonly $p = 2$ is chosen, which will henceforward be the case.

$$\boldsymbol{x} = [x_1, x_2, x_3, \ldots, x_m]^T \tag{D.5}$$

$$\boldsymbol{y} = [y_1, y_2, y_3, \ldots, y_m]^T \tag{D.6}$$

$$\boldsymbol{c} = [c_1, c_2, c_3, \ldots, c_n]^T \tag{D.7}$$

$\boldsymbol{x}$ is the input sequence, $\boldsymbol{y}$ is the output sequence.
$\boldsymbol{F}$ is the $m \times n$ functional matrix. Its elements are defined as:

$$f_{i,j} = f_j(x_i) \quad \begin{cases} i = 1, 2, 3, \ldots, m \\ j = 1, 2, \ldots, n \end{cases} \tag{D.8}$$

Using matrix notation, the residues may be written as:

$$\boldsymbol{r} = \boldsymbol{y} - \boldsymbol{F}\,\boldsymbol{c} \tag{D.9}$$

The LS estimate of $\boldsymbol{c}$ is given by:

$$\boldsymbol{c}^* = \left(\boldsymbol{F}^T \boldsymbol{F} \right)^{-1} \boldsymbol{F}^T \boldsymbol{y} \tag{D.10}$$

More details on the LS–method may be found in [Madsen, 1989, Chapter 2], [Hansen, 1985] and [Haykin, 1991, Chapter 10].

Appendix E

Markov Models

Considering the possible number of states an electrical network may be in, it is true that the number of possible states is finite, though limiting to infinity.
If the process of switching between the m states is regarded as a stochastic process, $X(n)$, and Equation E.1 is fulfilled the process is termed a *Markov Chain*.

$$P\{X(n) = k_n | X(n-1) = k_{n-1}, \ldots, X(0) = k_0\} = P\{X(n) = k_n | X(n-1) = k_{n-1}\} \quad \forall k_j |\, 1 \leq k_0, k_1, \ldots, k_n \leq m,\ (m,n) \in \mathcal{N}_0 \tag{E.1}$$

If also the conditional probability is independent of the time n, then the process is a stationary Markov Chain.
In the following is assumed stationarity.

Let p_{ij} denote the probability $P\{X(n) = j | X(n-1) = i\}$. If all possible p_{ij}'s are arranged in a matrix, we get the stochastic matrix $\boldsymbol{P}$:

$$\boldsymbol{P} = \begin{array}{c} \\ E_1 \\ E_2 \\ \vdots \\ E_m \end{array} \begin{array}{c} \begin{array}{cccc} E_1 & E_2 & \cdots & E_m \end{array} \\ \begin{pmatrix} p_{11} & p_{12} & \cdots & p_{1m} \\ p_{21} & p_{22} & \cdots & p_{2m} \\ \vdots & \vdots & \ddots & \vdots \\ p_{m1} & p_{m2} & \cdots & p_{mm} \end{pmatrix} \end{array} \tag{E.2}$$

$$p_{ij} \geq 0,\ \forall\, i,j \tag{E.3}$$

$$\sum_{j=1}^{m} p_{ij} = 1 \tag{E.4}$$

The P_{ij} are termed the *state transition probabilities*.
The *state probabilities* are termed $p_i^{(n)}$ and are defined by:

$$p_{i,n} = P\{X(n) = i\},\ i = 1, 2, \ldots, m;\ n \in \mathcal{N}_0 \tag{E.5}$$

$$\boldsymbol{p}_n = (p_{1,n}, p_{2,n}, \ldots, p_{m,n}) \tag{E.6}$$

$\boldsymbol{p}_0$ is the start distribution.

$\boldsymbol{p}_n$ may be determined from $\boldsymbol{p}_{n-1}$ and $\boldsymbol{P}$:

$$\boldsymbol{p}_n = \boldsymbol{p}_{n-1}\boldsymbol{P} \tag{E.7}$$

$$= \boldsymbol{p}_0 \boldsymbol{P}^n \tag{E.8}$$

Equation E.8 calls for a way of calculating $\boldsymbol{P}^n$

A stochastic matrix is regular if:

$$\forall\, i,j\ \exists\, n \in \mathcal{N} : p_{ij,n} > 0$$

A probability vector, $\boldsymbol{\alpha}$, is invariant if:

$$\boldsymbol{\alpha}\,\boldsymbol{P} = \boldsymbol{\alpha}$$

If $\boldsymbol{P}$ is a regular $m \times m$ stochastic matrix we have:

- $\lim_{n \to +\infty} \boldsymbol{P}^n = \boldsymbol{G}$
- All rows in $\boldsymbol{G}$ is the same probability vector $\boldsymbol{g}$.
  $\boldsymbol{g} = (g_1, g_2, \ldots, g_m)$
- All $g_i > 0$.
- $\lim_{n \to +\infty} \boldsymbol{p}\,\boldsymbol{P}^n = \boldsymbol{g}$
- $\boldsymbol{g}$ is the only invariant probability vector.

Appendix F

Calculation of $\Delta\varphi$.

Let s_n denote the n^{th} sample of a signal, then the average of the m previous samples of this signal is:

$$\widehat{\mathrm{E}}(s_n|s_{n-m:n-1}) = \frac{1}{m}\sum_{i=1}^{m} s_{n-i} \tag{F.1}$$

The estimation of the average using Expression F.1 requires that m samples of the signal s are stored. Alternatively one might consider to use weights that diminish with how old the sample is.

$$\widehat{\mathrm{E}}(s_n|s_{0:n-1}) = \frac{1-\lambda}{1-\lambda^n}\sum_{i=0}^{n-1} \lambda^i s_{n-1-i} \tag{F.2}$$

Which for large values of n approximately is the exponential weighting:

$$\widehat{\mathrm{E}}(s_n|s_{0:n-1}) = (1-\lambda)\sum_{i=0}^{n-1} \lambda^n s_{n-1-i} \tag{F.3}$$

With Expression F.3 a recursive calculation of the estimate may be easily made:

$$\begin{aligned} \widehat{\mathrm{E}}(s_{n+1}|s_{0:n}) &= (1-\lambda)\, s_n + \lambda\, \widehat{\mathrm{E}}(s_n|s_{0:n-1}) \\ s_n &= 0, \quad n < 0 \end{aligned} \tag{F.4}$$

Values of λ between 0,7 and 0,999 are frequently cited.

With one of the above estimates of the average of s, the mean may be adaptively extracted from a time series.

Let $\varphi(n)$ denote the phase of a current relative to the corresponding voltage then:

$$\Delta\varphi = \varphi(n) - \widehat{\mathrm{E}}(\varphi) \tag{F.5}$$

is an estimate of the phase difference between the n^{th} sample of the phase and the "level" of the phase prior to sample n.

Appendix G

Listings of ATP Model

Though EMTP dates back to long before ideas of structured programming emerged, it is possible to write data cases in a way that lets the structure of the system become clear.

It was attempted to write this data so that it would be easy to make changes to parts of the entire model, without having to make large changes.
E.g. if one wants to model cables differently than was described in Section 3.3.1, one only needs to replace the file(s) of the cable(s) that one wants to change.
One must, of course, assure that the node names at the terminals still correspond.

The entire data case is run from the ATP–file `A28.DAT`. This file calls all other necessary files.

The files are listed from "top to bottom", i.e. from substation to transformer stations.

All node names are chosen according to the system used by NESA, hence `5408` means the transformer station by that name. `54080925` means the cable from node `5408` to node `0925`, moving away from the substation.

To reduce the volume of the listing only one cable section and two loads are shown.

File: `A28.DAT`:

```
 1  BEGIN NEW DATA CASE
 2  C |-------------------------------------------------------------------------------|
 3  C |Created: 1993.02.19 by Steen M. Munk.              Last modified: 1994.07.26|
 4  C |     FILE: EMTP benchm-A:\INPUT\A28\A28.DAT                                    |
 5  C |-------------------------------------------------------------------------------|
 6  C | This EMTP-input file contains definitions which define radial A28, that     |
 7  C | starts from NESA's transformer station GLENTEGÅRD.                           |
 8  C |   ----------------------- GLN3     132kV Busbar at GLENTEGÅRD                |
 9  C |   |-(Y)  132kV/50kV                                                          |
10  C |   \ (D)                                                                      |
11  C |TER-  |                                                                       |
12  C |   ----------------------- GLN5      50kV Busbar at GLENTEGÅRD                |
13  C |               |       |-/---------------|                                    |
14  C |               |                         |                                    |
15  C |               |                         C Capacitor bank                     |
16  C |               |                         -                                    |
17  C |         |----(Y)  50kV/10kV           TERRA                                  |
18  C |   Arc   \    (D)  TRF1, TRF3 or TRF4                                         |
19  C |   Supp. L     |   19/24 MVA (Thrige or AEG)                                  |
20  C |   Coil  -     |                                                              |
21  C |       TERRA   |                                                              |
22  C |           ----------------------- GLN1      10kV Busbar at GLENTEGÅRD      |
23  C |                   |   |                 |                                    |
```

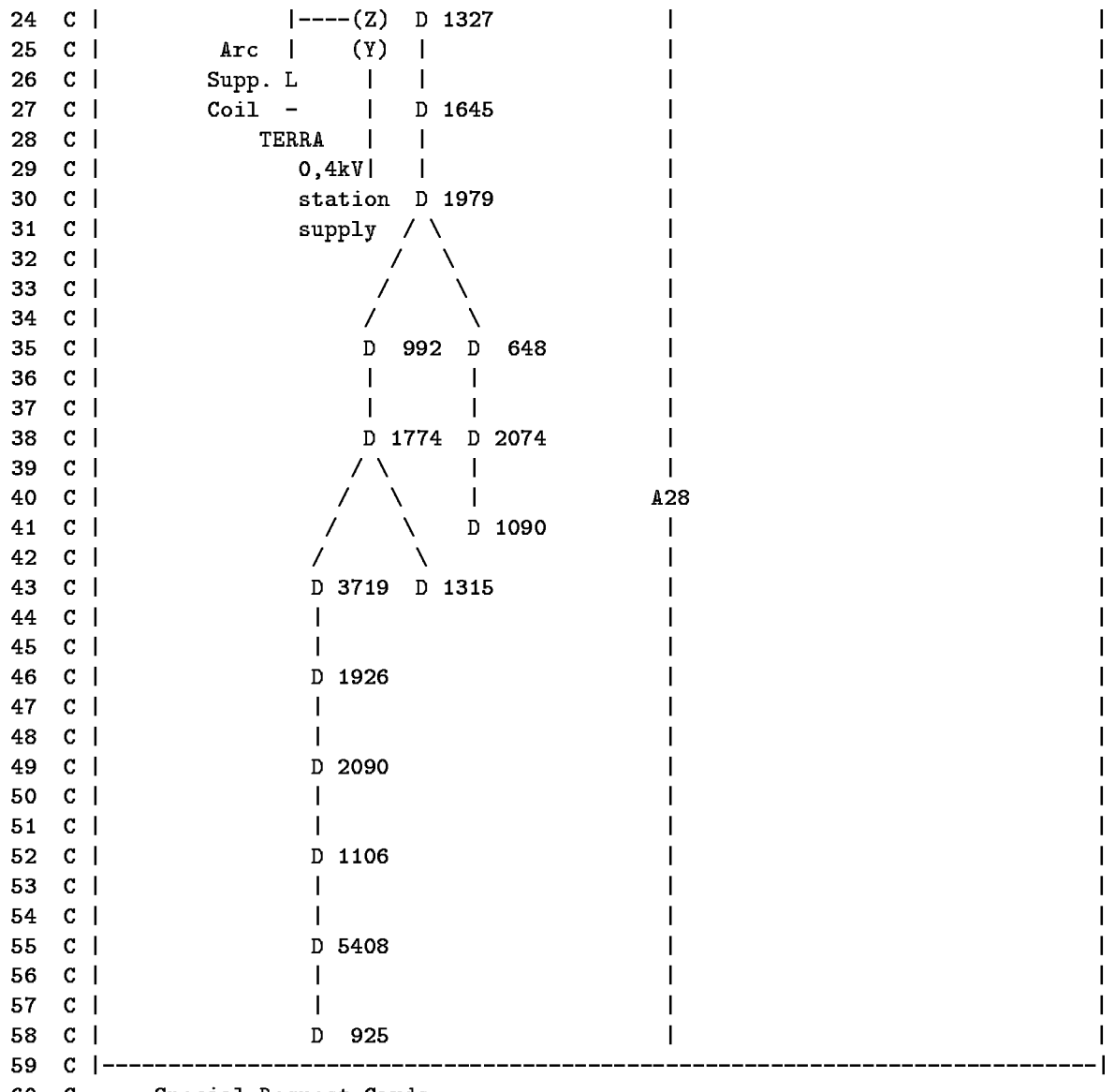


```
C      Special Request Cards
C FIX SOURCE
C 3456789012345678901234567890123456789012345678901234567890123456789012345678901234567890
C -------+---------+---------+---------+---------+---------+---------+---------+---------+
C        1         2         3         4         5         6         7         8
POWER FREQUENCY                    50.00
FREQUENCY SCAN           0.1            100000.0      40
C                    Miscellaneous Data Parameter Cards
C 3456789012345678901234567890123456789012345678901234567890123456789012345678901234567890
C -------+---------+---------+---------+---------+---------+---------+---------+---------+
C        1         2         3         4         5         6         7         8
C DELT >< TMAX >< XOPT >< COPT ><EPSILN><TOLMAT><TSTART>
   2.E-5   0.100      50       0
C                 XOPT = 0 => inductances are given in mH
C                 XOPT neq 0 => reactance in Ohm's at the frequency XOPT
C                         COPT = 0 => capacitances are given in microF
C                         COPT neq 0 => susceptance in microMho's at the
C                                       frequency COPT
C 3456789012345678901234567890123456789012345678901234567890123456789012345678901234567890
```

```
C -------+---------+---------+---------+---------+---------+---------+---------+
C        1         2         3         4         5         6         7         8
C  IOUT>< IPLOT><IDOUBL><KSSOUT><MAXOUT>< IPUN ><MEMSAV>< ICAT ><NENERG><IPRSUP>
C      20        5        1        0        1        0        0        1        0        0
     2000       95        1        0        1        0        0        1        0        0
C
C The feeder is defined. Each section is specified in a file. Every file is cal-
C led using the "$INCLUDE" command.
C It is therefore possible to change the model (pi, distributed...), without
C having to change this file.
C All files are given names according to this structure: FFFFTTTT.dat.
C FFFF is the "from node name" and TTTT is the "to node name".
C
C First comes MODELS. This is a constraint of EMTP.
C $INCLUDE, MODELS.DAT
C
C BEGIN defining A28
C <BUS1><BUS2><BUS3><BUS4><res ><ind ><cap >
 OGLN1R GLN1RM                .1                                                3
 OGLM1S GLN1SMGLN1R GLN1RM                                                      3
 OGLM1T GLN1TMGLN1R GLN1RM                                                      3
$INCLUDE, GLN11327.DAT
$INCLUDE, 13271645.DAT
$INCLUDE, 16451979.DAT
$INCLUDE, 19790992.DAT
$INCLUDE, 09921774.DAT
$INCLUDE, 17743719.DAT
$INCLUDE, 37191926.DAT
$INCLUDE, 19262090.DAT
$INCLUDE, 20901106.DAT
$INCLUDE, 11065408.DAT
$INCLUDE, 54080925.DAT
$INCLUDE, 17741315.DAT
$INCLUDE, 19790648.DAT
$INCLUDE, 06482074.DAT
$INCLUDE, 20741090.DAT
C END defining A28
C BEGIN Definition of loads:
$INCLUDE, 1327.DAT
$INCLUDE, 1645.DAT
$INCLUDE, 1979.DAT
$INCLUDE, 0992.DAT
$INCLUDE, 1774.DAT
$INCLUDE, 3719.DAT
$INCLUDE, 1926.DAT
$INCLUDE, 2090.DAT
$INCLUDE, 1106.DAT
$INCLUDE, 5408.DAT
$INCLUDE, 0925.DAT
$INCLUDE, 1315.DAT
$INCLUDE, 2162.DAT
$INCLUDE, 0648.DAT
$INCLUDE, 2074.DAT
$INCLUDE, 1090.DAT
C END Definition of loads.
```

```
134  C BEGIN Definition of source impedance
135  $INCLUDE, GLN1SIMP.DAT
136  C END Definition of source impedance
137  C BEGIN Include definition for the Petersen Coil
138  $INCLUDE T3.PCH          {T3.PCH contains definitions for the station supply Zy
139  C                           transformer, to which the Petersen Coil is attached
140  C END Include definition for the Petersen Coil
141  BLANK CARD TERMINATING BRANCHES
142  C BEGIN Definition of switches
143  $INCLUDE, MEASURE.DAT
144  C END Definition of switches
145  BLANK CARD TERMINATING SWITCHES
146  C BEGIN Definition of sources:
147  $INCLUDE, GLN1SOUR.DAT
148  C END Definition of sources.
149  BLANK CARD TERMINATING SOURCES
150  C $INCLUDE OUTPUTRE.DAT       {Request output. Has been commented out because
151  C program execution otherwise crashes. Output requests are made directly from
152  C within the main data case.
153    GLN1R GLN1S GLN1T GLN1RSGLN1SSGLN1TS
154    1327R 1327S 1327T 1645R 1645S 1645T
155    1979R 1979S 1979T 0992R 0992S 0992T
156    1774R 1774S 1774T 3719R 3719S 3719T
157    1926R 1926S 1926T 2090R 2090S 2090T
158    1106R 1106S 1106T 5408R 5408S 5408T
159    0925R 0925S 0925T 1315R 1315S 1315T
160    2162R 2162S 2162T 0648R 0648S 0648T
161    2074R 2074S 2074T 1090R 1090S 1090T
162    GLN1RMGLN1SMGLN1TM5408RX
163  BLANK CARD TERMINATING OUTPUT
164  BLANK CARD TERMINATING PLOT
165  BEGIN NEW DATA CASE
166  BLANK CARD ENDING TOTAL EMTP INPUT
```

File: GLN1SIMP.DAT:

```
 1  C |-------------------------------------------------------------------------|
 2  C |Created: 1993.04.13 by Steen M. Munk.            Last modified: 1993.10.18|
 3  C |     FILE: EMTP benchm-A:\INPUT\A28\GLN1SIMP.DAT                          |
 4  C |-------------------------------------------------------------------------|
 5  C
 6  C Definition of source impedance.
 7  C
 8  C 34567890123456789012345678901234567890123456789012345678901234567890123456789
 9  C -------+---------+---------+---------+---------+---------+---------+---------+
10  C        1         2         3         4         5         6         7         8
11  C <BUS1><BUS2><BUS3><BUS4><res ><ind ><cap >
12   0GLN1RSGLN1R             .00907.34621
13   0GLN1SSGLN1S             .00907.34621
14   0GLN1TSGLN1T             .00907.34621
15  C The arc-supression coil is attached to the network.
16  C The definitions are courtesy of Mr. Harald Wehrend, Hannover University.
17  $INCLUDE PETERSEN.DAT
```

File: T3.PCH:

```
C  <++++++>  Cards punched by support routine on  22-Sep-93  08.57.40  <++++++>
C ACCESS MODULE BCTRAN
C C
C $ERASE
C C
C C ============ excitation test and construction data; output requests ========
C C <  FREQ  >< IEXPOS ><  SPOS  >< LEXPOS >< IEXZERO><  SZERO >< LEXZERO>NPITIW
C  3       50.       0.9        5.       6.5       0.9        5.      6.5 0 3 3
C C
C C ============ transformer winding cards ====================================
C C K<  VRAT  ><    R   > <BUS1><BUS2><BUS3><BUS4><BUS5><BUS6>
C   3    0.0635    1.0E-6 T3OU_AT3OUSPT3OU_BT3OUSPT3OU_CT3OUSP
C   1    3.3333     0.076 T3IN_AT3Z1_AT3IN_BT3Z1_BT3IN_CT3Z1_C
C   2    3.3333     0.076 T3INSPT3Z2_AT3INSPT3Z2_BT3INSPT3Z2_C
C C ============ short-circuit test cards ( NW*(NW-1)/2 cards ) ================
C C  J<  Pij   >< ZPOSij >< SPOS   >< ZZEROij>< SZERO  >IDIL
C  1 3      1.0        7.0        5.      0.7         5. 0
C  2 3      1.0        7.0        5.      0.7         5. 0
C  1 2     0.01       0.01        5.     0.01         5. 0
C BLANK card ============== ending short-circuit test data ====================
$VINTAGE, 1,
 1T3OU_AT3OUSP             1.8610843917411
 2T3OU_BT3OUSP             0.0
                           1.8610843917411
 3T3OU_CT3OUSP             0.0
                           0.0
                           1.8610843917411
  USE AR
 1T3IN_AT3Z1_A             472018.09448731           .076
 2T3INSPT3Z2_A             -470667.1073262            0.0
                           472018.09448731           .076
 3T3OU_AT3OUSP             -70917.25203539            0.0
                           -70917.25203538            0.0
                           .744646275736E7          1.E-6
 4T3IN_BT3Z1_B              507.1298030053            0.0
                            507.1298029828            0.0
                           -53241.44164788            0.0
                           472018.09448731           .076
 5T3INSPT3Z2_B              507.1298029828            0.0
                           507.12980300531            0.0
                           -53241.44164788            0.0
                           -470667.1073262            0.0
                           472018.09448731           .076
 6T3OU_BT3OUSP             -53241.44164788            0.0
                           -53241.44164788            0.0
                           .558959676992E7            0.0
                           -70917.25203539            0.0
                           -70917.25203538            0.0
                           .744646275736E7          1.E-6
 7T3IN_CT3Z1_C              507.1298030053            0.0
                            507.1298029828            0.0
                           -53241.44164788            0.0
                            507.1298030053            0.0
                            507.1298029828            0.0
                           -53241.44164788            0.0
```

```
56                              472018.09448731            .076
57   8T3INSPT3Z2_C               507.1298029828             0.0
58                              507.12980300531            0.0
59                              -53241.44164788            0.0
60                               507.1298029828            0.0
61                              507.12980300531            0.0
62                              -53241.44164788            0.0
63                              -470667.1073262            0.0
64                              472018.09448731            .076
65   9T3OU_CT3OUSP              -53241.44164788            0.0
66                              -53241.44164788            0.0
67                              .558959676992E7            0.0
68                              -53241.44164788            0.0
69                              -53241.44164788            0.0
70                              .558959676992E7            0.0
71                              -70917.25203539            0.0
72                              -70917.25203538            0.0
73                              .744646275736E7          1.E-6
74  $VINTAGE, 0,
75  $UNITS, -1.,-1.
76    USE RL
77  C ------------------ << case separator >>> -----------
```

File: GLN1SOUR.DAT:

```
 1  C |-------------------------------------------------------------------------|
 2  C |Created: 1993.04.14 by Steen M. Munk.              Last modified: 1994.01.13|
 3  C |     FILE: EMTP benchm-A:\INPUT\A28\GLN1SOUR.DAT                          |
 4  C |-------------------------------------------------------------------------|
 5  C
 6  C Definition of source.
 7  C
 8  C 34567890123456789012345678901234567890123456789012345678901234567890123456789012345678901234567890
 9  C -------+---------+---------+---------+---------+---------+---------+---------+
10  C        1         2         3         4         5         6         7         8
11  C The following three generators are used to ensure a steady-state history
12  C <BUS1>VC<AMPLITUD><FREQUENC><TIME-0  ><A1      ><TIME-1  ><TSTART  ><TSTOP   >
13  C 14GLN1RS 0    1.E-18       50.    0.                        -1.0
14  C 14GLN1SS 0    1.E-18       50.  120.                        -1.0
15  C 14GLN1TS 0    1.E-18       50. -120.                        -1.0
16  C 145408RX 0     10000       50.    0.                        -1.0
17  C <BUS1>VC<AMPLITUD><FREQUENC><TIME-0  ><A1      ><TIME-1  ><TSTART  ><TSTOP   >
18  C 14GLN1RS 0     8165.       50.34.1748074                    -1.0     150.E-8
19  C 14GLN1SS 0     8165.       50.154.174807                    -1.0     150.E-8
20  C 14GLN1TS 0     8165.       50.274.174807                    -1.0     150.E-8
21  14GLN1RS 0     8165.       50.    0.                        -1.0       150.E-8
22  14GLN1SS 0     8165.       50.  120.                        -1.0       150.E-8
23  14GLN1TS 0     8165.       50. -120.                        -1.0       150.E-8
24  C The following three generators (Type 60) add harmonics and noise
25  C 60GLN1RS
26  C 60GLN1SS
27  C 60GLN1TS
```

File: GLN11327.DAT:

```
 1  C  <++++++>  Cards punched by support routine on  05-May-93  08.55.52  <++++++>
```

```
 2  C CABLE CONSTANTS
 3  C $ERASE                                    { Empty buffer to be flushed at LUNI
 4  C PUNCH
 5  C C MISCELLANEOUS DATA CARD
 6  C C 345678901234567890123456789012345678901234567890123456789012345678901234567890
 7  C C -------+---------+---------+---------+---------+---------+---------+-------
 8  C C        1         2         3         4         5         6         7
 9  C C IT><ISY><NPC><IEA><KMO><IZF><IYF><NPP><NGR>
10  C     3   -1    3    0    0    0    0    1    2
11  C C PI-CIRCUIT SPECIFICATION CARD
12  C C 345678901234567890123456789012345678901234567890123456789012345678901234567890
13  C C -------+---------+---------+---------+---------+---------+---------+-------
14  C C        1         2         3         4         5         6         7
15  C C NP><NCR><IRS><XMAJOR  ><  RSG   >
16  C    11    0        109.636        .1A {Here the length is defined:
17  C C                                    {Length = NP * XMAJOR = 1206m
18  C C PIPE PARAMETER CARD
19  C C 345678901234567890123456789012345678901234567890123456789012345678901234567890
20  C C -------+---------+---------+---------+---------+---------+---------+-------
21  C C        1         2         3         4         5         6         7
22  C C   RP1  ><   RP2  ><   RP3  ><   RHO  ><  my-r  >< eps-1  >< eps-2  >
23  C    0.0212    0.0222    0.02475   21.4E-8   1.0       4.5       4.5
24  C C CROSS-SECTION LOCATIONS CARD
25  C C 345678901234567890123456789012345678901234567890123456789012345678901234567890
26  C C -------+---------+---------+---------+---------+---------+---------+-------
27  C C        1         2         3         4         5         6         7
28  C C  DIST1 >< THETA1 ><  DIST2 >< THETA2 ><  DIST3 >< THETA3 ><  DIST4 >< THETA4
29  C    0.01400   0.00000   0.01400   120.000   0.01400   240.000
30  C C The preceding dimensions were calculated from the dimensions of the sectio-
31  C C nized condunctors.
32  C C CARD INDICATING NUMBER OF CONDUCTORS
33  C C 345678901234567890123456789012345678901234567890123456789012345678901234567890
34  C C -------+---------+---------+---------+---------+---------+---------+-------
35  C C        1         2         3         4         5         6         7
36  C C NC><NC2><NC3><NC4><NC5><NC6><NC7><NC8><NC9><N10><N11><N12><N13><N14><N15><N1
37  C     1    1    1
38  C C GEOMETRICAL & PHYSICAL DATA CARD
39  C C First conductor
40  C C 345678901234567890123456789012345678901234567890123456789012345678901234567890
41  C C -------+---------+---------+---------+---------+---------+---------+-------
42  C C        1         2         3         4         5         6         7
43  C C   R1   ><   R2   ><   R3   ><   R4   ><   R5   ><   R6   ><   R7   >
44  C          0   0.00549   0.00808
45  C C 345678901234567890123456789012345678901234567890123456789012345678901234567890
46  C C -------+---------+---------+---------+---------+---------+---------+-------
47  C C        1         2         3         4         5         6         7
48  C C  rhoc  ><  my-c  ><  my-I1 >< eps-I1 ><  rhos  ><  my-s  ><  my-I2 >< eps-I2
49  C      18E-9         1         1       4.5
50  C C GEOMETRICAL & PHYSICAL DATA CARD
51  C C Second conductor
52  C C 345678901234567890123456789012345678901234567890123456789012345678901234567890
53  C C -------+---------+---------+---------+---------+---------+---------+-------
54  C C        1         2         3         4         5         6         7
55  C C   R1   ><   R2   ><   R3   ><   R4   ><   R5   ><   R6   ><   R7   >
56  C          0   0.00549   0.00808
```

```
C C 3456789012345678901234567890123456789012345678901234567890123456789012345678
C C -------+---------+---------+---------+---------+---------+---------+--------
C C        1         2         3         4         5         6         7
C C  rhoc  ><  my-c  ><  my-I1 >< eps-I1 ><  rhos  ><  my-s  ><  my-I2 >< eps-I2
C      18E-9         1         1       4.5
C C GEOMETRICAL & PHYSICAL DATA CARD
C C Third conductor
C C 3456789012345678901234567890123456789012345678901234567890123456789012345678
C C -------+---------+---------+---------+---------+---------+---------+--------
C C        1         2         3         4         5         6         7
C C   R1   ><   R2   ><   R3   ><   R4   ><   R5   ><   R6   ><   R7   >
C          0   0.00549   0.00808
C C 3456789012345678901234567890123456789012345678901234567890123456789012345678
C C -------+---------+---------+---------+---------+---------+---------+--------
C C        1         2         3         4         5         6         7
C C  rhoc  ><  my-c  ><  my-I1 >< eps-I1 ><  rhos  ><  my-s  ><  my-I2 >< eps-I2
C      18E-9         1         1       4.5
C C The preceding dimensions were calculated from the dimensions of the sectio-
C C nized condunctors.
C C PIPE LOCATION CARD
C C 3456789012345678901234567890123456789012345678901234567890123456789012345678
C C -------+---------+---------+---------+---------+---------+---------+--------
C C        1         2         3         4         5         6         7
C C center >
C       1.00                                          { One metre below the surfac
C C FREQUENCY & EARTH RESISTIVITY CARD
C C 3456789012345678901234567890123456789012345678901234567890123456789012345678
C C -------+---------+---------+---------+---------+---------+---------+--------
C C        1         2         3         4         5         6         7
C C     rho     ><      freq   >
C          25.000                                           { Ground resistivi
$VINTAGE, 1
 1GLN1RMA 11 1              2.9711093E-02   2.0767641E-01   3.6522242E-02
 2GLN1SMA 11 2              2.6688466E-02   1.7740610E-01  -4.4793224E-03
                            2.9711093E-02   2.0767641E-01   3.6522242E-02
 3GLN1TMA 11 3              2.6688466E-02   1.7740610E-01  -4.4793224E-03
                            2.6688466E-02   1.7740610E-01  -4.4793224E-03
                            2.9711093E-02   2.0767641E-01   3.6522242E-02
 1A 11 1A 21 1GLN1RMA 11 1
 2A 11 2A 21 2
 3A 11 3A 21 3
 1A 21 1A 31 1GLN1RMA 11 1
 2A 21 2A 31 2
 3A 21 3A 31 3
 1A 31 1A 41 1GLN1RMA 11 1
 2A 31 2A 41 2
 3A 31 3A 41 3
 1A 41 1A 51 1GLN1RMA 11 1
 2A 41 2A 51 2
 3A 41 3A 51 3
 1A 51 1A 61 1GLN1RMA 11 1
 2A 51 2A 61 2
 3A 51 3A 61 3
 1A 61 1A 71 1GLN1RMA 11 1
 2A 61 2A 71 2
```

```
112   3A 61 3A 71 3
113   1A 71 1A 81 1GLN1RMA 11 1
114   2A 71 2A 81 2
115   3A 71 3A 81 3
116   1A 81 1A 91 1GLN1RMA 11 1
117   2A 81 2A 91 2
118   3A 81 3A 91 3
119   1A 91 1A101 1GLN1RMA 11 1
120   2A 91 2A101 2
121   3A 91 3A101 3
122   1A101 11327R GLN1RMA 11 1
123   2A101 21327S
124   3A101 31327T
125  $VINTAGE, 0
```

File: 1327.DAT:

```
 1  C |-------------------------------------------------------------------------|
 2  C |Created: 1993.04.13 by Steen M. Munk.            Last modified: 1994.11.09|
 3  C |                              FILE:  1327.DAT                            |
 4  C |-------------------------------------------------------------------------|
 5  C
 6  C Definition of load.
 7  C
 8  C 345678901234567890123456789012345678901234567890123456789012345678901234567890
 9  C -------+---------+---------+---------+---------+---------+---------+---------+
10  C        1         2         3         4         5         6         7         8
11  C <BUS1><BUS2><BUS3><BUS4><res ><ind ><cap >
12   01327R                   1176.5                                            3
13   01327S       1327R                                                         3
14   01327T       1327R                                                         3
```

File: 5408.DAT:

```
 1  C |-------------------------------------------------------------------------|
 2  C |Created: 1993.04.13 by Steen M. Munk.            Last modified: 1994.11.09|
 3  C |                              FILE:  5408.DAT                            |
 4  C |-------------------------------------------------------------------------|
 5  C
 6  C Definition of load.
 7  C
 8  C 345678901234567890123456789012345678901234567890123456789012345678901234567890
 9  C -------+---------+---------+---------+---------+---------+---------+---------+
10  C        1         2         3         4         5         6         7         8
11  C <BUS1><BUS2><BUS3><BUS4><res ><ind ><cap >
12  C $INCLUDE, 54081004.DAT
13  C 05408RS5408Z             0.2974                                           3
14  C 05408SS5408Z 5408RS5408Z                                                  3
15  C 05408TS5408Z 5408RS5408Z                                                  3
16  C 05408Z                     1.00                                           3
17   05408R                   185.87
18   05408S       5408R
19   05408T       5408R
20   05408R 5408RX                1.                                          3
```

File: MEASURE.DAT:

```
 1  C |------------------------------------------------------------------------|
 2  C |Created: 1993.08.11 by Steen M. Munk.              Last modified: 1993.09.13|
 3  C |     FILE: EMTP benchm-A:\INPUT\A28\MEASURE.DAT                          |
 4  C |------------------------------------------------------------------------|
 5  C
 6  C C Measuring switch call
 7  C C 345678901234567890123456789012345678901234567890123456789012345678901234567890123456789012345678
 8  C C -------+---------+---------+---------+---------+---------+---------+--------
 9  C C        1         2         3         4         5         6         7
10  C <BUS1><BUS2><TIME CRI><TERIA   >                    <REQUEST >               0
11  C These switches measure the current flowing into the feeder
12  C  GLN1R GLN1RM                                        MEASURING                1
13  C  GLN1S GLN1SM                                        MEASURING                1
14  C  GLN1T GLN1TM                                        MEASURING                1
15  C ------------ Schalter fuer ohmsche Sternpunkterdung an T3 --------------------
16  C <BUS1><BUS2>< T CLOSE>< T OPEN >< NSTEP  >< V FLA  ><        ><BUS5><BUS6>
17    T3INSPR_ESPU     9998.     9999.
18  C interconnections of Zy transformer windings within the main data case
19  C ------------ Verschaltung der Z-Wicklung Trafo T3 ---------------------------
20    T3Z1_AT3Z2_B                                       MEASURING
21    T3Z1_BT3Z2_C                                       MEASURING
22    T3Z1_CT3Z2_A                                       MEASURING
23  C The following three switches connect the transformer to the busbar:
24    GLN1R T3IN_A                                       MEASURING
25    GLN1S T3IN_B                                       MEASURING
26    GLN1T T3IN_C                                       MEASURING
27  C Miscellaneous switches for monitoring events on the network
28    5408R 5408RM                                       MEASURING                1
29    5408S 5408SM                                       MEASURING                1
30    5408T 5408TM                                       MEASURING                1
31    5408RL5408RS                                       MEASURING                1
32    5408SL5408SS                                       MEASURING                1
33    5408TL5408TS                                       MEASURING                1
34    1090R 1090RM                                       MEASURING                1
35    1090S 1090SM                                       MEASURING                1
36    1090T 1090TM                                       MEASURING                1
37    1090RL1090RS                                       MEASURING                1
38    1090SL1090SS                                       MEASURING                1
39    1090TL1090TS                                       MEASURING                1
40  C Switches that change the load.
41  C 5408RL5408Z  0.015    4.000     10.E8
42  C 5408S        0.015    4.000     10.E8
43  C 5408T        0.015    4.000     10.E8
44  C 1090RS1090RX 0.005    4.000     10.E8
45  C 1090SS1090SX 0.005    4.000     10.E8
46  C 1090TS1090TX 0.005    4.000     10.E8
```

Appendix H

Matlab Simulator of DISMO–System

During the work that is documented in [Jespersen, 1994] a simulator of the DISMO–system was implemented in the MATLAB-environment.

Based on v. 4 of MATLAB, this simulator gives the user simple control via menus.

Details on the program will not be released. In this appendix is only given examples on how to interact with the program.

The user interface is in Danish. Therefore translations are given in the captions of the figures.

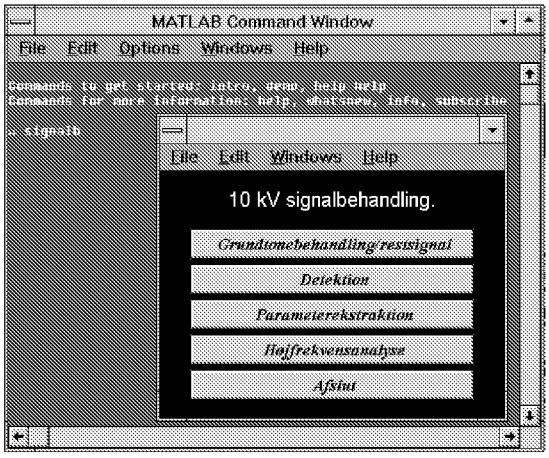

Figure H.1: First Menu of DISMO–Simulator. The Five Possibilities Are: Processing of Fundamental Component/Residual Component. Detection. Extraction of Parameters. High Frequency Analysis. Exit.

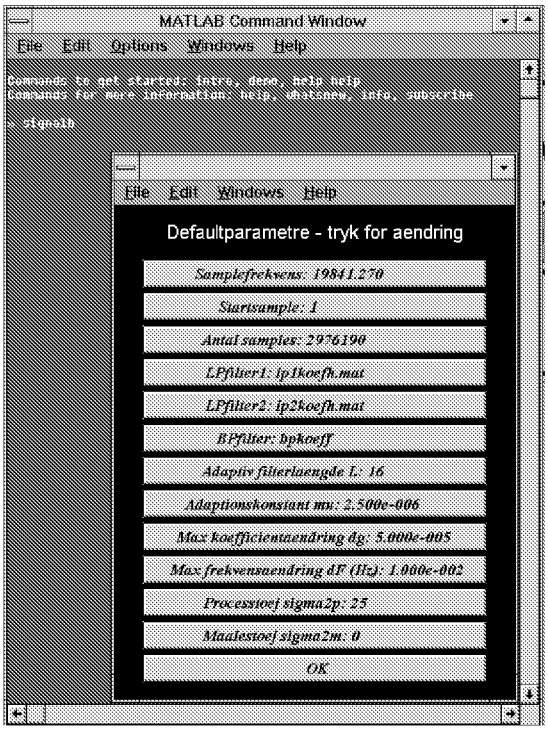

Figure H.2: First Menu under Processing of Fundamental Component/Residual. It Is Possible to Change Parameters Such As Sampling Frequency. Start Sample. Number of Samples to be Processed. The Lowpass Filters Used for Decimation. Bandpass Filter. Parameters of the Frequency Estimator.

The simulator is implemented as a so-called TOOLBOX and is to be installed along with other TOOL-

BOXes.
Besides the simulator TOOLBOX, called DISMO, it is required that the two TOOLBOXes SIGNAL PROCESSING TOOLBOX and OPTIMIZATION TOOLBOX are installed.

The simulator is started by giving the command `signalb` at the MATLAB-prompt.

[Jespersen, 1994] contains a users manual to the program.

Appendix I

SH-GR Viewer for Large Files in Matlab-Format

It was found necessary to create a viewer for MATLAB-files, because the first version of MATLAB; v. 3.5, used in this project was unable to handle the excessively large data files.
Though the newer versions of MATLAB may read files sequentially, the program is still relevant, because it runs much faster than MATLAB does.

In Figure I.1 is shown the screen image. The program runs only on an Intel 386/87 or higher. The screen must be a VGA.

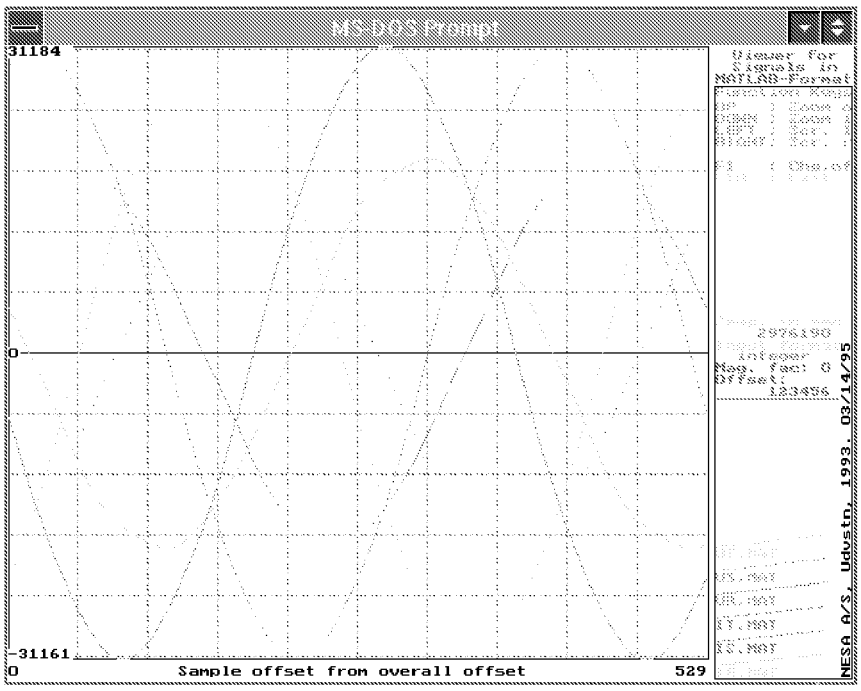

Figure I.1: Screen Image of **SH-GR**–File Viewer Program.

The file **EGAVGA.BGI** supplied with the BORLAND C–compiler must be in the default directory. Though this file is part of a commercial product, it is allowed to copy and distribute it.

The program handles up to six files at the time. These files must have the same length. ./.

Data stored as either **integer** or **double** (16bits or 64bits per sample) can be handled. Information on the type of data is stored in the compulsory header of MATLAB-files.

Start the program by typing **SH-GR** at the DOS–prompt.
After a short "commercial", where the version number of the program is shown, one proceeds into defining which files one wishes to view.
Notice the **b** in the version number. The program works, but is not completely tested. It does, at times, behave as a β-release.
The present version number is: **1.3b**.
Therefore, when entering file names DO NOT mis-type. Though it is possible on the screen to correct the error, the program unfortunately mis-interprets the input.

The program starts by asking where the input files are located. It is assumed that all input files are in the same directory, which must be the default directory. If one starts the program from the directory which is the default directory just type: [.] [Return].
If you enter a non-existing directory the program will ask once again.
If you regret, you can at this time say so, and the program will ask again where to go.

Then start entering the filenames **without** the extension.
If you wish to view fewer than the maximum number of files enter: [.] [Return] when the program asks for the name of the next file.
When the sixth filename has been entered the program proceeds into showing the curves.
Since the input-files must be in MATLAB-format, they must have the "**.MAT**"-extension, (which is automatically given when one exports data from MATLAB).
Data is assumed to be stored as real row-vectors. For some unexplainable reason the variable name may only be one character long. Longer variable names will do that what appears on the screen is completely nonsense.

One moves around using the four arrow-keys: $\leftarrow$, $\downarrow$, $\rightarrow$ and $\uparrow$.
$\leftarrow$ and $\rightarrow$ are used to move back and forth in the files. Each key-press will do that the next or previous window is shown.
$\downarrow$ and $\uparrow$ control the window length. The default window length is 529 samples, indicated on the screen as: **Mag. fac: 0** and **529** as the maximum value on the x-axis.

Mag. fac:	Nb. of samples
-2	**52**
-1	**88**
0	**529**
1	**2645**
2	**5290**

See also Figure I.1.

Does one need to go far into the signals, e.g. several hundred thousands of samples, press [F1]. The program asks for the Δ-offset. The Δ-offset is the number of samples one wishes to go back or forth in the files.

To exit press [F10].

Appendix J

Paper Presented at the PQA–'95 Conference in New York

The paper has been formatted to match the lay-out and notation of the thesis. Otherwise it is rendered without modification.

DISTRIBUTION NETWORK MONITORING

Steen M. Munk
NESA A/S
Strandvejen 102
DK-2900 Hellerup
udvsnesa@inet.uni-c.dk
&
John Aa. Sørensen
Electronics Institute
Technical University of Denmark
DK-2800 Lyngby
jaas@ei.dtu.dk

Abstract

This paper describes initial research in centralized monitoring of radial cable based distribution networks. The hypothesis that it is possible to monitor distribution networks on the basis of very few measuring points is shown to be valid for a certain set of events.

The paper describes experiments that have been made to verify that specific events may be distinguished from other events.

One method of classifying specific events is demonstrated, and it is shown that it is possible to distinguish two types of events (start/stop of large motors) that are much alike and take place at the same location on the feeder.

Keywords: *Distribution network. Monitoring. **O**bservation **P**oint. High quality measurements. Event detection. Signal classification.*

Distribution Network Monitoring

It is believed that distribution utilities in the future must monitor their networks better than today. Both to ensure high power quality and to be able to quickly locate and clear faults.

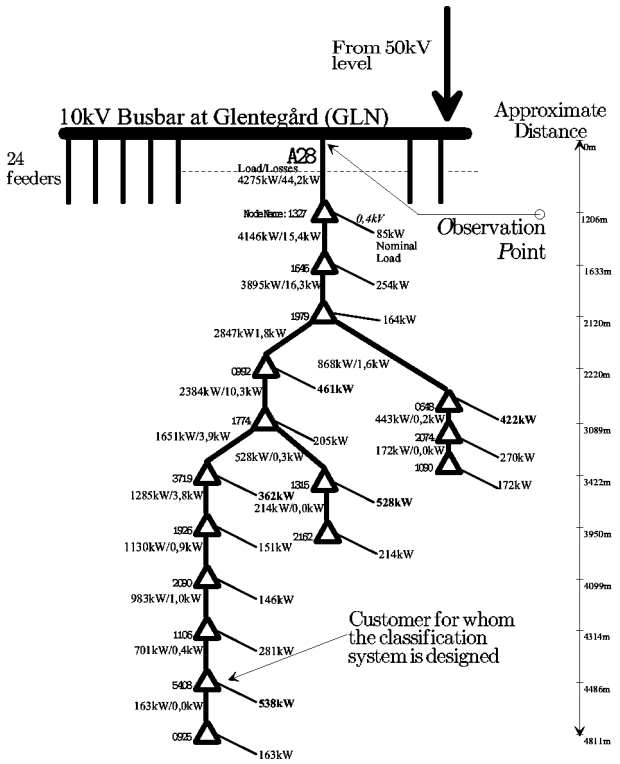

Figure J.1: Schematic of Feeder where Experiments were Carried Out with Indication of Nominal Load.

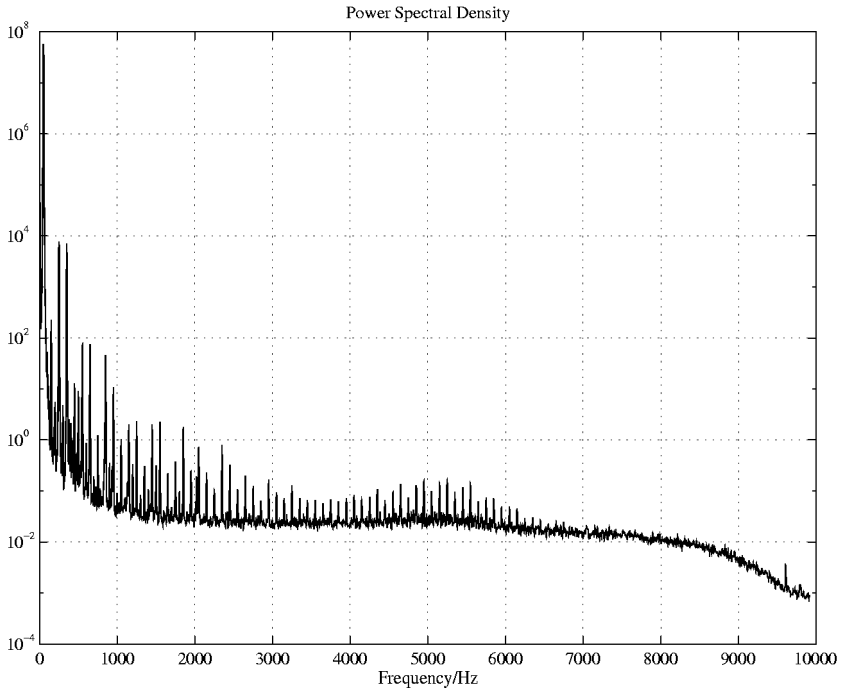

Figure J.2: Estimate of Power Spectrum of Phase Current.

The one extremity of distribution network monitoring would be to equip all transformer stations with measuring systems and transmit the measurements to locations in the network where they are processed. This, however, would be extremely expensive.
It has been estimated that in NESA's area of operation only[1], the expense would be DKK200.000.000 ($30.000.000) to establish measuring points and communication channels.
Such an investment is not believed to be profitable. Therefore, in order to be able to fulfill the demands of better monitoring, it is necessary to investigate how few measuring points are sufficient for properly monitoring of the network.

NESA A/S, the Electronics Institute & the Power Engineering Department of the Technical University of Denmark and the Danish Electrical Research Institute, have initiated research on the topic **C**entralized **M**onitoring of **D**istribution **N**etworks, henceforward denoted the DISMO–project.

This paper reports on experiences gained so far.

Main Questions Addressed in the Monitoring Project

The work was initiated with the most simple configuration: How much information can be derived about the state of a 10,4kV radial cable based distribution feeder, if only measurements are available at the substation, henceforward denoted the *O*bservation *P*oint (*OP*), see Figure J.1.
The limited number of measuring points imposes strict demands on the measuring equipment. An important result therefore is what are the requirements to the measuring system, i.e. bandwidth, noise and dynamic range.
Having acquired high quality measurements, the next problem is to assign methods that are capable of extracting the state information contained. Therefore an important question is what are the requirements to the analysis system?

A fundamental assumption is that since protection is not a part of DISMO–monitoring, there is sufficient time to process signals after the detection of an event.

Distribution Network Used for Initial Investigations

As a basis for the investigations one 10,4kV cable based feeder was chosen. This feeder supplies both residential and industrial areas.
The *OP* is located at the substation GLENTEGÅRD in the northern suburbs of København.

The total yearly consumption on this feeder is about 13GWh.
Among the approximately 2200 customers connected to this feeder, only 20 have a yearly consumption that exceeds 50MWh.
One customer has a yearly consumption that exceeds 1GWh.
This customers impact on the feeder was believed to be so significant, that it was chosen as a source of signals for the initial studies of signal propagation from a node in the network to the substation.
The customer alone is connected to the transformer station **5408**, see Figure J.1. At the plant there are several large asynchronous motors. Two of these, a 90kW and a 75kW motor, were chosen for the investigations: Fully loaded these machines were in turn turned on and off, while measurements were taken at the *OP*.

During the second part of the experiments, low voltage fuses (0,4kV) were burnt out at the secondary side of the transformer at node **1327**.

Outline of Monitoring System and Signal Model

In Figure J.3 is shown a diagram of the elements of the monitoring system. The system has a four-level structure:

[1] Approximately 500.000 customers supplied from 6.000 transformer stations and 60 substations.

1. Acquisition of three phase currents and voltages in 10kHz bandwidth.
2. Splitting up the signals into the fundamental component (50Hz) and the residual component.
3. Event detection.
4. Event classification.

At the *OP* is assumed that both currents and voltages may be described by the model in Equations J.1 and J.2:

$$i_{OP}(t) = x_{p,i}(t) + x_{t,i}(t) + \nu_i(t) \quad \text{(J.1)}$$

$$v_{OP}(t) = x_{p,v}(t) + x_{t,v}(t) + \nu_v(t) \quad \text{(J.2)}$$

$\nu_v(t)$ and $\nu_i(t)$ are band limited Gaussian white noise signals.
The p-subscript denotes the periodic component and the t-subscript denotes the transient component respectively.

Description of Monitoring System

Data Acquisition System

The fundamental component (50Hz) is no longer the sole component of interest.
During the initial research the hypothesis was that frequency components up to 10kHz needed to be acquired by the measuring part of the DISMO–system.

This leads to strict demands to the equipment. The fundamental component of both currents and voltages are orders of magnitude larger than the residual components.

On top of this, capturing transients is an important source of information about the activity on the feeder.

The voltages, 8,5kV$_{\text{peak}}$, were measured using high-voltage oscilloscope probes, and the currents were measured using an enhanced optical current sensor.
The current sensors are the most critical components of the measuring system. Their SNR is about 90dB over the entire frequency range from 1Hz to 10kHz, which corresponds to 14,5 bit resolution.
Steady state frequency components up to about 6,5kHz may be distinguished, see Figure J.2.
To eliminate unnecessary equipment, the signals were converted, using a 16 bit simultaneous sample and hold A/D–converter, and stored on a computer at the *OP*.

The output from this level therefore is the six measured signals in digital format.

Splitting the Broad Band Signal into the Fundamental and Residual Components

The fundamental frequency component poses a problem; it is orders of magnitude larger than the rest of the spectrum. The signal processing therefore takes place in two parts:

1. The *fundamental part.*
2. The *residual part.*

Due to implementation constraints the residual part is divided into two regions: Respectively below and above the fundamental component, see Figure J.3.
The splitting up of the signals is done by multi rate signal processing. All filters are FIR in order to have control over phase delay.

Furthermore, on the fundamental component is estimated the instantaneous amplitude and phase. The phase is indicated relative to a chosen reference. This reference is one of the phase voltages.

The output from this level thus becomes: The decomposed signal and the estimates of the amplitude and phase of the fundamental component.

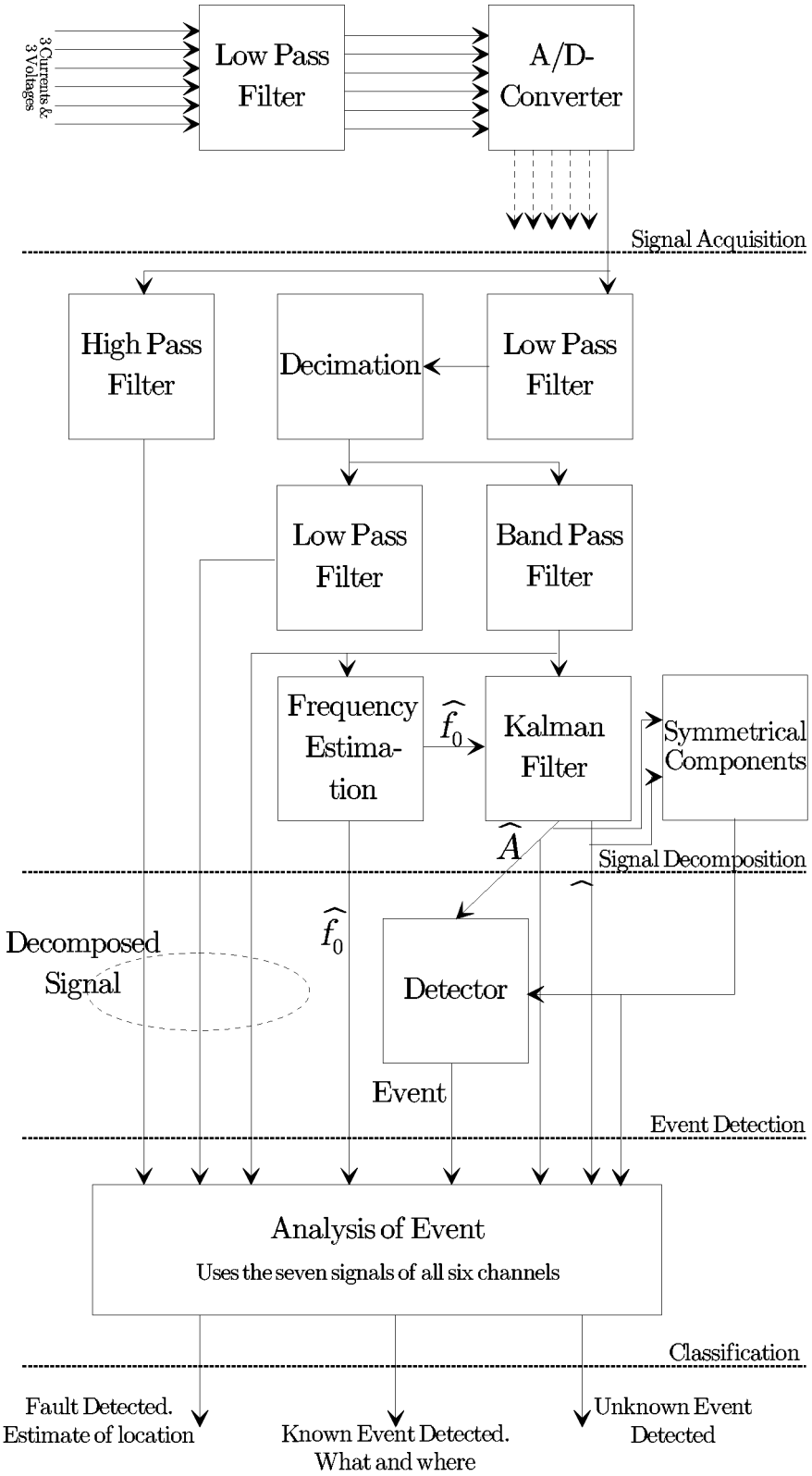

Figure J.3: Diagram of DISMO–System

The amplitude and phase are estimated using a modified Kalman filter, which requires an estimate of the instantaneous fundamental frequency. This estimate therefore is also part of the output from this level.
The estimates of the amplitudes and phases are used to estimate the symmetrical components.

Kalman filter.

The detection scheme is based on Kalman filter estimates of the current amplitudes, see [Haykin, 1991, Chapter 7].
To reduce the computational requirements, the Kalman filter operates on the estimate of the fundamental component only, i.e. the output from the band pass filter.
For this signal a two state model is defined:

$$\boldsymbol{x}(n+1) = \boldsymbol{\Phi}(n+1,n)\,\boldsymbol{x}(n) + \boldsymbol{v}_1(n) \tag{J.3}$$

$$\boldsymbol{y}(n) = \boldsymbol{C}(n)\,\boldsymbol{x}(n) + \boldsymbol{v}_2(n) \tag{J.4}$$

Equation J.3 is the process equation and Equation J.4 is the measurement equation.
$\boldsymbol{\Phi}(n+1,n)$ is a 2×2 state transition matrix. $\boldsymbol{v}_1(n)$ and $\boldsymbol{v}_2(n)$ are Gaussian white noise signals.
Assuming a constant frequency sinusoidal signal, $\boldsymbol{y}(n)$, leads to the transition matrix:

$$\boldsymbol{\Phi}(n+1,n) = \begin{pmatrix} \cos(\omega_0\,\Delta T) & -\sin(\omega_0\,\Delta T) \\ \sin(\omega_0\,\Delta T) & \cos(\omega_0\,\Delta T) \end{pmatrix} \tag{J.5}$$

The measurement matrix, $\boldsymbol{C}$, that combines the state variables, $\boldsymbol{x}(n)$, and the observations, $\boldsymbol{y}(n)$, is an 1×2 matrix.

$$\boldsymbol{C}(n) = \begin{pmatrix} 1 & 0 \end{pmatrix} \tag{J.6}$$

However tests have shown that the small variations in the frequency of the fundamental component leads to poor performance of the Kalman filter with fixed state transition matrix.
Instead is used a modified Kalman filter. The modification is based on an estimate of the fundamental frequency for the state transition matrix:

$$\boldsymbol{\Phi}'(n+1,n) = \begin{pmatrix} \cos(\widehat{\omega_{0,n}}\,\Delta T) & -\sin(\widehat{\omega_{0\,n}}\,\Delta T) \\ \sin(\widehat{\omega_{0\,n}}\,\Delta T) & \cos(\widehat{\omega_{0\,n}}\,\Delta T) \end{pmatrix} \tag{J.7}$$

The instantaneous frequency can be estimated in several ways. It was chosen to base the estimation on extraction of parameters from the linear prediction spectrum, see [Haykin, 1991, Griffiths, 1975].

Furthermore the frequency estimate will be used to detect extreme situations on the feeder, i.e. the loss of power plants, faults in the transmission system, etc., during which the monitoring system temporarily will be halted.

Event Detection

As expected, the voltages at the substation exhibit low sensitivity to state changes on the feeder. Therefore event detection is based on the estimates of the current amplitudes, complemented by use of the symmetrical components.

In Figure J.4 is shown an example of the amplitude estimate. To filter the fluctuations of the estimates a standard median (SM) filter is applied before the estimates enter the detector, see [Haavisto *et al.*, 1988, Heinonen and Neuvo, 1988].
The median filter is a filter that outputs the median of a given input sequence.

At this stage events may be classified into three categories: One- two- or three phase events. Therefore three detectors run simultaneously. In Table J.1 the function "MED" denotes the median filter. The table shows the test quantities in the three cases.

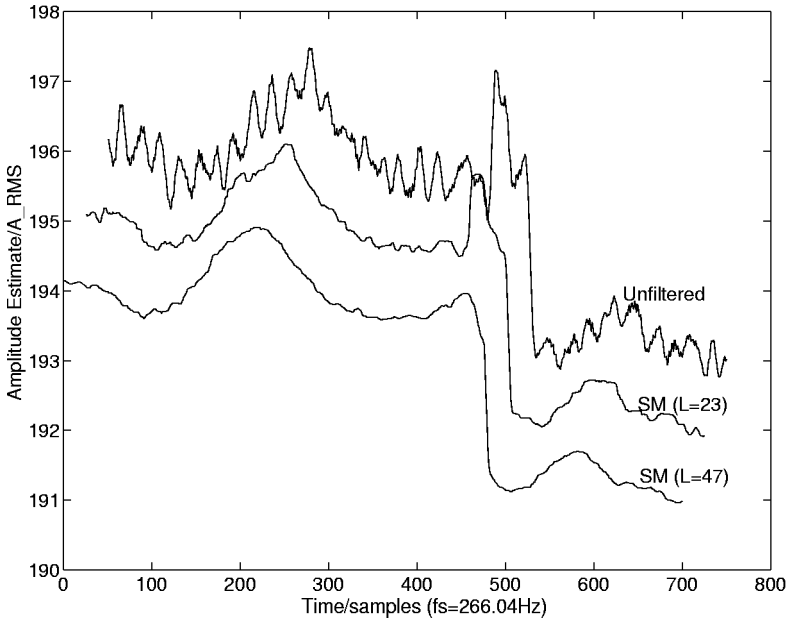

Figure J.4: Estimate of Amplitude of Current before and After Median Filtering. The Curves of the Two Filtered Versions are moved $1A_{eff}$ and $2A_{eff}$ Respectively and 25 samples and 50 samples Respectively.

Type of Event	Test Quantity
Three Phase	$A_{RST}(k) = \frac{1}{3}\left(\text{MED}(\widehat{\lvert i_R \rvert}(k)) + \text{MED}(\widehat{\lvert i_S \rvert}(k)) + \text{MED}(\widehat{\lvert i_T \rvert}(k))\right)$
Two Phase	$A_{RS}(k) = \frac{1}{2}\left(\text{MED}(\widehat{\lvert i_R \rvert}(k)) + \text{MED}(\widehat{\lvert i_S \rvert}(k))\right)$ $A_{ST}(k) = \frac{1}{2}\left(\text{MED}(\widehat{\lvert i_S \rvert}(k)) + \text{MED}(\widehat{\lvert i_T \rvert}(k))\right)$ $A_{TR}(k) = \frac{1}{2}\left(\text{MED}(\widehat{\lvert i_T \rvert}(k)) + \text{MED}(\widehat{\lvert i_R \rvert}(k))\right)$
One Phase	$A_R(k) = \text{MED}(\widehat{\lvert i_R \rvert}(k))$ $A_S(k) = \text{MED}(\widehat{\lvert i_S \rvert}(k))$ $A_T(k) = \text{MED}(\widehat{\lvert i_T \rvert}(k))$

Table J.1: Test Quantities in the Three Sub Cases.

Using the detector in Equation J.8, based on the test quantities defined in Table J.1, time stamps as indicated in Figure J.5 are obtained.

$$d(k) = A(k+p) - A(k) \tag{J.8}$$

$$d(k) > \Delta A_+ \quad \vee \quad d(k) < \Delta A_- \tag{J.9}$$

The thresholds ΔA_+ and ΔA_- are found as a function of the desired sensitivity and the allowed rate of false alarm.

The output from this level is binary; '0' for no event detected and '1' for event detected.

Event Classification

When an event is detected the classification scheme is initiated.
This part of the system is based on all the frequency components of the input signal. The output from this level is one of the three statements indicated in Figure J.3.

Time–frequency analysis of the residual signal during an event has shown frequency components up to about 2,5kHz.
The event investigated was the burning out of a fuse. It is therefore remarkable that such high frequency components occur, since the signals have passed through a distribution transformer. Distribution transformers behave much like low pass filters, with a cutoff frequency not much higher than about 1kHz.
Investigations on the transfer capabilities of cables have shown that cables may transmit frequencies up to some tens of kiloHertz for lengths which are within the normal for distribution feeders in NESA's area of operation, < 10km. Therefore events directly on the feeder (e.g. faults) are expected to cause much higher frequencies at the *OP*.

The work on event classification was initiated with signals from the operation of the two machines at the former factory. They are connected to the same transformer and trying to distinguish these two, would be a very good indication of the performance one could expect from a centralized monitoring system.

A time–frequency analysis has revealed that these events mostly cause fundamental frequency components. It was therefore decided to start the investigation by the development of methods that work on the estimate of the fundamental components of the currents.

The classifier selected for the initial investigation has relatively few parameters.

From Figure J.7 one may identify the two events that are associated with the 90kW machine; turning on and off. The waveform would look almost the same for the 75kW machine. But, as will be seen, it is possible to extract features so that one may distinguish between the two events.

The second order polynomial current amplitude model for starting of the machine has four parts which are described by the functions of Equation J.11, see Figure J.6.

$$\boldsymbol{\theta}_{on}^T = \begin{pmatrix} t_{1_{on}} & t_{2_{on}} & t_{3_{on}} & \alpha_{1_{on}} & \alpha_{2_{on}} & \alpha_{3_{on}} & \alpha_{4_{on}} \end{pmatrix} \tag{J.10}$$

$$f(t, \boldsymbol{\theta}_{on}) = \begin{cases} \alpha_1 & \text{for } t_{min} \le t < t_1 \\ \alpha_1 + \alpha_2 \frac{t-t_1}{t_2} & \text{for } t_1 \le t < t_1 + t_2 \\ \alpha_1 + \alpha_2 + \alpha_3 \frac{t-(t_1+t_2)}{t_3} + \alpha_4 \left(\frac{t-(t_1+t_2)}{t_3}\right)^2 & \text{for } t_1 + t_2 \le t < t_1 + t_2 + t_3 \\ \alpha_1 + \alpha_2 + \alpha_3 + \alpha_4 & \text{for } t_1 + t_2 + t_3 \le t \le t_{max} \end{cases} \tag{J.11}$$

t_1 denotes the start of the event.
$\alpha_{1_{on}}$ and $\alpha_{4_{on}}$ describe the level of the current before and after the event.
During the event the course of the current is divided into two parts; a linear and a second order part.
The parameters $\boldsymbol{\theta}_{on}$ were LS–estimated.

$$J(\boldsymbol{\theta}_{min}) = \min_{\boldsymbol{\theta}} \sum_{k=1}^{k_{max}} (f(k,\boldsymbol{\theta}) - \boldsymbol{y}_k)\,(f(k,\boldsymbol{\theta}) - \boldsymbol{y}_k)^* \tag{J.12}$$

Here $\boldsymbol{y}$ is the observed event, represented in complex format, i.e. on the basis of the estimates of amplitude and phase from the Kalman filter.

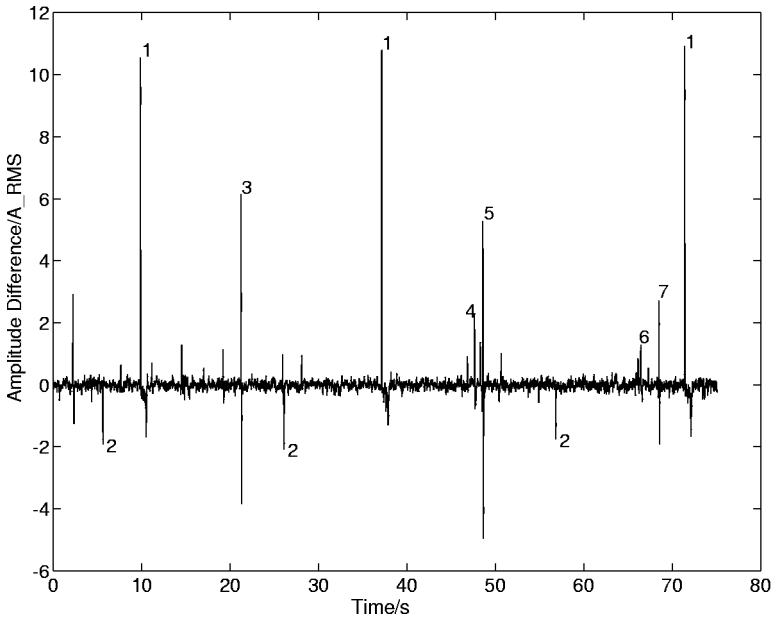

Figure J.5: Test Quantities During Operation of 90kW Machine at Factory. Event 1 is Starting of Machine. Event 2 is Stopping. Other Events are Unknown. Median Filter Length 23samples. p of Equation J.8 is 8.

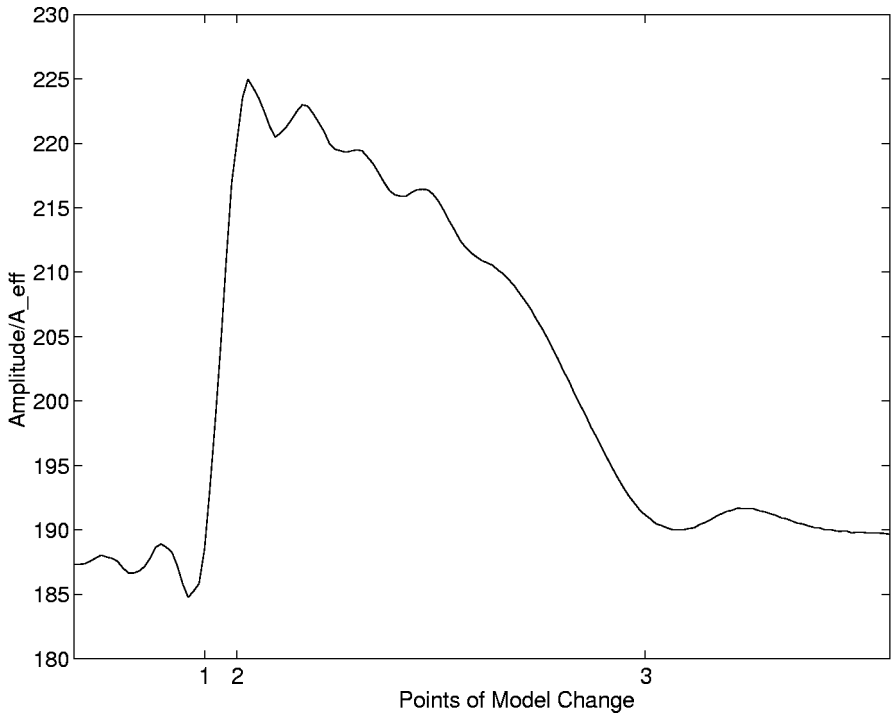

Figure J.6: Times t_{1on}, t_{2on} and t_{3on} of the Model Used for Starting of Motors at the Factory.

Figure J.4 shows the current when the 90kW machine is turned off. The model of Equation J.14 seems appropriate to describe this.

$$\boldsymbol{\theta}_{off}^T = \begin{pmatrix} t_{1_{off}} & t_{2_{off}} & \alpha_{1_{off}} & \alpha_{2_{off}} \end{pmatrix} \tag{J.13}$$

$$f(t, \boldsymbol{\theta}_{off}) = \begin{cases} \alpha_{1_{off}} & \text{for } t_{min} \leq t < t_{1_{off}} \\ \alpha_{1_{off}} + \alpha_{2_{off}} \frac{t - t_{1_{off}}}{t_{2_{off}}} & \text{for } t_{1_{off}} \leq t < t_{1_{off}} + t_{2_{off}} \\ \alpha_{1_{off}} + \alpha_{2_{off}} & \text{for } t_{1_{off}} + t_{2_{off}} \leq t \leq t_{max} \end{cases} \tag{J.14}$$

For several occurrences of the events the parameters were estimated. The results are shown in Table J.2.

A similar fitting of real parameters yielded results that hardly could be distinguished from one another. The information contained in the phase angle of the signals therefore has been shown to be very important.

Experimental Results

Two sets of experiments have been carried out:

1. Start and stop of asynchronous motors at the far end of the feeder.
2. Blowing out of low voltage fuses.

These two types of events are very different in nature. The first being slow, lasting some seconds, the second being very fast, only lasting about 10ms.

In Figures J.7 and J.8 are shown samples of currents from either experiment.
The starting and stopping of machines was done in cooperation with the afore-mentioned factory.

The fuses were burnt out by simply forcing a short circuit. This experiment was carried out on the secondary side of a distribution transformer that supplies customers. Therefore, while the experiments took place, the customers were disconnected from the transformer and supplied from a mobile power station.

In summary, it was possible to detect and classify both types of events.

Initial Implementation of Monitoring System

At this moment the monitoring system has been implemented as a simulator in the MATLAB environment. In this system the algorithms have been developed and their functionality verified.

Work is carried out on implementing the system first into ANSI–C and from there on to the signal processor chip ADSP 21020.

Conclusion

Thus far the DISMO-project has proven the feasibility of the principle of centralized monitoring.
In this stage of the project it has been possible to detect and distinguish start/stop of large motors connected to the same distribution transformer on the feeder and the burning out of fuses.

The experiments have revealed that currents and voltages need not be measured in the same quality. Most information is contained in the currents. These need therefore to be measured with high quality equipment in a bandwidth of about 10kHz.
The voltages serve an important role; they are used as reference for phases. It has, however, been seen that also in the voltages high frequency components occur. It therefore still need to be determined what the required quality of voltage measurements needs to be.

	t_2	t_3	α_2	α_3	α_4
90kW (on)	6,12	201,65	12,675∠5,114°	2,205∠−179,813°	0,406∠160,895°
	5,20	211,24	11,358∠5,599°	2,076∠−174,401°	0,554∠161,610°
	6,02	219,51	12,814∠6,373°	2,253∠−173,374°	0,493∠159,331°
75kW (on)	6,27	79,92	39,247∠4,807°	8,144∠−169,219°	1,086∠160,755°
	6,37	77,23	40,590∠4,959°	8,446∠−170,264°	1,000∠159,466°
	6,62	76,70	38,666∠4,125°	8,245∠−170,514°	0,956∠174,027°
	6,52	76,94	40,260∠3,413°	8,493∠−172,688°	0,992∠172,696°
	6,69	73,35	37,604∠6,522°	8,251∠−167,333°	0,717∠156,841°
	6,80	85,92	41,236∠6,564°	9,860∠−169,982°	0,749∠128,827°
	6,33	80,21	39,659∠3,815°	8,600∠−172,068°	0,950∠177,023°
	6,97	76,77	43,405∠5,955°	8,776∠−172,749°	0,951∠172,912°
90kW (off)	20,00	—	2,714∠179,585°	—	—
	7,02	—	2,630∠−165,502°	—	—
	9,75	—	2,604∠−165,632°	—	—
75kW (off)	17,82	—	3,844∠166,913°	—	—
	8,81	—	4,040∠163,801°	—	—
	12,33	—	4,040∠151,465°	—	—

Table J.2: Estimated Complex Parameters of Known Motor Events.

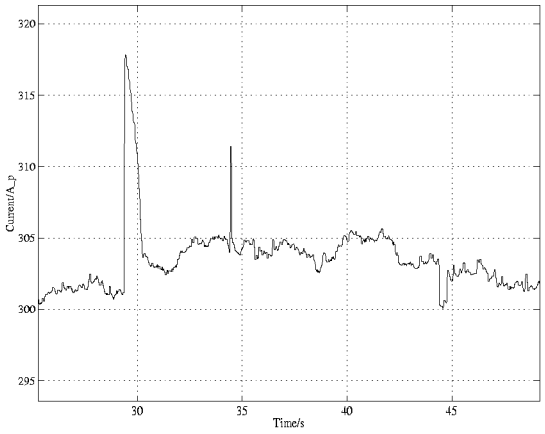

Figure J.7: Kalman Filter Estimate of Amplitude of Current During Operation of Motor at Factory.

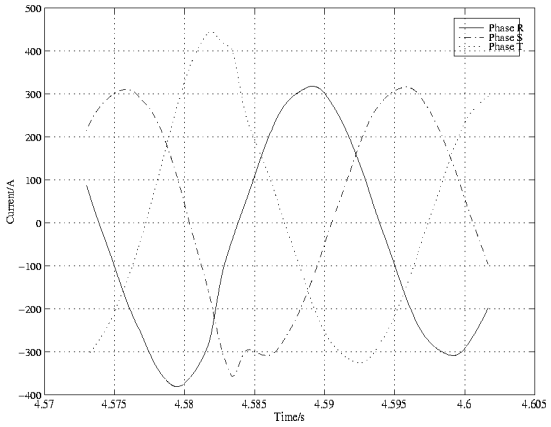

Figure J.8: Currents During Two Phase Fuse Burning Out.

Future Developments

The DISMO project aims at installing an on-line network monitor on a feeder in operation.

Important aspects need further attention. It needs to be investigated what the pay-off is of installing auxiliary measuring points along the feeder and what should be measured at such points.

It is expected that the degree of decentralized electricity production will increase in the years to come. It is therefore necessary to investigate what will be the impact of production units along the feeder.

It also needs to be clarified how many feeders may be monitored using only one analysis system. The requirement might well be to give higher priority to the cost of equipment to how well the system may react to events. In this case it must be investigated how often events may be detected and classified as a function of the number of feeders one analysis system is to monitor. In relation to that it may be acceptable that there is a dead time after the detection of an event, during which the system cannot detect new events.

References

See bibliography on pages 109–116.

List of Figures

List of Tables

Index